universitätbonn

Characterization of the structural-functional impact of heterozygous missense mutations in genes of the blood coagulation factor XIII that cause mild Factor XIII deficiency

Dissertation

zur Erlangung des Doktorgrades (Dr. rer. nat.)
der Mathematisch-Naturwissenschaftlichen Fakultät
der Rheinischen Friedrich-Wilhelms Universität Bonn

vorgelegt von

Anne Thomas

aus Weimar

Bonn, 2016

Aus dem Institut für experimentelle Hämatologie
und Transfusionsmedizin der Rheinischen
Friedrich-Wilhelms Universität Bonn

Angefertigt mit Genehmigung der Mathematisch-Naturwissenschaftlichen Fakultät der Rheinischen Friedrich-Wilhelms Universität Bonn

1. Gutachter:	Prof. Dr. med. Johannes Oldenburg
2. Gutachter:	Prof. Dr. rer. nat. Evi Kostenis

Tag der Promotion: 14.11.2017

Erscheinungsjahr: 2018

Betreffend die vorgelegte Dissertation:

Characterization of the structural-functional impact of heterozygous missense mutations in genes of the blood coagulation factor XIII that cause mild Factor XIII deficiency

hiermit versichere ich an Eides Statt:

dass die Dissertation von mir selbständig und ohne unzulässige fremde Hilfe angefertigt und verfasst wurde und andere Hilfsmittel als die in der Dissertation angegeben nicht benutzt habe; insbesondere, dass wörtlich und sinngemäß aus Veröffentlichungen entnommene Stellen als solche kenntlich gemacht worden sind.

Des Weiteren versichere ich, dass ich mich bis zu diesem Tag noch keiner Doktorprüfung unterzogen habe bzw. hat die von mir vorgelegte Dissertation noch keiner anderen Fakultät vorgelegen.

Zudem versichere ich, dass weder ein Dienststraf- noch ein Ehrengerichtsverfahren gegen mich vorliegen.

Bonn, 16.09.2016

Anne Thomas

Meinem Großvater in Memorandum

Index

Summary

The coagulation Factor XIII is a key player in hemostasis that is responsible for the last step of the coagulation cascade in which it covalently cross-links preformed fibrin clots to make them resistant to premature fibrinolysis. The plasma circulating FXIII zymogen is a heterotetrameric complex comprising two catalytic A ($FXIIIA_2$) and two protective carrier B-Subunits ($FXIIIB_2$) which are synthesized and secreted into the plasma as homo-dimers from various cell types like monocytes/ macrophages, megakaryocytes, and platelets for the A subunit and hepatocytes for the B subunit. Deficiency of FXIII results in a bleeding predisposition for the individual carrying it. This deficiency can have congenital or acquired origins. The inherited form of FXIII deficiency can be classified into two types based on severity of symptoms: severe and mild FXIII deficiency. While the homozygous inherited form of this deficiency caused by *F13A1* (OMIM #613225) (FXIIIA subunit) or *FXIIIB* (OMIM #613235) (FXIIIB subunit) gene mutations is rare (1 in 2-4 million), the milder heterozygous form is more frequent. Only recently, focus has shifted to the mild/heterozygous form of this deficiency that is associated with mild or even an asymptomatic phenotype (unless the affected individual is exposed to some kind of a trauma for e.g. peri-operative settings, accident etc.). Recent investigations from our group in the past five years have shown that inherited mild heterozygous deficiency does have clinical relevance. Identification of heterozygous FXIII deficient patients and extended causality determining research on the related mutations is crucial since the risk of provoked bleeding events (surgery, tooth extraction, trauma) in heterozygous patients can be minimized through early detection. In the last five years, our group has reported 23 mutations from patients with mild FXIII deficiency. Sixteen of these mutations were identified in the *F13A1* and seven in the *F13B* gene. In the present study we have performed a comprehensive investigation on the causality of these reported missense mutations using parallel *in silico* and *in vitro* approaches to structurally and functionally characterize their underlying pathophysiology. The *in vitro* methods have been complemented by *in silico* strategies in which modeling of protein subunits/domains/mutations and simulation/docking based approaches have been applied to explain the *in vitro* findings. Our analysis shows that these mutations can act on different aspects of FXIII activation and regulation based on the structure functional impact of the particular mutation.

Publication list

The thesis is a cumulative thesis based on the following three published/accepted for publication articles:

1. Biswas A.*, **Thomas A.***, Bevans C.*, Ivaškevičius V., Oldenburg J. *In vitro secretion deficits are common among human coagulation factor XIII subunit B missense mutants: correlations with patient phenotypes and molecular models.* **Hum Mutat.** 2013, 34(11):1490-500.

2. **Thomas A.** *, Ivaskevicius V., Oldenburg J., Biswas A*. *Structural and functional influences of coagulation factor XIII subunit B heterozygous missense mutants.* **Mol Genet Genomic Med.** 2015, 3(4):258-71.

3. **Thomas A.***, Biswas A.*, Dodt J., Philipou H., Smith E., Ensikat H.J., Ivaskevicius V., and Oldenburg J. *Factor XIII A subunit missense mutations affect structure and function at the various steps of factor XIII action.* **Hum Mutat.** 2016, 37(10):1030-1041

*These authors contributed equally to this work

Chapter I: Introduction

1.1 Part 1: Blood coagulation with special focus on the structure and function of factor XIII (FXIII)

Blood coagulation

The coagulation of blood is a highly conserved physiological response to prevent blood loss from injured or damaged vessels involving a complex regulated activation cascade of many proteins circulating in an inactive mode in the blood[1]. The generation of a haemostatic plug is a highly regulated process mainly to prevent unrestricted intravascular clotting. Most of the proteins of the coagulation cascade are serine proteases[2] reaching their activation through proteolytic cleavage when triggered, for example by vascular damage. For the conversion of fibrinogen (factor I [FI]) to fibrin (FIa), the transformation of prothrombin (FII) to thrombin (FIIa) is the central necessary process. The formation of stable, stiff and resistant blood clots resulting from polymerisation of fibrin occurs via two major steps:

A) The primary (cellular) haemostasis includes the formation of a loose primary haemostatic thrombotic clot accompanied by vessel constriction, platelet adhesion, aggregation and activation [3,4]. These primarily cellular reactions lead to a change in the polarity of the membrane surface to a negative charge that in turn induces the activation of the plasma blood coagulation factors [5].

B) During the secondary (plasmatic) haemostasis a more stable and resistant fibrin clot is formed out of the primary platelet plug [3,4]. The secondary haemostasis is activated either by the intrinsic or the extrinsic pathway.

Normally, an intact endothelium layer exposes factors like nitric oxide (NO), ecto-ADPase, prostacyclin (PGI_2), heparin sulfate, thrombomodulin and TFPI having anticoagulant and anti-inflammatory functions to prevent thrombus formation and maintain blood fluidity [6].

The primary haemostasis is initiated in case of injury: blood vessels get damaged, the endothelium breaks and the collagen layer in the subendothelium comes in contact with circulating platelets to initiate their adhesion, aggregation and activation. Collagen, which is located directly below the endothelium, binds to the platelets directly with its specific glycoprotein (GP)Ia/IIa (α2β1) and GPVI surface receptor complex[7]. Indirectly, platelets are bound via bridging of von Willebrand factor (vWF). Therefore, the vWF connects platelet surface GPIb/IX/V receptors and collagen fibrils [8,9]. Von Willebrand factor is a multimeric glycoprotein synthesized, located in weibel palade bodies and secreted by platelets and endothelial cells [10,11]. Platelet adhesion to collagen over the GPVI receptor activates the platelets in the extracellular matrix of the injury site and subsequently leads to thrombin and fibrin formation [12]. After collagen binding, activated platelets release different factors like vWF, serotonin, ADP, thromboxane A_2 and platelet-activating factor (PAF) stored in their α-granules to initiate activation of further platelets [13–16]. These agonists trigger several signalling pathways to increase the intracellular Ca^{2+} concentration [17]. High Ca^{2+} levels are necessary for platelet shape change and degranulation and for further activation of integrin α2β3 and finally to increase blood coagulation cascade to form a fibrin clot [18–20]. Integrin α2β3 is an important bridging factor for platelet aggregation via interaction with fibrinogen [18–20].

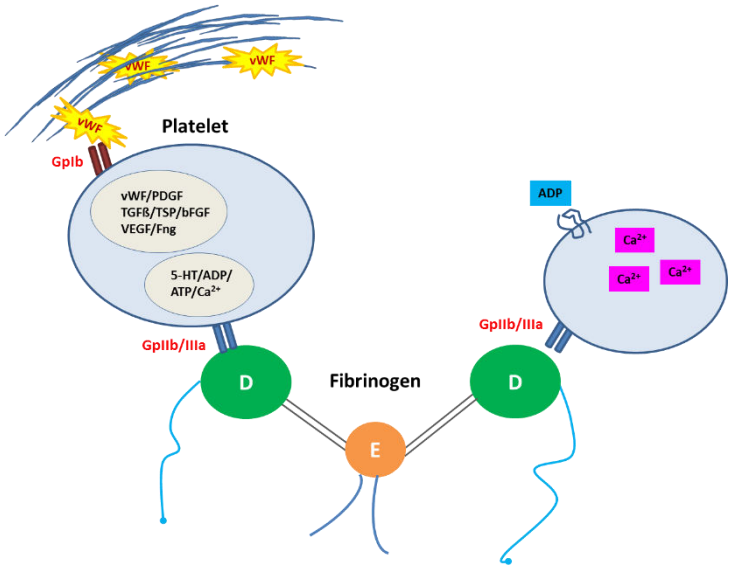

Figure 1: Platelet adhesion to collagen and fibrinogen and granula storage of platelets.

Fibrin formation is part of the secondary haemostasis which either is started by the contact activation pathway (intrinsic pathway) or primary tissue factor way (extrinsic pathway) both ending in a common pathway activating factor X, factor XIII, thrombin and fibrin. The two pathways are composed of different coagulation factors: mostly serine proteases, glycoproteins (FV/ FVIII) or a transglutaminase (FXIII) which circulate as zymogens in the plasma and get proteolytically activated to finally generate and covalently cross-link fibrin [4].

The extrinsic pathway (Tissue Factor (TF) pathway) is initiated if there is a tissue injury with blood vessel damage leading to release of the tissue factor from tissue cells like fibroblasts and leukocytes. The TF a integral cell surface protein is part of an enzyme complex acting as the positive regulator for the extrinsic pathway. The other subunit of this enzyme complex is the blood coagulation factor FVII [21] having catalytic function. Therefor FVII is anchored by TF to the cell surface acting

together in complex (TF:FVII) in activation of blood coagulation . This triggers a coagulation cascade involving a series of different reactions to activate or deactivate enzymes near the surface of activated platelets. This finally leads to the activation of thrombin for blood clotting. In the presence of Calcium, the contact with tissue factor (TF) starts the activation of zymogen FVII, which itself is activated by thrombin, FXIa, FXIIa and FXa. Activated FVII activates FIX [6] and FX [21]. FXa and its cofactor FVa form a prothrombinase complex to generate thrombin out of prothrombin [22]. With the generation of the serine protease thrombin the common pathway starts.

The intrinsic pathway plays a minor role in blood coagulation only in vitro more related to the inflammatory system showing *in vivo* no contribution to haemostasis [23,24]. The smaller physiological importance is supported by the fact that no severe bleeding occurs in case of severe Factor XII deficiency [24]. Recent publications with murine models in FXII deficient mice found unstable formed thrombi and discovered its central role in venous and arterial thrombosis [24]. Activation of the intrinsic pathway is forced in case of contact with negatively charged surfaces (non-physiological substances like glass or kaolin) by the heavy chain of FXII (Hageman factor) [22]. FXII starts activation of prekallikrein (PK) and high-molecular weight kininogen (HMWK) [25,26].The formation of a primary complex composed out of HMWK, prekallikrein and FXII is important to start the complex cascade for activation of thrombin [22,27]. Additionally, FXIIa activates FXI into FXIa, while FXIa converts FIX. FIXa forms a tenase complex with FVIIIa to finally stimulate FX to FXa. Thrombin is important to activate further factors of blood clotting like FV, FVIII, FXI, Fibrin and FXIII. The coagulation contact pathway is linked to the inflammatory system over activation of kallikrein which activates HMWK to release bradykinin. The small peptid bradykinin binds to the kinin B2 receptor on endothelial cells resulting in activation of inflammation like chemotaxis of neutrophils, vasodilation and increased permeability

of vascular system (Smith 2016). Next to the function in inflammation [2] found contribution to fibrinolysis, angiogenesis and part of inhibition of thrombin-induced platelet activation.

Finally, a complex called prothrombinase activator complex is formed out of FVa, FVIIIa, FXa, Ca^{2+} and phospolipids to cleave prothrombin to thrombin [28]. Thrombin cleaves fibrinogen into soluble fibrin monomers that polymerize to form a primary clot. For this, thrombin converts FXIII to FXIIIa and activates FVIII and FV [29]. Additionally, it stimulates further platelets via protease activating receptor 1 and 4 (PAR1/PAR4) to further mobilize the coagulation cascade [30]. In the presence of thrombomodulin, direct activation of its inhibitor protein C appears to regulate thrombin generation [31]. Vitamin K dependent protein C additionally inactivates both FVIIIa and FVa in presence of cofactor protein S [32,33]. Further regulation of coagulation occurs in different positions of the cascade. For example, inhibition of the TF/VIIa complex occurs via the TF inhibitor [34], antithrombin III inhibits both thrombin and FIXa. The fibrinolytic system is an important regulator to prevent unfunctional clot formation by downregulation of the thrombin generation and clot dissolving by plasmin.

In the final step of blood coagulation, the produced Fibrin is further stabilized and covalently cross-linked by thrombin-cleaved FXIIIa, which will be in the focus of this thesis. The understanding of pathogenic disease-causing mutations is important to understand coagulation, its enzymatic reactions and its molecular mechanism in more detail.

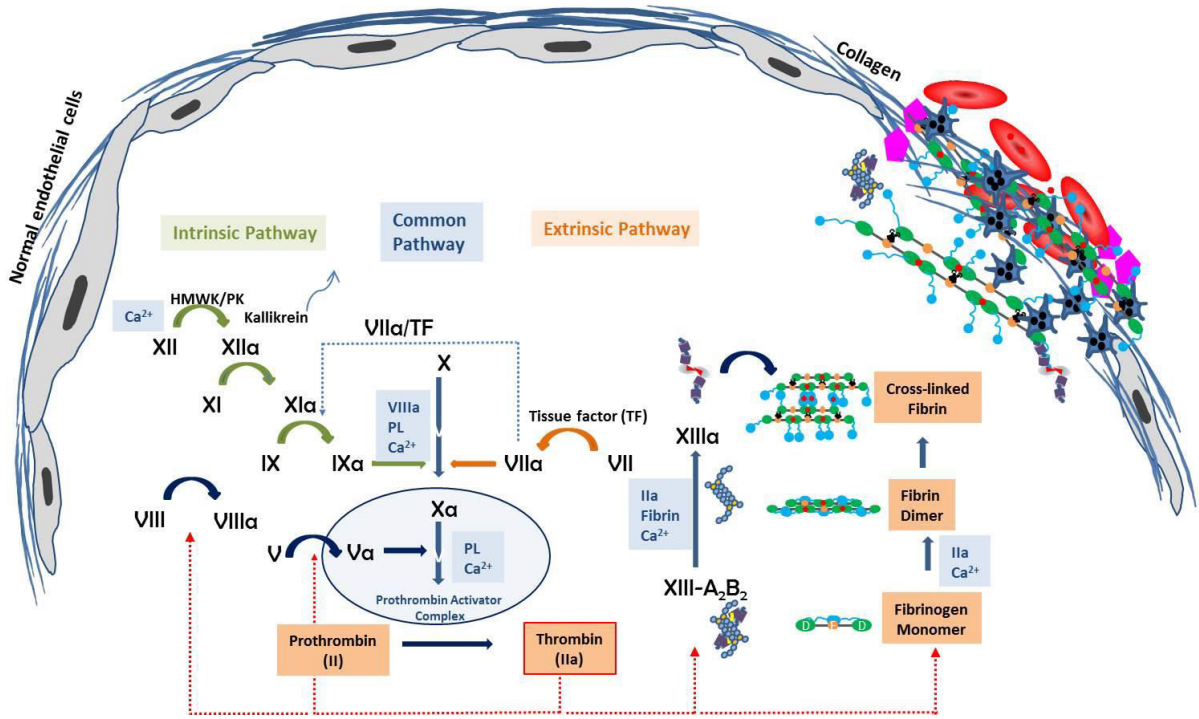

Figure 2: Overview of the coagulation cascade (secondary hemostasis).

The extrinsic pathway is triggered by contact of blood coagulation factor VII (FVII) with the membrane glycoprotein tissue factor (TF), while the intrinsic pathway is a result of contact with negatively charged surfaces like activated platelets. Both, the extrinsic and the intrinsic pathways result in a tenase complex including activated FVIIIa and FIXa, which are necessary for activating FX. Activated FXa and Va build up the prothrombinase complex important for thrombin generation. Thrombin generated Fibrin monomers polymerize to a soluble clot. Thrombin activated FXIIIa introduces covalent cross-links to the preformed primary clot. During the fibrin formation the fibrinolytic pathway is activated by tissue plasminogen activator (t-PA) binding to fibrin. The t-PA is necessary to activate Plasmin which degrades the fibrin clot.

Historical view on FXIII

Factor XIII is a key player in the coagulation pathway since it covalently cross-links preformed fibrin clots to form a more stable, stiff and resistant clot at the last step of the blood coagulation cascade. Barkan and Gaspar in 1923 made the first observation that fibrin clots become insoluble in weak bases in the presence of Calcium [35]. In 1944, Robbins, while studying purified fibrinogen from plasma, recognized that besides Calcium some other serum factor is needed to form this insoluble fibrin clot [36]. The two Hungarian researchers Laki and Lorand finally were the first to describe this factor, which is responsible for the fibrin clot insolubility observed in urea solution [37–39]. They characterized and named it the fibrin stabilizing factor that was thermo-labile and non-dialyzable. After Duckert et al. [40] reported a patient suffering from bleeding diathesis in 1960, the clinical relevance of the fibrin stabilization factor became more evident. The lack of this fibrin stabilization factor was found to result in a severe bleeding phenotype [40]. In 1961, Leowy [41–45] purified this plasma component and Buluk [46] suggested a reaction sequence for this new factor. Soon the International Committee on Blood Clotting Factors acknowledged the fibrin-stabilizing factor as a clotting factor and termed it factor XIII in 1963 [47]. Between 1986 and 1990, more important steps in FXIII research followed: the elucidation of the complete cDNA sequence of human placental FXIII-A by Takahashi et al. [48] and for the B subunit of factor XIII [49,50] by Grundmann in 1986 [51].

In 1994, the first three dimensional molecular structure for the homodimeric inactive A-Subunit was identified by the group of Yee et al. 1994 [52]. Recently, the first crystal structure of the non proteolytically activated FXIII (FXIIIa$^{\circ}$) in complex with an inhibitor was reported [53]. So far, there is no structure for the filamentous B-Subunit dimer

accessible. Since 1961, more than 606 articles have been published, including case reports and reviews about FXIII deficiency, revealing a considerable interest in FXIII clinical research [54].

Classification of FXIII deficiency

Coagulation factor XIII (FXIII) is a member of the transglutaminase (TGs; EC 2.3.2.13) family which consist of 9 zymogens (TG1 to TG7, TG9 and one protein 4.2 lacking catalytic activity), each sharing a similar structure of 4 domains (catalytic core, ß-sandwich, ß-barrel 1&2 domains) in a compact conformation [55]. The most conserved sequential homologies between the different TGs can be found in the middle region between amino acids 180 and 500 [56]. While the N-terminal region shows moderate similarity, the most outstanding differences can be found in the C-terminal region [56]. TGs cross-link peptide chains by ε (γ-glutamyl)-lysyl bonds. All TGs are monomers, except for FXIIIa, which appears as a homo-dimer [56]. Out of all TG´s, FXIII is the only TG which carries an activation peptide to protect the catalytic triad. A proteolytic cleavage in front of the ß-sandwich was found to be part of the protein-activation of TG-1[57], similar to the situation in FXIII. So far, three-dimensional structures of the three human TGs FXIII-A_2[52], TG-2[58] and TG-3[59] have been resolved. X-ray crystallographic analysis of the orthorhombic[52] and monoclinic[60] forms revealed the same structure for the inactive FXIIIA subunit dimer. Recently, the first high-resolution crystal structure (1.98 Å) of an active state of FXIII was published [53].

Genetic background and Structure for both of the FXIII Subunits

FXIII-A Subunit

The gene for the alpha chain (*F13A*) was found to appear earliest in sea lamprey, fishes and tetrapod's [61]. The gene coding for the subunit A is located on the short arm of chromosome 6 (p24-p25) [62] and consists of 160 kilobases (kb) including 15 exons and 14 introns [62,63]. The DNA coding for the human FXIII-A protein (F13A1 gene) is transcribed into a 3.9-kb mRNA. The mRNA is divided into an 84-bp 5´-untranslated region, a 2.2-kb open reading frame and a 1.6-kb 3´-untranslated region. The mature non glycosylated FXIII-A subunit protein reaches 732 amino acids including an initiator methionine (http://www.uniprot.org/uniprot/P00488) and is 1.15 times bigger than the FXIII-B protein reaching a molecular mass of 83 kDa [64]. Quite often the N-terminal methionine residue is acetylated or removed by Met-aminopeptidases [65]. The initiating methionine in the FXIII-A protein is followed by serine. The methionine is found to be removed and the serine is N-acetylated [65]. N-acetylated proteins are known to be catabolized by the proteasome pathway in the cytosol if protein folding is incorrect [65]. The protein harbours 9 cysteine residues, including the active site cysteine in the catalytic trait, Cys314. The FXIII-A dimer protein does not possess a hydrophobic leader sequence [66] indicating that the protein is not secreted in a constitutive pathway. FXIIIA is known to show PDI activity, but the responsible cysteine has not been not detected yet [67]. The deactivated protein is built up by 4 main structural domains: ß-sandwich from exon II-IV [38-184AS], the catalytic core containing exon IV-XII [185-515], ß-barrel 1 containing exons XII-XIII [516-628] and ß-barrel 2 with exons XIII-XV [629-731]. The N-terminal activation peptide (AP-FXIII) of exon II (amino acid 1-37) is cleaved off by thrombin [68]. Next to the cleavage site Arg37 another thrombin cleavage site at Lys513-Ser514 is found in the FXIII-A subunit [69]. Thrombin cleavage on the second site leads to the release of a 51 kDa (Gly38-Lys513) fibrin binding domain [70] hindering FXIIIa function.

Close Ca^{2+} binding sites protect the subunit from this secondary hydrolysis by thrombin [52].

The catalytic triad, which is completely buried by AP-FXIII, is composed of three amino acid residues Cys314, His373 and Asp396. The ß-sandwich and barrel 1 (516-628) & 2 (629-731) domains are built up by ß-sheets with only a few helical structural elements [56]. The core domain contains ß-sheets as well as helices and can be further divided into NH_2- (189-332) and COOH-terminal (333-515) subdomains [71]. The two central core domains of the FXIII-A subunit monomers are surrounded by six ß-sheets in the dimeric structure. In the core domain are two non-proline cis-peptide bonds [60] which were observed in the human TG-2 [58] and TG-3 [59], too. Overall, the solvent excluded surface of the FXIII-A is negatively charged, except for the thrombin cleavage site Arg37 residue which is positively charged. It is still unknown, in which way the two monomeric A-subunits are linked together. Mutational expression studies found that the residue Arg260 forms a salt bridge with Asp404 of the opposite monomer implying a function in binding of the two monomers [72]. Aside from Arg260, another residue, Tyr283 [73], is highly conserved among the TGs and also playing a role in dimer formation[73].

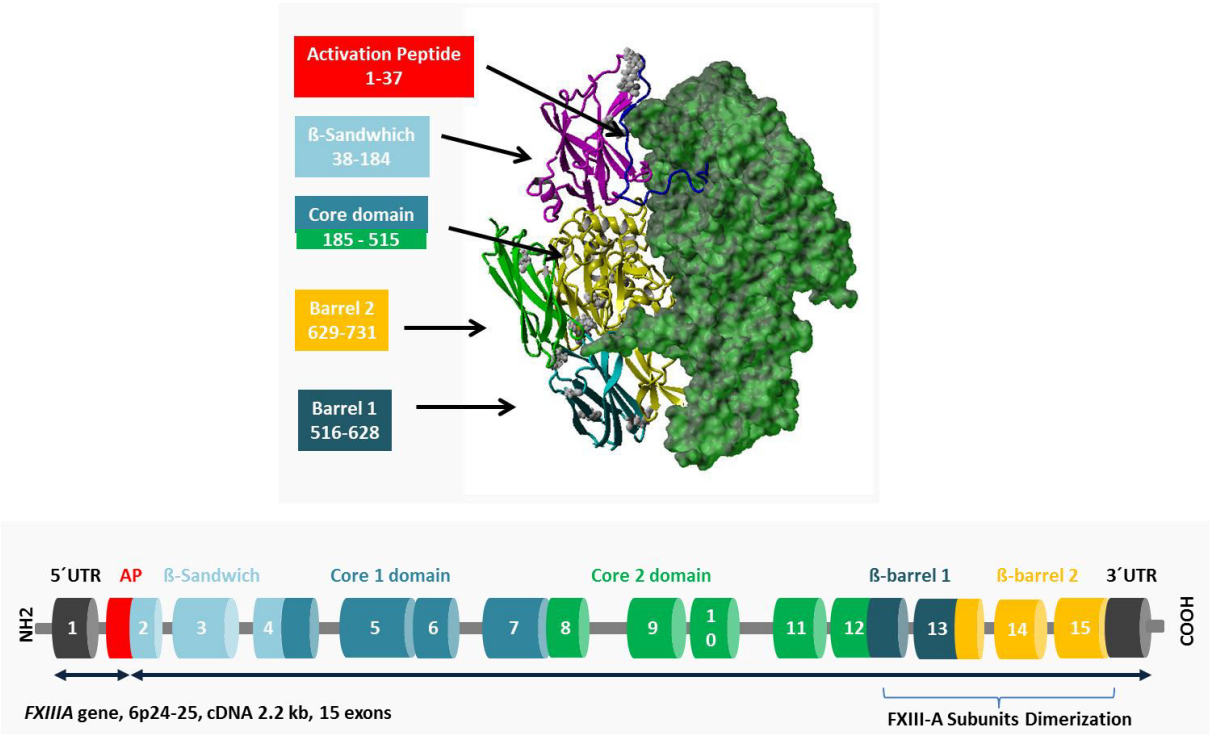

Figure 3: Illustrating the FXIII-A Subunit gene and the protein structure.

Catalytic triad

The Cys314, His373 and Asp396 are part of the catalytic triad of the cysteine protease which catalyses the interchain peptide bond formation between the glutamine and lysine side chains of two substrates [52]. Therefore the NH group of the indole side chain of the highly conserved Trp279 (shown to be involved in TG reaction by TG-2 [74] and Cys314) forms an oxyanion hole [75]. The catalytic cysteine residue Cys314 is completely buried by AP-FXIII, because a salt-bridge from the side chain of Arg11 in AP-FXIII reaches to the opposite subunit and a second side chain of Asp343 of the core domain blocks the access to the Cys314 for substrates [56]. The entrance to the active site is also blocked by strong hydrogen bonds between the Oη atom of the Tyr560, which is located on a loop of the β-barrel 1 domain, and Sγ atom of Cys314 residues [53,56]. This H-bond is important to prevent early TG reaction by blocking the Sγ atom of Cys314 residue from binding to the Gln side chain carbonyl

carbon of the potential substrate [56,75]. The highly conserved Trp279 [76] is found to prevent the substrate from reaching Cys314, if the protein appears in its inactive form [56].

Figure 4: The catalytic core domain of the Factor XIII-A subunit.

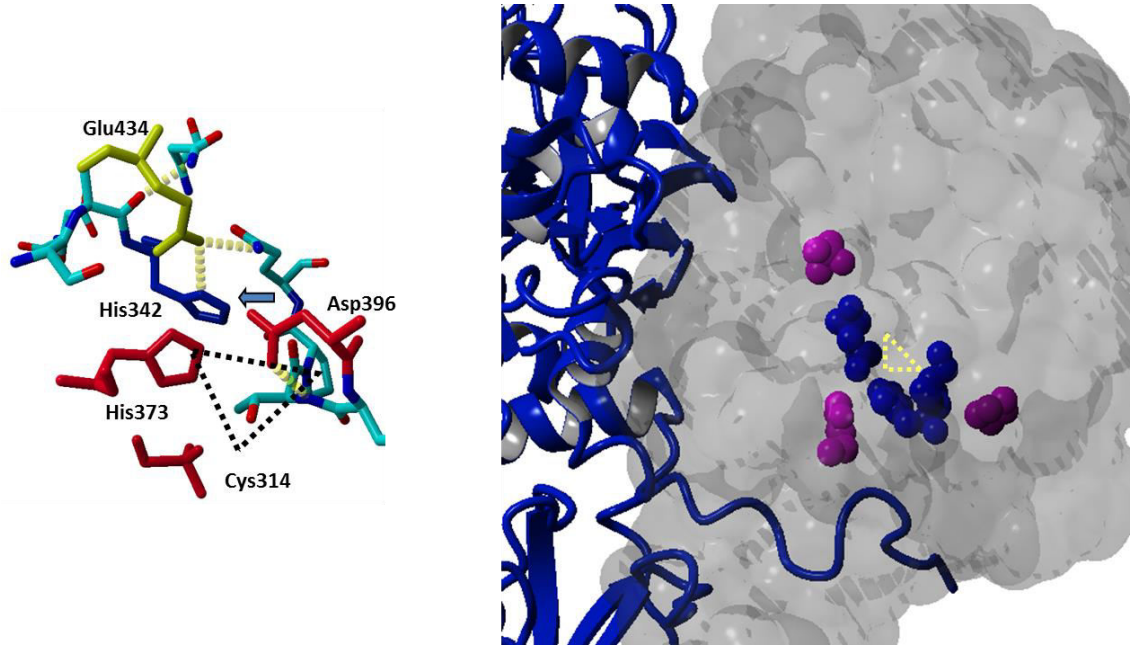

Ca^{2+}-binding sites

Ca^{2+}-binding is necessary for the activation of FXIII. Therefore, Ca^{2+} binds FXIII-A with high affinity (K_d = 0.1 mM) [1], but also additional low affinity binding sites are found. Ca^{2+}-binding on the FXIII-A subunit directly or through water bridging is located at the carboxylated groups of Asp438, Glu485, Glu490 side chains and the carbonyl O-atom of Asn436 and the backbone carbonyl O-atom of Ala457 [69,77], which create a Ca^{2+} binding pocket[56]. Direct Ca^{2+} binding happens by Ala457, Glu485 and Glu490 [56,69,77](74/75/172). Ca^{2+} binding to the catalytic core was found to be involved in the conversion from inactive FXIII to the active state. Therefore one Ca^{2+}-ion interacts with the Ca^{2+} binding site 1 via Ala457 in the inactive state [53]. During the activation process the Ca^{2+}- ion substitutes the bound water molecules on the other coordination sites with binding to Asn436, Glu485 and Glu490 which is necessary to move a loop and α helix forming a more compact Ca^{2+} surrounding environment [53]. During activation process, the second Ca^{2+}- binding site leads to the formation of a hydrophobic pocket next to the catalytic triad mainly through Ca^{2+} binding to Asp367

and Asp351 [53]. Next to the pocket formation, which is important for guiding the substrate to the catalytic core, the Ca^{2+} binding on site 2 further supports the development of the catalytic triad by binding Ca^{2+} to the Asp343 residue bringing His342 and Glu401 in proximity [53].

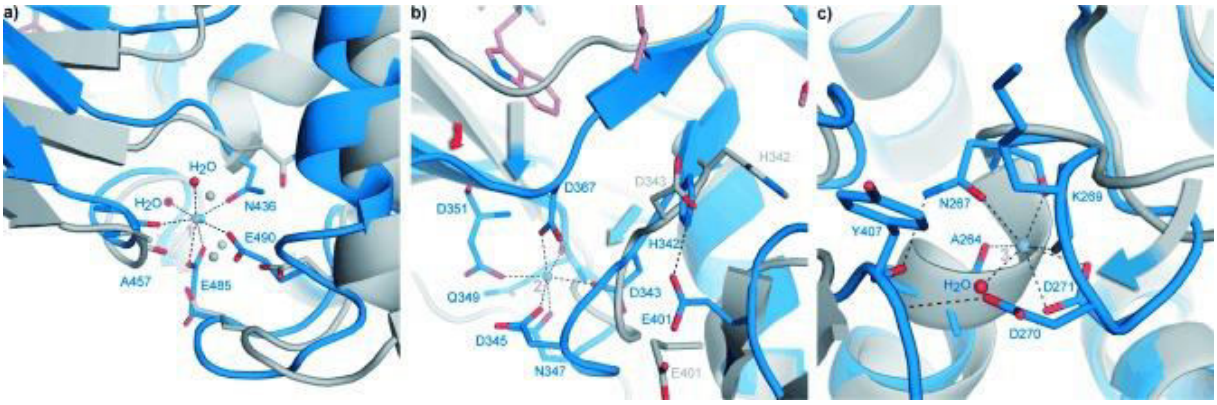

Figure 5: Calcium binding sites necessary on the non-activated and activated FXIIIa.

Activation Peptide and Thrombin cleavage site

FXIII-AP

The AP-FXIII is located to the A-Subunit in a special way that it is covering the ß-sandwich and part of the core domain of one A-Subunit monomer [78]. The N-terminus of the bound AP-FXIII overlaps with the barrel 1 domain of the other A-Subunit monomer [78]. The close interaction between the FXIIIA molecule environment and the AP concerning 17 H-bonds is necessary to bury the active site cysteine (Cys314). The interaction of the AP with both monomers of the A-Subunit includes 13 hydrogen bonds (Asn17-Arg107, Asn17-Tyr108, Asn17-Leu249, Asn18-Arg252, Asn20-Lys156, Ala21-Asp243, Glu23-Arg174 (2H-bonds), Asp24-Arg158, Pro27-Arg171, Thr28-Arg171, Glu30-Val169, and Gln32-Tyr167) with residues from one monomer and 4 hydrogen bonds (Gly10-Thr561, Arg11-Asp343 (2 H-bonds), and Arg11-

Pro399) with the other monomer, while three further hydrogen bonds (Ser19-Ala21, Ser19- Ala22, and Gln32-Gly33) are formed within the AP itself [78]. The salt bridge between Asp343 and Arg11´ (AP-FXIII) of the opposing monomer keeps the AP-FXIII in a position that covers the active site along with another amino acid, the Tyr560 of barrel 1. It buries the cavity in which the amino acids residues play a key role in the activation process. A small change in this complex binding process, which involves binding between FXIII and FXIII-AP and interaction between FXIII-AP and Thrombin, can have a fatal effect on the substrate cleavage process.

Thrombin binding for FXIII-AP cleavage

For activation of heterotetrameric pFXIII, proteolytic cleavage of the N-terminal AP-FXIII via the serine protease thrombin is necessary. The AP-FXIII is located on the flexible loop on the surface of the molecule promoting its release into cell plasma after cleavage. Arg37 and Gln38 are sticking out from the loop region for better accessibility of thrombin catalytic triad (Asp102, His57 and Ser195) [79]. Thrombin, which is composed of two ß-barrel domains, carries the cleavage site consensus sequence LTPRGVRL [80], which is critical for FXIIIA-AP cleavage carrying VVPRGVNP as cleavage site sequence. The region P(4) to P(1) region [nomenclature for the substrate: The thrombin hydrolysis site is marked as P1-P1´, the amino acids on the left side of the cleavage site are labelled as P2 to P4 and the amino acids on the right side are named as P2´, P3´ and so on [81]] is known to be very critical for the FXIII-A binding to the thrombin surface. Cleavage of the AP-FXIII involves the burying of the consensus substrate P1 Arg side chain deep into the S1 pocket of thrombin, allowing proximity of the sessile bond to the nucleophilic thrombin Ser195 residue [82]. This is aided by contacts formed by the positively charged Arg residue side chains with residues in the thrombin catalytic cavity that bear a strong

negative electrostatic potential [83]. In the thrombin cleft, the hydrophobic interaction takes place down to the guadinine group which forms a two pronged salt bridge with Asp189 at the base of the pocket [82]. The P4 (hydrophobic/ aromatic) interacts with the aryl binding pocket (S4) of thrombin [82]. The insertion loops can interact directly with the substrate peptide, with the 60-loop helping form the S2/ S4 sites and the γ-loop forming contacts with the P´side [82]. The loops are necessary for the thrombin specificity restricting the access to the active site cleft [82]. Thrombin is known to bind amino acids 33 to 37 (P4-P1) of FXIII-AP by hydrogen bonds with W60, L99, I174, W296, S195 and E217 [84,85]. W215 is the key residue for effective binding and hydrolysis of FXIII-AP by supporting the binding of main chain backbone residues V34 and V35 of FXIII-AP [84]. The other key supporting residue for the thrombin ligand E217 builds hydrogen bonds between P5 (G) and P4 (L) to E217 [84]. The L99 helps to align the FXIII-AP substrate into the active cleft for more effective hydrolysis [84]. The backbone of the Val residue (P3/ P4) of the V34 position is located above the thrombin W215 residue and the Proline at the P2 residue interacts with thrombin L99, Y60a and W60d. The hydrophobic bond between P2 to L99 is necessary for an appropriate binding and catalysis of thrombin substrates. L34 of the FXIII-AP appears to be interacting with thrombin L99 through the side chain and thrombin W215 through the main chain.

FXIII-B2 Subunit

The B subunit gene composed of 28 kb length is mapped on the long arm of chromosome 1 (q31-q32.1) [49,86] and consists of 12 exons and 11 introns coding for a 2.2 kb mRNA. Evolutionary, the beta-chain (F13B) appears to be present in cave fish (Astyanax mexicanus) and medaka (Oryzias latipes) [61]. The flexible, thin and linear 641 amino acid long glycoprotein (proved by electron microscopy [87]) has a molecular

mass of ~80 kDa. It is build up by 10 GP-1 structures called sushi domains of about 60 amino acids. Each of them is held together by two conserved disulphide bonds between the first and third cysteine and the second and the fourth cysteine [56]. The structure is similar to more than 50 other proteins, mostly belonging to the complement system, like Factor H, which is also composed out of complement control proteins (CCP) [88]. Evolutionary exon shuffling and gene duplication is responsible for the high degree of homology of the sushi domains building up Factor XIII-B protein [89,90].

Exon I encodes for a 20 amino acid leader sequence necessary for the classical secretion [91,92] and is cleaved off during the export process. Exon II-XI code for the 10 single sushi domains and exon XII codes for the 3´-untranslated COOH-terminal region. The transcription is regulated by the HNF1α and HNF4α transcription factors [93,94]. So far there is no crystal structure detected, but via the technique of electron microscopy the FXIII-B protein was described as a thin, kinked strand and flexible protein.

N-glycosylation of the protein appears at the amino acid Asn142 in the third sushi domain and Asn525 which is located in the ninth sushi domain [95,96]. Gel filtration analysis reveals that probably the first sushi domain is part of binding to the A-subunit in heterotetramer formation [97] and the fourth/ ninth sushi domains function in dimer assembly of the B-subunit [98].

The carrier protein has no enzymatic function and is part of the FXIII-A subunit in the plasma. It is supposed to stabilize and prevent non-proteolytic activation of plasma FXIII with high Ca^{2+} levels [99] and therefore increasing half-life of the FXIII-A protein [25]. It has been found recently that FXIII-B is participating in the formation of a ternary

complex between FXIII zymogen, fibrinogen, and activator thrombin and is especially involved in binding the pFXIII-A2B2 to the fibrinogen γ-chain over its D-domain[100].

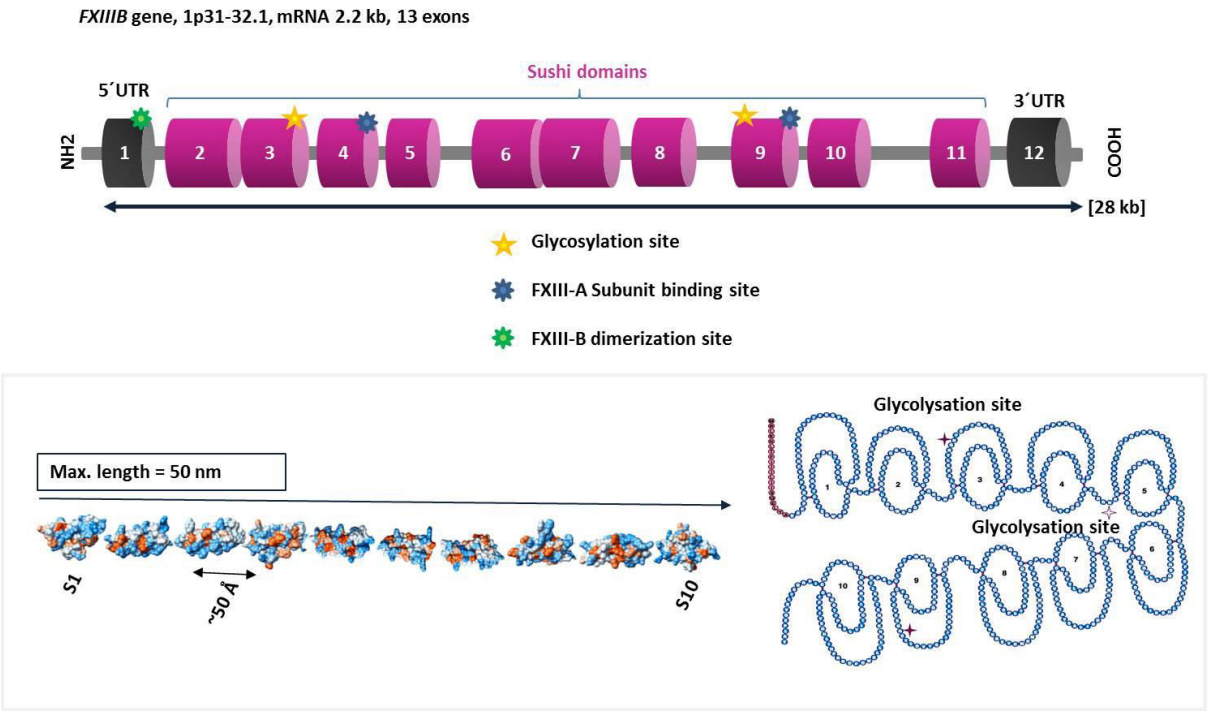

Figure 6: Illustrates the Factor XIII-B subunit gene and its possible protein structure.

Synthesis and secretion of both FXIII-A and FXIII-B Subunits

FXIII is located in the body in two forms, one is the intracellular dimer called cellular FXIII (cFXIII) and the other form is the heterotetrameric plasma FXIII (pFXIII). The function and activation of pFXIII is well studied, but less understood for the cFXIII, consisting of only two A-Subunits. Plasma-circulating FXIII (pFXIII) appears as a 320 kDa heterotetramer ($FXIIIA_2B_2$) composed of two catalytic A and two carrier/ protective B Subunits, held together by non-covalent interaction ($FXIIIA_2B_2$). Half of the FXIII in the body is cFXIII [101,102] synthesized in platelets and functioning mostly in

wound healing, bone development and tissue remodelling like cytoskeleton remodelling during platelet activation [55,103,104]. Missing the B-subunit and not in proximity to thrombin, the intracellular FXIII can only be activated non-proteolytically (without cleavage of the activation peptide) by high intracellular, non-physiological Ca^{2+} concentration (50-200mM) [105–107]. By the presence of the FXIII-B subunit, pFXIII is prevented from non-proteolytic activation in the plasma and needs thrombin as an activator [99].

Cellular FXIII (cFXIII)

The cFXIII is expressed in cells of the bone marrow origin like chondrocyte, chondrocytes/ osteoblast/osteocyte lineages [108,109], megakaryocytes/platelets [103,110,111] and their precursor cells and synthesized in the cytoplasm of monocytes/ macrophages [103]. Macrophages from different tissues like alveolar, dendritic, tumor or lymph node derived express cFXIIIA [112,113]. The cFXIII synthesis happens only during the differentiation step from monocytes to macrophages where it appears in the nucleus [114]. Additionally, cFXIII was found to be located in podosomes or other membrane structures of the macrophages [114].

Platelets contain huge amount of cFXIII [101,102,115], reaching FXIII-A_2 concentration 150-fold higher in platelet cytoplasm [101,102] than compared to plasma [112]. The average cFXIII content of a single platelet is found to be 60+/-10 fg (3% of total platelet proteins) [116],. The secretion mechanism of cFXIII out of platelets remains elusive [114]. Recently, *Mitchel et al 2014* [117] found that platelet cFXIII is released on the activated platelet surface in the form of protruding caps [117]. They showed under flow that activated platelets secrete the whole cytoplasmatic pool of cFXIII-A on the platelet surface where it cross-links α2-antiplasmin (a fibrinolytic inhibitor) to fibrin to increase fibrinolytic resistance of the thrombi [117]. However, several questions

regarding the exact mechanism of translocation of cFXIII to the outer surface membrane in platelets and other cFXIII containing cells remain open.

Another source of cFXIII are placenta/ uterus [118,119], and tear drops [120,121] . Placenta [122] and uterine [123] cFXIII come from monocyte-derived tissue macrophages origin [122]. The amount of cFXIII in tears is 3 times lower than in plasma [124]. Regulation mechanisms of cFXIII are found to be different in different body fluids [124].

Plasma FXIII (pFXIII):

Another question that has not been answered yet concerns the origin of secreted plasma FXIIIA subunit. FXIII-A_2 appears in the plasma fully complexed with the FXIII-B_2 subunit, while only a small amount i.e. <1% circulates in free functional non-complexed form [97]. Studies have shown that the main source of FXIII-A subunit for pFXIII are cells of bone marrow origin [125,126] like monocytes/ macrophages or platelets. In two transgenic mouse models, where mice showed thrombocytopenia plasma levels, the amount of pFXIII was not significantly reduced [114,117]. Therefore, Cordell et al. (2010)[114] suggested that instead of platelets maybe cells of monocyte lineage are the main source of pFXIII-A. Supported by the fact that patients who undergo bone marrow removal during autologous peripheral blood stem cell transplantation have reduced platelets with over 90 % decrease [127], but pFXIII levels fall off only ~25%[127], these data implicate that platelets are not the only source for pFXIII.

In embryos, FXIII-A is already synthesized in mesenchymal histiocytes and liver cells before bone marrow development starts [128]. Recently, Griffin et al 2015 [129] identified the cells that maintain the plasma pool by creating a MpP-/- (thrombopoietin receptor knockout) thrombocytopenic murine model out of a floxed mouse in coding exon 7 of the *F13A1* gene crossed with mice transgenic for Pf4-Cre-recombinase

(thrombopoietic deletion) or Cd11b-Cre-recombinase (myeloid deletion) [129], the research group found a 40% decrease of pFXIII-A activity in Cd11b mice and 85% decrease of pFXIII-A activity and a lack of platelets in Pf4 mice. Mpl mice showed normal pFXIII activity [129]. In combination with results from a human stem cell study they found the possibility that a unique Pf4-dependent and Mpl-independent progenitor cell is the major source of the plasma pool [129]. Another source of pFXIII-A are hepatocytes which have been reported to express low levels of the pFXIII-A subunit [113,127,130].

All the current findings show that FXIII-A, which is present in pFXIII, is predominantly synthesized in human stem cells of bone marrow origin. Still, the question of the origin of pFXIII-A cannot be answered fully and also the secretory mechanism remains unanswered.

The FXIII-B Subunit is only expressed by hepatocytes [131], also supported by following liver transplantation where the phenotype of the recipient FXIII-B changed to that of the donor phenotype for the B-Subunit [126]. Almost 50% of FXIII-B Subunit is found in non complexed free form in the plasma [132].

recombinant FXIII (rFXIII):

In all vertebrates investigated so far FXIII-A has been found to be expressed. Production of recombinant FXIII-A_2 (rFXIII-A_2) which is similar to cellular FXIII-A_2 was done in Escherichia coli [133], Saccharomyces cerevisiae [134,135], Schizosacharomyces pombe [136], tobacco plant cells and whole tobacco plants [137].

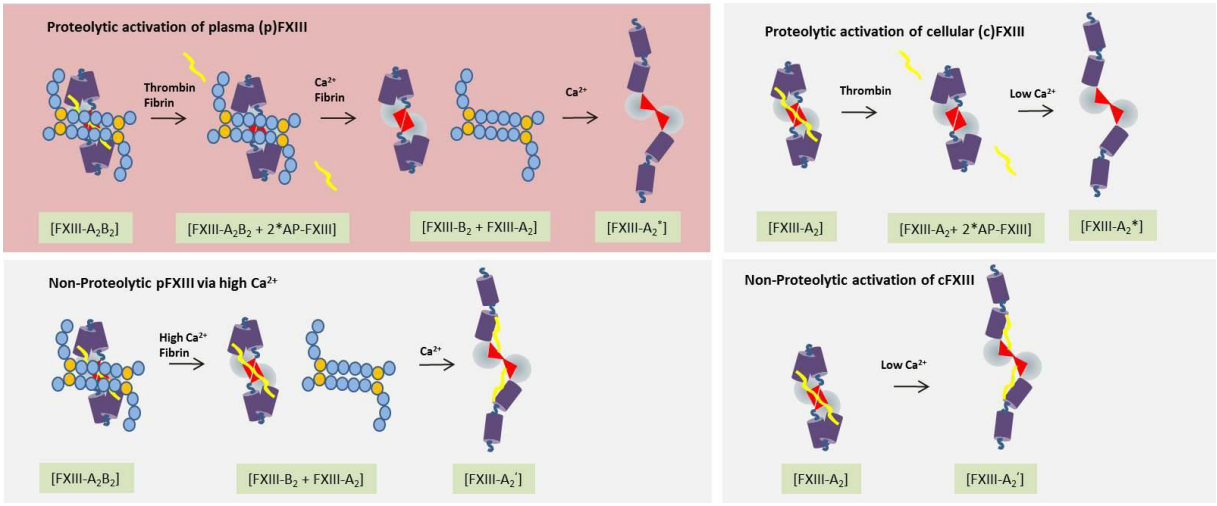

Figure 7: Proteolytic and non-proteolytic of cellular and plasma FXIII.

Activation of FXIII

There are two ways of activating Factor XIII: the proteolytic and the non-proteolytic activation [138].

Cellular FXIII: Non-proteolytic activation

Homodimeric cellular FXIII requires high Ca^{2+} concentration [138] for activation. The Ca^{2+} levels >50mM fully activates rFXIIIA [138]. The process is fully reversible and the enzyme can undergo a new activation round [99]. cFXIII can be activated with thrombin and Ca^{2+} like pFXIII in extracellular conditions [71], which is not the normal way of activation for cFXIII. Cleavage by Calpain, a Ca $^{2+}$ activated cysteine protease in platelets [139], was also detected for cFXIII.

Plasma FXIII: Heterotetramerformation and Proteolytic activation

In human plasma, $FXIIIA_2B_2$ circulates as a tight bound heterotetramer with a binding constant of 10^{-10} M [97] and an amount of 14-28 mg/l [116]. A minor fraction - approximately 1% of free non-complexed FXIII-A_2 - exist [97] next to ~50% free FXIII-B non-complexed form. pFXIII appears bound to fibrinogen (K_d~10^{-8} M) independent of

Ca^{2+} [140,141] and reaches its full functional active state only if Ca^{2+}, thrombin and fibrinogen are present [97]. For the heterotetramer formation, probably the first sushi domain is responsible for the binding of the FXIII-B to the FXIII-A subunit [97], while the fourth and ninth Sushi domain participate in the FXIII-B homodimer assembly. The other domains responsible for the heterotetramer assembly still remain unclear [97,98].

Proteolytic cleavage by thrombin of FXIII-AP is enhanced in the presence of fibrin [140]. Therefore, the FXIII-A_2B_2 is bound via FXIII-B_2 to non-cross-linked fibrin polymers on the γ-chain of the D-domain of fibrinogen in the plasma [107].The conformational change leads to the exposure of the catalytic triad. Thrombin cleaves off the 37th residue N-terminal AP-FXIII of FXIII-A_2 Subunit by hydrolysing the Arg37-Gly38 peptide bound only in the presence of Ca^{2+} and fibrin. The AP-FXIII dissociates from the molecule and appears in the plasma [142]. Plasma dimeric FXIII-A_2 reaches its full activity even if only one of the two activation peptides is cleaved off [143]. The proteolytic cleavage weakens the strong covalent binding between the two FXIII Subunits [68,144]. Upon high affinity Ca^{2+} binding to the A subunits, the B subunit dimer dissociates and the enzyme undergoes conformational change to an active conformation FXIII-A2* form [145,146]. Binding of Ca^{2+} ions on one of the A subunits is sufficient to dissociate the subunits and activate the released FXIII-A dimer [143,145]. This process finally leads to the exposure of the catalytic triad important to reach substrate access [56,147].

The FXIII-A_2 undergoes a remarkable strutural transition when converting from the zymogenic to its activated conformation. This involves the movement of the ß-barrel domains to reach the open active conformation [56] which is a very complex process and not fully understood up to now.

The process of FXIII activation is accelerated by Fibrin acting as a cofactor [148]. Important for the fibrin enhanced factor XIII activation are some surface residues of thrombin (His66, Tyr71 and Asn74) within exosite 1 which serves as a binding site for fibrin [149]. Another binding partner on these particular residues is thrombomodulin which serves as a cofactor-enhanced activator of protein C [150] but inhibits the fibrin enhanced factor XIII activation [149].

FXIII: Alternative activation

It has earlier been shown that next to Calcium activation both plasma and cellular FXIII also get cleaved by a human neutrophile elastase (HNE) which cleaves preferably valine and induces a limited cleavage of FXIII-A resulting in reaching 52.5% and 67.4% of thrombin-activated FXIII [151]. The preferable cleavage site for the HNE was identified in the middle of the flexible loop the V39-N40 as primary cleavage-site [151]. A few other proteases like Trypsin [64,152], batroxobin marajoensis [153], thrombocytin [154] and activated factor X [155] are also found to activate pFXIII in the presence of Ca^{2+} the potential cleavage sites are not identified yet. Only the mannan-binding lectin associated serine protease 1 (MASP1) which is involved in the complement system and possesses thrombin-like activity and cleaves FXIII-A at same position Arg37-Gly38 but slower [156].

Activated FXIIIa* cross-linking

The activated transglutaminase FXIII cross-links its substrates via an acyl transfer reaction in two steps [55,56,74]. Therefore it forms covalent ε-(-γ-glutamyl) lysine cross-links between the γ-carboxy-amine group of a glutamine (amine acceptor) and the ε-amino group of a lysine residue presenting the amine donor. The catalytic process of

protein cross-linking involves three main types of reactions the transamidation, esterification and hydrolysis [55].

FIRST STEP - ACYLATION

The reaction starts with the recognition of protein bound glutamine residues of the potential substrate (amine acceptor protein) and its catalysed thioester bond with the active site cysteine Cys314 of the $FXIIIA_2^*$. This is followed up by forming an oxyanion intermediate utilizing the side chain of Trp279 and the release of ammonia from the glutamine as the acyl-enzyme intermediate is formed [55,112].

SECOND STEP - DEACYLATION STEP

In the second part the created enzyme-glutamine substrate complex is bound to a primary amine (transamidation) which is a lysine ε-amino group of the second substrate, a polyamine or another primary amine [55,56,112]. Because the thioester intermediate is highly reactive there is rapid formation of the isopeptide bond. If a substrate primary amine group is present the acyl group is transferred to the acyl acceptor amine through a second oxyanion intermediate. The amine becomes attached to the γ-glutamyl residue via peptide bond (isopeptide) and the active-site cysteine becomes deacylated [157].

If there are no primary amines in the active-site pocket, the enzyme substrate complex will react with water (hydrolysis) releasing the enzyme and converting glutamine to glutamic acid. In the absence of a substrate amine deamidation of the substrate glutamine residue happens. If an ε-amino group of a peptide-bound lysine residue is the acyl acceptor primary amine for the reaction a ε(γglutamyl) lysyl is formed and the two peptide bonds become cross-linked [55,71,74].

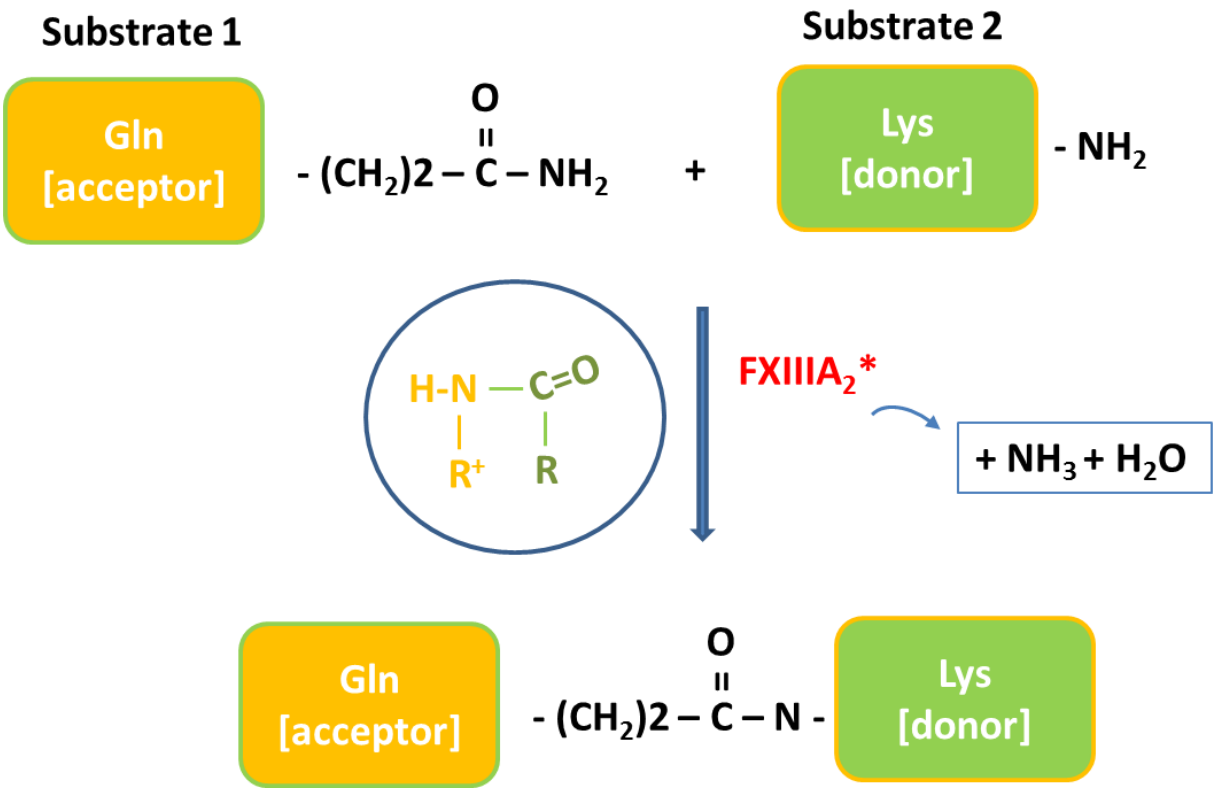

Figure 7: Cross-linking of two substrates by activated FXIII

Inhibition/inactivation of activated FXIII

Interestingly once cross linking of 40% of fibrin γ-chains occurs the effect of fibrin on FXIII-A_2 activation is lost giving fibrin cross-linking down regulation function for FXIII-A activation [1,140]. Additionally down regulation of activated factor XIII by polymorphonuclear granulocyte proteases [158] and recently discovered plasmin within the fibrin clot [159] was also observed. Another inhibitor is thrombomodulin which competitively decrease the effect of fibrin on factor XIII activation [160].

FXIII and its substrates

FXIII main substrate Fibrinogen/ Fibrin

Fibrinogen is an essential blood coagulation factor in the last step of the extrinsic blood coagulation pathway by building up the basic network of the blood clots to prevent blood loss and promote wound healing. It is the most abundant coagulation factor in the plasma reaching average concentration of 2-4mg/ml. The genes for the coagulation factor I FGA, FGB and FGG are clustered on chromosome 4q32.1 coding for the 3 chains Aα, Bß and γ which build up the molecule. The 340 kDa large glycoprotein FGG consists of six-chain $A\alpha_2$, $B\beta_2$- and γ_2 covalently bound by 29 disulfide bonds [161]. Two molecules build up the two outer D domains and one central E domain were the N-terminus of each chain coiled-coil contributes to constitute the central E domain [162,163]. The assembly of the trinodular structured molecule takes place in the endoplasmatic reticulum. The protein is finally secreted by hepatic parenchymal cells into the plasma. Synthesized Fibrinogen molecules are elongated 45 nm structures [162] which get converted during the clotting process to fibrin by serine protease thrombin cleavage of the two short N-terminal fibrinopeptides (FP)A and FPB from the Aα and Bß-chains on the central E domain [164]. After thrombin cleavage of the short fibrinopeptides A and B Fibrinogen converts into fibrin. Thrombin-mediated cleavage of fibrinogen initiates fibrin protofibril formation [164,165]. Polymerisation and formation of double stranded fibrin protofibrils and finally there lateral aggregation for fiber formation throught the αC interactions [166] is followed**.** Fibrin fibres branchpoints are formed by three fibers at a node leading to a trimolecular or tetramolecular joints strengthened by FXIIIa cross-linking [160]. Next to its role in branch-point formation FXIIIa is covalent cross-linking the fibrin aC-region

which increases the fibrin clot structure and support aC-aC interactions [167,168]. Therefore FXIII cross linking leads to reducing the space between the laterally protofibrils and leads to reduced average of fiber diameter [168].

FXIII and Fibrin

FXIII circulates bound to fibrinogen in the plasma showing a Kd of ~10^{-8} mol L^{-1} [140]. The presence of fibrin enhances the activation of pFXIII by ~100-fold [56,169]. FXIII-B Subunit binding to Fibrin gamma chain is important for the optimal orientation of pFXIII to thrombin for the proteolysis of FXIII-A [107,170]. A complex fibrin clot is created by lateral aggregation and formation of trimolecular and tetramolecular branch points connected by FXIIIa induced cross-links between fibrin γ- and α -chains [168]. The γ-dimer formation is more rapid intermolecular bond formation appearing in the first 5-10 min during clot formation between γ406 lysine of one γ-chain and γ398/399 glutamine residue of another –chain [168,170,171] performing first clot rigidity and maximum clot stiffness [172]. Cross-linking between α-chains glutamine and lysine residues appears with a slower rate [170] reaching better clot stability and rigidity by thicker fibers [160,167]. Less impact in fibrin fiber strength show γ-α-cross-links [173].

Different glutamine residues of the α –chain have been detected like Gln221, Gln237, Gln328 and Gln366 [170,173,174] and also a number of lysine donor sites Lys556, Lys539, Lys508, Lys580, Lys418, Lys448, Lys601, Lys606, Lys427, Lys429, Lys208, Lys224 and Lys219 which were detected by their ability to incorporate N-terminal peptide of α2-antiplasmin and other plasma proteins [173,175]. The combinations of Gln223 and Lys508 or Lys539, between Gln237 and Lys418, Lys508, Lys539 or Lys556, between Gln366 and Lys539, and between Gln563 and either Lys539 or Lys601 are cross-linking sites [176]. Next to γ-γ and α-α, smaller amounts of α-γ-chain heterodimers and γ-chain trimers and tetramers are also found in fibrin clots [157,177].

The cross-linking process increases the stiffness of the clot and reduces the network stretch of thrombus [168].

Next to its function in the blood clotting process, Fibrinogen is also known to be an acute phase protein which is why it is not surprising that fibrinogen disorders can lead to thrombotic problems as well [178].

Further substrates

FXIII is a highly pleiotrophic enzyme with a variety of substrates belonging to different body systems like blood coagulation, immune response (complement activation and inflammatory response), wound healing, cell adhesion, extracellular matrix organization (plasma proteins, bone and cartilage [179,180]), angiogenesis, proteolysis, adipogenesis [181] and pregnancy in females [182].

Next to the main primary substrates Fibrin and α_2-PI (α_2 plasmin inhibitor) 147 other substrates in plasma were recently detected [182] and 48 of these were confirmed to get incorporated into the fibrin clot [182] having functions like complement activation, inflammatory and immune response.

Twenty three of these substrates of FXIII are well characterized and listed already in the TRANSDAB database. These include several extracellular and intracellular proteins like myosin [183], actin [109], vinculin [184], filamin [185] fibronectin [174], vitronectin, collagen, Factor V [186], von Willebrand Factor [187], thrombospondin, PAI, and TAFI (thrombin activatable fibrinolysis inhibitor) which are well studied and play important roles in cytoskeletal remodelling during platelet adhesion, aggregation and contraction [117,188].

Consensus sequence

No consensus sequence has been identified yet for marking FXIII substrates. Only the glutamine and the surrounding hydrophobic residues seem to be important for substrate binding and recognition [173]. N-terminal to the reactive Gln residues on position 1 and 2 a higher frequency of acidic residues (Glu and Asp) was recently recognized [182] and for the position 4-12 a higher frequency of basic residues (Arg, Lys and His) was reported [182]. Reactive Gln residues can occur on a helix, strand or turn but for most of the proteins (61%) they are present on a loop [182].

Substrates influencing the blood clot structure

Formation of a stable and stiff thrombus involves apart from covalent fibrin dimer, the cross-linking of several other potential substrates like the glycoprotein Factor V (FV) [186,189] and thrombospondin-1 released by activated platelets [190] . These are found to be cross-linked to the fibrin α chain increasing the density of the fibrin clot [191]. Another glycoprotein Fibronectin is also cross-linked to the fibrin α-chain to produce a more dense clots with smaller pores [174] and has roles in cell adhesion, migration and tissue repair [192]. Collagen type I, II, III, V are found to be cross-linked by FXIIIa to fibronectin also playing an important role in thrombus formation and wound healing process [193]. Another substrate cross-linked by FXIII is the multimeric plasma glycoprotein vWF which is synthesized and stored in α-granules of platelets and endothelial weibel-palade bodies functioning as a carrier/ protector of Factor VIII from early degradation and functions in the early platelet adhesion to subendothelial collagen on injury-site [194,195].

Activation of Thrombus formation through platelets is mainly activated by collagen (type I and V) and thrombin [173]. COAT (collagen- and thrombin activated) platelet formation occur only in the presence of α granule secretion, exposure of

phospatidylserine, GPIIb/IIIa receptor activation and FXIII-A activation [173]. Next to the cross-linking of these secreted surface proteins from α granules (FV, vWF, fibrinogen, fibronectin, α2-antiplasmin and thrombospondin) [173] to fibrin, the transglutaminase additionally cross-links these proteins to serotonin [196,197]. These surface protein serotonin complexes are further cross-linked to fibrinogen and thrombospondin. Fibrinogen and FV are bound to the platelet GPIIb/IIIa receptor followed by thrombospondin binding. Finally the serotonin surface protein complexes are cross-linked via serotonin-binding sites to fibrinogen and thrombospondin performing a complex protein network [197].

Substrates influencing fibrinolysis of the clot

The cross-linking of fibrinolysis inhibitors is important for protecting the clot from plasmin-mediated lysis. Therefore further prolongation of lysis is achieved through cross-links between Gln^{2} within the α2-antiplasmin and the Lys^{303} of the fibrin α chain [198]. Modulation of clot lysis is found to be influenced by TAFI, vitronectin and α2-macroglobulin [173]. FXIIIa cross-links the pro-carboxypeptidase TAFI to fibrin through the reactive glutamine sites Gln^{2}, Gln^{5} located within the activation peptide of TAFI and also Gln^{292} [199] to Lys^{212}, Lys^{77} and Lys^{79} of the fibrin α chain [188]. These steps are necessary for localizing TAFI to the sites of thrombus formation [173]. Another fibrinolysis and proteolysis inhibitor of the preformed thrombus is PAI-2 (Plasmin activator inhibitor) which is cross-linked to fibrin α-chain [200,201] .

Vitronectin produced in megakaryocytes and platelets α-granules is found to form homodimers in the presence of FXIII [202]. Incorporation of vitronectin into fibrin clots is mediated by FXIII cross-linking [203] but the fibrin bound vitronectin also binds PAI and therefore prevent fibrinolysis [173,203]. The glycoprotein α_2-Macroglobulin, which is also a inhibitor of fibrinolysis [204] is another substrate of FXIII [173].

Substrates influencing the extracellular matrix formation

Myosin, Actin, Vinculin and Filamin are important cytoskeleton proteins functioning during clot retraction in the change of the plasma membrane shape in platelets to form filopodia. Stabilizing the platelet cytoskeleton proteins by cross-linking is an important factor for later clot retraction and fibrinogen binding to the platelets [183].

Platelet activation and aggregation is essential for binding cFXIII to platelet actin and its further translocation to the platelet periphery [185]. On the platelet periphery cFXIII is cross-linking next to actin other cytoskeleton proteins like vinculin and filamin to perform high-molecular complexes [109,184,185].

FXIII function in cross-linking of receptors

The angiotensin type 1 receptor (AT1R) is a G-protein-coupled receptor of the renin-angiotensinogen system functioning to regulate blood pressure [205]. Binding of its ligand AngII (AngiotensinII) and increased Ca^{2+} levels leads to dimerization and cFXIII promoted covalent cross-linking in the cytoplasmic tail domains of the receptor [206].

FXIII is also interacting with the vascular endothelial growth factor receptor 2 (VEGFR2) and the integrin $\alpha V\beta_3$ having pro-angiogenic function [207–209].

FXIII as a biomarker

Recently FXIII-A was detected as a novel prognostic marker for heart healing after acute myocardial infarction (MI) [210].

Higher expression of cFXIII-A in malignant monocytes is used as an intracellular marker for detection and differentiation of acute and chronic myelomonocytic and

monocytic leukemias from acute B cell leukemia were it is normally found to be absent in the lymphocytes and their precursors [211].

Immunohistochemical FXIII-A detection is used for diagnosis of dermatological pathologies like eczematous dermatitis, psoriasis or for example in aids associated cutaneous Kaposi´s sarcomas [212,213] or to differentiate macrophages from dendritic cells [214].

1.2 Part II: Clinical presentation of severe and mild FXIII deficiency

Clinical picture of the deficiency

Deficiency of Factor XIII leading to insufficient fibrin cross-linking with the consequence of late de novo bleeding occur with a frequency of 6 % from all rare bleeding disorders [215] . The FXIII bleeding diathesis is either acquired or inherited. Severe inherited FXIII deficiency is a rare bleeding disorder caused by homozygous or complex heterozygous mutations (both alleles affected) in *F13A1* or *F13B* genes and affecting one out of 2-4 million people [216]. Mild FXIII deficiency which is symptomatic only on provocation/trauma is a more frequent form (suspected prevalence: 1 out of 1000 in the German caucasian population) of inherited FXIII deficiency resulting from isolated (only one allele affected) heterozygous mutations in F13A1 or F13B genes [217].

Acquired FXIII deficiency

Acquired FXIII deficiency is mainly caused by hyperconsumption, hyposynthesises or rare by autoantibody development causing a more mild (plasma FXIII levels between 30-70%) up to severe phenotype (below 30%) [218]. Decreased production of FXIII-B (Hepatitis or acute liver failure) or increased consumption of FXIII subunits as cause of primary diseases like leukaemia, inflammatory bowel disease (crohn´s disease or ulcerative colitis), Henoch schoenlein purpura, systemic lupus erythematosus, disseminated intravascular coagulation, pulmonary embolism, liver disease, sepsis, stroke, surgery, trauma are related with more mild decrease requiring rarely replacement therapy [219,220]. Another reason for acquired FXIII deficiency next to primary diseases could also be the treatment itself like recently reported for patients suffering from rheumatoid arthritis treated with anti-interleukin-6-receptor monoclonal antibody (tocilizumab) resulting in impaired synthesis of FXIII-A and B-Subunit [221].

More severe is the development of autoantibodies (mostly IgG) [220] against FXIII-A (most) and FXIII-B (rare) subunits with neutralizing or non-neutralizing effect which was reported in 83 cases worldwide [218,222,223] mostly found in elderly patients around 70 years [223]. A third of cases having autoantibodies had systemic lupus erythematosus (SLE) as primary disease [24].

Inherited severe FXIII deficiency

Inherited severe FXIII deficiency is found more frequent in families with consanguineous marriages from South Asia especially in Middle Eastern countries like Iran/southwest Afghanistan and the Indian subcontinent [225,226]. People of all races and sexes are equally affected. Non consanguineous detected patients show a higher incidence for combined compound heterozygous mutations [25,227]. Congenital FXIII deficiency affecting 1 in 2 million [228] belonging to an autosomal recessive trait is associated with defects in both the FXIII-A and FXIII-B genes [25]. The severe form of the disease comes mostly from homozygous or compound heterozygous mutations were the mild form is related to heterozygous mutations.

Most of the missense mutations are found in the FXIII-A1 gene leading to a more severe phenotype then defects affecting the FXIII-B protein showing a moderate up to mild phenotype with reduced plasma levels of both subunits. FXIII-A deficient patients show a reduced total amount of FXIII-B in the plasma while the concentration of free B subunits remains constant. The inherited FXIII-A deficiency leads either to a quantitative Type I defect resulting in decreased unstable protein synthesis or to a qualitative (type II deficiency) functional defect with normal or mild decreased antigen levels but a dysfunctional protein. The type I deficiency lacks not only of the FXIII-A subunit in plasma, platelets and monocytes in females it's also missing in the placenta [229].

Homozygous FXIII deficiency

The severe congenital deficiency is characterized by critical life threatening bleeding events. Intracranial bleeding is the leading cause of death in FXIII deficiency. Congenital FXIII deficiency manifests itself immediately after birth in the form of umbilical stump bleeding that is detected in 80% of the cases [228]. This deficiency is characterized by a wide variety of bleeding phenotypes like epistaxis [226,230], subcutaneous bleeding, muscle haematoma, haemarthrosis, intracerebral bleeding (34%), mucosal tract bleeding mostly in the oral cavity (lips, tongue and gum) and intraperitoneal bleeding[231]. In women symptoms like menorrhagia and bleeding at the time of ovulation (20%), recurrent pregnancy loss are the common cause of habitual spontaneous abortion [227,228]. Lifelong bleeding tendency and abnormal wound healing (29%) probably caused by defective angiogenesis and fibrinolytic system are the result of a lack of FXIII-A protein [162].

Heterozygous FXIII deficiency

Mild FXIII deficiency has come to the fore only in the past few years, since this deficiency is difficult to detect owing to it's primarily asymptomatic phenotype. However the high risk of bleeding complication in case of a surgery or trauma in mild FXIII deficiency presents a realistic clinical danger. Additionally, the potentially high incidence of mild FXIII deficiency for the German population i.e. 1 out of 1000 individuals, implicates a high number of undiagnosed carriers that presents a clinical challenge to clinicians across the globe. Isolated heterozygous mutations act in a variable way on the FXIII enzyme activity and stability resulting in a wide range of phenotype from severe clinical symptoms up to an asymptomatic phenotype because of its pleiotropic nature [217,232]

Heterozygous deficiency is defined by FXIII activity levels between 30 – 60% that is considered enough to prevent spontaneous bleeding, but can cause a delayed bleeding diathesis in carriers when provoked. Some carriers show bleeding symptoms or wound healing problems in spite of nearly normal FXIII activity while others with lower FXIII activity are asymptomatic making this deficiency even more difficult to detect and phenotypically perplexing. Heterozygous Females suffer from menorrhagia, postpartum haemorrhage and face difficulties in *in vitro* fertilization if not treated with factor concentrates [26,233]. The functional impact of the heterozygous mutations are often explained by the the heterotetrameric nature of the FXIII protein. One allele carrying a mutation or polymorphism can influence the phenotype of the protein in a dominant/ semi-dominant manner if this mutation can impact the hetero-merization process negatively.

The range of FXIII activity of standard normal plasma pools is very high showing normal activity between 60-250% which is influenced by age, sex, smoker or non-smoker. Levels below 60% are observed in mild or severe FXIII deficiency. An associative classification was recently developed on the measured FXIII activity and clinical symptoms i.e.

1) Mild deficiency characterised through FXIII activity levels > 30% showing mostly an asymptomatic phenotype

2) Moderate deficiency with FXIII activity levels < 30% showing mild bleeding symptoms which can be provoked or spontaneous

3) Severe FXIII deficiency with undetectable FXIII activity is associated with severe spontaneous bleeding diathesis

Another study for the European Network of Rare Bleeding Disorders [231] classified bleeding of FXIII deficiency in three grades. Therefore grade 3 stands for spontaneous major bleeding like umbilical cord bleeding, gastrointestinal or intramuscular bleeds which they found for 48.5% of their patients. Only 6.1 % of patients showed minor spontaneous bleeding events like oral epistaxis, cavity bleeding or menorrhagia which is classified as grade 2. Grade 1 bleeding which appears after provocation like surgery, trauma or drug induced was also found in small minority of the patients (6,1%). The rest of the patients were asymptomatic 39,3% showing a mean activity level of 31 U/dl (10.83-51.31U/dl) [231].

Diagnosis

FXIII deficiency is hard to detect because normal standard global coagulation tests like the prothrombin time (PT) or activated partial thromboplastin time (aPTT) are not influenced by FXIII deficiency. Special specific tests are required to diagnose the FXIII deficiency. The qualitative clot solubility tests which is used since detection of the first FXIII deficiency case in 1960 but which unfortunately can only detect the severe FXIII deficiency can be only used if activity values are nearly zero [25].

Newly developed quantitative functional tests are used to determine the FXIII activity which is abnormal if the patient carry a defect in the FXIII-A subunit or the FXIII-A protein is non-functional. Therefore the chromogenic assay which determines FXIIIa activity indirectly by measuring ammonia (during a FXIII specific transglutaminase-NADH coupled reaction) release is used in most of the laboratories but is not accurate in the low ranges (activity below 20%) if compared with the incorporation assay which is more fitted to the natural function of FXIII. The incorporation assay is a functional test used to measure the FXIII activity through incorporation of a biotinylated amine substrate [5-(biotinamido) pentylamine] into fibrinogen which is

immobilized on a microtiter plate. Recalcification and the addition of thrombin serve to activate the zymogenic FXIII. The incorporated amine is labelled with a streptavidin-enzyme and coupled with an chromogenic substrate to detect the colour change or the amount of ammonia release is detected. Both detection methods are proportional to the transglutaminase reaction rate which indicates the activity.

To examine if the low activity is owing to A or B subunit deficiency the ELISA based measurement of FXIII-A_2, FXIII-B_2 or FXIIIA_2B_2 antigen is recommended. According to the ISTH joint SSC committee rules for the diagnosis of FXIII deficiency the standard protocol involves first to measure the FXIII activity. If FXIII activity is less an Elisa to detect antigen of FXIII heterotetramer has to be followed. Screening the lack of the individual subunits in order to identify the type of deficiency is the last step before genetic gene screening (*F13A1* or *F13B* genes) of the individual subunit can be done.

Treatment

FXIII deficiency whether congenital or acquired, needs next to a good detection system adequate and quick treatment because of the high risk for fatal bleeding diathesis in case of intracranial haemorrhage or massive joint bleeding. Primary prophylaxis (10-20 U/kg FXIII once per month) to prevent severe bleeding complications for FXIII deficient patients especially for patients with levels below 1 U/dL is recommended [250,251]. Factor replacement therapy is necessary for women suffering from congenital FXIII deficiency if pregnancy is a wish [26].

In general physicians follow the hypothesis that >10% of FXIII activity of the normal population is enough to prevent spontaneous severe bleeding episodes and therefore prophylaxis is not recommended. Still,10% of the patients with levels above 10% have a risk of cutaneous bleeding diathesis [250,251]. Provoked bleeding in case of

trauma or surgery might occur or pregnancy is planned and therefore higher levels of FXIII activity are needed.

Patients suffering of FXIII-A_2 deficiency are recently treated with recombinant FXIII-A_2 (rFXIII-A_2) which is produced in yeast *Saccharomyces cerevisiae* and therefore free of human or mammalian contamination originally developed by ZymoGenetics but recently aquired by Novo Nordisk (Novo Nordisk A/S, Copenhagen, Denmark) in 2004 [251,252]. In the best case the free rFXIII-A_2 binds in the plasma to the free FXIII-B_2 to form a heterotetramer showing half-life of approximately 10-14 days similar to native heterotetramer FXIII. rFXIII-A_2 is not suitable for Patients suffering from FXIII-B deficiency having short FXIII half-life times of because of lacking the B-Subunit [251,253].

rFXIII are a more safe and efficient option containing no human/ mammalian product then treating with plasma-derived sources of FXIII from fresh frozen plasma, cryoprecipitate or plasma-derived, virally inactivated FXIII concentrates which show a high risk for allergic reaction and infection (Hepatitis, HIV or other pathogens). No development of neutralizing alloantibodies or worse threatening complications came out in three trials detecting the pharmacokinetics of the product [54,253]. For bleeding prophylaxis of FXIII-A deficient patients a dosing of 35 IU/kg of rFXIII-A_2 independent of age and gender is suggested [54,251,253].

FXIII Mutation Profile and Protein misfolding

Mutations changing the amino acid sequence can lead to remarkable effects on protein stability. Several point mutations in genes coding for coagulation proteins have been found to reduce their stability and therefore their function [234]. The function of proteins is related to its stability which can be measured by the change in folding

energy i.e. ΔΔG of the protein structure [61,234]. Disease causing mutations destabilize the protein structure depending on the type of amino acid substitution, although some may also stabilize the protein structure [61]. Most of the missense mutations reported so far destabilize the protein and lead to loss of function because of protein instability.

Worldwide over 500 cases of severe FXIII deficiency have been reported since Webb et al. published in 1992 the first genetic mutation causing FXIII deficiency [86]. The majority of the mutations found to cause congenital severe FXIII deficiency are localized in the *F13A1* gene leading to a Type-I defect while the B subunit deficiency results mostly in a mild bleeding phenotype [235].

Only one well known polymorphism, the Val34Leu, has been reported from F13A1 gene which leads to a Type 2 FXIII deficiency i.e. impaired enzyme function in spite of normal antigen levels. This polymorphism (Val34Leu) in the activation peptide increases the activation rate of FXIII-A 3.2-fold faster [236] because of more efficient thrombin cleavage but leading to abnormal clot formation. The opposite effect was found for the peptide model rFXIII V34A variant located on the same position resulting in decreased activation rates [85,236,237]. Out of 200 patients from a pilot study in Bonn 23 novel heterozygous missense mutations (16 in the F13A1) and 7 in the *F13B* were detected in the mild form of FXIII deficiency. This suggested that in this form of FXIII deficiency a higher proportion of mutations existed in the FXIII B subunit gene [217,235,238,239].

Out of 112 reported mutations so far the majority (96 %) are located in the *F13A1* gene. Most of the mutations are of the missense type followed by splice site and deletions.

Polymorphism in the FXIII-A gene

Racial variations in the FXIII-A subunit gene have been listed for the Asian, Caucasians and African populations in the International HapMap project (**www.hapmap.org**). Out of 5 *F13A1* nucleotide variations, only the V34L (c.103G>T, rs5985) polymorphism was characterized and described further, especially in regard of the risk of coronary artery disease (CAD)[240,241]. The variant was found to have a protective effect against venous thromboembolism [242] and myocardial infarction [243] by increasing the rate of FXIII activation. The Leu34 allele was found to decrease the risk for CAD only in patients with an elevated fibrinogen concentration[241] followed by meta-analysis showing an overall protective effect against CAD [242,243].

Another polymorphism, Pro564Leu, leads to lower FXIIIA antigen levels but increased enzymatic activity, while Tyr204Phe was found to have low antigen levels as well as lowered activity leading to recurrent pregnancy loss [227,244]. Both the Pro654Leu as well as the Tyr204Phe polymorphism lead to a higher risk for nonfatal haemorrhagic stroke in young women (<45 years) [245].

Polymorphism of FXIII-B gene

Three major population-associated phenotypes were found to be characteristic for Europeans, Africans and Asian populations: FXIII-B*1, FXIII-B*2, FXIII-B*3. Board et al. was the first who reported a gene polymorphism of the *F13B* gene [246]. One of the polymorphism the FXIII-B*2 is a His95Arg transversion located within the exon 3 [247] which is the major allele among black Africans with 72.5% (International Hapmap

Project available online: http://hapmap.ncbi.nlm.nih.gov/ (accessed on 15 October 2014) but rare in white people (7,5%) and not found in Asien (International Hapmap Project). The polymorphism leads to a higher risk of venous thromboembolism [247] and an increased risk of mortality after cerebral ischemia of arterial origin [248,249]. Additional it was found to decrease the risk for nonfatal MI in postmenopausal women in case of homozygous expression [249].

Another polymorphism was detected in the intronic region of the B-subunit at the position of intron K nt29756 C>G (IVS11+144, rs12134960) and found frequently in the Asian population (International Hapmap Project). 14,2% of white population are carrier of this polymorphism and Africans don't show it at all (International Hapmap Project). The C to G exchange leads to a novel splice site acceptor site with a new splicing product exchanging the last 10 C-terminal located amino acids by 25 other amino acids. Therefore carriers show lower FXIII activity and lower antigen levels [241] with significant protection against coronary atherosclerosis (CAS) and myocardial infarction (MI) [241].

1.3 Part III: Objectives and thesis outline

Primary Objectives of this Thesis

1.) To heterologously express FXIIIB subunit missense mutations detected in patients with mild FXIII deficiency and study their effect on the B subunits antigenic stability and secretion phenotype in order to establish their causality.

2.) To model and simulate structures for the FXIIIB subunit sushi domains in order to predict the structural impact of FXIIIB subunit missense mutations and to correlate it with the expression data obtained from Objective 1.

3.) To heterologously express FXIIIA subunit missense mutations detected in patients with mild FXIII deficiency and study the expression phenotype in order to establish causality as well as the impact of these mutations on the different functional aspects of FXIII.

4.) To use *in silico* structural data from known crystal structures of FXIIIA subunit to understand the structural and functional correlations for the FXIIIA subunit missense mutations being expressed for Objective 3.

Thesis outline

This thesis outlines a study undertaken to develop a thorough understanding of the patho-molecular mechanisms underlying the functional impact of isolated heterozygous mutations that occur in the *F13A1* and *F13B* genes and result in mild FXIII deficiency. While the severe form of FXIII deficiency (FXIII activity < 1%) is an extremely rare event/disease, the mild or moderate form of this deficiency characterized by isolated heterozygous mutations in *F13A1* and *F13B* genes and

FXIII activity levels of 30 – 60% is believed to affect a significantly larger proportion of the general population. Mild FXIII deficiency is hard to detect because the patients are often asymptomatic unless they are exposed to some kind of a physical trauma. This is also the reason why in spite to its anticipated high frequency (1 out of 1000 in Germany = 80,000 potential carriers) it has not been reported in literature so far. In addition, there exists no strict correlation between bleeding symptoms and activity/ antigen levels making it difficult to develop a clinical definition for this deficiency. However, the fact that this deficiency is associated with a primarily asymptomatic phenotype does not make it clinically irrelevant. A large number of patients suffering from this deficiency are at a significant risk of bleeding when exposed to physical trauma especially in such situations involving hemorrhagic shock. Hemorrhagic shock presents a dangerous clinical situation involving severe trauma. It is associated with high mortality and morbidity since it leads to inadequate blood perfusion to vital organs and tissues. Such conditions are collectively known as trauma-hemorrhagic shock (THS) which might lead to insufficient microcirculation, tissue hypoxia and finally organ damage. These patients also develop severe coagulation related issues due to the transient loss of vital coagulation and fibrinolytic proteins because of sudden blood loss and/or consumption. Therefore the pre-identification of such individuals (i.e. who carry the mild FXIII deficiency) is of prime importance in order to be able to “prevent” blood loss in such conditions. Since phenotypically diagnosis of this deficiency is not easy, identifying genotypes that correspond to this disorder will go a long way in diagnosing this disease. Also since detection of a genotype in such a disorder which often does not show a clinical phenotype is not enough (since there is no way of knowing from the clinical data that the genotype is causal), the characterisation of mutations corresponding to these genotypes is very important.

On these grounds the purpose of this study was to characterize 23 missense variants that had been detected in the *F13A1* and *F13B* genes from patients with mild FXIII deficiency. These mutations had been detected and reported by Ivaskevicius and Biswas et. al. in a series of articles that have for the first time highlighted the concept of mild FXIII deficiency and its clinical relevance[235 239]. These articles had several unique observations, one of them being that mutations in the F13B gene occur proportionately at a higher rate in mild FXIII deficiency than that observed in its severe form. Therefore, a significant part of this thesis deals with characterizing the B subunit missense mutations i.e. the first two articles submitted as part of this cumulative thesis. The third and last article describes the analysis done for the A subunit mutations. All this analysis was performed using a combined *in vitro* and *in silico* approach.

The first publication that has been included in this thesis sheds light on the structure of the B subunit. The structure of the FXIIB subunit has not been resolved so far crystallographically or by NMR. However, this protein shares significant homology with certain proteins from the complement system like complement Factor H and like CFH is entirely comprised of repetitive predominantly beta sheeted sushi domains. Since sushi domains have a highly conserved (3+2 beta sheet interrupted by disordered variable length loops) core structure and high resolution structures of many sushi domains including that of CFH exist in the protein structure database, we adopted a homology modelling approach in order to generate protein models for the 10 sushi domains which form one monomer of the B subunit dimer. We used conserved structural disulphide bonded cysteines as guidepost residues in order to generate close spaced multiple alignments of template CFH sushi domain sequences and B subunit sushi domain sequences. Closer alignments were selected on the basis of a generated NJ (neighbourhood joining)-tree and fed into the Modeler

molecular modeling software to generate the models for the sushi domains. Later we analysed the structural positioning of the residues on which the 7 FXIIIB sububnit missense mutations had been reported, on these models. We found that many of these mutations were on residues that were surface exposed. However, the ones affecting the cysteines that are part of structural disulphide bonds were deep seated within the core of the sushi domains. In the same article we also expressed these 7 missense mutations in *HEK293t* cells and determined their intracellular and extracellular antigenic levels at different time points. We observed that all these 7 mutations showed different patterns of secretion.

This work was then followed up by work that is included in the next article (Publication 2) that is part of this thesis. In this article, we performed heterologous expression of the same 7 missense mutations but in heterozygous form (i.e. co-transfected with the wild type) in order to mimic their patient heterozygous status. We also performed confocal microscopy in order to determine if the differences in secretion pattern observed in the first article corresponded to a genuine secretion defect or not. Furthermore, we mixed expression products of these mutations with rFXIIIA (recombinant FXIIIA) subunit in order to study if these mutations influence the B subunit´s interaction with the A subunit. Structurally, we modelled these mutations on the sushi domain homology models generated, validated and published in the first article and simulated these domains in order to understand better the structural impact of these mutations. To summarize, from the second follow up article we could categorize these 7 mutations into ones that had a genuine secretion defect, ones that influenced interaction with the A subunit and the ones which had purely an affect on the antigenic stability.

In the third and last article from this cumulative thesis we have expressed and analysed 16 variants detected in the FXIIIA subunit gene (*F13A1*) in Cos-1 cell lines. Since the A subunit of FXIII is its catalytic part, the A subunit mutations expression phenotype had to analysed for several aspects. Therefore, apart from investigating the impact of these mutations on the antigenic stability and activity status, we analysed the expression phenotype for many other aspects like alpha-2-antiplasmin incorporation, non proteolytic activation, rate of activation and deactivation, rate of fibrin polymerization and clot thickness. In addition we also investigated the structural impact of these mutations by *in silico* modelling them on reported crystal structures of the zymogenic and activated forms of FXIIIA. The overall picture to emerge from this analysis was that mutations in the *F13A1* gene influence different aspects of FXIIIA subunit function and therefore can be categorized accordingly. These mutations could be categorized under those that influence thrombin cleavage of FXIIIA at the activation peptide region, influence incorporation of alpha-2-antiplasmin, and therefore affect alpha-2-antiplasmin/FXIII i.e. substrate enzyme interaction, influence rate of fibrin polymerization and therefore have an impact on FXIII/fibrinogen interaction, affect the rate of FXIII activation. Almost all mutations were found to finally influence clot thickness.

Chapter II: Publications

Publication 1

Published in *Human mutation* as a Research article

Title: *In vitro* secretion deficits are common among human coagulation factor XIII subunit B missense mutants: Correlations with patient phenotypes and molecular models

Authors: Arijit Biswas[1†], Anne Thomas[1†], Carville G. Bevans[2†], Vytautas Ivaskevicius[1], and Johannes Oldenburg[1]

[1]Institute of Experimental Haematology and Transfusion Medicine, University Clinic Bonn, 53105 Bonn, Germany;

[2]Im Hermeshain 6, 60388 Frankfurt am Main, Germany

[†]Equally contributing first author

Abstract

Coagulation factor XIII (FXIII) pro-enzyme circulates in plasma as a heterotetramer composed of two each of A and B subunits. Upon activation, the B subunits dissociate from the A subunit dimer which gains transglutaminase activity to cross-link preformed fibrin clots increasing mechanical strength and resistance to degradation. The B subunits are thought to possess a carrier/protective function prior to FXIII activation. Mutations in either A or B subunits are associated with pathological patient phenotypes characterized by mild to severe bleeding. *In vitro* expression of FXIII B subunit (FXIIIB) missense variants in HEK293T cells revealed impaired secretion for all seven variants studied. To investigate the likely molecular environments of the missense residues, we created molecular models of individual FXIIIB Sushi domains using phylogenetically similar complement factor H (CFH) Sushi domain structural templates. Assessment of the local molecular environments for the models suggested surface or buried positions for each mutant residue and possible pathological mechanisms. The *in vitro* expression system and *in silico* analytical methods and models we developed can be used to further investigate the molecular basis of FXIIIB mutation pathologies.

RESEARCH ARTICLE

Human Mutation

OFFICIAL JOURNAL
HGVS
HUMAN GENOME VARIATION SOCIETY
www.hgvs.org

In Vitro Secretion Deficits are Common Among Human Coagulation Factor XIII Subunit B Missense Mutants: Correlations with Patient Phenotypes and Molecular Models

Arijit Biswas,[1*†] Anne Thomas,[1†] Carville G. Bevans,[2†] Vytautas Ivaskevicius,[1] and Johannes Oldenburg[1*]

[1] *Institute of Experimental Haematology and Transfusion Medicine, University Clinic Bonn, Bonn, Germany;* [2] *Im Hermeshain, Frankfurt am Main, Germany*

Communicated by John McVey

Received 16 April 2013; accepted revised manuscript 18 July 2013.
Published online 2 August 2013 in Wiley Online Library (www.wiley.com/humanmutation). DOI: 10.1002/humu.22391

ABSTRACT: Coagulation factor XIII (FXIII) proenzyme circulates in plasma as a heterotetramer composed of two each of A and B subunits. Upon activation, the B subunits dissociate from the A subunit dimer, which gains transglutaminase activity to cross-link preformed fibrin clots increasing mechanical strength and resistance to degradation. The B subunits are thought to possess a carrier/protective function before FXIII activation. Mutations in either A or B subunits are associated with pathological patient phenotypes characterized by mild to severe bleeding. *In vitro* expression of FXIII B subunit (FXIIIB) missense variants in HEK293T cells revealed impaired secretion for all seven variants studied. To investigate the likely molecular environments of the missense residues, we created molecular models of individual FXIIIB Sushi domains using phylogenetically similar complement factor H Sushi domain structural templates. Assessment of the local molecular environments for the models suggested surface or buried positions for each mutant residue and possible pathological mechanisms. The *in vitro* expression system and *in silico* analytical methods and models we developed can be used to further investigate the molecular basis of FXIIIB mutation pathologies.
Hum Mutat 34:1490–1500, 2013. © 2013 Wiley Periodicals, Inc.

KEY WORDS: factor XIII deficiency; FXIIIB; *F13B*; homology modeling; expression analysis

Introduction

Coagulation factor XIII (FXIII) is a heterotetrameric protein complex composed of two A subunit (FXIIIA) and two B subunit (FXIIIB) homodimers encoded by separate *FXIIIA* and *FXIIIB* genes [Lorand et al., 1980]. FXIIIA is a transglutaminase enzyme responsible for covalently cross-linking fibrinogen and other proteins involved in regulation of clot maintenance and, subsequently, fibrinolysis during wound healing. Thus, it has a primary role in clot stabilization after the primary coagulation process is completed. Contrastingly, FXIIIB has no enzymatic activity and is thought to be a carrier protein that stabilizes FXIIIA dimers before activation in blood plasma, increasing their circulating half-life [Souri et al., 2008b]. Deficiencies in FXIII activity arise through two distinct pathological mechanisms. Acquired deficiencies are more common than inherited genetic deficiencies and are caused by either inhibitors (autoimmune antibodies) or systemic depletion of FXIII by chronic inflammatory conditions [Ichinose, 2011]. Inherited FXIII deficiency caused by *FXIIIA* (MIM #613225) or *FXIIIB* (MIM #613235) gene mutations is a rare condition, currently estimated to affect approximately one in six million individuals, for example, in the general German population. These mutations result in a broad spectrum of bleeding pathologies, usually only discovered incidentally in patients suffering traumas or undergoing surgical procedures [Peyvandi et al., 2012]. This suggests the number of undiagnosed patients may be much higher than previously believed [Biswas et al., 2011]. The broad implications for heritable FXIII deficiencies on patient health have been highlighted in the literature and notably include detrimental effects on wound healing (fibrinolysis) [Muszbek et al., 2008], complications following myocardial infarction [Nahrendorf et al., 2006a, 2006b], thrombosis risk [Muszbek et al., 2010], angiogenesis of significance to tumorigenesis and cancer [Dardik et al., 2005, 2006], and carrying pregnancy to term [Inbal and Muszbek, 2003; Muszbek et al., 2011; Palumbo et al., 2008; Vossen et al., 2011]. Until the 1980s, the research literature in the field predominantly comprised descriptive reports of homozygous *F13A1* (RefSeq NM_000129.3; MIM #134570) and *F13B* (RefSeq NM_001994.2; MIM #134580) mutations with associated severe patient pathological phenotypes [Biswas et al., 2011; Levy and Greenberg, 2012]. Recently, the Project on Consensus Definitions in Rare Bleeding Disorders suggested an associative classification of FXIII deficiency severity based on measured FXIII activity and clinical bleeding severity [Peyvandi et al., 2012]. Accordingly, FXIII deficiency is described by the following three-tier classification

Additional Supporting Information may be found in the online version of this article.

†These authors contributed equally to this work.

*Correspondence to: Arijit Biswas, Institute of Experimental Haematology and Transfusion Medicine, University Clinic Bonn, Sigmund Freud Str. 25, 53127 Bonn, Germany. E-mail: arijit.biswas@ukb.uni-bonn.de; Johannes Oldenburg, Institute of Experimental Haematology and Transfusion Medicine, University Clinic Bonn, Sigmund Freud Str. 25, 53127 Bonn, Germany. E-mail: johannes.oldenburg@ukb.uni-bonn.de

Contract grant sponsors: BONFOR(University of Bonn) to AB; Novonordisk to AB and JO.

Table 1. Tabular Overview of Reported FXIIIB Missense Mutations

cDNA	Protein	Literature reference
F13B:c.73T>C	FXIIIB:p.Cys5Arg	Ivaskevicius et al. (2010)
F13B:c.302T>A	FXIIIB:p.Ile81Asn	Ivaskevicius et al. (2010)
F13B:c.406C>T	FXIIIB:p.Leu116Phe	Ivaskevicius et al. (2010)
F13B:c.709G>A	FXIIIB:p.Val217Ile	Ivaskevicius et al. (2010)
F13B:c.1007G>T	FXIIIB:p.Cys316Phe	Ivaskevicius et al. (2010)
F13B:c.1262T>A	FXIIIB:p.Val401Glu	Ivaskevicius et al. (2010)
F13B:c.1342C>T	FXIIIB:p.Pro428Ser	Ivaskevicius et al. (2010)
F13B:c.1349G>T	FXIIIB:p.Cys430Phe	Hashiguchi et al. (1995)

Nucleotide numbering reflects cDNA numbering with +1 corresponding to the A of the ATG translation initiation codon in the reference sequence, according to journal guidelines (www.hgvs.org/mutnomen). The initiation codon is codon 1. All protein residue references are with regard to the processed prepropeptide, which begins with Glu1 corresponding to the 21st residue of the translated, unprocessed pre–pro sequence of FXIIIB.

system: (1) severe deficiency, undetectable FXIII activity associated with spontaneous major bleeding; (2) moderate deficiency, <30% FXIII activity associated with mild spontaneous or triggered bleeding; (3) mild deficiency, >30% FXIII activity associated with a mostly asymptomatic disease course. The majority of causative FXIII heterozygous or homozygous mutations affect the *F13A1* gene [Biswas et al., 2011], but seven different heterozygous *F13B* gene mutations were recently discovered that are associated with heritable mild FXIII deficiency [Ivaskevicius et al., 2010b]. Previously only five *FXIIIB* mutations, including only one missense mutation, were reported.

To date, there have been several expression-based analytical studies for mutations associated with severe FXIII deficiency [Balogh et al., 2000; Hettasch and Greenberg, 1994; Maeda et al., 2012; Mikkola et al., 1997; Vysokovsky et al., 2006; Wang et al., 2011; Zheng et al., 2011]. However, only one of these investigated a FXIIIB missense mutation that was at that time the only one known and that causes mild-to-moderate FXIII deficiency [Hashiguchi and Ichinose, 1995; Saito et al., 1990]. The current study investigates the molecular basis for moderate and mild FXIII deficiencies arising from seven additional FXIIIB missense mutations we previously identified in patients with reported clinical phenotypes (see Table 1 for a complete listing of known FXIIIB missense mutations) [Ivaskevicius et al., 2010b]. Specifically, we used a parallel strategy that included *in silico* comparative modeling of the human FXIIIB Sushi domains, in order to explore possible pathological mechanisms, and *in vitro* expression of the wild-type and mutant FXIIIB variants in HEK 293T cells to assess their intracellular expression and secretion levels.

Materials and Methods

Cloning and Site-Directed Mutagenesis

The human *FXIIIB* gene was cloned into the mammalian expression vector pEZ-MO1 (Genecopia, Rockville, MD, USA) according to the manufacturer's recommendations. Site-directed mutagenesis corresponding to the seven previously identified FXIIIB missense mutations (Table 1) was performed on the methylated pEZ-MO1-*FXIIIB* Vector using the Gene Tailor site directed mutagenesis kit (Invitrogen, Darmstadt, Germany) using primers shown in Supp. Table S1. Nucleotide numbering reflects cDNA numbering with +1 corresponding to the A of the ATG translation initiation codon in the reference sequence, according to journal guidelines (www.hgvs.org/mutnomen). The initiation codon is codon 1. All protein residue references are with regard to the processed prepropeptide, which begins with Glu1 corresponding to the 21st residue of the translated, unprocessed pre–pro sequence of FXIIIB.

Mutational Database Submissions

The eight previously reported *F13B* missense mutations have been registered with the Factor 13 Registry Database (http://www.f13-database.de/) and additionally updated to the Leiden Open Variation Database (LOVD version 2.0 Build 35; accessed on 11.06.2013 at http://www.lovd.nl/F13B).

Cell Culture, Transfection, and Protein Expression

FXIIIB variants were heterologously expressed in HEK 293T cells (DSMZ German Collection of Microoganisms and Cell Cultures, Braunschweig). The cells were cultured in 10 cm dishes with Dulbecco's Eagles Medium (DMEM Invitrogen) supplemented with 10% fetal bovine serum (Invitrogen), 1% penicillin–streptomycin (Invitrogen), and 0.1% Fungizone (Invitrogen) at 37°C in 5% CO_2. For transfection, 2.7×10^6 million cells were seeded into six-well plates with DMEM (with FBS) without supplements and transfected using Lipofectamin 2000 reagent (Invitrogen). Cotransfection of mutants was done at a 4:0.5 ratio with a pCMV-LacZ Vector (Clontech, Heidelberg, Germany) containing the *LacZ* gene for normalizing transfection efficiencies. All FXIIIB variant transfections were performed in triplicate ($n = 3$) for each of three separate HEK 293T cell passages ($N = 3$).

After 4 hr, incubation medium was changed and supernatants and lysed cells were collected after 12, 24, and 36 hr. The supernatants were centrifuged at 14,000*g* to remove cell debris. Collected cells were washed, lysed by incubation with 260 μl nondenaturing lysis buffer (native M-PER Mammalian Protein Extraction Reagent buffer; Thermo Scientific, Schwerte, Germany) containing 25 mM bicine, pH 7.6, supplemented with 0.1 mM PMSF for 10 min and centrifuged at 14,000*g* for 5 min at 4°C. Both supernatants and cell lysates were stored at −80°C for further analysis.

FXIIIB Antigen Quantitation

FXIIIB antigen was quantified for culture supernatants and cell lysates in cell lysis buffer using the Technozym FXIII-B:Ag Sub ELISA kit (Technoclone GmbH, Vienna, Austria) according to the manufacturer's instructions. Standard assay detection limit was 0.95 μg/ml; lower antigen concentrations to 0.009 μg/ml (sensitivity) were determined according to the manufacturer's dilution protocol. FXIIIB levels from normal pooled plasma and from high/low controls from the kit were measured as controls.

Normalization of Intracellular and Secreted FXIIIB Variant Levels for Transfection Efficiency

FXIIIB variant-transfected HEK 293T cells were cotransfected with a β-galactosidase encoding reporter vector in order to normalize transfection efficiencies among experiments. Equal aliquots of cells from triplicate wells for each time point and for three separate transfections of each FXIIIB variant ($n = 3$ replicates for each of $N = 3$ transfections on different cell passages, total nine samples) were pooled and frozen at −80°C for later evaluation of β-galactosidase expression by a standard colorimetric assay (Thermo Fisher Scientific, Schwerte, Germany) according to the

manufacturer's directions. The β-galactosidase levels for each of the FXIIIB variant transfections (Supp. Fig. S1) were divided by the wild-type FXIIIB-transfected β-galactosidase level to yield normalization constants for transfection efficiency. For each of three separate FXIIIB variant transfections ($N = 3$), the raw FXIIIB antigen concentrations were divided by the respective transfection efficiency normalization constants to yield the final normalized FXIIIB levels for both intracellular and secreted samples.

Comparison of Mean Intracellular and Secreted FXIIIB Variant Levels

From the intracellular FXIIIB variant expression and secretion levels presented in Figure 1, relative mean normalized FXIIIB levels for each of the mutant variants were calculated by dividing the mean for each triplicate of bars for the variant time points by the means of each triplicate of bars for the wild-type data. This yielded the equivalent fractional value of intracellular or secreted FXIIIB variant relative to the wild-type levels as shown in Figure 2 where a value of 1.0 at each time point represents the wild-type FXIIIB level.

Statistical Analysis

All transfections were repeated in triplicate ($n = 3$) for three different passages ($N = 3$) of the same cell line (i.e., yielding three independent mean ± SEM values; Fig. 1). Statistical differences in expression levels were analyzed using one-way ANOVA with Fisher's ad hoc post-test ($P < 0.05$ considered significant) using KaleidaGraph 4.1.3 (Synergy Software, Reading, PA, USA).

Modeling of FXIIIB Sushi Domains and Assessment of Predicted Local Protein Environments for FXIIIB Missense Mutations

High-quality homology models of the ten FXIIIB Sushi domains were constructed based on sequence similarity clustering with sequences for 13 available high-resolution Sushi domain structures for the human CFH protein (RefSeq NM_000186.3, Supp. Table S2). Template choices were determined by constructing a neighbor-joining (NJ) tree for individual FXIIIB and CFH Sushi domain sequences using the BLOSUM62 amino-acid substitution matrix (Supp. Fig. S2) [Henikoff and Henikoff, 1992; Saitou and Nei, 1987]. Accordingly, a protein multiple sequence alignment (MSA) for choosing optimal structural template/target pairs was created using a NJ algorithm implemented by MAFFT (L-INS-i option for small-scale accuracy-oriented alignment using a summation of a weighted sum-of-pairs score as objective function and all-to-all pairwise consistency scoring from local alignments) in the Jalview 2.7 java-based MSA editor implementing the Java Bioinfomatics Analysis Web Services system (JABAWS) [Katoh and Toh, 2008; Waterhouse et al., 2009]. The resulting MSA was refined by hand curation in order to achieve optimized close-spaced alignment (Supp. Fig. S3) (Supp. Methods). A phylogenetic NJ algorithm was used to sort the sequences into a relationship tree where sequences closest together share the highest sequence and structural homology. Thus, for any FXIIIB Sushi domain target sequence, the most appropriate structural template will correspond to the nearest CFH Sushi domain sequence in the tree (Supp. Fig. S2, cf. FH20, FXIIIB-S8 and FXIIIB-S10, for example). If the nearest CFH Sushi domain has no known solved structure, the next-nearest available structural template was chosen from the NJ tree (Table 2). In order to independently validate our NJ method choices for best target/template matches, we calculated% sequence identities using the European Bioinfomatics server implementation of ClustalW2 for all target/template sequence pairs (Table 2) [Goujon et al., 2010; Larkin et al., 2007]. Homology models were constructed using the Modeller 9v7 software package (Supp. Methods). Ten models were generated for each FXIIIB Sushi domain and the final model selected with the lowest value of the calculated MODELLER objective function. All-atom structure validation of final models (Table 3), as well as for five previously published FXIIIB Sushi domain models (Supp. Table S3) from Soares et al. (2005) for which the modeling template sequences are not available, was performed using the MolProbity server at http://molprobity.biochem.duke.edu/ [Chen et al., 2010]. Flipping of branched Asn, Gln, and His side-chain rotamers by 180° was performed when improvements in stereochemical parameters resulted for the FXIIIB Sushi domain models (Table 3) [Word et al., 1999]. Molecular model coordinate files for the FXIIIB Sushi domains were deposited in the Protein Modeling Database (http://mi.caspur.it/PMDB/) under accession numbers PM0078467 through PM0078476 [Castrignano et al., 2006]. Template appropriateness for 20 available models comprising 58 unique FXIIIB Sushi domains collected from public databases [ModBase (Pieper et al., 2011] and SWISS-MODEL Repository [Kiefer et al., 2009]) was evaluated as calculated% sequence identity for each aligned target/template sequence pair using ClustalW 2.0 as described above or as evaluated on the PSI Protein Model Portal at http://www.proteinmodelportal.org/query/uniprot/P05160 (accessed 22 October 2012; Supp. Table S4) [Arnold et al., 2009].

Results

Quantitation of Expression and Secretion for Wild-Type FXIIIB and Missense Mutations Causing FXIIIB Deficiency in Heterozygous Patients

We successfully expressed wild-type and seven FXIIIB missense variants, identified from our previously reported FXIII deficiency patient cohort [Ivaskevicius et al., 2010b], in HEK 293T cells and measured intracellular and secreted FXIIIB protein concentrations over 36 hr in 12 hr intervals (Fig. 1). In this *in vitro* system, intracellular and secreted levels of FXIIIB variants were highly reproducible at all time points for replicates ($n = 3$) of three separate transfections ($N = 3$) performed on different cell passages.

Although we observed significant differences among levels for only a minority (36 out of 144; 25%) of the repeated transfections ($P < 0.05$ for wild-type 24 hr I, 36 hr I&S; Cys5Arg 24 hr S; Ile81Asn 24 hr S, 36 hr I&S; Leu116Phe 36 hr S; Val217Ile 36 hr S; Cys316Phe 12 hr I, 24 hr I&S, 36 hr S; Val401Glu 24 hr S, 36 hr I; Pro428Ser 24 hr S, 36 hr I&S; I, intracellular; S, secreted), the intracellular or secreted levels for independent transfections in each group of three were significantly different ($P < 0.05$) from the levels at the neighboring time point(s) for all results (Fig. 1). This strongly suggests that results from our *in vitro* methods are statistically robust. With respect to intracellular protein levels at all time points, we found three distinct phenotypes: p.Cys5Arg (*F13Bc.73T>C*), p.Val217Ile (*F13Bc.709G>A*), and p.Cys316Phe (*F13Bc.1007G>T*) all exhibited lower than wild-type levels ($P < 0.05$); Leu116Phe (*F13Bc.406C>T*), Val401Glu (*F13Bc.1262T>A*), and Pro428Ser (*F13Bc.1342C>T*) all exhibited levels similar to wild-type ($P \geq 0.05$); Ile81Asn (*F13Bc.302T>A*)

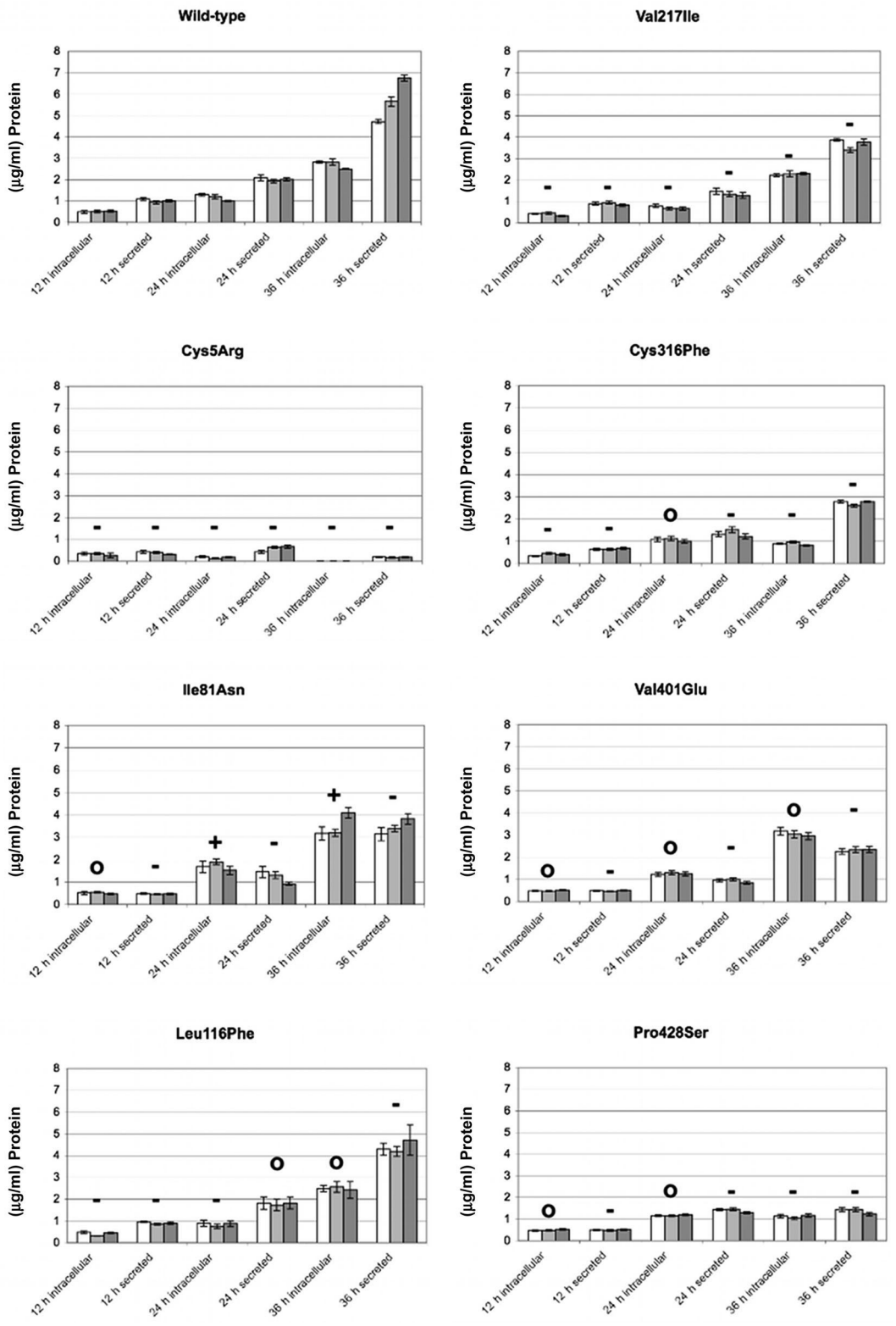

Figure 1. Time course of expressed and secreted levels of FXIIIB variants. For wild-type FXIIIB and seven missense mutation variants white, light gray, and dark gray bars represent results from three separate transfections on different cell passages ($N = 3$). Error bars represent ±standard error of the mean (±SEM) for triplicate parallel transfections of each variant ($n = 3$). Results indicated as 12, 24, 36 hr for 12, 24, 36 hr between transfection and separate harvesting of cells and culture supernatants, respectively. "Intracellular" results are for FXIIIB concentrations measured in cleared cell lysates (400 μl total volume); "secreted" results are for undiluted cell culture supernatants (2 ml total volume); all FXIIIB concentrations determined by ELISA assay (see *Materials and Methods* for details) and reported in units of μg/ml. Comparisons between results for wild-type FXIIIB and each missense variant are summarized by symbols appearing over the results bars: o, not significantly different; –, significantly lower variant concentration relative to wild-type; +, significantly greater variant concentration relative to wild-type (statistical significances determined by ANOVA with ad hoc Fisher's post-test; $P < 0.05$ was considered as significantly different).

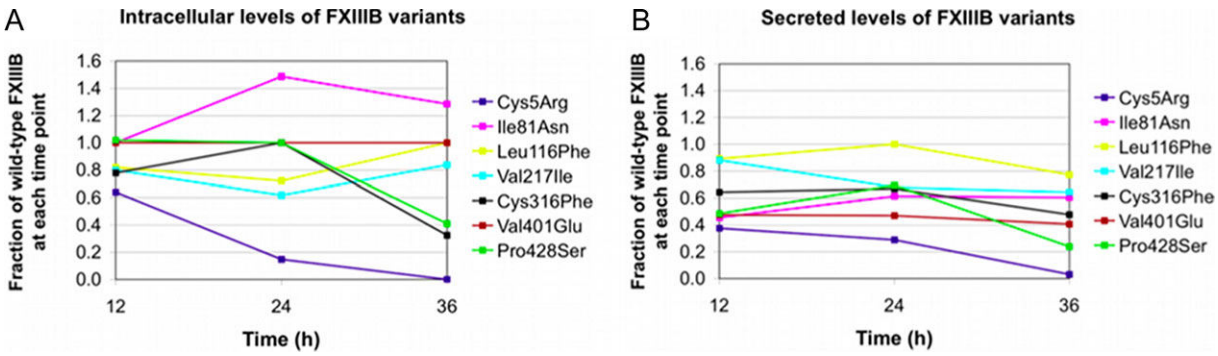

Figure 2. Fractional intracellular and secreted FXIIIB variant protein levels relative to wild-type levels for each time point. Panel A: Intracellular levels of FXIIIB variants expressed in HEK 293T cells at 12, 24, and 36 hr normalized for transfection efficiency by cotransfected LacZ reporter and normalized to intracellular wild-type FXIIIB mean expression level at each time point. Panel B: Secreted levels of FXIIIB variants expressed in HEK 293T cells at 12, 24, and 36 hr normalized for transfection efficiency by cotransfected LacZ reporter and normalized to wild-type FXIIIB mean secreted level at each time point. All values shown are means for three replicate measurements of each of three separate transfections using cells from different passages. A value of 1.0 on the ordinate axis represents intracellular or secreted levels equivalent to those for transfected wild-type FXIIIB.

Table 2. Choices of FXIIIB Sushi Domain Homology Modeling Template Structures from the NJ Tree in Supp. Figure S1

Target	Rank 1 template	Rank 2 template	Rank 3 template	Applied template	Resolution (Å)	Literature reference
FXIIIB-S1	FH8–2UWN	FH9	**FH6–2W81**	FH6–2W81	2.35	Schneider et al. (2009)
	32.3	28.6	**34.3**			
FXIIIB-S2	**FH8–2UWN**	FH9	FH6–2W81	FH8–2UWN	2.35	Prosser et al. (2007)
	40.0	25.4	26.2			
FXIIIB-S3	**FH8–2UWN**	FH9	FH6–2W81	FH8–2UWN	2.35	Prosser et al. (2007)
	34.8	30.2	22.7			
FXIIIB-S4	FH10	**FH3–2RLQ**	FH1–2RLP	FH3–2RLQ	Solution NMR	Hocking et al. (2008)
	29.2	**29.2**	24.6		lowest energy	
FXIIIB-S5	FH14	FH11	**FH19–3OXU**	FH19–3OXU	2.10	Morgan et al. (2011)
	39.4	31.3	**28.1**			
FXIIIB-S6	FH14	FH11	**FH19–3OXU**	FH19–3OXU	2.10	Morgan et al. (2011)
	34.8	29.9	**32.8**			
FXIIIB-S7	**FH19–3OXU**	FH11	FH14	FH19–3OXU	2.10	Morgan et al. (2011)
	42.2	32.8	34.4			
FXIIIB-S8	**FH20–3OXU**	FH2—2RLP	FH7–2W81	FH20–3OXU	2.10	Morgan et al. (2011)
	33.8	18.5	29.0			
FXIIIB-S9	**FH19–3OXU**	FH11	FH14	FH19–3OXU	2.10	Morgan et al. (2011)
	43.8	31.8	27.3			
FXIIIB-S10	**FH20–3OXU**	FH2–2RLP	FH7–2W81	FH20–3OXU	2.10	Morgan et al. (2011)
	36.8	16.9	21.0			

Symbol key: Under column "Target" FXIIIB-Sn (n = 1 through 10) indicates FXIIIB Sushi domain n; under columns "Rank 1 template," "Rank 2 template," "Rank 3 template," and "Applied template" FHn (n = 1 through 20) alone indicates factor H Sushi domain n for which no high-resolution structure has been reported, FHn-XXXX indicates factor H Sushi domain n for which the highest quality X-ray crystallographic or solution NMR structure is four-digit alphanumeric PDB entry number XXXX (see Table 2 for actual PDB entry numbers). Numbers below template ranking entries are % identity between target and template sequences as calculated using ClustalW2 on the EBI Web-based server (http://www.ebi.ac.uk/Tools/services/web/toolform.ebi?tool=clustalw2; accessed 14 October 2012). For template FH3–2RLQ the lowest energy NMR structure was chosen as modeling template from among the ensemble structures included in PDB entry 2RLQ.

exhibited significantly higher than wild-type levels ($P < 0.05$). Plotting the grande means for each variant at 12 hr shows that intracellular levels of all seven FXIIIB variants are in the range 60%–100% with respect to wild-type levels, but that variant intracellular levels achieved a broader range of 0%–130% with respect to wild-type levels by 36 hr (Fig. 2A). Notably, only for the Cys5Arg variant did the intracellular level appear to be consistent with protein production being a primary limiting factor associated with FXIIIB deficiency. However, secreted levels of all seven FXIIIB variants associated with FXIIIB deficiencies were significantly lower than wild-type secreted levels at all time points except for the Leu116Phe variant, which exhibited no significant difference from wild-type secretion at the intermediate 24 hr time point (Fig. 2B). By the 36 hr end point of the study, all mutant FXIIIB variants showed significantly lowered secretion ranging 0%–80% that of wild-type FXIIIB.

Modeling of Individual FXIIIB Sushi Domains for Assessment of Possible Underlying Molecular Mechanisms for the Seven FXIIIB Mutations of this Study

In order to explore possible structural correlates among the seven mutant FXIIIB variants that might suggest underlying pathological mechanisms, we produced high-quality homology models of the FXIIIB Sushi domains (Figs. 3 and 4). Accordingly, we identified appropriate modeling templates by a bioinformatics approach involving simultaneous alignment of 20 human CFH Sushi domain template sequences to the 10 FXIIIB Sushi domain target sequences, followed by calculation of a local-alignment NJ tree where the most appropriate target/template pairs lie closest to each other among the tree arborizations (Supp. Fig. S2). Because only 13 of the 20 CFH Sushi domains have solved high-resolution structures in the NCBI

Table 3. Validation Statistics Calculated Using the MolProbity Server for 10 FXIIIB Sushi Domain Models from the Present Study

FXIIIB subdomain	Goal value	S1	S2	S3	S4	S5	S6	S7	S8	S9	S10
Optimized side-chain flips	–	Q52	N11	H1, N11	N13, Q21, H34	N15, Q19	N17, N21	N13	N7, N12, Q38	–	N15, N24
Poor rotamers	<1%	4.84%	3.77%	**0%**	1.79%	**0%**	**0%**	**0%**	**0%**	**0%**	3.03%
Ramachandran outliers	<0.2%	**0%**	1.72%	1.72%	**0%**	1.82%	**0%**	**0%**	1.52%	**0%**	1.45%
Ramachandran favored	>98%	89.55%	93.10%	94.83%	**100%**	**98.18%**	**100%**	**100%**	95.45%	**100%**	94.20%
Cβ deviations >0.25Å	0	100%	1	2	1	**0**	**0**	**0**	1	**0**	**0**
Residues with bad bonds	0%	**0%**	**0%**	**0%**	**0%**	**0%**	**0%**	**0%**	**0%**	**0%**	**0%**
Residues with bad angles	<0.1%	**0%**	**0%**	1.67%	**0%**	1.69%	**0%**	**0%**	2.94%	**0%**	1.41%
Number of serious steric overlaps (>0.4 Å) per 1,000 atoms	0	139.75	125.27	104.64	116.35	40.57	14.69	15.12	144.81	31.22	138.84
Clash percentile	100%	0%	0%	30%	35%	8%	90%	90%	25%	77%	12%
MolProbity score	Lower is better	3.69	3.44	2.84	2.72	**2.09**	**1.67**	**1.68**	2.94	**1.98**	3.36

Symbol key: "Sn" (n = 1 through 10) indicates the modeled structure for FXIIIB Sushi domain n; "FHn XXXX" (n = 1–5, 7, 8, 12, 13, 15, 16, 19, 20) indicates an available solved, high-resolution structure for factor H Sushi domain n for which XXXX represents the PDB coordinate file used as structural template for homology modeling. Bold-face type indicates protein structural parameters meeting or exceeding X-ray crystallographic standards.

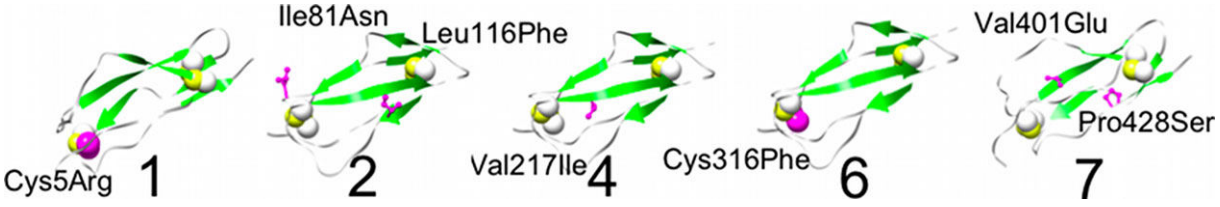

Figure 3. Homology models of five FXIIIB Sushi domains showing localization of seven FXIIIB mutations from this study. Numbers below each model indicate the FXIIIB Sushi domain identity. Models are represented as backbone ribbons with beta strands colored green (arrows pointing from N- to C-terminus), four cysteines in each domain shown as van der Waals space-filling balls (sulfur, yellow; carbon, white; hydrogen, not shown). Wild-type residue side-chains at positions of human mutations in this study are shown in magenta and labeled with the corresponding primary sequence number and amino-acid substitution.

Protein databank (PDB), for cases where the first-choice templates were not available, we chose 2nd or 3nd ranked modeling templates from the NJ tree and cross-validated the choices by calculating% sequence identities between the target/template pairs (Table 2). Overall, the target/template sequence identities were 28.1%–43.8% (mean 35.6%), all within the current de facto range for high-quality homology modeling [Vitkup et al., 2001]. Stereochemical parameter validation statistics assessed for the ten modeled FXIIIB Sushi domains are of similar quality to those for the 13 solved human factor H Sushi domain high-resolution structures (cf. Table 3 and Supp. Table S3). The 10 FXIIIB Sushi domains could be best modeled using just five different CFH template structures (Table 2, derived by nearest neighbor analysis of Supp. Fig. S2). Leu116Phe is the only substitution predicted to result in a surface-exposed change of residue side-chain, suggesting this mutation affects surface-mediated protein–protein interactions instead of formation and correct packing of the second FXIIIB Sushi domain fold (see structural and chemical properties summarized in Supp. Table S5; see also Fig. 4). For the six other missense variants, the respective side-chains are predicted to be buried in the respective Sushi domain fold, suggesting these mutations may affect protein folding and/or fold stability (Fig. 4).

Assessment of Previously Reported FXIIIB Sushi Domain Homology Models

We conducted literature and database surveys and found 63 previously reported FXIIIB Sushi domain models constructed by comparative/homology modeling methods (Table 3, Supp. Tables S2 and S3). Five of the 10 individual FXIIIB Sushi domains (S2, S5, and S6; Supp. Table S3) were previously modeled in an automated, high-throughput study [Soares et al., 2005]. At the time of that study, high-resolution structures were available for only three of the CFH Sushi domains and for a total of only 13 additional Sushi domain structures from more diverse proteins. Except for the three CFH Sushi domains, none of the template structures were from the Receptors of Complement Activation (RCA) gene cluster at chromosomal locus 1q32 that includes CFH and FXIIIB, suggesting a lack of appropriate modeling templates. The close proximity of the *CFH* gene to five *CFH*-like protein-encoding genes and *F13B* at this locus suggests that the respective genes may have arisen through multiple duplications, as has been reported for other Sushi domain proteins of the RCA cluster [Hourcade et al., 1990]. Additionally, Soares et al. (2005) previously presented sequence clustering results in support of this duplication hypothesis that further support our choice of CFH Sushi domain structures as FXIIIB modeling templates. However, because the original template structures and sequences are not available from this study, it was necessary to assess their model qualities by calculated stereochemical parameters from the MolProbity server instead of using % sequence identity as an objective measure of target/template choice compared with our models [Chen et al., 2010]. In all cases, the models from the present study are significantly superior by stereochemical measures (cf. Table 3 and Supp. Table S3).

Discussion

FXIIIB Subunit Missense Mutations

Two recent publications from our group describe investigation of heterozygous Factor XIII deficiency through a broad patient screening approach [Ivaskevicius et al., 2010a, 2010b]. Accordingly, *F13A1* and *F13B* genes were sequenced for a large group of patients with suspected FXIII deficiency operationally defined by a FXIII activity below the normal range of 65%–120% and/or a history of bleeding.

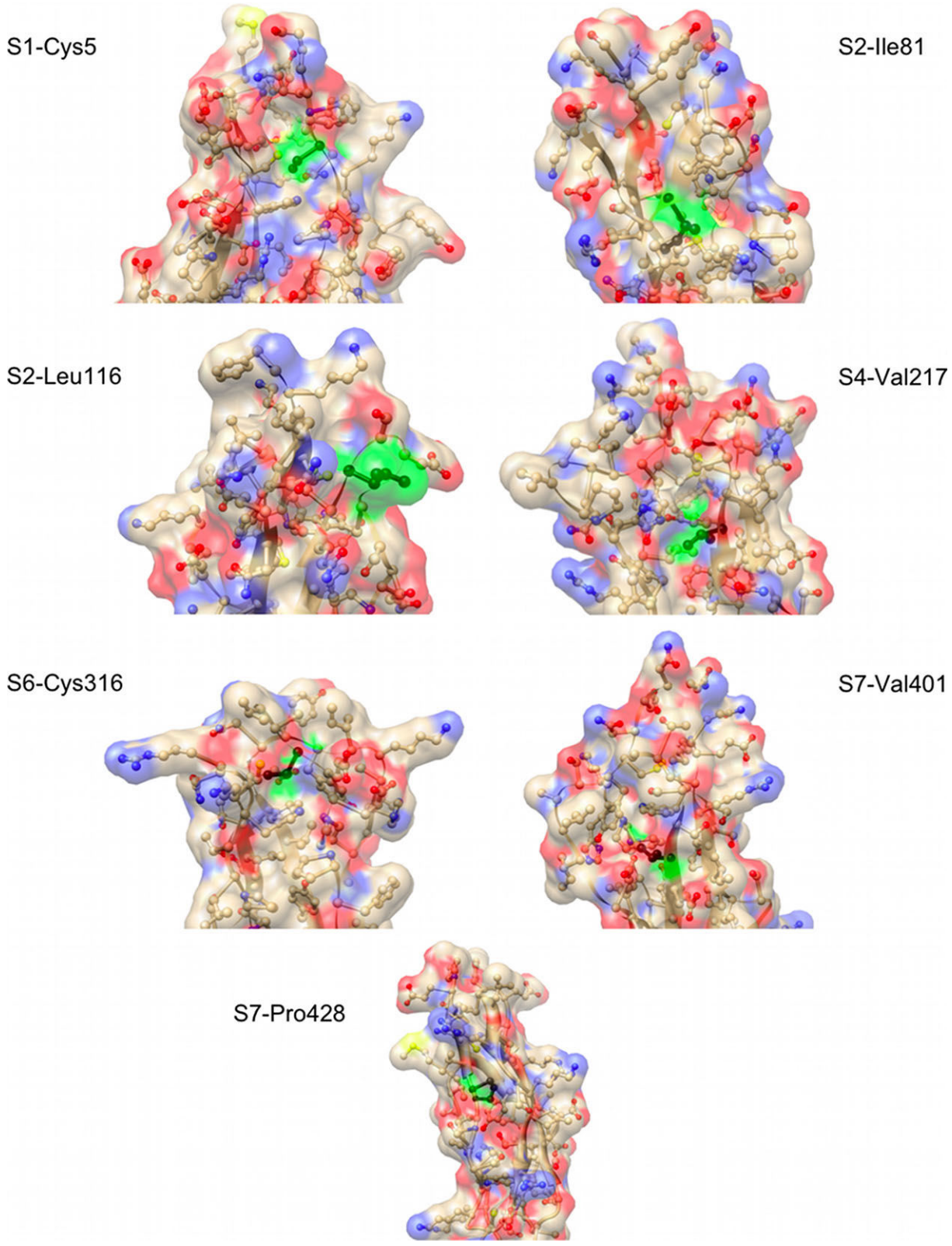

Figure 4. Detailed views of predicted local molecular environments surrounding the seven FXIIIB mutations from Sushi domain homology models generated in this study. Close-up, semi-transparent views of van der Waals space-filling models of homology modeled FXIIIB Sushi domains showing positions of known human missense mutations from the present study (green shading represents predicted solvent-accessible surface area for wild-type residues at mutation positions; Sushi domain number and wild-type residue identity and primary sequence number indicated for each model view). Calculated positive (blue) and negative (red) surface charges are shown. Atom coloring scheme for ball-and-stick backbone: tan, carbon; red, oxygen; blue, nitrogen; yellow, sulfur; hydrogens not shown; black, wild-type residue side-chain atoms at mutation positions. Model size scaling is same for all models except S7-Pro428, which is rendered at smaller scale in order to show a larger intramolecular environment adjacent to the mutation site.

We reported a surprisingly large number (25) of heterozygotes for FXIII deficiency among a pilot population of 150 patients selected for genetic analysis [Ivaskevicius et al., 2010a, 2010b]. Interestingly, mutational screening revealed seven novel FXIIIB missense mutations, which have been characterized in the present study (see Supp. Table S6 for patient phenotypes). To date, 53 FXIIIA and 20 FXIIIB nonsynonymous gene polymorphisms that result in single amino-acid substitutions have been described in the literature and indexed on the Factor XIII Registry Database (http://www.F13-database.de) [Biswas et al., 2011]. Of these, the majority are considered to be natural variants in various ethnic populations [Anwar and Miloszewski, 1999; Iwata et al., 2009; Komanasin et al., 2005]. However, only one missense mutation had been reported for FXIIIB associated with a severe FXIII deficiency [Ivaskevicius et al., 2010b; Saito et al., 1990]. An *in vitro* study found the FXIIIB:p.Cys430Phe (*F13B:c.1349G>T*) mutant protein was chiefly retained in the ER and not properly glycosylated, resulting in poor secretion compared with wild-type FXIIIB when expressed in BHK cells [Hashiguchi and Ichinose, 1995].

In Vitro Expression Time Courses of Mutations Highlight Secretion Deficits

In the present study, we characterized intracellular and secreted levels of the remaining seven mild FXIII deficiency-associated variants expressed in HEK 293T cells. Our results, when normalized for transfection efficiency differences using an exogenous β-galactosidase-encoding control vector (Supp. Fig. S1), showed lower than wild-type secretion levels for all seven variants at each of three time points (Figs. 1 and 2B—12, 24, and 36 hr). These results suggest a common underlying molecular mechanism for the corresponding patient phenotypes generally characterized as having mild measured deficits in plasma FXIII activity as well as in FXIIIA and FXIIIB antigen levels (Supp. Table S6). Concerning the only other *in vitro* study of a FXIIIB mutation, expression/secretion levels for the Cys430Phe mutant were reported only at 24 hr by Hashiguchi and Ichinose (1995). They concluded that reduced plasma level of the protective carrier subunit FXIIIB likely led to an overall reduction in the amount of FXIIIB-bound FXIIIA and considerably reduced FXIII activity and FXIIIA protein half-life in plasma [Hashiguchi and Ichinose, 1995]. Besides measuring *in vitro* secreted levels of FXIIIB variants from HEK 293T cells, we also measured the intracellular levels of these proteins at 12 hr intervals up to 36 hr. We identified three basic expression patterns for our system over the defined time course (Fig. 2A): (1) Ile81Asn and Val401Glu maintained or exceeded intracellular protein levels compared with wild-type FXIIIB over the entire time course; (2) Leu116Phe and Val217Ile were present at slightly attenuated intracellular levels, relative to wild-type FXIIIB, over the entire time course; (3) Cys5Arg, Cys316Phe, and Pro428Ser intracellular levels, compared with wild-type FXIIIB, were already considerably attenuated at 12 hr and fell significantly throughout the time course. The first expression pattern is consistent with initial accrual of wild-type levels of intracellular protein for Val401Glu, whereas Ile81Asn accrues at elevated levels, relative to that of wild-type, suggesting resistance to intracellular proteolysis and protein turnover. Interestingly, both substitutions are nonconservative, resulting in replacement of nonpolar residues by polar or charged ones. The second expression pattern is suggestive of upregulated intracellular turnover for the Leu116Phe and Val217Ile variants, both of which represent conservative, hydrophobic substitutions. The third expression pattern suggests a possible upregulation of the intracellular unfolded protein response (UPR) degradation pathways where conserved cysteine and proline residues are substituted. Conserved cysteines participate in disulfide cross-links that are invariant and well-characterized structural features buried in the cores of all Sushi domains [Schmidt et al., 2008], and proline is an amino acid that forms a unique structural kink in two highly conserved sites of all Sushi domains [Komaromi et al., 2011]. Notably, substitutions of both types of residues often result in structural instability and significant protein backbone rearrangement associated with UPR pathway upregulation. The Cys430Phe mutation previously studied by Hashiguchi and Ichinose (1995) and both the Val401Glu and Pro428Ser variants in the present study are located in the seventh Sushi domain. The in vivo phenotype for the female proband with compound heterozygous Cys430Phe/truncation variants of FXIIIB was no detectable protein in plasma for this variant, whereas the true heterozygous (wild-type/Cys430Phe) parents and children from the same family bearing this mutation exhibited 34%–52% FXIIIB wild-type levels. Taken together, these previous results suggest that low or no Cys430Phe variant is secreted into the plasma. These in vivo phenotypes are similar to those for Val401Glu and Pro428Ser where FXIII activities of 44%–48% of normal were reported (Supp. Table S6) [Ivaskevicius et al., 2010b]. Interestingly, the mean secretion level for the former was not significantly different from that of wild-type FXIIIB expressed in BHK cells (14.6 vs 34.6 $\mu g/10^7$ cells, mean 42% but $P = 0.21$) [Hashiguchi and Ichinose, 1995], whereas the secretion levels for the two Sushi domain 7 mutations from this study were significantly lower than wild-type FXIIIB when expressed in HEK 293T cells (Val401Glu 41%, Pro428Ser 24%; both $P < 0.0005$ compared with wild-type).

Generation of FXIIIB Subunit Sushi Domain Homology Models Based on Complement Factor H Sushi Domain Templates

Currently, no high-resolution structural data for FXIIIB exist. Therefore, in order to investigate molecular causalities for the seven FXIIIB mutations, we constructed high-quality homology models of the respective FXIIIB Sushi domains. Interestingly, the *F13B* and *CFH* genes are located in close proximity to each other at the Ch1q32 locus that is frequently referred to as the complement factor H (CFH) or regulators of compliment activation (RCA) gene cluster. At least 18 other genes encoding involved in the complement system are also encoded at this locus with five *CFH*-related genes (*CFHR1–CFHR5*) encoding proteins with multiple Sushi domains between *F13B* and *CFH* [Abrera-Abeleda et al., 2006]. The *CFHR* genes and splice-variants encode mature secretory proteins with four to nine Sushi domains exhibiting 32%–100% sequence identity with the CFH Sushi domains [Jozsi and Zipfel, 2008]. Interestingly, all of these complement proteins share similarity in structure and function to CFH Sushi domains 6–14 and 19–20 that include heparin binding, binding specificity to Complement receptor 3 (C3) subdomains as well as to C-reactive protein, binding to various pathogenic microbial surface proteins, and recognition and binding to anionic lipids and cell-surface glycosaminoglycans [Jozsi and Zipfel, 2008]. The genetic proximity of *F13B* in the RCA gene cluster, together with previously published experimental evidence that proteins encoded by the *CFHR* genes comprise Sushi domains that are involved in binding of some of the same physiological biomolecular targets as known to bind to CFH, suggests that FXIIIB might also possess similar binding modalities. For example, our primary sequence analysis indicates those FXIIIB Sushi domains S1 to S10 share significant sequence homologies to CFH Sushi domains 6, 8, 8, 3/10, 14, 14, 19, 20, 19, and 20, respectively

(Supp. Table S4). Based on these Sushi domain correspondences, FXIIIB S1–S3 appear to be homologous to the N-terminal Sushi domains of the CFHR proteins, suggesting functionally similar roles possibly including heparin binding as well as recognition and binding of bacterial, viral, fungal, and obligate parasitic pathogen surface proteins [Jozsi and Zipfel, 2008; Rodriguez de Cordoba et al., 2004; Zipfel et al., 2002]. Recently, experimental evidence implicated FXIIIB S1 and S2 in FXIIIB binding to the unactivated $FXIIIA_2$ dimer [Komaromi et al., 2011; Souri et al., 2008a]. FXIIIB S4-S6 bear homology to CFH Sushi domains 10 and 14 that are known to bind heparin, C reactive protein, sialic acid and Complement receptor 3 (C3) subdomains C3b and C3c [Hageman et al., 2005; Jozsi and Zipfel, 2008]. The four C-terminal FXIIIB Sushi domains (S7–S10) bear pronounced homology to CFH Sushi domains 19 and 20, suggesting functional similarities possibly including heparin and C3 binding, as well as cell surface recognition and binding of anionic lipids and glycosaminoglycans [Jozsi and Zipfel, 2008]. Interestingly, FXIIIB Sushi domains 4 and 9 were recently found to mediate $FXIIIB_2$ dimer formation in *in vitro* experiments [Souri et al., 2008a]. An exhaustive survey of literature and homology modeling databases revealed that five FXIIIB Sushi domains (S2, S5, S6, S7, S8; models available at http://www.bionmr.chem.ed.ac.uk/bionmr/public_html/ccp-models.html under accession number P05160) were modeled as a result of one study in 2005 aimed at creating 135 modeled Sushi domains and comparing surface features between these [Soares et al., 2005]. However, although an algorithm similar to our present NJ-tree method was developed and used for target/template matching, many of the 135 homology models are of low quality due to the automated, high through-put phylogenetic clustering analysis employed, and lack of suitable template structures. Interestingly, using this analysis, the authors resolved nine sequence-based clusters by a dynamic hidden Markov model algorithm, suggesting that their method found evidence for nine distinct Sushi domain structural clusters comprising ~70% from among an initial set of 243 unique Sushi domain sequences from 48, mostly human, Sushi domain proteins. However, only six of the nine clusters had associated high-resolution structural coordinate files in the NCBI Structure database. A further shortcoming of their method involved using a combination of ClustalX, an unweighted pair-group method using arithmetic averages (UPGMA) not intended for large MSA construction, resulting in large numbers of opened alignment gaps. As their alignment relied on only the four invariant Cys residues and one highly conserved Tyr residue as structural "guideposts" for MSA, the gaps created arbitrary target/template sequence alignment errors that propagated as structural errors built using Modeller. Our use of a larger number (13) of structurally conserved "guideposts" for alignment, together with post-alignment manual curation of the MSA to minimize opened gaps, yielded models of comparatively higher quality as assessed by both visual inspection and explicit calculation of protein stereochemical parameters. Although both studies used comparable state-of-the-art Modeller software for model building, we achieved an additional advantage in modeling accuracy due to our discrete treatment of only single Sushi domains. Database queries returned a total of 20 models of FXIIIB single and multiple (two to five) contiguous Sushi domain models comprising some 58 additional, unique single domain models (Supp. Table S4). Notably, when we calculated% sequence identity (%I) for the target/template pairs, we discovered a tendency for better target/template choices among the models with only one or two Sushi domains (Supp. Table S4). When we compared %I together with template choices between these models and ours, only four of the SWISS-MODEL generated models (Supp. Table S4, ID numbers 4, 5, 7, 8) had target/template pairs similar to those for our models. Specifically, ID numbers 4 and 5 are modeled on the same templates chosen by our method (ID4, FXIIIB S9-S10, and ID5, FXIIIB S7-S8, both modeled on CFH S19-S20), although the target/template sequence alignments were as or only slightly less optimal (average %I for both tandem Sushi domains S7-S8 and S9-S10 of 37%) as for our models (average %I of 38% for S7 and S8, 40.3% for S9 and S10) due to the automated alignment of the tandem Sushi domains and connecting linker sequence. Also, linked multi-Sushi domain templates tend to bias the geometry and spatial constraints of the final models due to the fact that the template structures often represent native bound protein–protein complexes that are likely not relevant to the biological structure and function of the targets. The automated SWISS-MODEL method also matched our target/template assignments for FXIIIB S1/CFH S6 (ID numbers 7 and 8, respectively), but resulted in the inferior choice of FXIIIB S2/CFH S7 compared with our FXIIIB S2/CFH S6 pairing. However, the 3rd (C-terminal) Sushi domain choice for ID8 (FXIIIB S3/CFH S8) again matched our best template choice, although both models suffer from template-imposed tertiary structural constraints and lack of target/template sequence alignment precision as for ID numbers 4 and 5. Other problems arising from the automated methods included partial structures due to short target or template sequences or misalignments (ID numbers 1, 2), inferior template choices (IDs 3 and 6–20—the majority of cases), overall low sequence identity (<25%) due to poor alignment, poor template choice, or both (IDs 11–20), and choice of non-Sushi domain template folds (C-terminal domains for IDs 19, 20).

Predicted Structural Implications of the Mutations

Since Sushi domains have a highly conserved protein backbone fold that comprises nearly equal numbers of amino acid residues that have either surface accessible or buried side chains, we thought it possible to ascertain if the positional locations of the mutations correlate with a negative impact on protein folding or stability due to structural mispacking (Figs. 3 and 4). Accordingly, we inspected our Sushi domain models to ascertain for each mutated residue the predicted position with respect to burial within the domain core or surface exposure, differences in possible hydrogen bonding between wild-type or mutant residues and neighboring residues, and differences in volume and formal charge with respect to wild-type and mutant residues at each position (Supp. Table S5). The Cys5Arg substitution ablates one of the two conserved disulfide bonds in Sushi domain 1, introduces a formal positive charge together with three possible hydrogen bond (H-bond) donor groups. Each of these effects would tend to disrupt the overall structural fold of Sushi domain 1. Experimental evidence has been reported that this domain is important for binding to the $FXIIIA_2$ dimer [Souri et al., 2008a]. The substitutions Ile81Asn and Val217Phe are considered to be semiconservative from a physicochemical point of view. However, molecular modeling analysis (Supp. Table S5) suggested that these substitutions occur within the cores of the corresponding folded Sushi domains 2 and 4, respectively. The second Sushi domain 2 substitution is Leu116Phe, conservative with respect to hydrophobicity, but nonconservative with respect to size. Notably, only Leu116 in Sushi domain 2 is predicted to be a surface exposed residue with its aliphatic side-chain fully solvent exposed. Sushi domain 2 has been reported to also interact with the $FXIIIA_2$ dimer [Komaromi et al., 2011]. All other mutant positions correspond to residues that are substantially buried in the cores of the respective

Sushi domains (Fig. 4). The fairly conservative substitution for the Val217Phe mutant may affect protein fold and packing for Sushi domain 4. Additionally, since Sushi domains 4 and 9 have been reported to interact in stabilizing the $FXIIIB_2$ dimer, this substitution might affect the surface portion of Sushi domain 4 responsible for binding Sushi domain 9 [Souri et al., 2008a]. The Cys316Phe substitution in Sushi domain 6 is expected to have a similar effect on domain fold and stability as the Cys5Arg substitution in Sushi domain 1, although any specific interaction of this domain with other FXIIIB or FXIIIA domains is currently unknown. The Val401Glu and Pro428Ser substitutions are both nonconservative and located in Sushi domain 7.

Functional Implications for FXIIIB Missense Mutations

There is experimental evidence that FXIIIB Sushi domains 1 and 2 are involved in binding to $FXIIIA_2$, so mutations in these two domains may affect FXIII tetramer formation and stability [Komanasin et al., 2005; Souri et al., 2008a]. Similarly, FXIIIB Sushi domains 4 and 9 have been shown to mediate FXIIIB dimerization, so mutations in these domains might affect formation and stability of FXIIIB dimers, thought to be in equilibrium with FXIII tetramers in plasma.

Interestingly, however, the His95Arg nondisease phenotype polymorphism reported in FXIIIB Sushi domain 2 confirms that missense mutations do not necessarily have detrimental effects on the properties of secreted FXIIIB variants, especially when the plasma levels are found to be normal [Iwata et al., 2009]. Contrastingly, a similar substitution in CFH Sushi domain 15 (His875Arg) is associated with defective secretion for the mutant allele [Dragon-Durey et al., 2004]. Furthermore, in all heterozygous CFH missense mutation patients to date for which CFH antigen was measured, the variant alleles apparently resulted in complete loss of secretion of the mutant CFH protein (35%–50% of normal CFH antigen levels) except for one case where secretion was found to be ~100%, but for which there was no measurable complement binding activity [Dragon-Durey et al., 2004]. Apparently, this single His to Arg substitution was sufficient to completely eliminate protein binding activity, in stark contrast to the apparent effect of FXIIIB:His95Arg, which is secreted at normal levels and apparently binds $FXIIIA_2$ normally with no apparent deficit for FXIII activity level [Iwata et al., 2009].

In conclusion, we have shown that FXIIIB missense mutations associated with patient mild bleeding tendencies exhibit a common *in vitro* secretion deficit when expressed in HEK 293T cells. This suggests that reduced in vivo FXIII activity might arise from either pathologically low circulating levels of FXIIIB, altered interaction with $FXIIIA_2$ to form FXIII tetramers with reduced stability, or both effects together. Additionally, we have developed molecular models of the 10 FXIIIB Sushi domains, based on phylogenetic sequence similarity to CFH Sushi domains with solved high-resolution structures, that will be useful in planning future hypothesis-driven investigation of FXIIIB structure/function relationships and molecular mechanisms underlying FXIIIB missense mutation pathologies.

Acknowledgments

The authors acknowledge technical and laboratory help from Zaid Aburubaiha and Sophie Lyonga.

Disclosure statement: The authors declare no conflict of interest.

References

Abrera-Abeleda MA, Nishimura C, Smith JL, Sethi S, McRae JL, Murphy BF, Silvestri G, Skerka C, Jozsi M, Zipfel PF, Hageman GS, Smith RJ, et al. 2006. Variations in the complement regulatory genes factor H (*CFH*) and factor H related 5 (*CFHR5*) are associated with membranoproliferative glomerulonephritis type II (dense deposit disease). J Med Genet 43(7):582–589.

Anwar R, Miloszewski KJ. 1999. Factor XIII deficiency. Br J Haematol 107(3):468–484.

Arnold K, Kiefer F, Kopp J, Battey JN, Podvinec M, Westbrook JD, Berman HM, Bordoli L, Schwede T. 2009. The protein model portal. J Struct Funct Genomics 10(1):1–8.

Balogh I, Szoke G, Karpati L, Wartiovaara U, Katona E, Komaromi I, Haramura G, Pfliegler G, Mikkola H, Muszbek L. 2000. Val34Leu polymorphism of plasma factor XIII: biochemistry and epidemiology in familial thrombophilia. Blood 96(7):2479–2486.

Biswas A, Ivaskevicius V, Seitz R, Thomas A, Oldenburg J. 2011. An update of the mutation profile of Factor 13 A and B genes. Blood Rev 25(5):193–204.

Castrignano T, De Meo PD, Cozzetto D, Talamo IG, Tramontano A. 2006. The PMDB protein model database. Nucleic Acids Res 34(Database issue):D306–D309.

Chen VB, Arendall WB, 3rd, Headd JJ, Keedy DA, Immormino RM, Kapral GJ, Murray LW, Richardson JS, Richardson DC. 2010. MolProbity: all-atom structure validation for macromolecular crystallography. Acta Crystallogr D Biol Crystallogr 66(Pt 1):12–21.

Dardik R, Loscalzo J, Eskaraev R, Inbal A. 2005. Molecular mechanisms underlying the proangiogenic effect of factor XIII. Arterioscler Thromb Vasc Biol 25(3):526–532.

Dardik R, Loscalzo J, Inbal A. 2006. Factor XIII (FXIII) and angiogenesis. J Thromb Haemost 4(1):19–25.

Dragon-Durey MA, Fremeaux-Bacchi V, Loirat C, Blouin J, Niaudet P, Deschenes G, Coppo P, Herman Fridman W, Weiss L. 2004. Heterozygous and homozygous factor h deficiencies associated with hemolytic uremic syndrome or membranoproliferative glomerulonephritis: report and genetic analysis of 16 cases. J Am Soc Nephrol 15(3):787–795.

Goujon M, McWilliam H, Li W, Valentin F, Squizzato S, Paern J, Lopez R. 2010. A new bioinformatics analysis tools framework at EMBL-EBI. Nucleic Acids Res 38(Web Server issue):W695–W699.

Hageman GS, Anderson DH, Johnson LV, Hancox LS, Taiber AJ, Hardisty LI, Hageman JL, Stockman HA, Borchardt JD, Gehrs KM, Smith RJ, Silvestri G, et al. 2005. A common haplotype in the complement regulatory gene factor H (*HF1*/*CFH*) predisposes individuals to age-related macular degeneration. Proc Natl Acad Sci USA 102(20):7227–7232.

Hashiguchi T, Ichinose A. 1995. Molecular and cellular basis of deficiency of the b subunit for factor XIII secondary to a Cys430-Phe mutation in the seventh Sushi domain. J Clin Invest 95(3):1002–1008.

Henikoff S, Henikoff JG. 1992. Amino acid substitution matrices from protein blocks. Proc Natl Acad Sci USA 89(22):10915–10919.

Hettasch JM, Greenberg CS. 1994. Analysis of the catalytic activity of human factor XIIIa by site-directed mutagenesis. J Biol Chem 269(45):28309–28313.

Hourcade D, Miesner DR, Bee C, Zeldes W, Atkinson JP. 1990. Duplication and divergence of the amino-terminal coding region of the complement receptor 1 (CR1) gene. An example of concerted (horizontal) evolution within a gene. J Biol Chem 265(2):974–980.

Ichinose A. 2011. Hemorrhagic acquired factor XIII (13) deficiency and acquired hemorrhaphilia 13 revisited. Semin Thromb Hemost 37(4):382–388.

Inbal A, Muszbek L. 2003. Coagulation factor deficiencies and pregnancy loss. Semin Thromb Hemost 29(2):171–174.

Ivaskevicius V, Biswas A, Bevans C, Schroeder V, Kohler HP, Rott H, Halimeh S, Petrides PE, Lenk H, Krause M, Miterski B, Harbrecht U, et al. 2010a. Identification of eight novel coagulation factor XIII subunit A mutations: implied consequences for structure and function. Haematologica 95(6):956–962.

Ivaskevicius V, Biswas A, Loreth R, Schroeder V, Ohlenforst S, Rott H, Krause M, Kohler HP, Scharrer I, Oldenburg J. 2010b. Mutations affecting disulphide bonds contribute to a fairly common prevalence of *F13B* gene defects: results of a genetic study in 14 families with factor XIII B deficiency. Haemophilia 16(4):675–682.

Iwata H, Kitano T, Umetsu K, Yuasa I, Yamazaki K, Kemkes-Matthes B, Ichinose A. 2009. Distinct C-terminus of the B subunit of factor XIII in a population-associated major phenotype: the first case of complete allele-specific alternative splicing products in the coagulation and fibrinolytic systems. J Thromb Haemost 7(7):1084–1091.

Jozsi M, Zipfel PF. 2008. Factor H family proteins and human diseases. Trends Immunol 29(8):380–387.

Katoh K, Toh H. 2008. Recent developments in the MAFFT multiple sequence alignment program. Brief Bioinform 9(4):286–298.

Kiefer F, Arnold K, Kunzli M, Bordoli L, Schwede T. 2009. The SWISS-MODEL repository and associated resources. Nucleic Acids Res 37(Database issue): D387–D392.

Komanasin N, Catto AJ, Futers TS, van Hylckama Vlieg A, Rosendaal FR, Ariens RA. 2005. A novel polymorphism in the factor XIII B-subunit (His95Arg): relationship to subunit dissociation and venous thrombosis. J Thromb Haemost 3(11):2487–2496.

Komaromi I, Bagoly Z, Muszbek L. 2011. Factor XIII: novel structural and functional aspects. J Thromb Haemost 9(1):9–20.
Larkin MA, Blackshields G, Brown NP, Chenna R, McGettigan PA, McWilliam H, Valentin F, Wallace IM, Wilm A, Lopez R, Thompson JD, Gibson TJ, et al. 2007. Clustal W and Clustal X version 2.0. Bioinformatics 23(21):2947–2948.
Levy JH, Greenberg C. 2012. Biology of Factor XIII and clinical manifestations of Factor XIII deficiency. Transfusion 53:1120–1131.
Lorand L, Losowsky MS, Miloszewski KJ. 1980. Human factor XIII: fibrin-stabilizing factor. Prog Hemost Thromb 5:245–290.
Maeda S, Zhang WG, Souri M, Yee VC, Ichinose A. 2012. Impaired dimer assembly and decreased stability of naturally recurring R260C mutant A subunit for coagulation factor XIII. J Biochem 152:471–478.
Mikkola H, Muszbek L, Haramura G, Hamalainen E, Jalanko A, Palotie A. 1997. Molecular mechanisms of mutations in factor XIII A-subunit deficiency: in vitro expression in COS-cells demonstrates intracellular degradation of the mutant proteins. Thromb Haemost 77(6):1068–1072.
Muszbek L, Bagoly Z, Bereczky Z, Katona E. 2008. The involvement of blood coagulation factor XIII in fibrinolysis and thrombosis. Cardiovasc Hematol Agents Med Chem 6(3):190–205.
Muszbek L, Bereczky Z, Bagoly Z, Komaromi I, Katona E. 2011. Factor XIII: a coagulation factor with multiple plasmatic and cellular functions. Physiol Rev 91(3):931–972.
Muszbek L, Bereczky Z, Bagoly Z, Shemirani AH, Katona E. 2010. Factor XIII and atherothrombotic diseases. Semin Thromb Hemost 36(1):18–33.
Nahrendorf M, Hu K, Frantz S, Jaffer FA, Tung CH, Hiller KH, Voll S, Nordbeck P, Sosnovik D, Gattenlohner S, Novikov M, Dickneite G, et al. 2006a. Factor XIII deficiency causes cardiac rupture, impairs wound healing, and aggravates cardiac remodeling in mice with myocardial infarction. Circulation 113(9):1196–202.
Nahrendorf M, Weissleder R, Ertl G. 2006b. Does FXIII deficiency impair wound healing after myocardial infarction? PLoS ONE 1:e48.
Palumbo JS, Barney KA, Blevins EA, Shaw MA, Mishra A, Flick MJ, Kombrinck KW, Talmage KE, Souri M, Ichinose A, Degen JL. 2008. Factor XIII transglutaminase supports hematogenous tumor cell metastasis through a mechanism dependent on natural killer cell function. J Thromb Haemost 6(5):812–819.
Peyvandi F, Di Michele D, Bolton-Maggs PHB, Lee CA, Tripodi A, Srivastava A, for the Project on Consensus Definitions in Rare Bleeeding Disorders of the Factor VFIXSaSCotISoTaH. 2012. Classification of rare bleeding disorders (RBDs) based on the association between coagulant factor activity and clinical bleeding severity. J Thromb Haemost 10(9):1938–1943.
Pieper U, Webb BM, Barkan DT, Schneidman-Duhovny D, Schlessinger A, Braberg H, Yang Z, Meng EC, Pettersen EF, Huang CC, Datta RS, Sampathkumar P, et al. 2011. ModBase, a database of annotated comparative protein structure models, and associated resources. Nucleic Acids Res 39(Database issue):D465–D474.
Rodriguez de Cordoba S, Esparza-Gordillo J, Goicoechea de Jorge E, Lopez-Trascasa M, Sanchez-Corral P. 2004. The human complement factor H: functional roles, genetic variations and disease associations. Mol Immunol 41(4):355–367.
Saito M, Asakura H, Yoshida T, Ito K, Okafuji K, Yoshida T, Matsuda T. 1990. A familial factor XIII subunit B deficiency. Br J Haematol 74(3):290–294.
Saitou N, Nei M. 1987. The neighbor-joining method: a new method for reconstructing phylogenetic trees. Mol Biol Evol 4(4):406–425.
Schmidt CQ, Herbert AP, Hocking HG, Uhrin D, Barlow PN. 2008. Translational mini-review series on complement factor H: structural and functional correlations for factor H. Clin Exp Immunol 151(1):14–24.
Soares DC, Gerloff DL, Syme NR, Coulson AF, Parkinson J, Barlow PN. 2005. Large-scale modelling as a route to multiple surface comparisons of the CCP module family. Protein Eng Des Sel 18(8):379–388.
Souri M, Kaetsu H, Ichinose A. 2008a. Sushi domains in the B subunit of factor XIII responsible for oligomer assembly. Biochemistry 47(33):8656–8664.
Souri M, Koseki-Kuno S, Takeda N, Degen JL, Ichinose A. 2008b. Administration of factor XIII B subunit increased plasma factor XIII A subunit levels in factor XIII B subunit knock-out mice. Int J Hematol 87(1):60–68.
Vitkup D, Melamud E, Moult J, Sander C. 2001. Completeness in structural genomics. Nat Struct Biol 8(6):559–566.
Vossen CY, Hoffmeister M, Chang-Claude JC, Rosendaal FR, Brenner H. 2011. Clotting factor gene polymorphisms and colorectal cancer risk. J Clin Oncol 29(13):1722–1727.
Vysokovsky A, Rosenberg N, Dardik R, Seligsohn U, Inbal A. 2006. Effect of four missense mutations in the factor XIII A-subunit gene on protein stability: studies with recombinant proteins. Blood Coagul Fibrinolysis 17(2):125–130.
Wang W, Huang L, Ma Q, Xiao D, Chen X, Yang Z, Wang X, Zhou K, Li G, Xiao M, Du G, Hao X, et al. 2011. Homozygous intronic mutation leading to inefficient transcription combined with a novel frameshift mutation in *F13A1* gene causes FXIII deficiency. J Hum Genet 56(6):460–463.
Waterhouse AM, Procter JB, Martin DM, Clamp M, Barton GJ. 2009. Jalview Version 2—a multiple sequence alignment editor and analysis workbench. Bioinformatics 25(9):1189–1191.
Word JM, Lovell SC, Richardson JS, Richardson DC. 1999. Asparagine and glutamine: using hydrogen atom contacts in the choice of side-chain amide orientation. J Mol Biol 285(4):1735–1747.
Zheng WD, Liu YH, Luo Y, Yao ZB. 2011. Molecular mechanisms of Arg77Cys missence mutation and Arg174stop nonsense mutation of factor XIII A gene causing severe factor XIII deficiency. Zhongguo Shi Yan Xue Ye Xue Za Zhi 19(6): 1456–1461.
Zipfel PF, Skerka C, Hellwage J, Jokiranta ST, Meri S, Brade V, Kraiczy P, Noris M, Remuzzi G. 2002. Factor H family proteins: on complement, microbes and human diseases. Biochem Soc Trans 30(Pt 6):971–978.

Supp. Methods

FXIIIB sequences for modeling

For these sequences, the naturally occurring proximal and distal linkers were truncated to just after the C-terminal cysteine of the preceding Sushi domain and just before the N-terminal cysteine of the following Sushi domain.

MSA construction details

By hand curation, the number of columns containing opened gaps was minimized, while maintaining alignment of 13 highly conserved structural "guidepost" residues including four cysteines, three glycines, three aromatics (phenylalanines or tyrosines), two prolines and one tryptophan (Supp. Figure S3, astrices below sequences indicate guidepost residues in panel B). Where guidepost residues were absent in specific sequences, the positions of variant residues at the corresponding guidepost positions was contextually determined by adjacent residue conservation among all sequences. Notably, the aim of this type of MSA refinement is alternative to the aim of usual methods that are intended for building phylogenetic trees using inference models accurately reflecting evolutionary processes. The chief aim of a close-spaced MSA is to optimally align conserved structural "guidepost" residues that define conserved topological features of the protein domain fold. Accordingly, variable sequence stretches, which often represent solvent-accessible surface regions and variable-sized loops, are allowed to span and define clusters of multicolumn gaps in the MSA. Thus, opening as few gaps (clusters) as possible is a primary driving principle in constructing a useful close-spaced MSA for successful structural alignment of target and template sequences (Supp. Figure S3).

Set-up for Modeller files

Input files included pairwise alignments of target and template sequences in PIR format and PDB-format atomic coordinate files for the following template structures: CFH Sushi domain 6 (FH6) from PDB entry 2W81(2.35 Å resolution)(Schneider, et al., 2009), FH8 from 2UWM(2.35 Å) (Prosser, et al., 2007), FH3 from 2RLQ(lowest energy structure of 29 solution NMR models)(Hocking, et al., 2008), FH19 and FH20 from 3OXU()(Morgan, et al., 2011). Calculated stereochemical validation measures for 13 CFH Sushi domains with solved high-resolution structures are given in Supp. Table S2. The single solution NMR template (2RLQ) used for modeling FXIIIB Sushi domain 4 in this study has stereochemical parameters that are comparable in quality to those of the X-ray structures used as templates. Individual CFH Sushi domain template files were created by manual editing/truncating the available PDB files for multiple Sushi domain structures and residues were renumbered using the pdbset command of the standard CCP4 macromolecular crystallography package (Evans, 1992; Winn, et al., 2011).

We refrained from further model optimization as it is not currently general practise to refine homology models when detailed experimental intramolecular structural constraints are not available (Punta, et al., 2007).

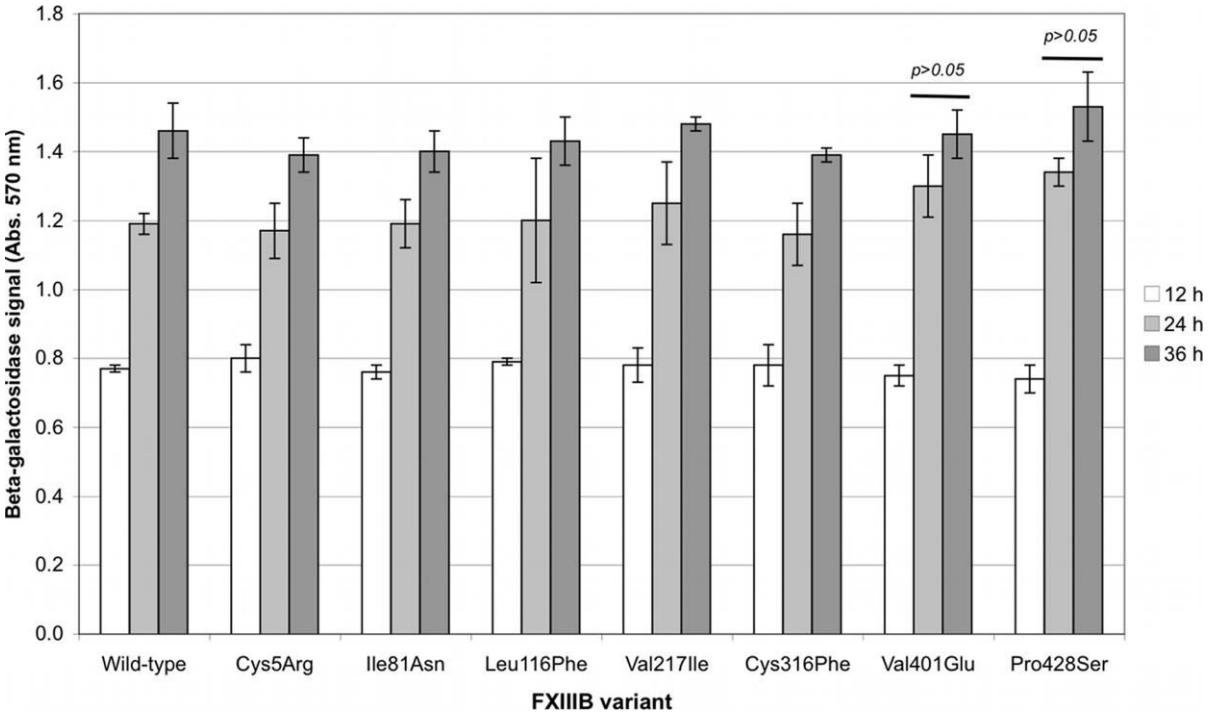

Supp. Figure S1. Measured LacZ reporter values for transfection normalization. Pooled data for cotransfected *LacZ* gene assessed as expressed beta-galactosidase. A *LacZ*-encoding vector was mixed with FXIIIB variant vectors at a constant proportion for measuring transfection efficiency. Mean values and error bars are for pooled equal volume aliquots of cell lysates for n=9 samples (*i.e.*, triplicates of each of three separate transfections) for each FXIIIB variant and time point. ANOVA analysis with *ad hoc* Fisher's post-test revealed that mean values are not significantly different across all FXIIIB variant transfections at each of the three time points (*i.e.*, comparing across all bars of the same color shading). Also, for each FXIIIB variant, there is significant difference ($p<0.05$) between each time point except for Val401Glu and Pro428Ser transfections measured at 24 h and 36 h (indicated as horizontal lines above bars).

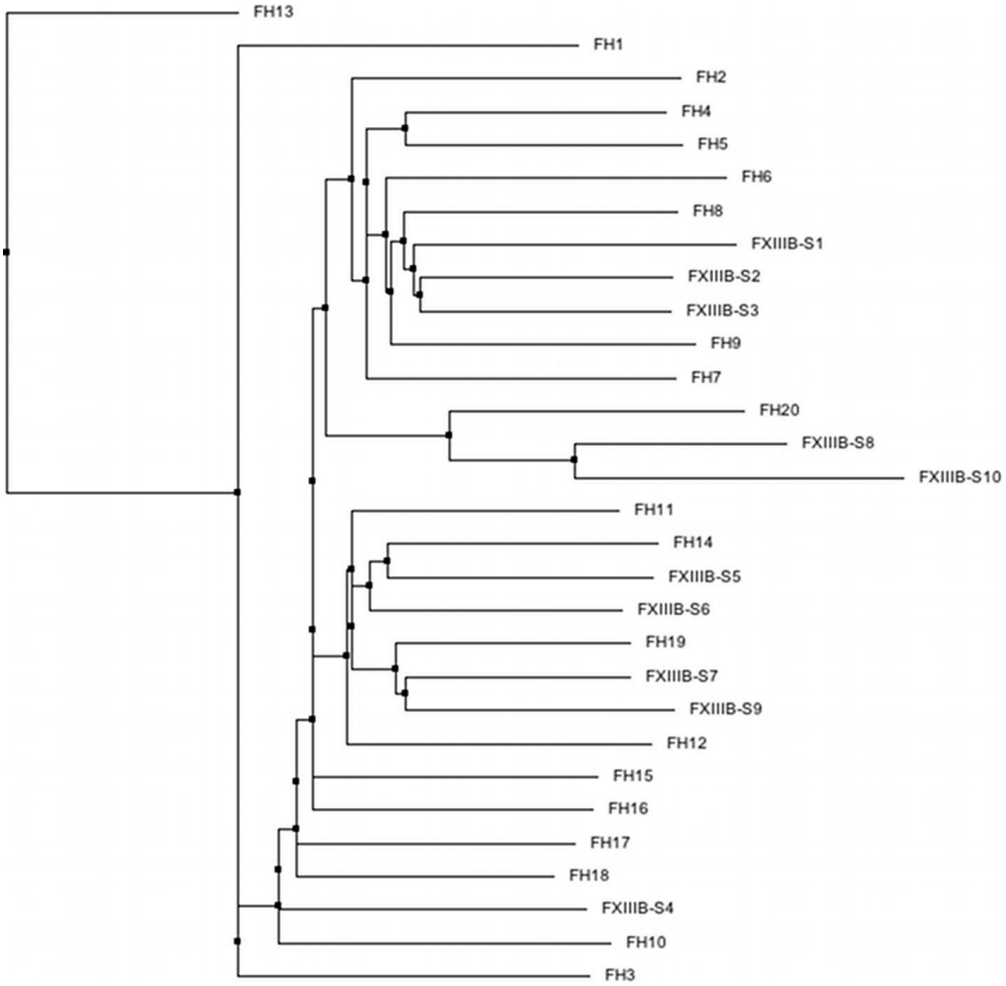

Supp. Figure S2. Neighbor-joining tree from close-spaced MSA of FXIIIB and CFH Sushi domain sequences. Symbol key: FHn (n=1 through 20) are template factor H Sushi domain sequences 1 through 20; FXIIIB-n (n=1 though 10) are target FXIIIB Sushi domain sequences 1 through 10. Appropriate CFH Sushi domains for structural modeling templates are located topologically nearest to the FXIIIB Sushi domain target sequences; *e.g.*, FH20 (13^{th} branch from top of tree) is the best template structure for modeling both FXIIIB-S8 and FXIIIB-S10 which lie adjacent on the two next lower branches.

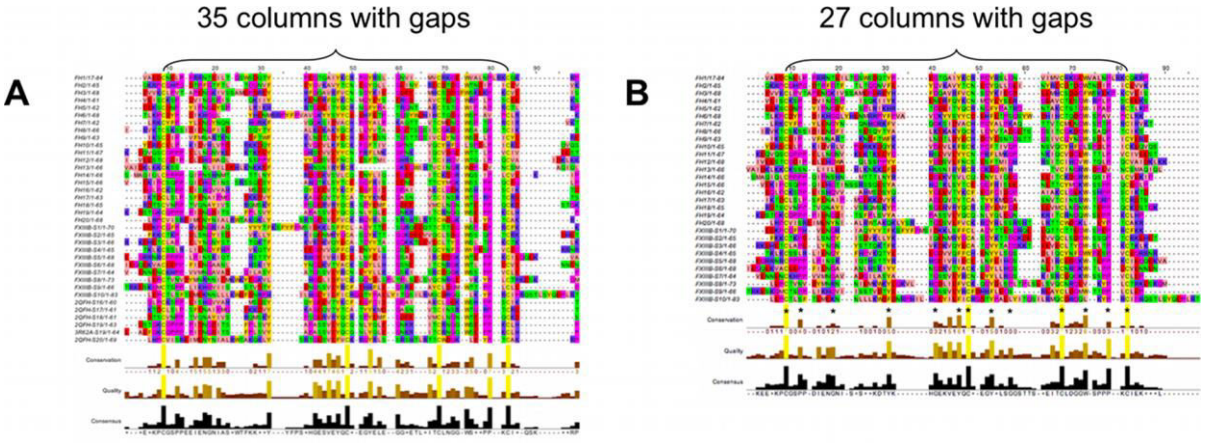

Supp. Figure S3. Comparison of multiple sequence alignments optimized for guiding phylogenetic studies *versus* selecting target/template pairs for homology modeling. Panel A: A high-quality, single-pass MSA created by MAFFT using an accuracy-oriented L-INS-i algorithm for automated iterative refinement by local pairwise alignment. This type of MSA is used as input data for building phylogenetic trees by inference models that accurately reflect evolutionary processes. Panel B: A high-quality, MSA for choosing optimal structural taget/template pairs created by a low-stringency alignment algorithm followed by hand curation. Astrices in panel B indicate 13 conserved structural "guidepost" positions. The MSA in panel A has 35 columns with gaps, while the MSA in panel B has only 27 columns with gaps.

Supp. Table S1. PCR primers for FXIIIB site-directed mutagenesis

Cys5ArgF	5´-CTCTATGCAGAAGAGAAACCCCGTGGTTTTCCTCAT-3´
Cys5ArgR	5´-GGGTTTCTCTTCTGCATAGAGTTCTCCTGAG-3´
Ile81AsnF	5´-CCTGACCTGAGTAATGGTTACAACTCTGATGTAAAG-3´
Ile81AsnR	5´- GTAACCATTACTCAGGTCAGGCTTAGTGCAT-3´
Leu116PheF	5´- GATGAAGAAGTGGTTCAATGTTTCTCTGATGGATGG-3´
Leu116PheR	5´- ACATTGAACCACTTCTTCATCCTTCCCTCCA-3´
Val217IleF	5´- ACCTATGAAGAAGGAGATGTCATTCAGTTTTTCTGT-3´
Val217IleR	5´- GACATCTCCTTCTTCATAGGTTTGCTTTACA-3´
Cys316PheF	5´- GAAGGACAGGAGAAGGTAGCCTTTGAGGAACCACCC-3´
Cys316PheR	5´- GGCTACCTTCTCCTGTCCTTCAATGCATTTT-3´
Val401GluF	5´- AGCTATGCAACAGGATCCTCAGAGGAATATAGATGC-3´
Val401GluR	5´- TGAGGATCCTGTTGCATAGCTTGCCAATATC-3´
Pro428SerF	5´- CAAGGAAAATGGTCATCCCCATCTGTTTGCTTGGAA-3´
Pro428SerR	5´- TGGGGATGACCATTTTCCTTGTTCGCAACGA-3´

Supp. Table S2. Stereochemical validation statistics for 13 solved high-resolution CFH Sushi domains

Factor H Sushi domain, PDB entry ID	Goal value	FH1 2RLP	FH2 2RLP	FH3 2RLQ	FH4 2WII	FH6 2W81	FH7 2W81	FH8 2UWM	FH12 2KMS	FH13 2KMS	FH15 1HFH	FH16 1HCC	FH19 3OXU	FH20 3OXU
Optimized side-chain flips	-	-	-	N154	-	-	-	-	-	-	-	-	-	-
Poor rotamers	<1%	0.00%	4.00%	3.64%	0%	7.14%	10.87%	5.77%	7.69%	5.66%	8.93%	8.16%	1.92%	5.00%
Ramachandran outliers	<0.2%	1.64%	0.00%	1.64%	0%	0%	0%	0%	7.02%	1.85%	16.39%	3.51%	0%	0%
Ramachandran favored	>98%	91.80%	89.66%	88.52%	98.18%	98.36%	88.89%	90%	73.68%	92.59%	68.85%	84.21%	98.25%	95.31%
Cβ deviations >0.25Å	0	0%	0	1	0	1	3	0%	0	0	0	1	0	0
Residues with bad bonds	0%	0%	1.67%	0%	0%	0%	0%	3.23%	1.69%	1.79%	0%	0%	0%	0%
Residues with bad angles	<0.1%	0%	0%	0%	0%	3.17%	3.77%	1.61%	0%	0%	1.59%	0%	0%	0.00%
Number of serious steric overlaps (> 0.4 Å) per 1000 atoms	0	9.95	13.61	6.28	15.91	20.33	74.52	15.23	36.49	34.33	22.65	13.92	2.26	15.86
Clash percentile	100%	71%	55%	90%	91%	62%	1%	81%	9%	11%	26%	54%	99%	60%
MolProbity score	lower is better	2.01	2.66	2.36	1.70	2.45	3.71	2.81	3.52	3.05	3.42	3.02	1.22	2.56

Supp. Table S3. Stereochemical validation statistics for five FXIIIB Sushi domain models from Soares *et al.* (2005)

FXIIIB subdomain fom Soares *et al.* 2005	Goal value	Soares-S2	Soares-S5	Soares-S6	Soares-S7	Soares-S8
Optimized side-chain flips	-	not applied	not applied	not applied	not applied	not applied
Poor rotamers	<1%	3.77%	3.77%	2.04%	0%	1.85%
Ramachandran outliers	<0.2%	2%	0.00%	0%	0%	0%
Ramachandran favored	>98%	91.38%	96.43%	94.64%	94.74%	96.49%
Cβ deviations >0.25Å	0	0	0	0	0	0
Residues with bad bonds	0%	0%	0%	0%	0%	0%
Residues with bad angles	<0.1%	1.67%	1.72%	0%	1.69%	0%
Number of serious steric overlaps (> 0.4 Å) per 1000 atoms	0	159.74	119.6	113.27	110.86	142.06
Clash percentile	100%	0%	0%	0%	0%	0%
MolProbity score	lower is better	3.61	3.21	3.12	2.87	3.05
Current study model MolProbity score (for comparison)	-	3.44	2.09	1.67	1.68	2.94

Supp. Table S4. Assessment of FXIIIB single and multiple Sushi domain homology models from ModBase and SWISS-MODEL databases

ID	Rel.	Provider	Type	Templates	%Seq id	from	to	Target FXIIIB Sushi domain(s)	Template name	Comments
1	good	MODBASE	SC	1srzA	52%	418	450	S8	S2 of GABA(A) receptor 1a	Only half of Shushi domain sequence
2	fair	SWISSMODEL	SC	1srzA	44%	417	451	S8	S2 of GABA(A) receptor 1a	Only half of Shushi domain sequence
3	fair	SWISSMODEL	SC	1hfhA	38%	333	451	S6-S7	S15-S16 of factor H	Better templates are factor H S11, S12, S14, S19
4	fair	SWISSMODEL	SC	2bzmA	37%	521	649	S9-S10	S19-S20 of factor H	Best templates chosen, but tertiary structure constrained, alignment not optimal
5	fair	SWISSMODEL	SC	2bzmA	37%	392	517	S7-S8	S19-S20 of factor H	Best templates chosen, but tertiary structure constrained, alignment not optimal
6	fair	SWISSMODEL	SC	1hfhA	31%	273	385	S5-S6	S15-S16 of factor H	Better templates are factor H S11, S12, S14, S19
7	fair	SWISSMODEL	SC	2ybyA	31%	22	147	S1-S2	S6-S7 of factor H	Best template for S1, but not for S2; better S2 templates are factor H S8, S9; alignment not optimal
8	poor	SWISSMODEL	SC	2uwnA	30%	21	207	S1-S2-S3	S6-S7-S8 of factor H	Best templates for S1 & S3, but not for S2; better S2 templates are factor H S8, S9; alignment not optimal
9	poor	SWISSMODEL	SC	1ghqC	29%	213	318	S4-S5	Compliment receptor 2	Better templates are factor H S3, S19; tertiary structure constrained
10	poor	SWISSMODEL	SC	1hfhA	25%	451	579	S8-S9	S15-S16 of factor H	Better templates are factor H S20, S19; tertiary structure constrained; alignment not optimal
11	poor	SWISSMODEL	SC	2o39D	24%	152	259	S3-S4	S1-S2 of MCP (CD46)	low sequence identity
12	poor	SWISSMODEL	SC	3erbA	24%	213	400	S4-S5-S6	C2b (complement C2)	low sequence identity
13	poor	SWISSMODEL	SC	1c1zA	24%	89	327	S2-S3-S4-S5	apolipoprotein-H (ApoH)	low sequence identity
14	poor	SWISSMODEL	SC	3o8eB	24%	152	391	S3-S4-S5-S6	S1-S2-S3-S4 of MCP (CD46)	low sequence identity
15	poor	SWISSMODEL	SC	3o8eB	23%	214	453	S4-S5-S6-S7	S1-S2-S3-S4 of MCP (CD46)	low sequence identity
16	poor	SWISSMODEL	SC	1ok3A	23%	336	579	S6-S7-S8-S9	S1-S2-S3-S4 of DAF	low sequence identity
17	poor	SWISSMODEL	SC	2xrbA	22%	273	517	S5-S6-S7-S8	S1-S2-S3-S4 of CRRY	low sequence identity
18	poor	SWISSMODEL	SC	3o8eB	22%	25	257	S1-S2-S3-S4	S1-S2-S3-S4 of MCP (CD46)	low sequence identity
19	poor	SWISSMODEL	SC	1c1zA	22%	152	455	S3-S4-S5-S6-S7	apolipoprotein-H (ApoH)	low sequence identity, 5th domain not Sushi fold
20	poor	SWISSMODEL	SC	1c1zA	21%	211	518	S4-S5-S6-S7-S8	apolipoprotein-H (ApoH)	low sequence identity, 5th domain not Sushi fold

Sequence-Centric Models (SC) are generated by searching the best available template structures to build a model for a given protein target sequence, while Template-Centric Models (TC) result from using a specific solved structure as a template to build a number of models for a series of target protein sequences.

MCP = membrane cofactor protein
DAF = DECAY ACCELERATING FACTOR (CD55)
CRRY = COMPLEMENT REGULATORY PROTEIN CRRY (rat)

Supp. Table S5. Predicted physical and chemical properties of FXIIIB mutations from the present study homology modeling

Amino acid substitution[1]	Sushi domain	Wild-type residue surface exposure	Possible H-bonds for mutation[2] (A:Acceptor, D:Donor)	ΔVolume (Å^3) for mutation	ΔCharge for mutation
Cys5Arg	S1	CA, CB surface	D: NE, NH1(2), NH2(2)	+64.9	+1
Ile81Asn	S2	CA, CG2 surface	A: OD1(2), D: ND2(2)	-52.6	0
Leu116Phe	S2	surface[3]	none	+23.2	0
Val217Ile	S4	CB, CG1 surface	none	+26.7	0
Cys316Phe	S6	burried	none	+81.4	0
Val401Glu	S7	CA surface	A: OE1(2), OE2(2)	-1.6	-1
Pro428Ser	S7	CB surface	A: OG(2), D: OG	-23.7	0

[1]Amino acid numbering according to Bottenus *et al.* 1990 for which residue 1 is equivalent to Glu21 of the translated full-length precursor.(Bottenus, et al., 1990) [2]No H-bond donor o acceptor groups are predicted for wild-type residues at these positions. [3]Only Leu116 is predicted to be a fully surface-exposed residue.

Supp. Table S6. Patient data for carriers of the FXIIIB mutations investigated in the present study

Family/Patient ID (gender)	Birth date	Bleeding symptoms[1]	FXIII activity[2] (% of normal)	FXIIIA:Ag[3] (% of normal)	FXIIIB:Ag[3] (% of normal)	Amino acid substitution
GER05/ Patient E (f)	1947	After abdomen surgery	47-53	43	32	Cys5Arg
GER01/ Patient A (f)	1968	None reported	50-60	46	60	Ile81Asn
Mother of patient A (f)	1937	None reported	74	60	99	Ile81Asn
GER02/ Patient B (f)[4]	1990	None reported	46-59	40	86-94	Ile81Asn
Mother of patient B (f)	1965	After every delivery (n=4)	80	71	67	Ile81Asn
GER06/ Patient F (m)	1983	Epistaxis	54-71	58	64	Leu116Phe
Father of patient F (m)	1962	None reported	73	42	52	Leu116Phe
GER13/ Patient M (f)	1988	None reported	50	n.d.	n.d.	Val217Ile
Mother of patient M (f)	1962	After tonsillectomy	76	n.d.	n.d.	Val217Ile
GER07/ Patient G (m)	1971	Epistaxis	45-48	n.d.	n.d.	Cys316Phe
GER08/ Patient H (f)	1955	Haematoma in the neck after brain surgery[5]	20-41	n.d.	n.d.	Cys316Phe
GER14/ Patient N (f)	1966	After tonsillectomy	45	n.d.	n.d.	Val401Glu
GER09/ Patient I (m)	1985	None reported	44-48	n.d.	n.d.	Pro428Ser

Symbol key: GER, German origin; IND, Indian origin; MOZ, African (Mozambique) origin; red-shaded entries indicate lower than normal values (FXIII activity determined by a photometric assay(Fickenscher, et al., 1991) and, for one family, by an incorporation assay (Pefakit FXIII Incorporation Assay, Pentapharm Ltd, Basel, Switzerland); FXIIIA:Ag andFXIIIB:Ag determined in citrated plasma by ELISA using a polyclonal anti-FXIII tetramer antibody (Binding Site, Birmingham, England) for coating and polyclonal anti-subunit A or anti-subunit B antibodies (Diagnostica Stago, Asnières, France) for detection.(Ariens, et al., 1999) Antigen levels were expressed as a percentage relative to levels in normal pooled plasma.); n.d., not determined; [1]No patients were reported to suffer gennerally impaired wound healing; [2]photometric assay (normal range 65-120%); [3]normal range 70-120%; [4]Patient B had one successful pregnancy wherein a Caesarean section was performed in the 37th week of gestation due to abnormal position of the fetus (breech presentation). The patient was perioperatively administered 2500 U (25 U/kg) FXIII concentrate; [5]Patient supplemented with FXIII concentrate (2500 IU).

Supp. References

Ariens RA, Kohler HP, Mansfield MW, Grant PJ. 1999. Subunit antigen and activity levels of blood coagulation factor XIII in healthy individuals. Relation to sex, age, smoking, and hypertension. Arterioscler Thromb Vasc Biol 19(8):2012-6.

Bottenus RE, Ichinose A, Davie EW. 1990. Nucleotide sequence of the gene for the b subunit of human factor XIII. Biochemistry 29(51):11195-209.

Evans P. 1992. PDBSET - Various useful manipulations on coordinate files. Cambidge: MRC LMB.

Fickenscher K, Aab A, Stuber W. 1991. A photometric assay for blood coagulation factor XIII. Thromb Haemost 65(5):535-40.

Hocking HG, Herbert AP, Kavanagh D, Soares DC, Ferreira VP, Pangburn MK, Uhrin D, Barlow PN. 2008. Structure of the N-terminal region of complement factor H and conformational implications of disease-linked sequence variations. J Biol Chem 283(14):9475-87.

Morgan HP, Schmidt CQ, Guariento M, Blaum BS, Gillespie D, Herbert AP, Kavanagh D, Mertens HD, Svergun DI, Johansson CM and others. 2011. Structural basis for engagement by complement factor H of C3b on a self surface. Nat Struct Mol Biol 18(4):463-70.

Prosser BE, Johnson S, Roversi P, Herbert AP, Blaum BS, Tyrrell J, Jowitt TA, Clark SJ, Tarelli E, Uhrin D and others. 2007. Structural basis for complement factor H linked age-related macular degeneration. J Exp Med 204(10):2277-83.

Punta M, Forrest LR, Bigelow H, Kernytsky A, Liu J, Rost B. 2007. Membrane protein prediction methods. Methods 41(4):460-74.

Schneider MC, Prosser BE, Caesar JJ, Kugelberg E, Li S, Zhang Q, Quoraishi S, Lovett JE, Deane JE, Sim RB and others. 2009. Neisseria meningitidis recruits factor H using protein mimicry of host carbohydrates. Nature 458(7240):890-3.

Winn MD, Ballard CC, Cowtan KD, Dodson EJ, Emsley P, Evans PR, Keegan RM, Krissinel EB, Leslie AG, McCoy A and others. 2011. Overview of the CCP4 suite and current developments. Acta Crystallogr D Biol Crystallogr 67(Pt 4):235-42.

Publication 2

Published in *Molecular Genetics & Genomic Medicine* as a Research article

Title: Structural and functional influences of coagulation factor XIII subunit B heterozygous missense mutants

Authors: Anne Thomas[1†], Arijit Biswas[1†], Vytautas Ivaskevicius[1], Johannes Oldenburg[1]

[1]Institute of Experimental Haematology and Transfusion Medicine, University Clinic Bonn, 53127 Bonn, Germany

[†]Equally contributing first author

Abstract

The coagulation Factor XIII(FXIII) is a plasma circulating heterotetrameric protransglutaminase that acts at the end of the coagulation cascade by covalently crosslinking preformed fibrin clots (to themselves and to fibrinolytic inhibitors) in order to stabilize them against fibrinolysis. It circulates in the plasma as a heterotetramer composed of two homomeric catalytic Factor $XIIIA_2$ ($FXIIIA_2$) and two homomeric protective/carrier Factor $XIIIB_2$ subunit ($FXIIIB_2$). Congenital deficiency of FXIII is of two types: severe homozygous/compound heterozygous FXIII deficiency which results in severe bleeding symptoms and mild heterozygous FXIII deficiency which is associated with mild bleeding (only upon trauma) or an asymptomatic phenotype. Defects in the *F13B* gene (Factor XIIIB subunit) occur more frequently in mild FXIII deficiency patients than in severe FXIII deficiency. We had recently reported secretion related defects for seven previously reported *F13B* missense mutations. In the present study we further analyze the underlying molecular pathological mechanisms as well as the heterozygous expression phenotype for these mutations using a combination of *in vitro* heterologous expression (in *HEK293T* cells) and confocal microscopy. In combination with the *in vitro* work we have also performed an *in silico* solvated molecular dynamic simulation study on previously reported FXIIIB subunit sushi domain homology models in order to predict the putative structure-functional impact of these mutations. We were able to categorize the mutations into the following functional groups that: a) affect antigenic stability as well as binding to FXIIIA subunit i.e. *Cys5Arg, Cys316Phe* and *Pro428Ser* b) affect binding to FXIIIA

subunit with little or no influence on antigenic stability i.e. *Ile81Asn* and *Val401Gln* c) influence neither aspects and are most likely causality linked polymorphisms or functional polymorphisms i.e. *Leu116Phe* and *Val217Ile*. The *Cys5Arg* mutation was the only mutation to show a direct secretion based defect since the mutated protein was observed to accumulate in the endoplasmic reticulum.

Molecular Genetics & Genomic Medicine

Open Access

ORIGINAL ARTICLE

Structural and functional influences of coagulation factor XIII subunit B heterozygous missense mutants

Anne Thomas[a], Arijit Biswas[a], Vytautas Ivaskevicius & Johannes Oldenburg

Institute of Experimental Haematology and Transfusion Medicine, University Clinic Bonn, 53127 Bonn, Germany

Keywords
Confocal microscopy, FXIIIB subunit, missense mutation, molecular dynamic simulation, secretion defects

Correspondence
Arijit Biswas, Institute of Experimental Haematology and Transfusion Medicine, University Clinic Bonn, Sigmund Freud Str. 25, 53127 Bonn, Germany.
Tel: +49 228 287 19428;
Fax: +49 228 287 14320;
E-mail: arijit.biswas@ukb.uni-bonn.de

Funding Information
The authors would like to acknowledge CSL Behring for funding research on FXIII.

Received: 17 November 2014; Revised: 6 February 2015; Accepted: 6 February 2015

Molecular Genetics & Genomic Medicine **2015; 3(4): 258–271**

doi: 10.1002/mgg3.138

[a]These authors contributed equally to this work.

Abstract

The coagulation factor XIII(FXIII) is a plasma circulating heterotetrameric protransglutaminase that acts at the end of the coagulation cascade by covalently cross-linking preformed fibrin clots (to themselves and to fibrinolytic inhibitors) in order to stabilize them against fibrinolysis. It circulates in the plasma as a heterotetramer composed of two homomeric catalytic Factor $XIIIA_2$ ($FXIIIA_2$) and two homomeric protective/carrier Factor $XIIIB_2$ subunit ($FXIIIB_2$). Congenital deficiency of FXIII is of two types: severe homozygous/compound heterozygous FXIII deficiency which results in severe bleeding symptoms and mild heterozygous FXIII deficiency which is associated with mild bleeding (only upon trauma) or an asymptomatic phenotype. Defects in the *F13B* gene (Factor XIIIB subunit) occur more frequently in mild FXIII deficiency patients than in severe FXIII deficiency. We had recently reported secretion-related defects for seven previously reported *F13B* missense mutations. In the present study we further analyze the underlying molecular pathological mechanisms as well as the heterozygous expression phenotype for these mutations using a combination of in vitro heterologous expression (in *HEK293T* cells) and confocal microscopy. In combination with the *in vitro* work we have also performed an *in silico* solvated molecular dynamic simulation study on previously reported FXIIIB subunit sushi domain homology models in order to predict the putative structure-functional impact of these mutations. We were able to categorize the mutations into the following functional groups that: (1) affect antigenic stability as well as binding to FXIIIA subunit, that is, *Cys5Arg*, *Cys316Phe*, and *Pro428Ser* (2) affect binding to FXIIIA subunit with little or no influence on antigenic stability, that is, *Ile81Asn* and *Val401Gln* c) influence neither aspects and are most likely causality linked polymorphisms or functional polymorphisms, that is, *Leu116Phe* and *Val217Ile*. The *Cys5Arg* mutation was the only mutation to show a direct secretion-based defect since the mutated protein was observed to accumulate in the endoplasmic reticulum.

Introduction

Factor XIII deficiency is a rare bleeding disorder that results from the deficiency of coagulation FXIII, a heterotetrameric protransglutaminase molecule that functions by cross-linking preformed fibrin clots to provide them mechanical stability and resistance to fibrinolysis (Lorand et al. 1980). The plasma circulating FXIII is composed of two catalytic $FXIIIA_2$ subunits and two protective $FXIIIB_2$ subunits. While the homozygous inherited form of this deficiency caused by *FXIIIA* (OMIM #613225) or *FXIIIB* (OMIM #613235) gene mutations is rare (1 in 4–6 million), the milder heterozygous form is more frequent (Biswas et al. 2011; Biswas et al. 2014a,b). Only recently, focus has shifted to the mild/heterozygous form of this deficiency that is associated with mild or even an asymptomatic phenotype (unless the affected individual is exposed to some kind of a trauma, for example, perioperative settings, accident etc.). Four publications from our group in the past 5 years have shown that inherited mild or heterozygous deficiency does have clinical relevance (Biswas et al. 2010; Ivaskevicius et al. 2010a,b; Biswas

et al. 2014a,b). One key observation from these articles is that the FXIIIB subunit mutations, which are rarely reported in the severe homozygous form of FXIII deficiency, occur at almost equal proportion when compared with the frequency of FXIIIA subunit mutations in mild heterozygous FXIII deficiency (Ivaskevicius et al. 2010b). It is secreted as a homodimer into the plasma where it associates with the $FXIIIA_2$ subunit to form the $FXIIIA_2B_2$ heterotetramer (Radek et al. 1993). It is secreted in excess of the $FXIIIA_2$ subunit in the plasma. Therefore, there is always free FXIIIB subunit aside from the complexed one circulating in the plasma. Despite early achievements investigating FXIIIB secondary structural elements and structural domains (Ichinose et al. 1986), progress on structure/function studies of this noncatalytic subunit have been slow and there are no high-resolution x-ray-based crystal/NMR structures for $FXIIIB_2$ dimers, or for the $FXIIIA_2$-bound conformation in $FXIIIA_2B_2$ tetramers. Based on gel filtration chromatographic data, the FXIIIB subunit appears to form a physiological dimer (Souri et al. 2008). High sequence homologies with proteins from the complement system suggest that the monomeric B subunit is composed of ten Sushi domains, each comprising ~60 amino acid residues and also designated in the literature as complement control protein (CCP) modules, or as short consensus repeats (SCR) (Ichinose et al. 1986). Knowledge of the structural interfaces between individual $FXIIIB_2$ subunit dimers as well as for the intermolecular interfaces of the $FXIIIA_2B_2$ heterotetramer has only recently started to emerge (Katona et al. 2014). The sushi domain folds into a small and compact hydrophobic core enveloped by six β-strands which are stabilized by two disulfide bridges on either end of this domain. All sushi structures share the relative structural orientation of the β-2 and β-4 strands. The other strands vary in topology relative to this central conserved core especially at the interdomain interfaces (Gaboriaud et al. 2000). There are more than 25 high-resolution structures for this highly conserved domain type and additional Sushi domain-containing protein (Soares et al. 2005). In a recent article we have reported homology-based models for all ten sushi domains of the FXIIIB subunit based on the templates of complement factor H (CFH) sushi domains (Biswas et al. 2013). We have so far reported 12 unique mutations in the $FXIIIB_2$ subunit from patients with heterozygous (mild) FXIII deficiency of which seven were missense mutations. In an earlier article using heterologous in vitro expression we had shown that almost all reported FXIIIB subunit missense mutations showed differences in secretion rate, with the highest impact being observed for two mutations affecting structural disulfide bonds and one mutation involving a Proline428 residue (Biswas et al. 2013). However, a few questions remained unanswered from this article which we have now attempted to answer in our present study. These questions are: (1) Do the differences in secretion rates correspond to a genuine secretion defect, that is, is there intraorganellar accumulation/aggregation or are they simply a reflection of the influence that the mutations have on the rate of biosynthesis and folding? (2) Does the in vitro expression data of the *F13B* mutations correlate with the heterozygous patient phenotype? (3) Which mutations are most likely to affect binding to the $FXIIIA_2$ subunit without compromising the antigenic stability of the $FXIIIB_2$ subunit? (4) What are the likely structure-functional correlations for these mutations? In our present study we have used a combination of heterologous *in vitro* expression, confocal microscopy and molecular dynamic simulation (MD) on homology-based models to address these questions.

Material and Methods

Cell culture, transfection, and protein expression and quantification

Site-directed mutagenesis for the seven FXIIIB missense mutations were performed on a mammalian expression pEZ-MO1-*FXIIIB* vector using the Gene Tailor site-directed mutagenesis kit (Life Technologies, Darmstadt, Germany). The seven FXIIIB mutant variants [pEZ-MO1-FXIIIB-p.Cys5Arg (*F13Bc.73T>C*), pEZ-M01-FXIIIB-p.Cys316Phe (*F13Bc.1007G>T*), MO1-FXIIIB-p.Ile81Asn (*F13B*c.302T>A), MO1-FXIIIB-p.Leu116Phe (*F13B*c.406C>T), MO1-FXIIIB-p.Val217Ile (*F13Bc.*709G>A), MO1-FXIIIB-p.Val401Glu (*F13B*c.1262T>A), MO1-FXIIIB-p.Pro428Ser (*F13B*c.1342C>T)] were expressed in *HEK 293T* cells (DSMZ [Institute of DSMZ-German Collection of Microorganisms and Cell Cultures, Germany]) in homozygous and heterozygous forms, that is, mutations or the wild type was expressed alone (homozygous), mutations were cotransfected with the wild type (heterozygous). Culturing of the cells was done in 10 cm dishes with Dulbecco′s modified Eagles medium (DMEM; Life Technologies) supplemented with 10% fetal bovine serum (FBS; Life Technologies), 1% penicillin-streptomycin (Life Technologies) and 0.1% Fungizone (Life Technologies) at 37% in 5% CO_2. For transfection 2.7×10^6 million cells were seeded out into 6-well plates with DMEM (with FBS) without supplements and transfected with wild-type and mutated DNA using Lipofectamine 2000 reagent (Life Technologies). Cotransfection of the variants was done at a 4:0.5 ratio with a pCMV-LacZ Vector (Clontech, Saint-Germain-en-Lay, France) containing the *LacZ* gene for normalizing the antigen values. All samples (supernatant and lysed cells) were collected 36 h after media change. The extracellular medium was centrifuged at 14,000*g* to remove cell debris and

the cells were washed with phosphate-buffered saline (PBS) and lysed by incubation with 260 μL nondenaturing lysis buffer "native M-PER Mammalian Protein Extraction Reagent buffer" (Life Technologies, Darmstadt, Germany) containing 25 mmol/L bicine pH 7.6 for 10 min incubation and centrifuged at 14,000*g* for 5 min at 4°C. Both extracellular medium and cell lysates were stored at −80°C for later analysis. Each transfection set was performed in triplicate and repeated a minimum of three times(total $n > 9$). Total $FXIIIB_2$ and $FXIIIA_2B_2$ antigen levels were evaluated for the expression supernatants using ELISA kits (Technoclone, Vienna, Austria).

Confocal microscopy

For confocal microscopy 270000 *HEK293T* cells were seeded on 12-mm Poly-D-Lysine coated coverslips (BD Biosciences, Heidelberg, Germany) in 24-well cell culture plates. The cells were transiently transfected with the Wild-type pEZ-MO1-FXIIIB and the seven FXIIIB mutant variants using Lipofectamine 2000 transfection reagent (Life Technologies) following the recommendations of the manufacturer. After 24 h cells were washed and fixed with 4% paraformaldehyde in PBS for 10 min and at room temperature. After washing with PBS and blocking (90% PBS azide [0.1% sodium azide], 10% FBS, 0.1% Triton-X100) incubation with 2.5 μg/mL primary antibody diluted in PBS azide (1% FBS, 0.1% Triton-X100) against the FXIIIB subunit (mouse monoclonal IgG) and the cell compartments ER (IgG rabbit polyclonal anti-calnexin; Abcam, Cambridge, England) and Golgi (rabbit anti-TGn46; Sigma, Hamburg, Germany) was done. Signal detection was performed using an IgG Alexa Fluor 488 IgG goat anti-mouse (Life technologies) against the FXIIIB subunit and an IgG goat anti-rabbit Alexa Flour 594 (Life technologies) against the ER and Golgi compartment. After washing the treated cells and Dapi (Life technologies) staining for nucleus visualization the samples were embedded with VectaShield mounting medium (Vector Laboratories, Peterborough, United Kingdom) and stored at 4°C for visual imaging with the Olympus Fluo View FV 1000 confocal microscope, Hamburg, Germany.

Image analysis

Colocalization analysis was performed using plugins embedded in the image visualization and analysis software ImageJ 1.43m (Schneider et al. 2012). Analysis was performed on a similar sized symmetrical region of interest (ROI) selected for each dye. Background levels were subtracted from each ROI before calculating the degree of colocalization (to a range of one standard deviation). Each colored image was split into the respective RGB (red, green, blue) channels. The comparative degree of colocalization for the wild-type and mutant variants was calculated as mean Pearson's and Mander′s R coefficients on the red and green channels using the embedded colocalization analysis plugin at default settings. The colocalization highlighter plugin was used also with default setting (50% threshold values for both channels) to further visualize the co-localized pixels rendered as white. Since Pearson's and Mander′s R coefficient showed good correlation (Mander′s R was almost consistently higher than Pearson's correlation coefficient), therefore only Pearson's correlation coefficient was used for comparing relative degree of colocalization between the mutant variants and wild-type (Adler and Parmryd 2010). A minimum of $n = 10$ ROI′s were evaluated for each pairwise comparison.

Expression and reconstitution study

Constant amount of the recombinant $FXIIIA_2$ subunit (Zedira, Darmstadt, Germany) (0.75 μg) was added to a final volume of 200 μL of transfection product (wild type as well as mutants), that is, the secreted medium for reconstituting the heterotetramer. In the event of a significant difference in the beta galactosidase reporter levels between the particular mutant and wild type the mixing volumes would have been altered to allow for differences in transfection efficiency. Since this set of expression and reconstitution showed no significant differences in beta galactosidase reporter levels the mixing volumes were not altered. Postincubation the mix was evaluated for $FXIIIA_2B_2$ heterotetrameric antigen levels. The results are normalized against total $FXIIIB_2$ antigen levels previously evaluated to give a representation of the respective variant's ability to form a heterotetramer, which are compared against the wild type. This ability we name as the comparative tetramerization potential (CTP) or potential percentage (CTPP). It is calculated by the following formula:

$$\begin{aligned} CTP = &(\text{Total FXIII-B antigen variant}/ \\ &\text{Total FXIII-}A_2B_2\text{antigen variant})/ \\ &(\text{Total FXIII-B antigen wild type}/ \\ &\text{Total FXIII-}A_2B_2\text{wild type})CTPP = CTP \times 100 \end{aligned}$$

Proteasomal inhibition

Typical 36 h transfection and collection with the wild type and different variants was performed as described above. The only difference was that after 24 h of transfection 10 mmol/L Lactacystin (to a final concentration 10 μmol/L) was added to the cell medium. Therefore, the cells were incubated with 10 μmol/L of Lactacystin for a

period of 12 h. This analysis was done only one time in triplicates.

Structural and sequence conservation analysis

Two different types of multiple sequence alignments were generated to evaluate the conservation of residues on which the mutations have been reported and their neighboring residues. The first alignment was generated by aligning individual FXIIIB sushi domain sequences with its near homolog CFH sushi domain amino acid sequences. Since elaborate functional information exists for the CFH sushi domains, this alignment helped us to functionally evaluate FXIIIB sushi domains with respect to functional definitions for CFH sushi domains (Perkins et al. 2012; Kopp et al. 2012). A more elaborate multiple sequence alignment was generated by first downloading sushi domain amino acid sequences of 50 mammalian proteins (Soares et al. 2005) and then aligning them with the ten FXIIIB sushi domain sequences in order to look for overall sequence conservation and identity. Alignment was done on Jalview 2.7 using MAFFT, L-insi-1 accuracy-based parameters (Waterhouse et al. 2009; Katoh and Standley et al. 2013). In addition to sequence conservation analysis, structural conservation of the FXIIIB subunit sushi domains was evaluated by submitting their homology-based models individually to the PROBIS server (http://probis.cmm.ki.si/) (Konc and Janezic 2010a,b).

MD simulation analysis

Previously published homology-based models were used as a primer for the MD simulation study (Biswas et al. 2013). The previously generated models were first refined by a short solvated refinement simulation run of 500 ps on YASARA version 13.9.8 (Krieger et al. 2002). Individual sushi domain models were housed in a simulation cell 2×7.5 Å larger than the model on each axis. The simulation cell was filled with water to a density of 0.997 g/L. The YASARA YAMBER03 force field derived originally from the AMBER force field was imposed. Periodic boundary conditions were used for the simulation run. The structure with the lowest energy from the simulation run was used for further study. Each of the refined sushi domain models (wild type) on which the mutations occur were individually run for a period of 25 ns with a different force field (AMBER03) than the one used for model refining. The remaining simulation protocol was similar to the one used for model refining. The same protocol was employed for a 25-ns run for sushi domains on which the individual missense variants were introduced and optimized for the best possible rotamer (using SCRWL parameters) (Krivov et al. 2009). The simulation trajectories were analyzed for DCCM (dynamic cross-correlation matrices), C-alpha backbone RMSDs (root mean square deviation), RMSF (root mean square fluctuation), radius of gyration, surface electrostatic potential, accessible surface area and other variable components. These analyses were performed for the complete trajectory as well as for the simulation-averaged structure. The simulation variables were compared between the wild-type and mutated sushi domains. All image rendering and structural analysis (of the simulation trajectories as well as the simulation averaged structures) was done using YASARA version 13.9.8 and SWISS-PDB viewer (Guex et al. 2009). Difference in folding free energies between mutant and wild-type structures were calculated using the following web servers: Imut 2.0, SDM, McSM, DUET, ERIS (Capriotti et al. 2005; Yin et al. 2007; Worth et al. 2011; Pires et al. 2014a,b) and also with the FOLDX plug in embedded in YASARA (Van Durme et al. 2011). The simulation averaged structures for both the wild type and mutants were used as an input for these web servers as well as for FOLDX-based calculations. The PIPSA web server (http://pipsa.eml.org/pipsa/) was used to calculate the surface electrostatic potential distances between wild type and mutated sushi domain (once again the simulation averaged structures were used as an input) (Richter et al. 2008).

Results

Heterologous expression of FXIIIB subunit variants in homozygous and heterozygous forms

The results of heterologous expression of the FXIIIB subunit wild type and mutations in homozygous form showed a pattern that was published recently (Fig. 1) (Biswas et al. 2013). Three of the mutations (*Cys5Arg*, *Cys316Phe*, and *Pro428Ser*) showed quite low levels of secreted FXIIIB subunit (mean levels ranging between 0.29 and 2.74 μg/mL) Another variant showed moderately reduced levels than the wild type (*Val401Glu*; mean level 3.65 μg/mL), three other variants (*Ile81Asn*, *Leu116Phe*, *Val217Ile*) showed levels close to that of the wild type (4.82 μg/mL). The heterozygous coexpression with the wild type for all variants afforded some degree of correction for the mutated expression phenotype. In fact in some of the variants (*Ile81Asn*, *Leu116Phe*, *Val217Ile, Cys316Phe*, and *Val401Glu*) the coexpressed phenotype $FXIIIB_2$ antigen levels (4.2–6.66 μg/mL) were quite similar to the wild type (Fig. 1) except for *Cys5Arg* and *Pro428Ser* which reached only 1.22–3.87 μg/mL FXIIIB antigen levels.

Confocal microscopy and Image analysis for B subunit variants

The comparative degree of colocalization expressed as Pearson and Mander's R coefficient showed an interesting

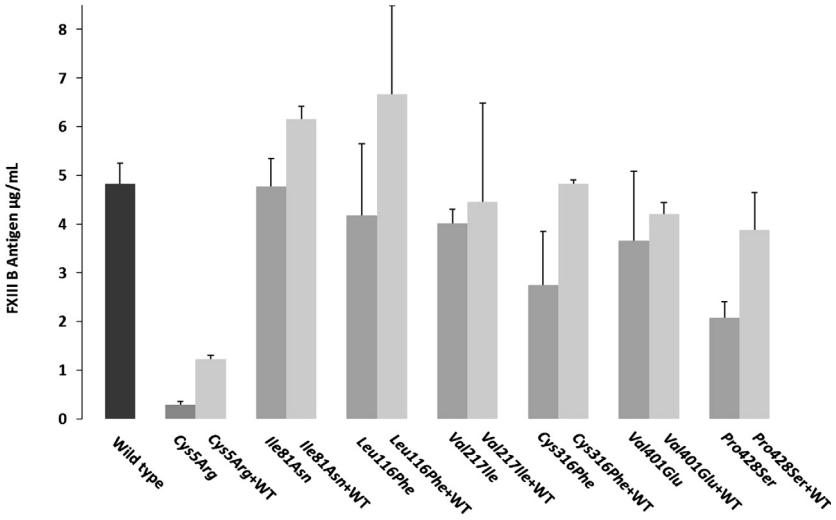

Figure 1. Transient homozygous/heterozygous expression of the reported missense mutations. This image represents comparative bar graph representations for the mutant and wild-type FXIIIB expression antigen values, homozygous as well as heterozygous. The leftmost black bar represents the wild type. Amongst the other bars, the dark gray represent homozygous mutant expression while the light represents the heterozygous expression (cotransfection with wild type). All values have already been normalized for transfection efficiency with beta galactosidase levels. The error bars represent the standard deviation.

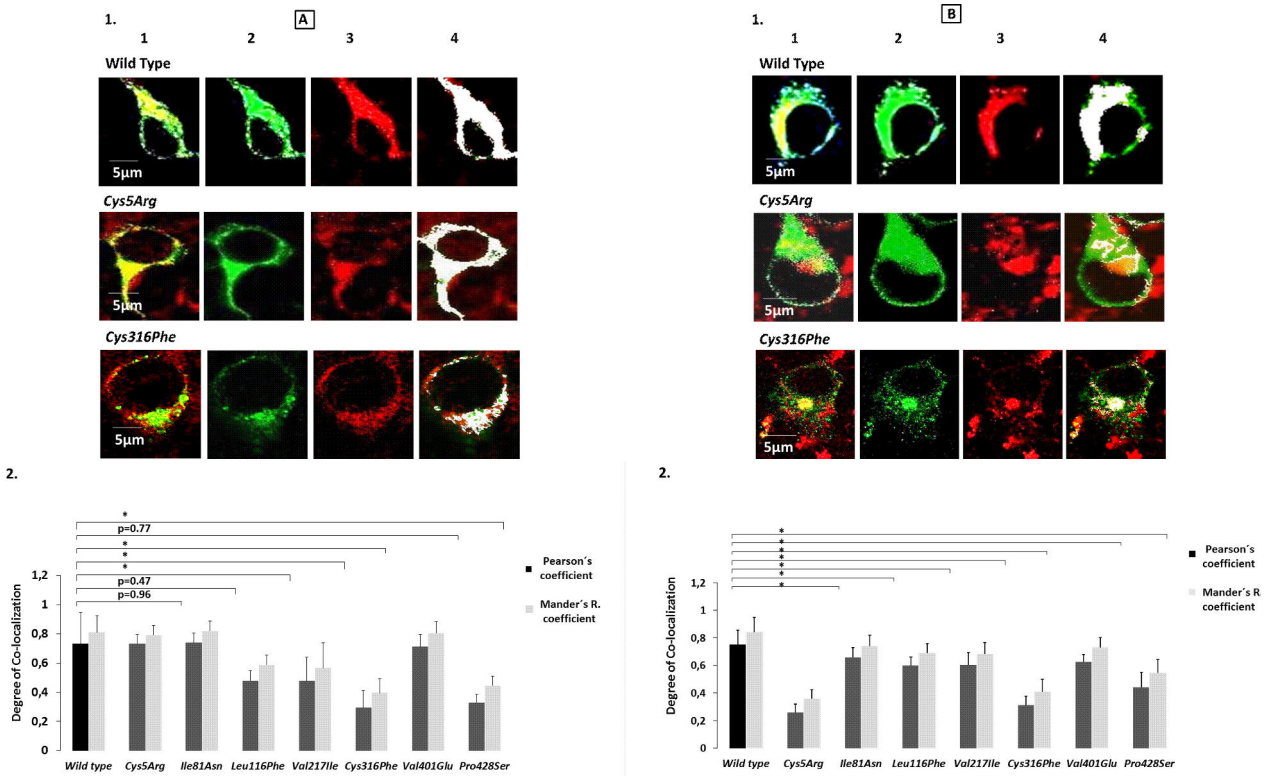

Figure 2. Confocal analysis and the degree of colocalization for wild-type and the reported missense mutations. A(1) Confocal images for colocalization of our wild-type and mutant variant FXIIIB subunit protein with ER. In order to avoid any confusion only the two cysteine-based mutations, *Cys5Arg* and *Cys316Phe* have been shown here. The images for all the missense mutations can be seen in Figure S3. Each representative confocal image is split into four sections: green staining representing the FXIIIB subunit protein, red staining representing the ER, yellow staining showing the colocalization of ER and FXIIIB subunit and finally white dots which also represents co-localization of ER and FXIIIB subunit. A(2) Bar graph representing comparative degree of ER colocalization with ER for the wild-type and mutant variant FXIIIB subunit protein. B(1) and B(2) is similar to A(1) and A(2), the main difference being that the red stain represents the Golgi network and the co-localization overlays shown are for the FXIIIB subunit protein with the Golgi network.

pattern with respect to one particular mutation, that is, *Cys5Arg*. The *Cys5Arg* variant showed similar levels of colocalization for ER (difference $P = 0.96$; Fig. 2A) but very low levels of colocalization for Golgi (lowest amongst all mutations; difference $P < 0.001$) (Fig. 2B). The degree of colocalization was also quite low in both ER and Golgi

for the mutations *Cys316Phe* and *Pro428Ser*. *Ile81Asn* and *Val401Glu* showed similar levels of colocalization in ER and lower but only borderline significant levels of colocalization in Golgi indicating that their secretion paths follow similar fates as that of wild type. The *Val217Ile* mutant shows significantly lower levels of colocalization for both ER and Golgi (but not of the order of other high impact mutations like *Cys316Phe* and *Pro428Ser*) which might account for the slight difference in secreted antigen levels for this mutant when compared with the wild type.

Proteasome inhibition by Lactacystin

The inhibition of the proteasome by Lactacystin showed a corrective effect for all mutations except *Ile81Asn* and *Val217Ile*. The mutations *Cys5Arg*, *Leu116Phe*, *Cys316Phe and Pro428Ser* show an increase in FXIIIB antigenic level more than that observed for the wild type (0.56 μg/mL) post-Lactacystin treatment (Fig. S1).

Expression and reconstitution study of the FXIIIB subunit variants with recombinant FXIIIA subunit

Reconstitution experimentation with recombinant FXIIIA subunit showed a significant impact on binding to the FXIIIA subunit and hence on heterotetramer assembly for four FXIIIB subunit mutations (*Ile81Asn*, *Val401Glu*, *Cys316Phe*, and *Pro428Ser*) (Fig. 3). The *Cys5Arg* variant showed nondetectable levels of $FXIIIA_2B_2$ antigen and therefore representative CTP or CTPP values were not calculated. The highest calculated impact on heterotetramer assembly was for the *Cys316Phe* mutation (only ~22% of the binding ability of wild type FXIIIB). Two mutations (*Leu116Phe* and *Val217Ile*) showed CTP and CTPP values similar to wild type indicating no effect on heterotetramer assembly.

Structural and sequence conservation analysis

Sequence alignment with CFH sushi domains as well as with sushi domains from 50 different mammalian proteins (containing sushi domains) suggest a number of consistently conserved residues aside from the cysteines which form the backbone structural disulfide bonds of the sushi domains [Fig. 4A(1) and (2)]. Interestingly most of these sequence conserved residues are hydrophobic (Proline, Tryptophan) in character suggesting a role for these residues either in binding/functional interactions or maintaining the hydrophobic core of their respective sushi domains. Structural alignment of the sushi domains differs from their sequence alignment in certain segments. We observed sequence conserved residues occurring in regions of structural variability in the FXIIIB sushi domains. This was quite frequent for the residues on the variable length loops connecting the sushi domain beta strands (Fig. 4B). The two reported cysteine missense mutations occur in highly conserved structural cores of their sushi domains and show practically no variability at all (structurally as well as sequence identity based). The Pro428 residue is also highly conserved. Only in the 13th factor H sushi domain it is substituted by another residue, which turns out to be a hydrophobically similar and small Val residue [Fig. 4A(2)]. The Ile81 residue occurs in a semiconserved sequence but a structurally variable region of the FXIIIB subunit S2 sushi domain. The Ile residue in the multiple sequence alignment with CFH sushi domain varies on most occasions to a hydrophobically similar Val residue [Fig. 4A(2)]. Only in sushi domains 14 of CFH we observe an Asn residue similar to the reported mutation (*Ile81Asn*). However, sushi domain 14 has no designated role in protein–protein interactions for CFH protein, therefore this sushi domain might be functionally redundant (Perkins et al. 2011). In the larger multiple alignment this residue is poorly conserved but

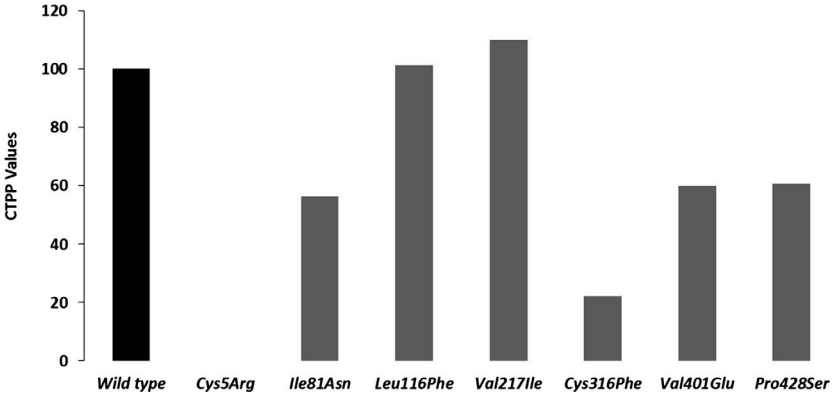

Figure 3. CTPP values representing FXIIIB-binding ability. This image is a comparative bar graph description of the wild type versus mutant FXIIIB subunit CTPP (comparative tetramerization potential percentage) values. The calculations for CTTP have been explained in the methods section. Since the CTTP values are a comparative representation when the wild type is considered to be 100%, therefore no error bars are shown for this figure.

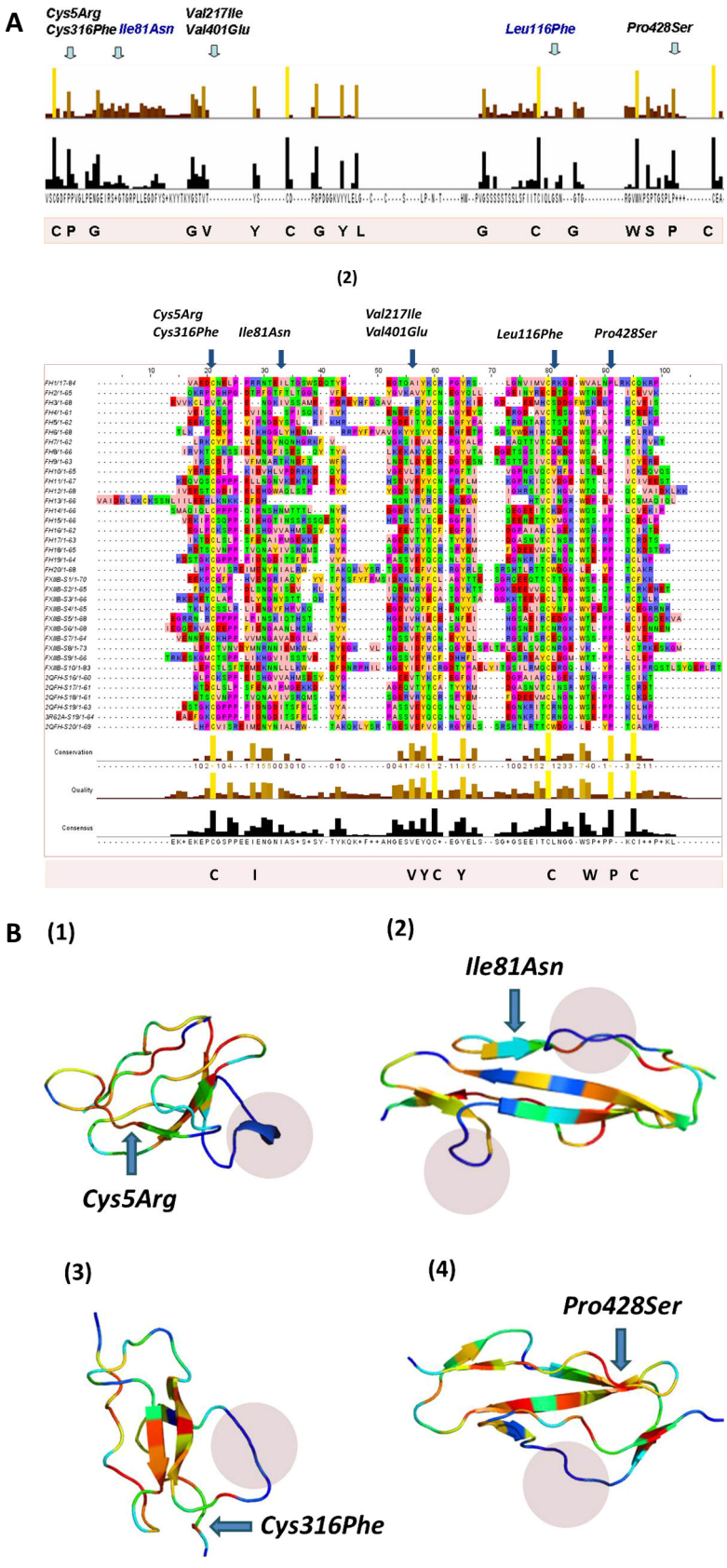

Figure 4. Sequence and structural conservation of sushi domains. A(1) Conservation results for the multiple sequence alignment of FXIIIB subunit sushi domains with sushi domains from 50 mammalian sushi domain-containing proteins. Owing to the large size of the actual alignment, it is not shown here. Only the conservation has been shown here with two bar graphs. The upper colored one depicts the degree of conservation and the lower bars show the consensus. Taller bars indicate higher sequence identity and also conservation. A(2) Multiple sequence alignment of FXIIIB subunit sushi domains with sushi domains of the complement factor H. The highly conserved residues are colored and also listed at the bottom of the multiple sequence alignment. The residues corresponding to each mutation have been marked at the position they occur in the alignment. (B) Structural alignment results for four sushi domains on which the mutations *Cys5Arg (S1; B1)*, *Ile81Asn (S2; B2)*, *Cys316Phe (S6; B3)* and *Pro428Ser (S7; B4)* occur. Structural conservation is depicted in a color gradient where blue represents lowest conservation level and red the highest. The variable length loops connecting the beta strands, which show the highest structural variability, are shown in blue shaded regions in each domain.

most of the variant residues are also hydrophobic in character. The Leu116 residue is located in a highly conserved sequence stretch (VQCLSDG) within which the Leu residue is the most poorly conserved residue. Interestingly, this residue varies between polar and nonpolar residues almost consistently between the various sushi domains in both the larger as well smaller (with CFH) multiple sequence alignments. The Val217 residue is a highly conserved residue and it aligns with the Val401 residue (on which another mutation *Val401Glu* has been reported) from sushi domain 7. The difference between the two mutations is that one is to a hydrophobically similar Ile residue and the other results in a negatively charged polar Glu residue.

MD simulation analysis for FXIIIB subunit sushi domain mutations on the FXIIIB subunit sushi domain homology-based models

A number of subtle as well as wide-ranging differences were observed during the analysis of the simulation trajectories/simulation averaged structures of individual mutations modeled on their respective homology modeled sushi domains. The *Cys5Arg* mutation showed deviation in structure indicated by higher RMSD values than its wild-type sushi domain 1 for the entire simulation time (Fig. 5A). Simulation RMSF values showed wide differences in flexibility upon mutation on neighboring hydrophobic variable length loops (Fig. 5B). Differences in cross-correlation maps were also observed especially in areas of surface exposure for the sushi domain 1 (Fig. S2). A number of hydrophobic patches were detected in the simulation averaged structure for the *Cys5Arg* mutation when compared with the wild type (Fig. 6A). Differences in surface electrostatic potentials for the simulation averaged structures (Fig. 6B) were observed for all mutations except for *Leu116Phe* and *Val217Ile* (not shown here). In fact the differences in calculated surface electrostatic potential between the wild-type and the mutated domain was the highest for the *Cys5Arg* mutation while the other mutations also showed modest to high differences (Table S1). The mutation to an Arg residue breaks the disulfide bond but also results in the gain of hydrogen bonds with

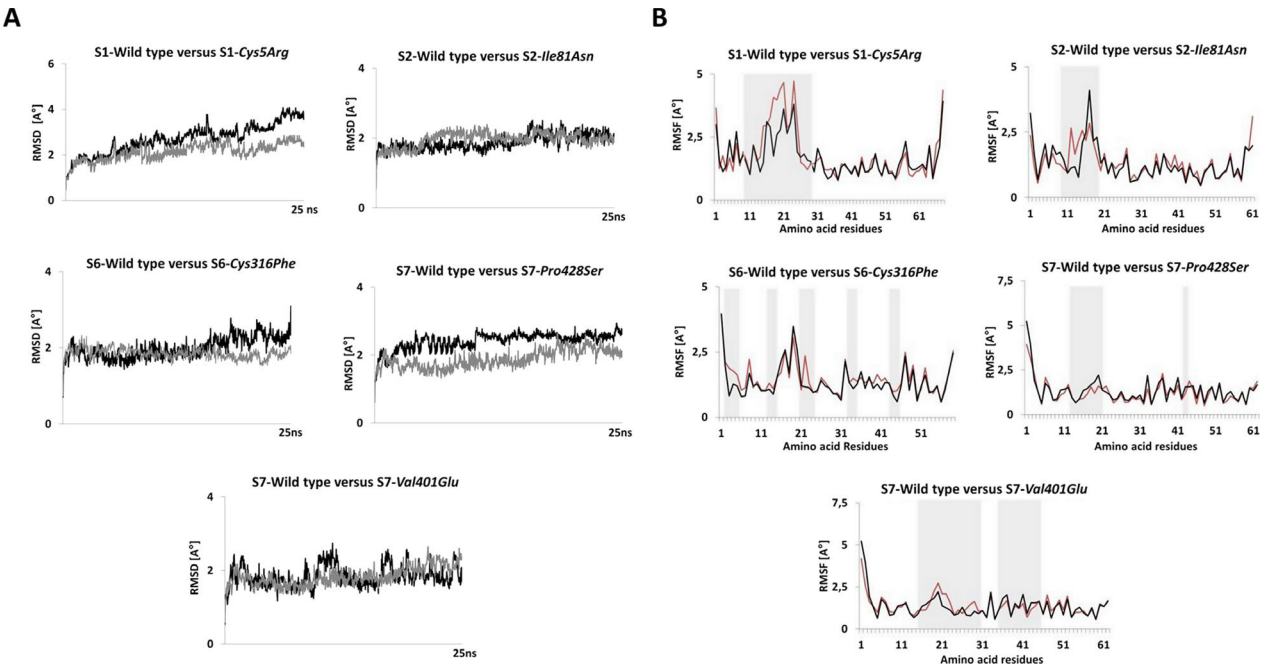

Figure 5. Simulation RMSD and RMSF comparisons for wild-type and mutated sushi domains. (A) Changes in RMSD during the 25 ns simulation for the mutated and wild-type sushi domains. Only the high impact mutations Cys5Arg, Cys316Phe, Pro428Ser that undergo significant changes in RMSD during simulation and one Ile81Asn mutation with no observable difference in RMSD are illustrated here. The dark black patterns represent wild-type RMSDs while the gray patterns represent the mutant RMSDs in each graph. (B) Observed RMSF per residue during simulation for the mutated and wild-type sushi domains. Only the high impact mutations Cys5Arg, Cys316Phe, Pro428Ser and two other mutations Ile81Asn and Val401Glu are shown here. The regions showing noticeable differences in RMSFs are shaded in gray. The red patterns represent the wild-type RMSFs while the black pattern represents the mutated RMSFs in each graph. The RMSD and RMSF calculation for the simulation trajectories were done on YASARA version 13.9.8. RMSD, root mean square deviation; RMSF, root mean square fluctuation.

Met29 (Fig. 7B). The mutation also results in the gain of accessible surface area for the mutated Arg residue side chain instead of the completely buried wild-type Cys residue (Table S2). Two other mutations, *Cys316Phe* and *Pro428Ser* also show higher RMSD values when compared with the wild type but not of the order of *Cys5Arg* (Fig. 5A). The *Cys316Phe* mutation in particular behaves close to the wild type for most of the simulation time. However, this mutation does show differences in RMSD values from that of its wild-type sushi domain when approaching the end of the stipulated simulation time, indicating a slower and lower impact mutation than the *Cys5Arg* mutation. The *Pro428Ser* mutation showed consistently higher RMSD values than the wild type during the entire simulation. The *Cys316Phe* and *Pro428Ser* mutations showed a number of differences in the cross-correlation maps (Fig. S2) indicating an impact on the correlated motion and therefore relative orientation of individual residues on the sushi domain surface. The mutation *Cys316Phe* showed one small hydrophobic patch when compared with the wild type (Fig. 6A; Table S3). This hydrophobic patch is dominated by the mutated surface exposed Phenylalanine (Phe316) which lies next to a Lys362 residue which is also surface exposed in the mutated sushi domain in comparison to its wild-type domain where it is partially buried (Fig. 7E). This hydrophobic patch is a likely target for the ubiquitin system for the clearance of this misfolded mutant variant by the proteasomal degradation pathway (since ubiquitin attaches itself to surface lysine residues) Mattiroli and Sixma et al. 2014. The *Pro428Ser* mutation shows conspicuous hydrophobic patches all over its sushi domain (Fig. 6A). The mutated Ser428 residue seems to mimic the wild-type Proresidue since there is no observable loss or gain of surface accessible surface area or a distinct change in backbone secondary structure of the residue (Fig. 7C). However, the interaction profile of the simulation averaged structure shows that this mutation leads to the loss as well as gain of several hydrogen bonds/salt bridges (Fig. 7D). This might be principally responsible for altering the native fold and exposing the observed hydrophobic patches. The simulation run for the *Val401Glu* mutation does not show remarkable changes in RMSD (Fig. 5A). The average RMSDs though do show small differences between the wild type and mutant (0.113 Å). The RMSF values for *Pro428Ser* and *Cys316Phe* mutations show small changes in flexibility in regions spread across the sushi domains (Fig. 5B). The mutations *Ile81Asn* and *Val401Glu* also show differences in RMSF values between the mutated and the wild-type sushi domains suggesting influences on domain flexibility. The other two mutations (*Leu116Phe* and *Val217Ile*) do not show any remarkable differences in RMSD or RMSF values (data not shown here). The free energy calculations made across different servers consensually suggest a destabilizing influence for almost all mutations except for *Leu116Phe* and *Val217Ile* (Table S4). Our simulation analysis agrees best with the results obtained with the FoldX tool, Eris and Imut 2.0 server in that the two Cys mutations and one Pro mutation seem to have the highest impact on domain stability. The *Val401Glu* mutation also had high destabilizing free energy values across almost all free energy evaluation servers tested in this study.

Discussion

The missense mutations investigated in our study have been reported in heterozygous form in patients with mild FXIII deficient phenotype. The occurrence of heterozygous mutations is a phenomenon not uncommon to sushi domain-containing proteins as was earlier observed by Goodship (2006) and Dragon-Durey et al. (2004) in CFH proteins. The heterozygous form of expression in our study conclusively demonstrates that these mutations can be classified into three major types: (1) Mutations which show influence on antigenic stability (and therefore are partially corrected for their phenotype when coexpressed with the wild type) (2) Mutations which have no influence on antigenic stability and therefore their impact is limited to interference in protein–protein interactions (i.e., dimer/heteromer assembly) and (3) Mutations which influence antigenic stability as well as binding interactions. The two cysteine mutations, *Cys316Phe* and *Cys5Arg* and the proline mutation, *Pro428Ser* clearly belong to the first as well as last group. In our earlier study we had observed differential rate/pattern of secretion for almost all FXIIIB missense mutations investigated (Biswas et al. 2013). In the current study, we have gone a step further to look for intracellular accumulation followed by possible downregulation of these mutations by the unfolded protein response. Amongst the high impact mutations, only *Cys5Arg* was observed to accumulate within the ER following which the mutant protein is cleared off by the unfolded protein response of the cell. This was clearly demonstrated since on one hand almost equivalent amount of protein was observed colocalized with the ER for the mutated protein (when compared with the wild type), almost none to nonsignificant amounts of protein was observed in the Golgi indicating an immediate response from the quality control system of the cell. The structural analysis also demonstrated that the mutation most likely results in structural destabilization (high RMSDs) and strong hydrophobic patches on the surface of the protein/domain which will elicit a strong unfolded protein response. As a result almost no protein is observed in the secreted medium for the *Cys5Arg* mutation. The influence of the unfolded protein

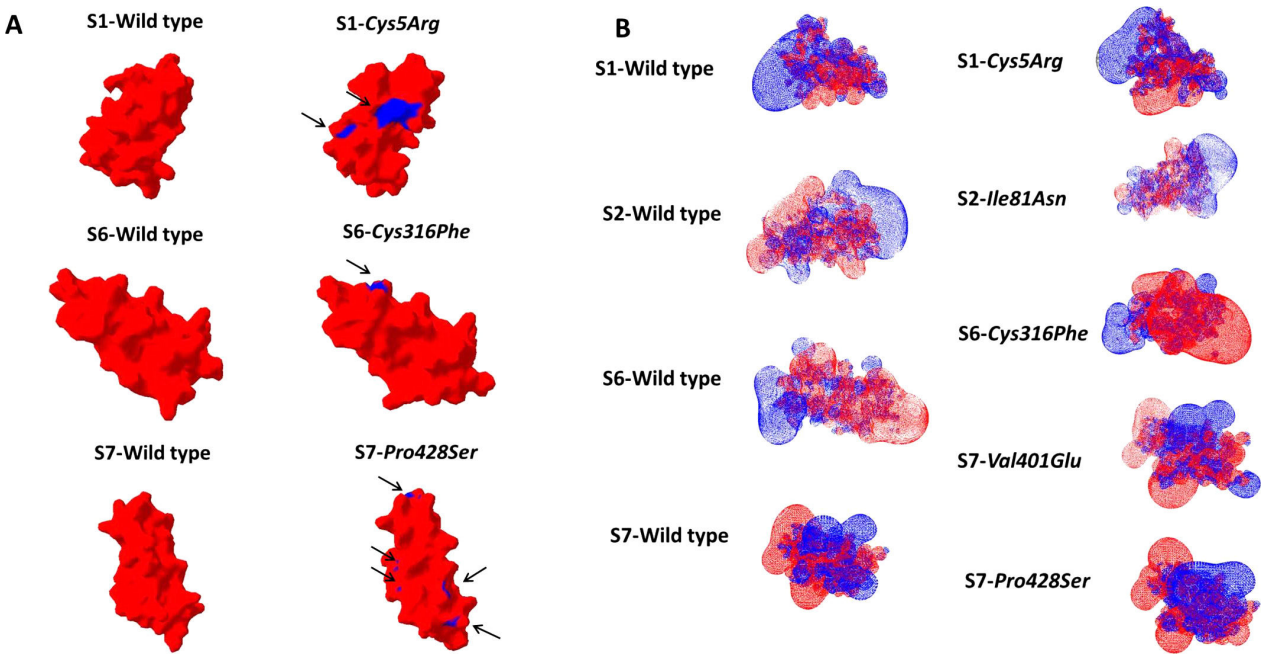

Figure 6. Surface electrostatic potential and Hydrophobic patch representations of Sushi domains. (A) Surface electrostatic potential map for the simulation averaged structures of wild-type sushi domains alongside the simulation-averaged structures of their corresponding mutated sushi domains. The images have been generated on SWISS-PDB viewer. The surface electrostatic potential calculations were made using the Poisson-Boltzmann method utilizing partial charges of atoms. The default dielectric constant of four for the protein and 80 for the solvent were used during calculations. An ionic strength of 50 mmol/L was used during calculations. Red color denotes negative potential while blue denotes positive potential. (B) Hydrophobic patches as determined with the SWISS-PDB viewer tool for simulation averaged structures of wild-type and mutated sushi domains. Surface representations of the sushi domains are shown. Hydrophobic patches are colored blue while the rest of the domain is colored red. The combined calculated areas of all hydrophobic patches for each sushi domain (in those detected) have been tabulated in Table S2.

response on the mutated protein is further demonstrated when upon inhibition of the proteasome (by Lactacystin) we observe a correction of the expression phenotype. The other two high impact mutations *Cys316Phe* and *Pro428-Ser* do not seem to have an accumulative influence on the respective variant proteins as no accumulation is seen in either ER or Golgi. However, structural analysis does show the presence of hydrophobic patches as well as a destabilizing influence (high RMSDs) on their respective domains. This is further supported by the fact that while the mutated variants are observed in both Golgi and ER, their amounts are significantly reduced. This suggests that these mutations do elicit a weak unfolded protein response (in comparison to *Cys5Arg*) which leads to reduced protein secretion. The highest difference in post-Lactacystin-induced antigenic values was observed for *Pro428Ser*. While some antigen from all three of these mutations (*Cys5Arg*, *Cys316Phe*, and *Pro428Ser*) does get secreted into the medium, this variant protein is still likely to be nonfunctional owing to altered surface electrostatics which will prevent its association with the $FXIIIA_2$ subunit and therefore also influence heterotetramer assembly. This is further demonstrated by the low CTP values for the *Pro428Ser* and *Cys316Phe* mutations (the *Cys5Arg* mutation was not evaluated as explained before owing to very low antigenic values). The high degree of structural and sequence conservation and the *in silico* calculated folding energy values observed for the wild-type residues corresponding to these three mutations (*Cys5Arg*, *Cys316Phe*, and *Pro428Ser*) lend further credence to the idea that these mutations primarily have a destabilizing effect on the protein. Furthermore, our confocal analysis confirms that amongst these three mutations, *Cys5Arg* is the only true accumulative/secretion-based defect resulting in ER accumulation and subsequent degradation. Interestingly, although *Cys5Arg* and *Cy316Phe* both break structural disulfide bonds their detailed expression/confocal phenotype (one results in accumulation/degradation while other shows no accumulation/lower rate of degradation) is different. This dichotomy has been observed in cysteine mutations from the sushi domains of CFH protein also. Saunders et al. (2006) tabulated that amongst eight reported cysteine substitutions which break structural disulfide bonds, six

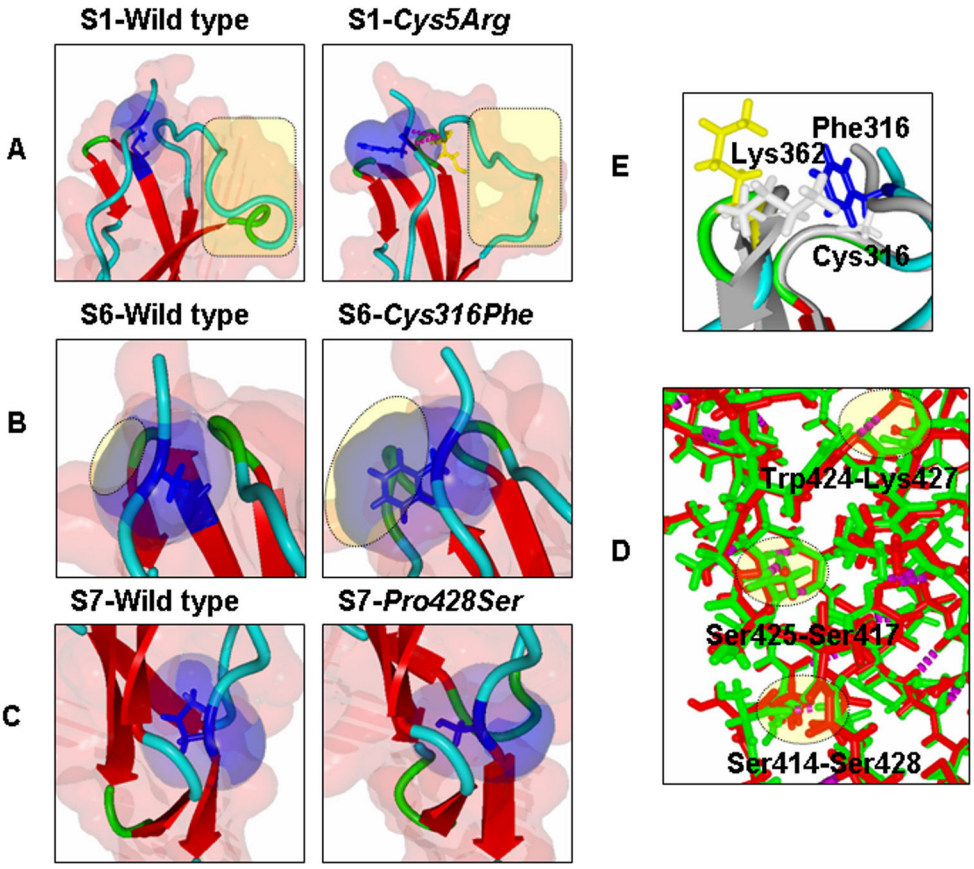

Figure 7. Close up views of the local molecular environment of reported missense mutations. (A–C) Depicts side-by-side local molecular environments for the mutations *Cys5Arg*, *Cys316Phe*, *Pro428Ser* with their wild-type sushi domains. The backbone is presented in ribbon format. Residue(s) of interest are depicted in stick format. Also depicted is the solvent accessible area (transparent red for the entire object and transparent blue for the residue of interest). In (A) and (B) it is quite apparent that mutation results in significant gain of accessible surface area. Also in (A) the mutated Arg residue is observed to form hydrogen bonds with Met 29. (C) Both the mutated Ser and the wild-type Proresidue look similar in terms of accessible surface areas and the secondary structure. (D) Close up view of superimposed structures of the mutated (for Cys316Phe) and wild-type S6 sushi domain. The backbones are depicted in ribbon format. The wild-type backbones as well as residues are colored gray while the backbone of the mutated sushi domain is colored with respect to its secondary structure. The mutated Phe316 residue is colored blue and the neighboring residue Lys362 is colored yellow in the mutated sushi domain. These residues are depicted as stick models in both wild-type and mutated sushi domain structures. The mutated Phe316 is surface exposed as opposed to the Cys316, which is completely buried. Also surface exposed is the Lys362 in the mutated structure while in the wild-type structure it is partially buried. (E) Superimposition of S7 wild-type sushi domain (green) and S7 mutated (for Pro428Ser) sushi domain (red) structures. Backbones are depicted as stick models. Hydrogen bonds are shown as magenta dots. The hydrogen bonds lost or gained are shaded yellow and also labeled with the residues participating in the particular bond. Structural alignments for (D) and (E) were done using the MUSTANG function embedded in YASARA.

resulted in the loss of stability/incorrect folding and reduced antigen levels. The other two mutations, *p.Cys630Trp* (*c.1890T>G*) and *p.Cys1043Arg* (*c.3127T>C*) in the 11th and 17th sushi domains, respectively, showed normal antigen levels. Therefore, we hypothesize that in spite of forming structural disulfide bonds; cysteines in FXIIIB subunit (and other sushi domain-containing proteins) are likely to show strong functional diversity. The mutations *Ile81Asn* and *Val401Glu* both show near wild-type-like phenotype and slightly attenuated level phenotype, respectively, in terms of secretion/confocal phenotype. *In silico* analysis did not show any major implications for these two mutations on the stability of their respective sushi domains. What both mutations clearly show are changes in the surface electrostatic potential for their respective domains. Previous literature suggests that sushi domain interactions are primarily electrostatic mediated and that sushi domains can be classified into functional groups on the basis of their surface electrostatic properties (Soares et al. 2005). This coupled with the fact that both show reduced CTPP values (when compared with the wild type) suggests that these mutations primarily influence binding to the $FXIIIA_2$ subunit and therefore $FXIIIA_2B_2$ heterotetramer assembly since

native PAGE ruled out any impaired dimer formation (data not shown; although a qualitative effect cannot be ruled out). Previous literature suggests that sushi domain interactions are primarily electrostatic mediated and that sushi domains can be classified into functional groups on the basis of their surface electrostatic properties (Soares et al. 2005). The *Val401Glu* mutation might additionally have a mild destabilizing effect in addition to influencing binding to the FXIIIA subunit (as evidenced by differences in average RMSDs from the wild type, minor gain of accessible surface area, radius of gyration over the wild type and folding free energy calculations). The sushi domain 2 of the FXIIIB subunit on which the *Ile81Asn* mutation occurs has now been conclusively shown to participate in interaction with the FXIIIA subunit (Katona et al. 2014). The interface region for this sushi domain shown in this study is proximal to our reported mutation. Sushi domain 7, on which the *Val401Glu* mutation occurs has so far showed no role in FXIIIA subunit interaction or FXIIIB subunit dimerization (Souri et al. 2008). However, since the entire heterotetramer assembly is assumed to be cooperative in nature the participation of other domains has not been ruled out as yet. This mutation results in the replacement of a highly sequence and structurally conserved non polar residue with a negatively charged Glu residue which explains for the difference in the electrostatic potential surface observed for the mutated sushi domain from the wild-type sushi domain. This also explains the reduced CTPP values from our study for the *Val401Glu* mutation which further confirms its impact on heterotetramer assembly.

The remaining two mutations, *Leu116Phe* and *Val217Ile* are observed to be pathologically neutral in terms of secretion, structural and functional stability. No effect on heterotetramer assembly was observed for these two mutations. Low degree of sequence and structural conservation further supports the neutral status of these two mutations. Minor influences on the rate of biosynthesis still cannot be ruled out for these two variant within the current experimental set up. Even in the event of a minor influence, these variants are most likely candidate functional polymorphisms rather than true causative mutations.

We have therefore using a host of functional, structural/computational analysis successfully determined the underlying molecular mechanisms for the causality of seven FXIIIB subunit variants which we had earlier reported in heterozygous form from patients with mild FXIII deficiency. We found that three of these mutations (*Cys5Arg*, *Cys316Phe*, and *Pro428Ser*) cause antigenic instability as well as reduced binding to FXIIIA subunit, two (*Ile81Asn* and *Val401Glu*) cause impaired FXIIIA subunit binding while maintaining antigenic stability. Only one mutation in the entire lot (*Cys5Arg*) showed a true accumulative/secretion-based defect while two (*Leu116Phe* and *Val217Ile*) others seem to have neutral status.

Acknowledgment

The authors acknowledge CSL Behring for funding research on FXIII, and Sophie Lyonga and the diagnostic laboratory for technical help. The authors also acknowledge Zaid Aburubaiha for technical support and advice. A. B. and J. O. are the principle investigators of the study. AT and the experimental data. A. B. performed and collected the *in silico* data. A. B., A. T. analyzed the data. A. B., A. T., V. I., and J. O. edited and co-wrote the article. A. B. designed the study.

Conflict of Interest

None declared.

References

Adler, J., and I. Parmryd. 2010. Quantifying colocalization by correlation: the Pearson correlation coefficient is superior to the Mander's overlap coefficient. Cytometry A 77:733–742.

Biswas, A., V. Ivaskevicius, R. Seitz, A. Thomas, and J. Oldenburg. 2011. An update of the mutation profile of Factor 13 A and B genes. Blood Rev. 25:193–204.

Biswas, A., A. Thomas, C. G. Bevans, V. Ivaskevicius, and J. Oldenburg. 2013. In vitro secretion deficits are common among human coagulation factor XIII subunit B missense mutants: correlations with patient phenotypes and molecular models. Hum. Mutat. 34:1490–1500.

Biswas, A., V. Ivaskevicius, A. Thomas, and J. Oldenburg. 2014a. Coagulation factor XIII deficiency. Diagnosis, prevalence and management of inherited and acquired forms. Hamostaseologie 34:160–166.

Biswas, A., V. Ivaskevicius, A. Thomas, M. Varvenne, B. Brand, H. Rott, et al. 2014b. Eight novel F13A1 gene missense mutations in patients with mild FXIII deficiency: in silico analysis suggests changes in FXIII-A subunit structure/function. Ann. Hematol. 93:1665–1676.

Capriotti, E., P. Fariselli, and R. Casadio. 2005. I-Mutant2.0: predicting stability changes upon mutation from the protein sequence or structure. Nucleic Acids Res. 33:W306–W310.

Dragon-Durey, M. A., V. Fremeaux-Bacchi, C. Loirat, J. Blouin, P. Niaudet, G. Deschenes, et al. 2004. Heterozygous and homozygous factor h deficiencies associated with hemolytic uremic syndrome or membranoproliferative glomerulonephritis: report and genetic analysis of 16 cases. J. Am. Soc. Nephrol. 15:787–795.

Gaboriaud, C., V. Rossi, I. Bally, G. J. Arlaud, and J. C. Fontecilla-Camps. 2000. Crystal structure of the catalytic domain of human complement c1s: a serine protease with a handle. EMBO J. 19:1755–1765.

Goodship, T. H. 2006. Factor H genotype-phenotype correlations: lessons from aHUS, MPGN II, and AMD. Kidney Int. 70:12–13.

Guex, N., M. C. Peitsch, and T. Schwede. 2009. Automated comparative protein structure modeling with SWISS-MODEL and Swiss-PdbViewer: a historical perspective. Electrophoresis 30(Suppl. 1):S162–S173.

Ichinose, A., B. A. McMullen, K. Fujikawa, and E. W. Davie. 1986. Amino acid sequence of the b subunit of human factor XIII, a protein composed of ten repetitive segments. Biochemistry 25:4633–4638.

Ivaskevicius, V., A. Biswas, C. Bevans, V. Schroeder, H. P. Kohler, H. Rott, et al.2010a. Identification of eight novel coagulation factor XIII subunit A mutations: implied consequences for structure and function. Haematologica 95:956–962.

Ivaskevicius, V., A. Biswas, R. Loreth, V. Schroeder, S. Ohlenforst, H. Rott, et al. 2010b. Mutations affecting disulphide bonds contribute to a fairly common prevalence of F13B gene defects: results of a genetic study in 14 families with factor XIII B deficiency. Haemophilia 16:675–682.

Katoh, K., and D. M. Standley. 2013. MAFFT multiple sequence alignment software version 7: improvements in performance and usability. Mol. Biol. Evol. 30:772–780.

Katona, E., K. Penzes, A. Csapo, F. Fazakas, M. L. Udvardy, Z. Bagoly, et al. 2014. Interaction of factor XIII subunits. Blood 123:1757–1763.

Konc, J., and D. Janezic. 2010a. ProBiS: a web server for detection of structurally similar protein binding sites. Nucleic Acids Res. 38:W436–W440.

Konc, J., and D. Janezic. 2010b. ProBiS algorithm for detection of structurally similar protein binding sites by local structural alignment. Bioinformatics 26:1160–1168.

Kopp, A., M. Hebecker, E. Svobodova, and M. Jozsi. 2012. Factor h: a complement regulator in health and disease, and a mediator of cellular interactions. Biomolecules 2:46–75.

Krieger, E., G. Koraimann, and G. Vriend. 2002. Increasing the precision of comparative models with YASARA NOVA–a self-parameterizing force field. Proteins 47:393–402.

Krivov, G. G., M. V. Shapovalov, and R. L. Jr Dunbrack. 2009. Improved prediction of protein side-chain conformations with SCWRL4. Proteins 77:778–795.

Lorand, L., M. S. Losowsky, and K. J. Miloszewski. 1980. Human factor XIII: fibrin-stabilizing factor. Prog. Hemost. Thromb. 5:245–290.

Mattiroli, F., and T. K. Sixma. 2014. Lysine-targeting specificity in ubiquitin and ubiquitin-like modification pathways. Nat. Struct. Mol. Biol. 21:308–316.

Perkins, S. J., R. Nan, K. Li, S. Khan, and A. Miller. 2012. Complement factor H-ligand interactions: self-association, multivalency and dissociation constants. Immunobiology 217:281–297.

Pires, D. E., D. B. Ascher, and T. L. Blundell. 2014a. mCSM: predicting the effects of mutations in proteins using graph-based signatures. Bioinformatics 30:335–342.

Pires, D. E., D. B. Ascher, and T. L. Blundell. 2014b. DUET: a server for predicting effects of mutations on protein stability using an integrated computational approach. Nucleic Acids Res. 42:W314–W319.

Radek, J. T., J. M. Jeong, J. Wilson, and L. Lorand. 1993. Association of the A subunits of recombinant placental factor XIII with the native carrier B subunits from human plasma. Biochemistry 32:3527–3534.

Richter, S., A. Wenzel, M. Stein, R. R. Gabdoulline, and R. C. Wade. 2008. webPIPSA: a web server for the comparison of protein interaction properties. Nucleic Acids Res. 36:W276–W280.

Saunders, R. E., T. H. Goodship, P. F. Zipfel, and S. J. Perkins. 2006. An interactive web database of factor H-associated hemolytic uremic syndrome mutations: insights into the structural consequences of disease-associated mutations. Hum. Mutat. 27:21–30.

Schneider, C. A., W. S. Rasband, and K. W. Eliceiri. 2012. NIH Image to ImageJ: 25 years of image analysis. Nat. Methods 9:671–675.

Soares, D. C., D. L. Gerloff, N. R. Syme, A. F. Coulson, J. Parkinson, and P. N. Barlow. 2005. Large-scale modelling as a route to multiple surface comparisons of the CCP module family. Protein Eng. Des. Sel. 18:379–388.

Souri, M., H. Kaetsu, and A. Ichinose. 2008. Sushi domains in the B subunit of factor XIII responsible for oligomer assembly. Biochemistry 47:8656–8664.

Van Durme, J., J. Delgado, F. Stricher, L. Serrano, J. Schymkowitz, and F. Rousseau. 2011. A graphical interface for the FoldX forcefield. Bioinformatics 27:1711–1712.

Waterhouse, A. M., J. B. Procter, D. M. Martin, M. Clamp, and G. J. Barton. 2009. Jalview Version 2–a multiple sequence alignment editor and analysis workbench. Bioinformatics 25:1189–1191.

Worth, C. L., R. Preissner, and T. L. Blundell. 2011. SDM–a server for predicting effects of mutations on protein stability and malfunction. Nucleic Acids Res. 39:W215–W222.

Yin, S., F. Ding, and N. V. Dokholyan. 2007. Eris: an automated estimator of protein stability. Nat. Methods 4:466–467.

Supporting Information

Additional Supporting Information may be found in the online version of this article:

Figure S1. Proteasomal inhibition by lactacystin. The bar graphs in this image represent the difference in FXIIIB antigen values with and without lactacystin treatment (Proteasome inhibition). The wild type is represented by dark black bar while all the other mutations are represented by dark gray bars. A dotted black line marks the difference in antigenic level (i.e., for the wild type) above

which any observation would be considered an effect on proteasome due to the mutation.

Figure S2. DCCM map for simulation trajectories. This image depicts the DCCM (dynamic cross-correlation matrices) map of each mutation's simulation trajectory compared with its wild-type sushi domain simulation trajectory. The yellow regions show positive correlation (proportional to its intensity) and the blue regions shows negative correlation.

Figure S3. Confocal microscopy images for all variants. This image shows the co-localization pattern for all missense mutations with ER and Golgi in comparison with the wild type. The image coding is the same as in the main Figure 2.

Table S1. Surface electrostatic potential differences between the mutant and wild-type sushi domains.

Table S2. Accessible surface area and radius of gyration for simulation averaged wild-type and mutant structures.

Table S3. Exposed hydrophobic patches for each mutation.

Table S4. Free energy changes calculated for each mutation across various protein stability prediction servers.

Molecular Genetics & Genomic Medicine

Supplementary files

Structural and functional influences of coagulation factor XIII subunit B heterozygous missense mutants

Anne Thomas[1†], Arijit Biswas[1†*], Vytautas Ivaskevicius[1], Johannes Oldenburg[1*]

[1]Institute of Experimental Haematology and Transfusion Medicine, University Clinic Bonn, 53105 Bonn, Germany;

Running head title: Molecular defects underlying FXIIIB missense mutations

[†]These authors contributed equally to this work.

*Correspondence to:

Arijit Biswas, Institute of Experimental Haematology and Transfusion Medicine, University Clinic Bonn, Sigmund Freud Str. 25, 53127 Bonn, Germany.
Email: arijit.biswas@ukb.uni-bonn.de
phone: +49 228 287 19428
fax: +49 228 287 14320

or

Johannes Oldenburg, Institute of Experimental Haematology and Transfusion Medicine,
University Clinic Bonn, Sigmund Freud Str. 25, 53105 Bonn, Germany.
Email: johannes.oldenburg@ukb.uni-bonn.de
phone: +49 228 287 15175
fax: +49 228 287 14783

Figure S1. Proteasomal inhibition by lactacystin. The bar graphs in this image represent the difference in FXIIIB antigen values with and without lactacystin treatment (Proteasome inhibition). The wild type is represented by dark black bar while all the other mutations are represented by dark grey bars. A dotted black line marks the difference in antigenic level (i.e. for the wild type) above which any observation would be considered an effect on proteasome due to the mutation.

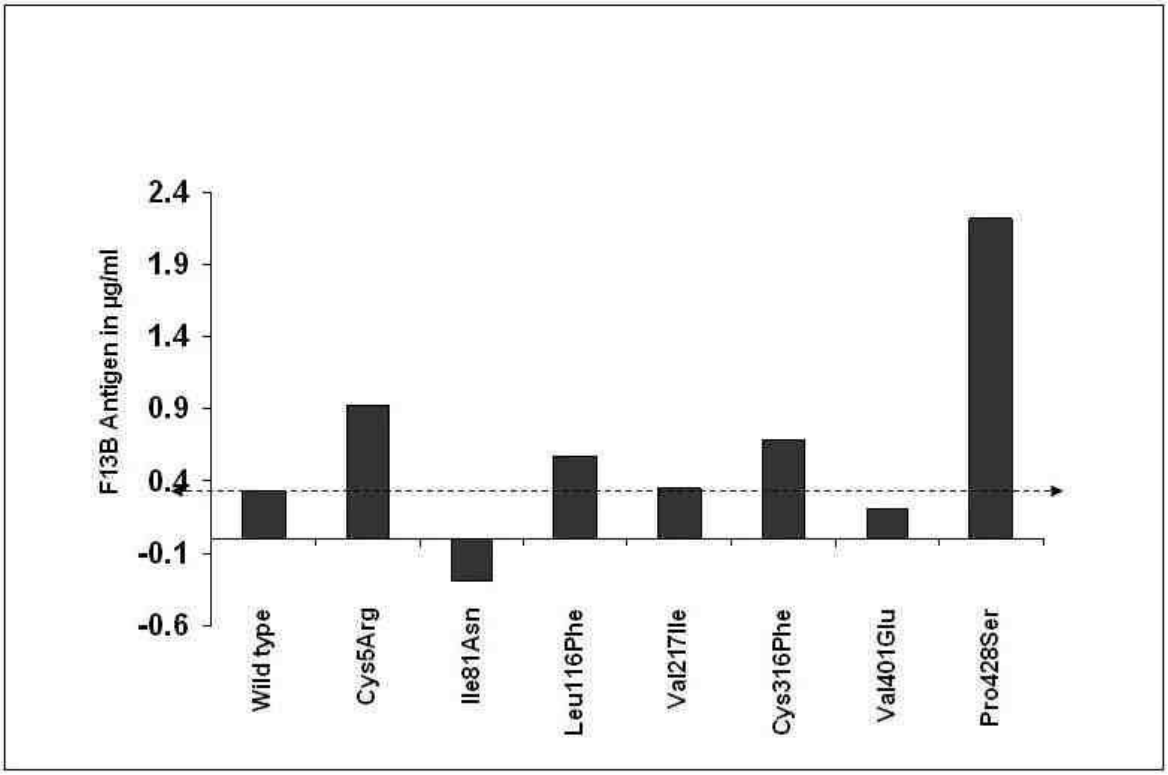

Figure S2. DCCM map for simulation trajectories. This image depicts the DCCM (dynamic cross correlation matrices) map of each mutation´s simulation trajectory compared with its wild type sushi domain simulation trajectory. The yellow regions show positive correlation (proportional to its intensity) and the blue regions shows negative correlation.

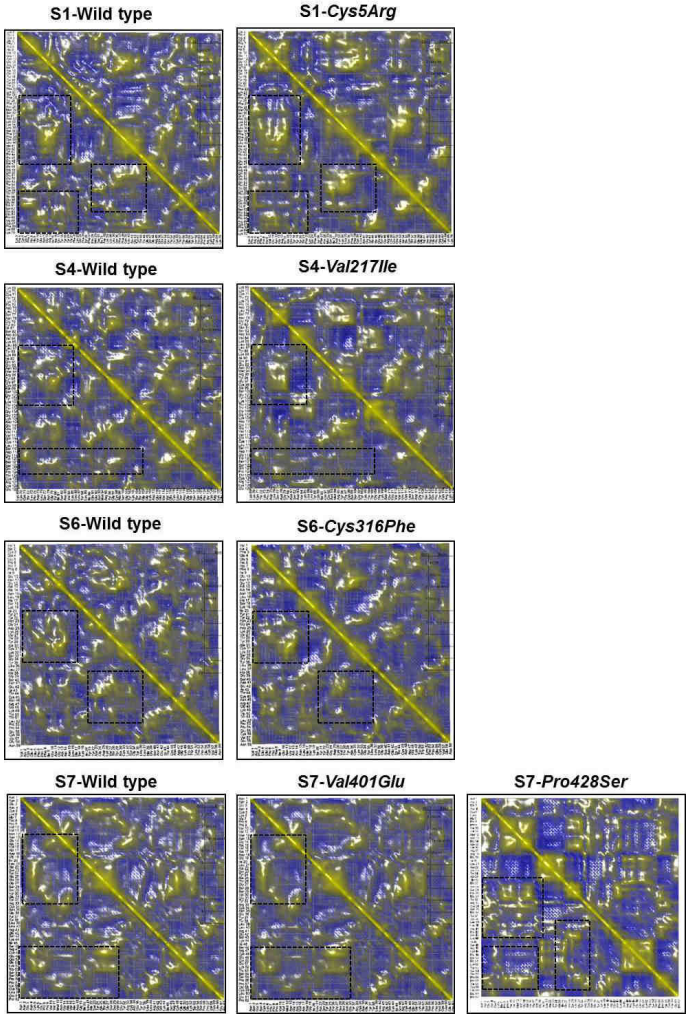

Figure S3. Confocal microscopy images for all variants. This image shows the co-localization pattern for all missense mutations with ER and Golgi in comparison with the wild type. The image coding is the same as in the main Figure 2.

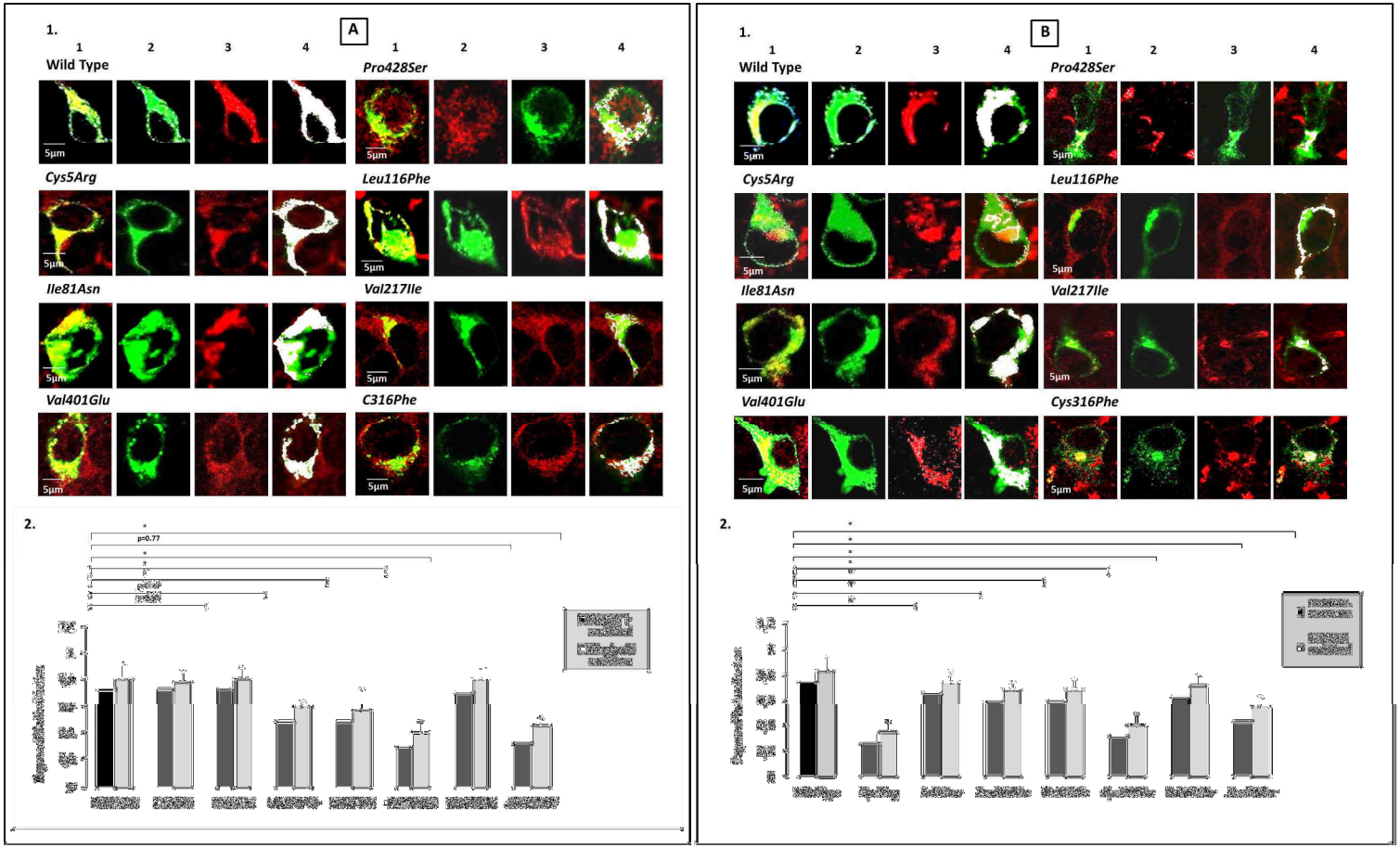

Table S1. Surface electrostatic potential differences between the mutant and wild type sushi domains.
Distance/difference values range from 0-2. Higher values represent larger differences/distances.

Mutation vs Wild type	Surface electrostatic potential difference/distance
Cys5Arg vs S1	0.61482
Ile81Asn vs S2	0.36878
Leu116Phe vs S2	0.10232
Val217Ile vs S4	0.11372
Cys316Phe vs S6	0.24495
Pro428Ser vs S7	0.48785
Val401Glu vs S7	0.38471

Table S2. Accessible surface area and radius of gyration for simulation averaged wild type and mutant structures.
Abbreviations: WT: Wild type, ROG: Radius of gyration, MT: Mutant type, ASA: Accessible surface area.

WT	ASA(Å^2)	ROG(Å)	MT	ASA(Å^2)	ROG(Å)	MT	ASA(Å^2)	ROG(Å)
S1	4823.9	12.421	Cys5Arg	5172.92	12.545			
S2	3959.05	11.852	Ile81Asn	4007.93	12.075	Leu116Phe	4008	11.932
S4	4155.98	12.089	Val217Ile	4162.06	12.124			
S6	3975.92	12.048	Cys316Phe	4164.9	12.263			
S7	3983.23	12.693	Val401Glu	4135.44	13.104	Pro428Ser	4427.03	12.157

Table S3. Exposed hydrophobic patches for each mutation.

Mutation	Surface area(Å^2)
Cys5Arg	175
Ile81Asn	None
Leu116Phe	None
Val217Ile	None
Cys316Phe	31
Val401Glu	None
Pro428Ser	184

Table S4. Free Energy changes calculated for each mutation across various protein stability prediction servers.
Free energy values (ΔΔG) expressed as Kcal/mol. Interpretation for the FOLDX and ERIS server: ΔΔG>0, mutation is destabilizing; for other servers: ΔΔG<0 mutation is destabilizing

Mutation	SDM	FoldX	mCSM	DUET	Imutant 2.0	Eris
Cys5Arg	-0.88	15.61	-1.07	-0.769	-1.95	3.32
Ile81Asn	-3.54	1.78	-1.17	-1.165	0.92	3.92
Leu116Phe	0.19	0.56	-1.332	-1.442	1.75	2.59
Val217Ile	0.17	0.72	-0.486	-0.159	0.7	1.06
Cys316Phe	-0.56	9.12	-0.951	-1.139	-2.14	>10
Val401Glu	-3.04	1.07	-1.652	-1.816	-1.02	>10
Pro428Ser	-1.92	12.41	-1.749	-1.833	-3.22	5.17

Publication 3

Accepted for publication in *Human mutation* as a Research article and features as the cover page for the October issue of *Human mutation*

Title: Coagulation Factor XIIIA subunit missense mutations affect structure and function at the various steps of factor XIII action

Authors: Anne Thomas[1†], Arijit Biswas[1†], Johannes Dodt[2], Helen Philippou[3], Emma Hethershaw[3], Hans Juergen Ensikat[4], Vytautas Ivaskevicius[1], Johannes Oldenburg[1]

[1]Institute of Experimental Haematology and Transfusion Medicine, University Clinic Bonn, 53127 Bonn, Germany

[2]Paul Ehrlich Institut, 63225 Langen, Germany.

[3]Leeds Institute for Cardiovascular and Metabolic Medicine, University of Leeds, Leeds, UK.

[4]Nees Institute for Biodiversity of Plants, University of Bonn, Bonn, Germany.

[†]Equally contributing first author

Abstract

Inherited defects of coagulation Factor XIII (FXIII) can be categorized into severe and mild forms based on their genotype and phenotype. Heterozygous mutations occurring in *F13A1* and *F13B* genes causing mild FXIII deficiency have been reported only in the last few years primarily because the mild FXIII deficiency patients are often asymptomatic unless exposed to some kind of a physical trauma. However, unlike mutations causing severe FXIII deficiency, many of these mutations have not been comprehensively characterized based on expression studies. In our current article we have transiently expressed 16 previously reported missense mutations detected in the *F13A1* gene of patients with mild FXIII deficiency and analyzed their respective expression phenotype. Complimentary to expression analysis we have used *in silico* analysis to understand and explain some of the *in vitro* findings. The expression phenotype has been evaluated with a number of expression phenotype determining assays. We observe that the mutations influence different aspects of FXIII function and can be functionally categorized on the basis of their expression phenotype. We identified mutations which even in heterozygous form would have strong impact on the functional status of the protein (namely mutations *p.Arg716Gly/ p.Arg704Gln/ p.Gln602Lys/ p.Leu530Pro/ p.His343Tyr/ p.Pro290Arg/ p.Arg172Gln*).

RESEARCH ARTICLE

Human Mutation

OFFICIAL JOURNAL HGVS HUMAN GENOME VARIATION SOCIETY www.hgvs.org

Coagulation Factor XIIIA Subunit Missense Mutations Affect Structure and Function at the Various Steps of Factor XIII Action

Anne Thomas,[1†] Arijit Biswas,[1*†] Johannes Dodt,[2] Helen Philippou,[3] Emma Hethershaw,[3] Hans Juergen Ensikat,[4] Vytautas Ivaskevicius,[1] and Johannes Oldenburg[1*]

[1]*Institute of Experimental Haematology and Transfusion Medicine, University Clinic Bonn, Bonn, Germany;* [2]*Paul Ehrlich Institut, Langen, Germany;* [3]*Leeds Institute for Cardiovascular and Metabolic Medicine, University of Leeds, Leeds, UK;* [4]*Nees Institute for Biodiversity of Plants, University of Bonn, Bonn, Germany*

Communicated by John McVey

Received 16 December 2015; revised 6 June 2016; accepted revised manuscript 17 June 2016.
Published online 1 July 2016 in Wiley Online Library (www.wiley.com/humanmutation). DOI: 10.1002/humu.23041

ABSTRACT: Inherited defects of coagulation Factor XIII (FXIII) can be categorized into severe and mild forms based on their genotype and phenotype. Heterozygous mutations occurring in *F13A1* and *F13B* genes causing mild FXIII deficiency have been reported only in the last few years primarily because the mild FXIII deficiency patients are often asymptomatic unless exposed to some kind of a physical trauma. However, unlike mutations causing severe FXIII deficiency, many of these mutations have not been comprehensively characterized based on expression studies. In our current article, we have transiently expressed 16 previously reported missense mutations detected in the *F13A1* gene of patients with mild FXIII deficiency and analyzed their respective expression phenotype. Complimentary to expression analysis, we have used in silico analysis to understand and explain some of the in vitro findings. The expression phenotype has been evaluated with a number of expression phenotype determining assays. We observe that the mutations influence different aspects of FXIII function and can be functionally categorized on the basis of their expression phenotype. We identified mutations which even in heterozygous form would have strong impact on the functional status of the protein (namely mutations *p.Arg716Gly*, *p.Arg704Gln*, *p.Gln602Lys*, *p.Leu530Pro*, *p.His343Tyr*, *p.Pro290Arg*, and *p.Arg172Gln*).

Hum Mutat 00:1–12, 2016.

KEY WORDS: molecular basis of inherited coagulopathies; Factor XIII(FXIII)deficiency; *F13A1*; *F13B*; expression analysis; in silico structural analysis

Introduction

One of the key players in hemostasis is the plasma circulating Factor (F) XIII, a protransglutaminase that is responsible for the last step of the coagulation cascade in which it covalently crosslinks preformed fibrin clots to make them resistant to premature fibrinolysis [Lorand et al., 1980]. The plasma FXIII zymogen is a heterotetrameric complex comprising of two catalytic A ($FXIIIA_2$) and two protective carrier B-subunits ($FXIIIB_2$), which are synthesized and secreted into the plasma as homodimers from various cell types like monocytes/macrophages, megakaryocytes, and platelets for the A subunit and hepatocytes for the B subunit [Muszbek et al., 2011]. The $FXIIIA_2B_2$ complex has been suggested to be associated with fibrinogen in plasma. The polymerized form of fibrinogen, fibrin is also a known cofactor for the activation of FXIII. Structurally, each A monomeric subunit is composed of an activation peptide (residues 1–38) and four distinct domains: beta-sandwich (residues 39–184), central core (residues 185–516), barrel 1 (residues 517–628), and barrel 2 regions (residues 629–732) [Komaromi et al., 2011]. The monomeric B subunit on the other hand is composed of 10 tandem repeats or glycoprotein-I (GP-I) structures designated as Sushi domains, which are also observed in proteins of the complement system [Ichinose et al., 1986]. The activation of plasmatic $FXIIIA_2B_2$ is the combined effect of the proteolytic cleavage (by thrombin) of a 37 amino acid long N-terminal peptide, the activation peptide (FXIII-AP), from the $FXIIIA_2$-subunit and calcium binding to specific $FXIIIA_2$ subunit calcium binding sites [Schroeder et al., 2007; Komaromi et al., 2011; Stieler et al., 2013]. These two actions lead to the dissociation of the $FXIIIB_2$-subunits and conformational changes in the zymogenic FXIII converting its closed structure to a more open activated form, thereby exposing the active site to substrate access [Komaromi et al., 2011; Stieler et al., 2013]. In addition, to mediating fibrin chain crosslinking, FXIII also crosslinks fibrinolytic inhibitors such as α-2-antiplasmin into the fibrin clot. Alpha-2-antiplasmin is a serine protease inhibitor (serpin), which renders the fibrin clot less susceptible to fibrinolysis by inhibiting plasmin within the clot [Fraser et al., 2011; van Giezen et al., 1993]. Therefore, the complete mechanism of FXIII activation and regulation is a complex process mediated by a number of protein–protein interactions and protein conformational changes. Defect in any of these steps can lead to the complete disruption of regulated FXIII activation and activity. FXIII deficiency can be of both acquired and congenital origin (MIM# 613225 and MIM# 613235) [Biswas et al., 2011; Biswas et al., 2014a]. The clinical manifestation of severe congenital FXIII deficiency resulting from homozygous/complex

Additional Supporting Information may be found in the online version of this article.

†These authors contributed equally to this work.

Contract Grant Sponsors: BONFOR Grant (2010–2012) (O-145.0009); NovoNordisk (2009–2012) (N.045.0141); CSL Behring (2015–2016) (N.045.0180).

*Correspondence to: Arijit Biswas, Institute of Experimental Haematology and Transfusion Medicine, University Clinic Bonn, Sigmund Freud Str. 25, 53127 Bonn, Germany. E-mail: arijit.biswas@ukb.uni-bonn.de; Johannes Oldenburg, Institute of Experimental Haematology and Transfusion Medicine, University Clinic Bonn, Sigmund Freud Str. 25, 53105 Bonn, Germany. E-mail: johannes.oldenburg@ukb.uni-bonn.de

heterozygous defects usually in the *F13A1* gene (RefSeq NM_000129.3, MIM# 134570), have been described well in previous literature, the first case being reported by Duckert et al. (1960). Reports of *F13B* gene (RefSeq NM_001994.2, MIM# 134580) mutations in the severe form of this deficiency are rarer. This rare disorder (severe FXIII deficiency) with a prevalence of approximately one in 2 million represents an autosomal inherited recessive congenital disorder leading to severe bleeding symptoms. Another form of this deficiency is the isolated heterozygous congenital FXIII deficiency (or mild FXIII deficiency) that is currently underreported; primarily because the carriers are often asymptomatic and therefore the symptoms become apparent only when the individual is exposed to trauma [Biswas et al., 2014a]. Identification of heterozygous FXIII-deficient patients and extended causality determining research on the related mutations is crucial since the risk of provoked bleeding events (surgery, tooth extraction, and trauma) in heterozygous patients can be minimized through early detection. The *F13A1* gene coding for the A subunit maps to the short arm of chromosome 6 (p24-25) and spans >160 kb of genomic DNA consisting of 15 exons encoding a mature protein of 732 amino acids (~83 kDa) including an initiator methionine [Ichinose et al., 1988]. No classical signal sequence has been detected in the *F13A1* gene and the mechanism by which it might be secreted extracellularly is presently unknown. Intracellularly FXIIIA subunit (c.FXIIIA) exists as a dimer unlike in plasma where it associates with the B subunit to form a heterotetramer. The *F13B* gene is located on the long arm of chromosome 1 (q32-32.1) and contains 12 exons encoding the mature protein of 641 amino acids (~80 kDa) (Schwartz et al., 1973). The *F13B* gene sequence contains a 20 amino acid long leader sequence indicative of a classically secreted protein [Ichinose et al., 1986; Webb et al., 1989]. The FXIIIB subunit is glycosylated at two glycosylation sites [Chen et al., 2009].

In the last 5 years, our group has reported 23 mutations from patients with mild FXIII deficiency [Ivaskevicius and Biswas et al., 2010a; Ivaskevicius and Biswas et al., 2010b; Biswas et al., 2014b; Ivaskevicius et al., 2012]. Sixteen of these mutations were identified in the *F13A1* and seven in the *F13B* gene. We have earlier studied and characterized the *F13B* gene mutations [Biswas et al., 2013; Thomas and Biswas et al., 2015]. In the present study, we have performed a comprehensive investigation on the causality of 16 previously reported FXIIIA subunit missense mutations [Ivaskevicius and Biswas et al., 2010a; Biswas et al., 2014b] using parallel in silico and in vitro approaches to structurally and functionally characterize their underlying pathophysiology. The in vitro methods have been complemented by in silico strategies in which modeling of mutations on defined crystal structures and protein docking has been applied to explain the in vitro findings. Our analysis shows that these mutations can act on different aspects of FXIII activation and regulation based on the structure functional impact of the particular mutation.

Material and Methods

Mutational Database Submissions

Protein and DNA sequence numbering has been done on the basis of the reference sequence: RefSeq NM_000129.3. All sequence variant descriptions were cross-checked by the Mutalyzer program (http://www.LOVD.nl/mutalyzer; accessed on 26.03.2016). The *F13A1* gene is composed of 732 amino acids including an initiator methionine. The amino acids are numbered starting with the initiator methionine as +1. The 16 previously reported *F13A1* missense mutations have been registered with the Factor 13 Registry Database (http://www.f13-database.de/) and additionally under submission to the Leiden Open Variation Database (LOVD version 3.0; http://www.lovd.nl/3.0/home; submission IDs: 0000089893-0000089878 in increasing order of amino acid numbering).

Heterologous Expression of the Wild Type and Mutated FXIIIA Subunit Variants in *COS-1* Cell Lines

Site-directed mutagenesis was performed, on the mammalian expression vector pDest^{TM}26 Vector (Invitrogen, Darmstadt, Germany), containing the human FXIIIA subunit cDNA using the Gene Tailor site-directed mutagenesis kit (Invitrogen), for 16 previously reported *F13A1* heterozygous gene mutations (*p.Arg38Pro*, *p.Arg38Gln*, *p.Pro167Leu*, *p.Tyr168Cys*, *p.Arg172Gln*, *p.Pro290Arg*, *p.His343Tyr*, *p.Gln416Arg*, *p.Leu530Pro*, *p.Arg541Gln*, *p.Gly593Ser*, *p.Gln602Lys*, *p.Arg612His*, *p.Asp669Gly*, *p.Arg704Gln*, and *p.Arg716Gly*) (Note: These mutations have been previously reported with the old nomenclature, that is, the residue after the initiator methionine which is a serine is regarded as +1) [Ivaskevicius and Biswas et al., 2010a; Ivaskevicius and Biswas et al., 2010b; Biswas et al., 2014b; Ivaskevicius et al., 2012]. All vector construct clones were verified by complete cDNA sequencing to avoid misincorporations within the expressed vector, that is, variants or the wild type. Wild type and mutated FXIIIA subunit carrying mammalian expression vectors were heterologous expressed in *COS-1* cells [DSMZ(Institute of DSMZ-German Collection of Microorganism's and Cell Cultures, Germany)], which had been cultured in 10 cm dishes with DMEM (Invitrogen) supplemented with 10 % FBS (Invitrogen), 1% (v/v) penicillin–streptomycin (Invitrogen) and 0.1% fungizone (Invitrogen) at 37°C in 5% CO_2. During transfection 70,000 cells/well were seeded into six-well plates or 1.8 million cells in one 6 cm dish using DMEM (with FBS but without supplements and phenol red). The mutated versions were expressed in homozygous (alone) or heterozygous form (cotransfected along with the wild type) using Lipofectamine 2000 (Invitrogen). Both forms of transfections were performed for wild type and mutated forms with a reporter pCMV-LacZ vector (Clontech, Saint-Germain-en-Laye, France) containing the *LacZ* gene for normalizing the transfection at a 4:0.5 (homozygous; Expression vector: Reporter vector) or 2:2:0.5 (heterozygous; Expression vector: Expression vector in heterozygous form: Reporter vector) ratio. Collection of the supernatant and lysed cells was performed after 12, 24, and 36 hr. Cells were lysed with 270 μl non-denaturing lysis buffer "native M-PER Mammalian Protein Extraction Reagent buffer" (Thermo Scientific, Darmstadt, Germany) containing 25 mM bicine pH 7.6 without supplement of protease inhibitors. Both supernatant and cell lysates were stored at –80°C until further use. Since the FXIIIA subunit lacks a leader sequence and a significantly higher amount of the protein is found intracellularly when performing heterologous expressions, therefore we used the cell lysates for evaluating the quality of the FXIIIA expression products and not the supernatant. Where required (i.e., FXIII generation assay addressed later) cell lysates were further concentrated using Amicon Ultra-4 Centrifugal Filter Units with an Ultracel-50 membrane (Merck Millipore, Darmstadt, Germany). Transfections were completed in triplicates and repeated a minimum of three times. Further measurement of activity and antigen levels for the expressed cell lysates were performed with commercial kits (more details in the supplementary methods).

Determination of FXIII Activity by Pentylamine Incorporation

Cell lysates were also tested for FXIII activity with a modification of a biotin-labeled pentylamine incorporation activity assay

previously described by Philippou et al. [2003] (details given in supplementary methods).

Determination of FXIII Activity by α2-Antiplamin Incorporation

The rate of α2-antiplasmin incorporation mediated by FXIII from the expressed cell lysates was performed as previously described by Smith et al. [2013] (details in supplementary methods).

Generation of Activated FXIII (FXIIIa) using Expressed Cell Lysates

In order to determine the real-time FXIII activity (activation and inhibition), the expressed cell lysates were spiked into FXIII-deficient plasma (Haemochrom, Essen, Germany) and the FXIIIa (activated FXIII) generation assay was performed [Dodt et al., 2013] (details in supplementary methods). The curve data were evaluated according to a biexponential model with first order absorption and elimination. Data were fitted to the equation: $C(t) = c*k_a/(k_a - k_b)*(\exp(-k_b*(t - t_{lag}))-\exp(-k_a*(t - t_{lag})))$ where: k_a—constant of absorption that describes the development of FXIIIa and kb—elimination constant. The parameters area under the curve (AUC), peak FXIIIa concentration (CP), and time to peak (TTP) were also evaluated.

Fibrin Crosslinking Monitored over SDS-PAGE

The effect of the mutations on FXIII-mediated fibrin crosslinking SDS-PAGE were performed under reducing conditions on clots generated by mixing the expressed cell lysates with deficient plasma (details in supplementary methods).

Scanning Electron Microscopy of Fibrin Clots Generated using FXIIIA Expressed Cell Lysates

To analyze the effect of the FXIIIA mutations on fibrin clot thickness the expressed FXIIIA subunit cell lysates were mixed with deficient plasma (in a 1:1 ratio), thrombin (0.2 U/ml) and $CaCl_2$ (1 mM) and reactions were stopped after 60 min with 150 μl EDTA (50 mM). Finally, the clots were subjected to scanning electron microscopy after an elaborate procedure of fixation (further details in supplementary methods).

Molecular Modeling and in silico Analysis

In silico analysis was performed toward obtaining complimentary evidence for the putative structural influence of the expressed missense mutations on (A) rate of activation and (B) interaction with α-2-antiplasmin, fibrinogen, and thrombin. All structural analysis and visual rendering was performed on the YASARA version 13.9.8 platform [Krieger and Vriend, 2014].

(A) Activation path modeling

Protein database (PDB) files for the crystal structures of the zymogenic FXIIIA (Species: *Homo sapiens,* PDB ID: 1f13; 2.1 Å resolution) and activated FXIIIA (FXIIIAa) (Species: *Homo sapiens,* PDB ID: 4kty; 1.98 Å resolution) were downloaded from the PDB (www.rcsb.org; accessed on the 05.11.2014) [Stieler et al., 2013; Weiss et al., 1998] and used as input files on the ANMpathway server (http://anmpathway.lcrc.anl.gov/anmpathway.cgi; accessed on 10.11.2014) [Das et al., 2014]. This server uses a coarse-grained modeling approach to construct a two-state potential calculated by combining two elastic network models representative of the experimental structures representing the beginning and end points of the simulation. Intermediate structures are extracted as snapshots along continuous steepest descent pathways generated for the protein atomic coordinates during the transition from beginning to end point structures. The input files (PDB files) were optimized by first removing or modeling residues, which are not common to either file. Only a single chain from each PDB file was used as an input file. The output files (also in PDB format) are a series of coarse-grained models that represent the macromolecular structure of a specific transition point. No additional cut-offs were assigned as the default mode applicable in the server was chosen for generating the intermediates. The transition pathway was analyzed to identify residues, which show structural consistency or inconsistency during the activation process. Experimental validation of any conformational transition pathway is difficult because of the short life of the transition intermediates; however, a limited amount of experimental validation for this server has been demonstrated by Das et al. [2014].

(B) Interaction with α-2-antiplasmin, fibrinogen, and thrombin

In order to investigate putative structural influences, our reported missense mutations were analyzed in the context of interaction with α-2-antiplasmin, fibrinogen, and thrombin. Therefore, constrained all atom docking models were generated for these interacting partners with zymogenic or activated FXIIIA subunit. The human α-2-antiplasmin has no well-defined NMR or X- ray crystal structure in the database and therefore a model of the same was generated on the ITASSER threading server (http://zhanglab.ccmb.med.umich.edu/I-TASSER/ accessed on 22.11.2014) and the ab initio Quark server ((http://zhanglab.ccmb.med.umich.edu/QUARK/; accessed on 24.11.2014) [Yang et al., 2015; Xu et al., 2012]. In the case of fibrinogen, high-resolution crystal structures for all three fibrinogen chains were available in the protein structure database (Species: *Homo sapiens*, PDB ID: 3GHG; 2.9 Å resolution) [Kollman et al., 2009]. However, missing regions in the structure were modeled on the ab initio Quark server ((http://zhanglab.ccmb.med.umich.edu/QUARK/; accessed on 03.12.2014) and fitted onto the original structure before it was used for docking purposes. Both α-2-antiplasmin and fibrinogen chain structures were docked onto the activated FXIIIA (FXIII Aa) crystal structure (Species: *Homo Sapiens*, PDB ID: 4kty; 1.8 Å resolution). For both modeling servers (threading: ITASSER and ab initio: Quark), the amino acid sequence in fasta format of the relevant protein/part of protein were the input files. The output files were in PDB format. Both servers have repeatedly been validated and ranked number one in CASP experimental competitions in their respective sections (an annually organized competition for protein molecular modeling) [Yang et al., 2015; Xu et al., 2012]. The input sequence was combined with a guiding constraint for α-2-antiplasmin (the murine α-2-antiplasmin crystal structure, i.e., PDB ID: 2r9y; 2.65 Å resolution, Species: *Mus musculus,* was used) but for all ab initio predictions default settings of the server were used. Interaction between thrombin and FXIIIA was investigated by docking the active thrombin heavy chain thrombin crystal structure (Species: *Homo sapiens,* PDB ID: 1PPB; chain: et al.; 1.92 Å resolution) on a monomeric chain of the zymogenic crystal structure of FXIII (Species: *Homo Sapiens*, PDB ID: 1f13; 2.1 Å resolution). All dockings were performed

on the cluspro server (http://cluspro.bu.edu/login.php; accessed between 08.12.2014 and 24.12.2014) [Kozakov et al., 2010; Kozakov et al., 2013] using PDB files of the corresponding interacting proteins as input files. Specific guiding constraint residues as was applicable for the specific interaction/dock were assigned on an individual case basis (More comprehensive detailed explanation on the docking and modeling can be found separately in the supplementary methods section). Output files were also in PDB format and were read and analyzed on the YASARA platform (specified earlier). This docking server (Cluspro) has been repeated been validated and ranked first in the automated docking section of the CASP experiments [Kozakov et al., 2013].

Results

Antigen and Activity Levels for the Expressed Mutations

The antigen and activity levels (Fig. 1) for the expressed mutations with respect to that of the wild type can be arranged into four groups: (I) severely decreased activity levels in spite of normal antigen levels, which is now classified as group II functional defect, mutations revealed no effect on either antigen or activity levels and most likely represent putative polymorphisms (II), (III) mutations showed a simultaneous but moderate reduction in antigen and activity levels, and (IV) mutations have a severe impact on both antigen and activity levels. The fourth group is the largest and comprises seven mutations (*p.Arg716Gly*, *p.Arg704Gln*, *p.Gln602Lys*, *p.Leu530Pro*, *p.His343Tyr*, *p.Pro290Arg*, and *p.Arg172Gln*) with severely decreased antigen levels [<10 % (<1 μg/ml)] and non-detectable FXIIIA activity (<20%) compared with wild type (mean antigen: 12.9 ± 3.4 μg/ml). Mildly reduced antigen levels in the range of 31%–78% [absolute values are presented in Fig. 1] of the wild type as well as similarly reduced activity levels in the range of 38%–83 % of the wild type were observed for 4 mutants (*p.Arg541Gln*, *p.Tyr168Cys*, *p.Arg612His*, and *p.Asp669Gly*) belonging to the third group (Fig. 1). Two mutations, *p.Pro167Leu* and *p.Gln416Arg* (second group) reached antigen and activity levels close to that of wild type (antigen: 96.8% and 97.2% of the wild type; activity 93.6% and 102% of the wild type), respectively. Interestingly, another mutation *p.Gly593Ser* belonging to the second group showed high activity levels (125% of the wild type). Two substitutions at the thrombin cleavage site, *p.Arg38Gln* and *p.Arg38Pro* lead to a functional group II defect [as per recent FXIII deficiency classification; Kohler et al., 2011] with mildly decreased to normal antigen levels (58% and 93%) but severely decreased FXIII A activity, that is, <20 % with respect to the wild type (the first group). The heterozygously coexpressed rFXIIIA levels (activity as well antigen) for all mutations showed correction in their respective expression phenotype. As expected, the correction was partial for the mutations in groups I and IV (correction only for activity levels for the first group) and absolute for the mutations belonging to in groups II and III. However, the term "correction" applied here to the simultaneous expression of wild type and mutant allele could have different connotations, that is, the observed increase in expression levels might be a result of both alleles expressing in the same cell or in different cells. We assume that in case of our transient transfections the overall effect levels out in their mean values. This might also explain the high standard deviations observed for some of the transfection sets especially for the cotransfections. Western blotting of neat cell lysates further confirmed and correlated with the antigenic variation observed for all the expressed mutations (Supp. Fig. S1). Although we do not know the exact prevalence of these variants as yet, in our earlier reports we have screened for only 200 healthy controls (of German-caucasian ethnicity) for these variants and these numbers might not be adequate.

All these variants were checked on the 1000 genome server (http://browser.1000genomes.org/Homo_sapiens/Gene/Variation_Gene/Table?db = core;g = ENSG00000124491;r = 6:6144318-6321246#missense_variant_tablePanel; accessed on 05.02.2016). Eight out of the 15 amino acids on which we have reported variations existed in the 1000 genomes database. Amongst these apart from *p.Pro290Arg* which showed a Thr substitution in the database, all other seven substitutions were the same as that observed in our study. The reported nucleotide substitution differed in all eight of the mutations in the 1000 genome database. The minor allele frequency for all the substitutions was <0.01 indicating a prevalence of less than 1% in the sequenced genomes. None of the substitution was linked to any previously reported clinical significance. The reference SNPs corresponding to the variants observed in the 1000 genome database are provided here: *p.Arg172Gln* (rs121913065), *p.Pro290Arg* (rs201752338; *p.Pro290Thr*), *p.Arg541Gln* (rs367679357), *p.Gly593Ser* (rs138754417), *p.Arg612His* (rs369187276), *p.Asp669Gly* (rs375129902), *p.Arg704Gln* (rs267606787), and *p.Arg716Gly* (rs147189258).

α-2-Antiplasmin Incorporation Assay

Four of the expressed mutants (*p.Arg38Gln, p.Arg38Pro, p.Arg172Gln*, and *p.His343Tyr*) showed significantly impaired α-2-antiplasmin crosslinking ability ranging between 6–19% of the wild-type activity (Fig. 2). Moderately defective α-2-antiplasmin cross-linking in the range between 40–48% of the wild type was detected for four mutations (*p.Leu530Pro, p.Arg612His, p.Arg704Gln* and *p.Arg716Gly*). Two mutants *p.Pro290Arg* and *p.Gln602Lys* showed almost no detectable α-2-antiplasmin crosslinking activity. Six mutations (*p.Pro167Leu, p.Tyr168Cys, p.Gln416Arg, p.Arg541Gln, p.Gly593Ser*, and *p.Asp669Gly*) showed α-2-antiplasmin cross linking comparable to that of the wild type (between 80% and 120%).

FXIIIAa generation assay

In the case of seven (*p.Arg172Gln*, *p.Pro290Arg*, *p.His343Tyr*, *p.Leu530Pro*, *p.Gln602Lys*, *p.Arg704Gln*, and *p.Arg716Gly*) out of the 16 expressed mutants the FXIIIa generation assay curves could not be plotted since the expression levels were below the detection limit (despite concentration of the cell lysates). All other mutations showed variable curves with respect to the wild type (Supp. Fig. S2). Except for *p.Arg38Pro*, all mutations showed a typical bell-shaped curvature during the time period of the generation assay (60 min) with variation in the AUC, TTP, CP, the constant for FXIIIa generation (k_a) and the FXIIIa elimination/ inactivation constant (k_b). Five mutations (*p.Arg38Gln*, *p.Arg38Pro*, *p.Gln416Arg*, *p.Arg612His*, and *p.Asp669Gly*) showed a moderate to severe decrease in the AUC values ranging between 8% and 34% of the wild-type AUC (Fig. 3A). Interestingly three of the mutations *p.Pro167Leu*, *p.Tyr168Cys*, and *p.Arg541Gln* showed higher AUC than the wild type although the TTP was comparable (Fig. 3A and B). The k_a values for the *p.Tyr168Cys* mutation were almost double that of the wild type but the k_b was similar to wild type (Fig. 3A). Except for *p.Asp669Gly*, these mutations had TTP values comparable to that of the wild type (TTP 75% of wild-type TTP; Fig. 3B). The k_b for the *p.Pro167Leu* mutant was extremely high which reflects a faster inactivation of FXIIIa (Fig. 3A). Only two mutations, that

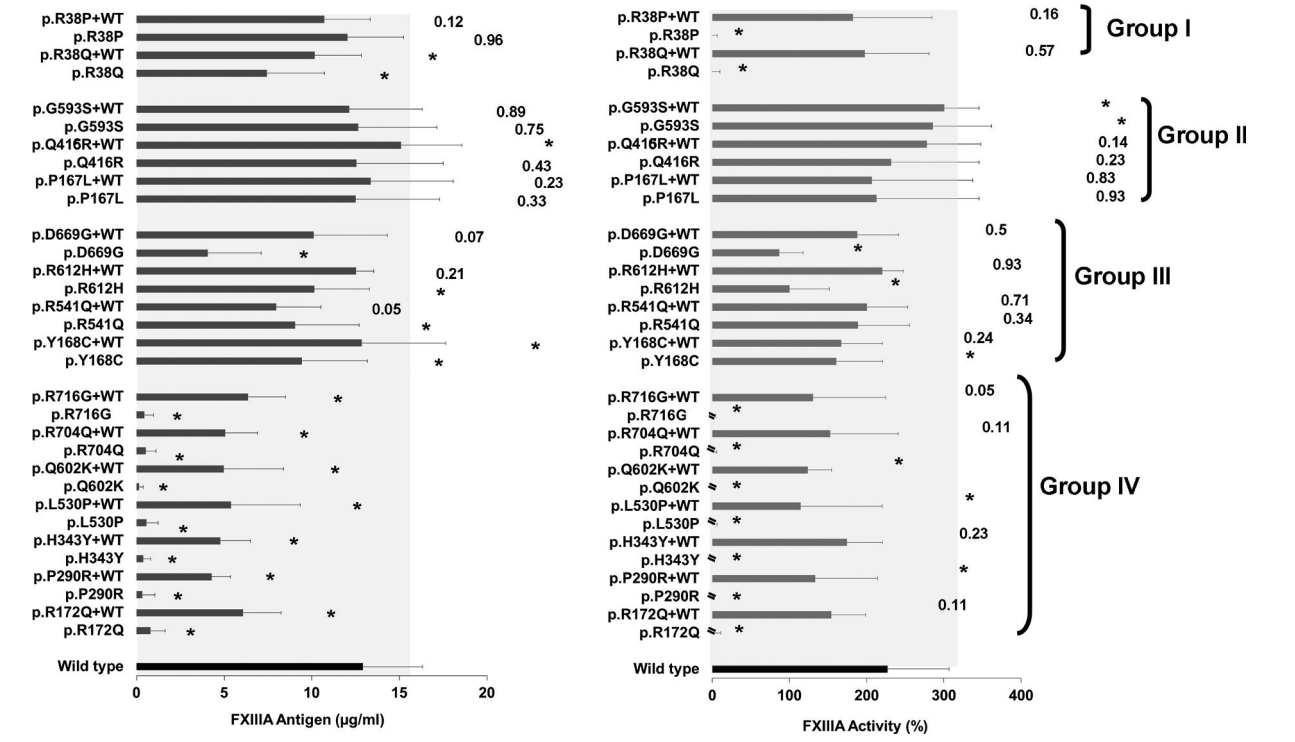

Figure 1. Antigen and activity levels for the expressed cell lysates. The figure illustrates the calculated mean antigen (μg/ml) and activity (in %) levels for the homozygous and heterozygous expressed intracellular cell lysates from a minimum of triplicate set of transient transfections on different cell passages [minimum $n = 3$ repeats; therefore number of values considered >9(3×3)]. The wild-type antigen/activity results are shown in dark gray and the missense mutations in light gray shades. Error bars represents standard deviation for each variant over the complete set of transfection. Intracellular antigen and activity results are from 36 hr post-transfection (further details see in *Material and Methods*). The *P* values >0.5 are mentioned on top of the bar graphs, *P* values <0.05 are depicted with a "$*$" sign.

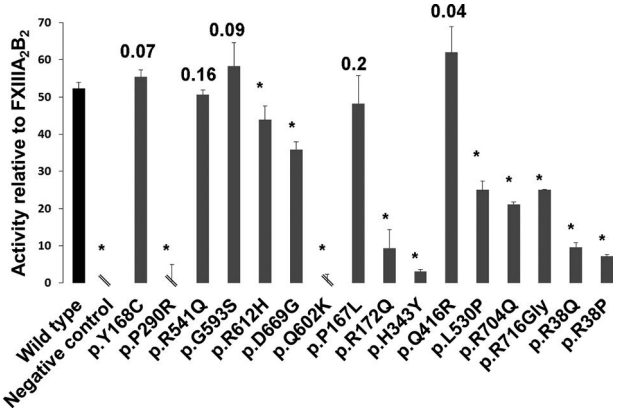

Figure 2. The α-2-antiplasmin incorporation assay for expressed cell lysates. Functional test results for the α-2-antiplasmin incorporation assay for the expressed intracellular cell lysates from transfected FXIIIA variants. All results are depicted as % activity of recombinant $FXIIIA_2B_2$. All values are means for three replicate measurements from one transfection. Error bars represents standard deviation of the mean for the triplicates of each variant ($n = 3$) from one transfection ($n = 1$). Wild-type transfection values are represented in light gray and variants in dark gray shades. The *P* values >0.5 are mentioned on top of the bar graphs, *P* values <0.05 are depicted with a "$*$" sign.

is, the *p.Arg38Pro* and *p.Asp669Gly* showed k_b values far greater than k_a values and also higher than that observed for the wild type (0.023 unit/sec) indicating a general tendency of faster inactivation (Fig. 3B). The second substitution at the thrombin cleavage site (*p.Arg38Gln*) did not show a higher rate of inactivation as observed for the Pro variant (Fig. 3A).

Fibrin Crosslinking Analyses

Analysis of the γ- and α-chain crosslinking using SDS-PAGE showed γ-chain dimers appearing between 5 and 10 min of crosslinking in the majority of the lysates (Fig. 4). A defect in γ–γ crosslinking was apparent for six out of 16 mutants. In three of these mutations (*p.Leu530Pro*, *p.Pro290Arg*, and *p.His343Tyr*), the effect was severe since no γ dimers were observed even after 60 min of crosslinking (Fig. 4). Three more mutations (*p.Arg172Gln*, *p.Gln602Lys*, and *p.Arg716Gly*) showed a time shift in the appearance of γ dimers indicating slower rate of γ dimerization (Fig. 4). Three (*p.Tyr168Cys*, *p.Pro167Leu*, and *p.Gln602Lys*) of the 16 mutants showed no α-chain crosslinking even after 60 min of crosslinking reaction. In six mutants (*p.Pro290Arg*, *p.Hi342Tyr*, *p.Arg172Gln*, *p.Arg704Gln*, *p.Asp669Gly*, and *p.Arg716Gly*), α-multimers were formed at a slower rate (Fig. 4). The remaining mutations did not show any major difference in the generation of γ dimers or α-multimers.

Fibrin Clot Fiber Thickness using SEM

Clots generated by mixing expressed cellular lysates and FXIII-deficient plasma showed a decrease in the clot thickness (μm) for all mutations (range: 0.145–0.195 μm) when compared with the wild-type FXIII (0.256 μm) (Fig. 5).

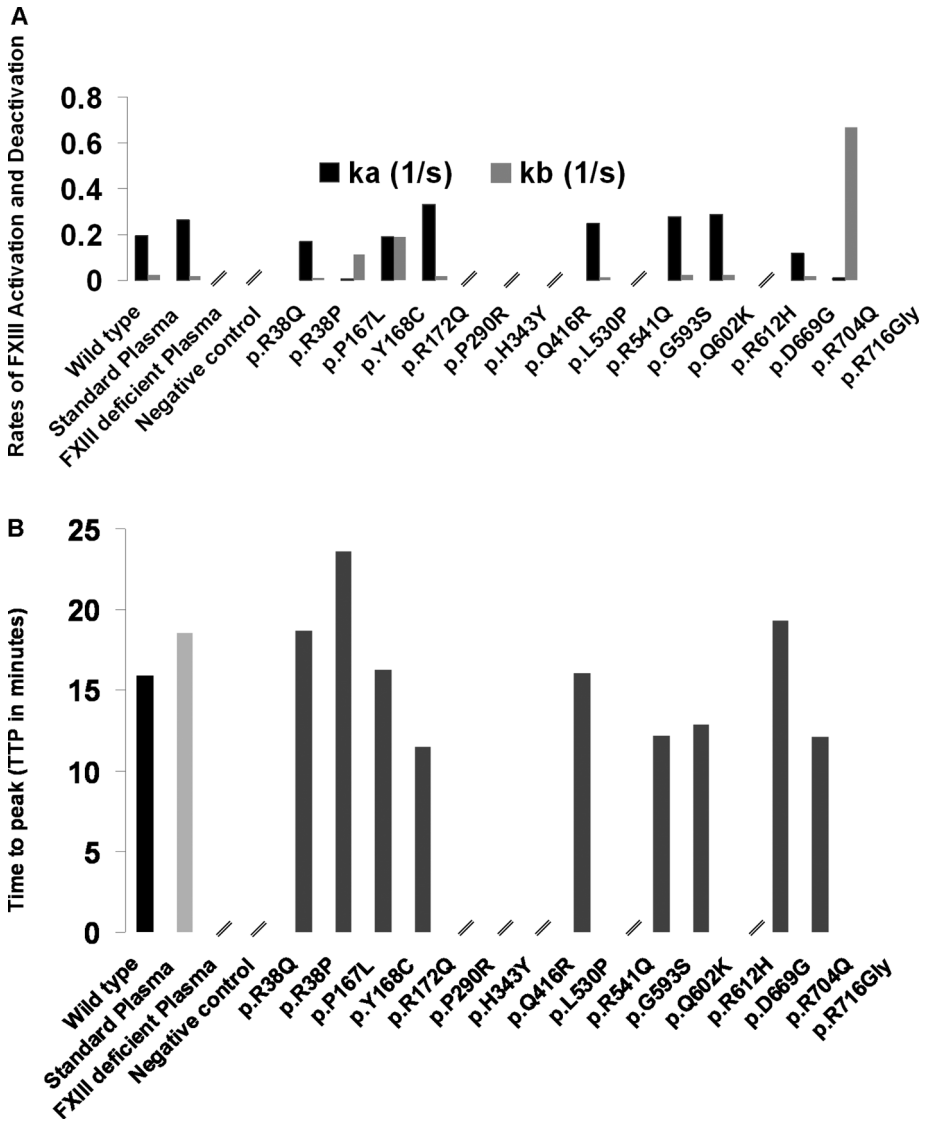

Figure 3. FXIIIa (Activated Factor XIII) generation assay for expressed cell lysates. This graph depicts a comparison of two key variables, that is, rate of activation and deactivation (k_a—constant of absorption that describes the development of FXIIIa and k_b—elimination constant) and the time to peak (TTP) for the intracellularly expressed FXIIIA wild type and variants when evaluated with the FXIIIa (Activated Factor XIII) generation assay. Panel **A** is the bar graph representation for the rate of activation and deactivation, whereas panel **B** represents a comparative bar graph illustration of the TTP. The k_a values are depicted in black and k_b values in light gray shades. Panel **B** represents the TTP values for all variants and the wild type calculated from the curves depicted in Supp. Figure S2. Wild-type values are represented in dark gray and variants in light gray shades.

Thrombin Cleavage/Non-Proteolytic Activation

Non-proteolytic activation of the expressed recombinant FXIIIA was probed using super physiological concentrations of calcium (100 mM) in the pentylamine incorporation assay without thrombin. Amongst the 16 expressed mutations, only those mutations on the activation peptide cleavage site (*p.Arg38Pro* and *p.Arg38Gln*) responded to high calcium levels shown in Figure 6, which restored the specific activity of these two mutations similar to that of the wild type. The other mutations showed no effect in the presence of super physiological levels of calcium, indicating no effect for these mutations on the activation peptide cleavage (Fig. 6). Five mutations (*p.Tyr168Cys*, *p.Arg541Gln*, *p.Gly593Ser*, *p.Arg612His*, and *p.Asp668Lys*) reached unusual high specific activity compared with the wild type when the incorporation assay was performed using low levels of calcium in the presence of thrombin (Fig. 6). No discordance between the antigen and activity levels was observed for the same set of mutations when the photometric assay was used. Interestingly all these mutations belonged mostly to the second group of mutations leading to mildly reduced antigen and activity levels.

Modeling of FXIII Complexes and the Activation Pathway

Zymogenic FXIII–thrombin complex

The zymogenic FXIII–thrombin complex showed an interface comprising of a stretch of residues within the FXIII activation peptide with the primary participants being the cleavage site residue *p.Arg38* and *p.Gly39*. Other participants were slightly distant from the sessile bond, for example, *p.Asn47* or *p.Glu31* but still within this particular stretch (Fig. 7A). The residues involved in the

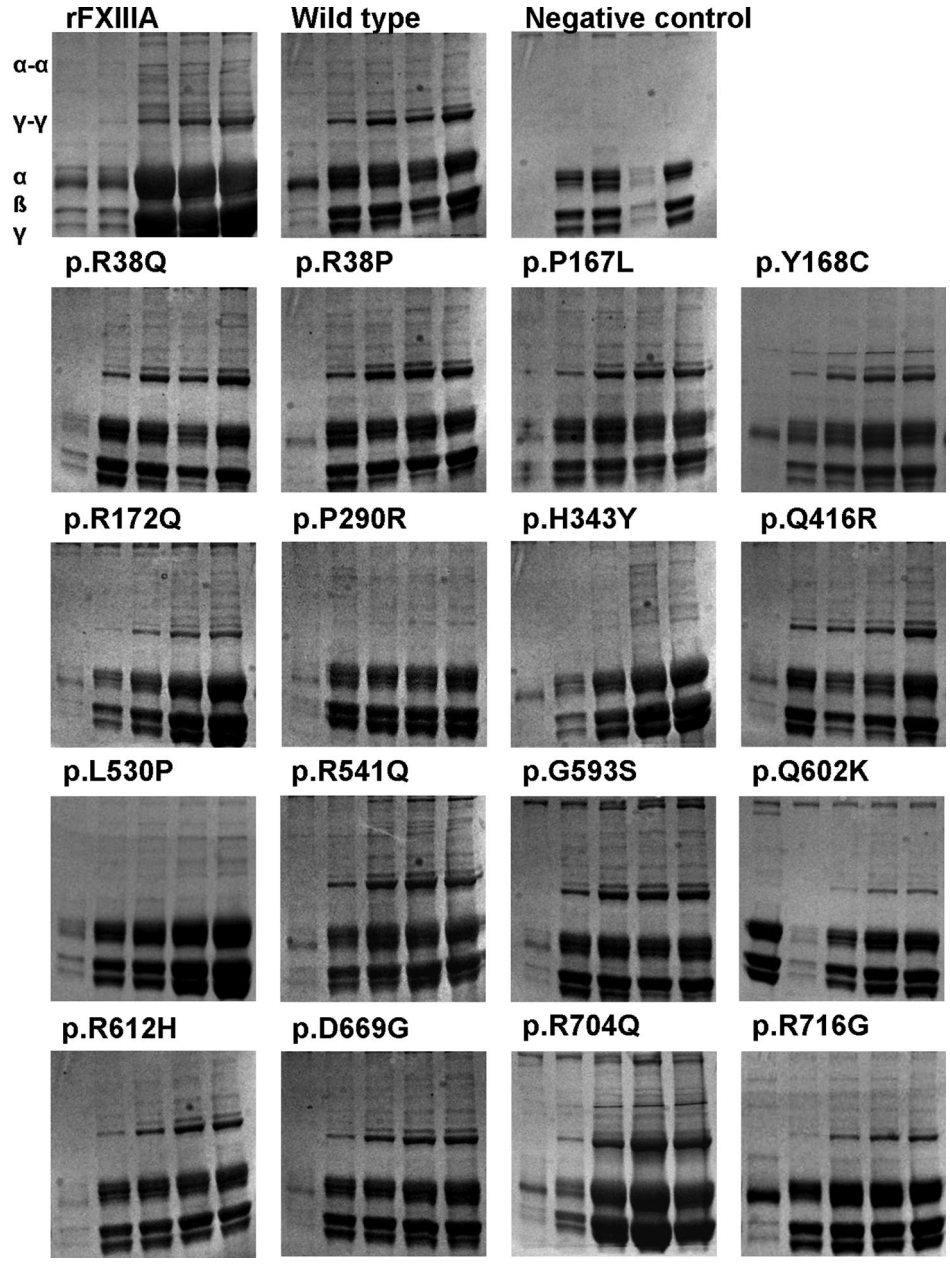

Figure 4. Fibrin crosslinking for the expressed cell lysate variants and wild type. The above figure shows the results of the functional test for the expressed FXIIIA variants compared with wild type for their ability to perform α–α and γ–γ crosslinking. Clots generated from a mix of the expressed cell lysates and deficient plasma was run on a 10% SDS-PAGE stained with Coomassie blue. Each panel in this figure represents a variant or the wild type. Additionally recombinant FXIIIA and only the deficient plasma (negative control) were also tested on this gel. Each gel shows five different lanes, which represent successively increasing times of crosslinking (from left to right: 0, 10, 30, 60, and 90 min). The respective fibrin chains as well the dimers and multimers formed as a result of crosslinking are labeled for reference in the first gel for the recombinant FXIIIA.

interaction on thrombin were mostly those neighboring thrombin's catalytic triad spatially. The interface residue interaction chart for this interface is presented in Supp. Table S1.

Activated FXIIIA–α-2-antiplasmin complex

The interface activated FXIIIA residues in the activated FXIIIA–α-2-antiplasmin complex were limited only to those from core domain. Notably, the *p.Trp280* residue which is believed to form an oxyanion hole that stabilizes the enzyme substrate complex is one of the participating residues (Fig. 7B). All mutations reported on the core domain were proximal to the binding interface but none of them were directly on the interface. The interface residue interaction chart for this interface is presented in Supp. Table S2.

Activated FXIIIA–fibrinogen α and γ chain complexes

The activated FXIIIA–fibrinogen α and γ chain complexes generated using putative reactive glutamine residues as constraints suggest four different orientations for the α and one orientation for the γ chain (i.e., corresponding to the number of putative reactive glutamine residues in these chains) (Fig. 7C; Supp. Table S3–S7). One

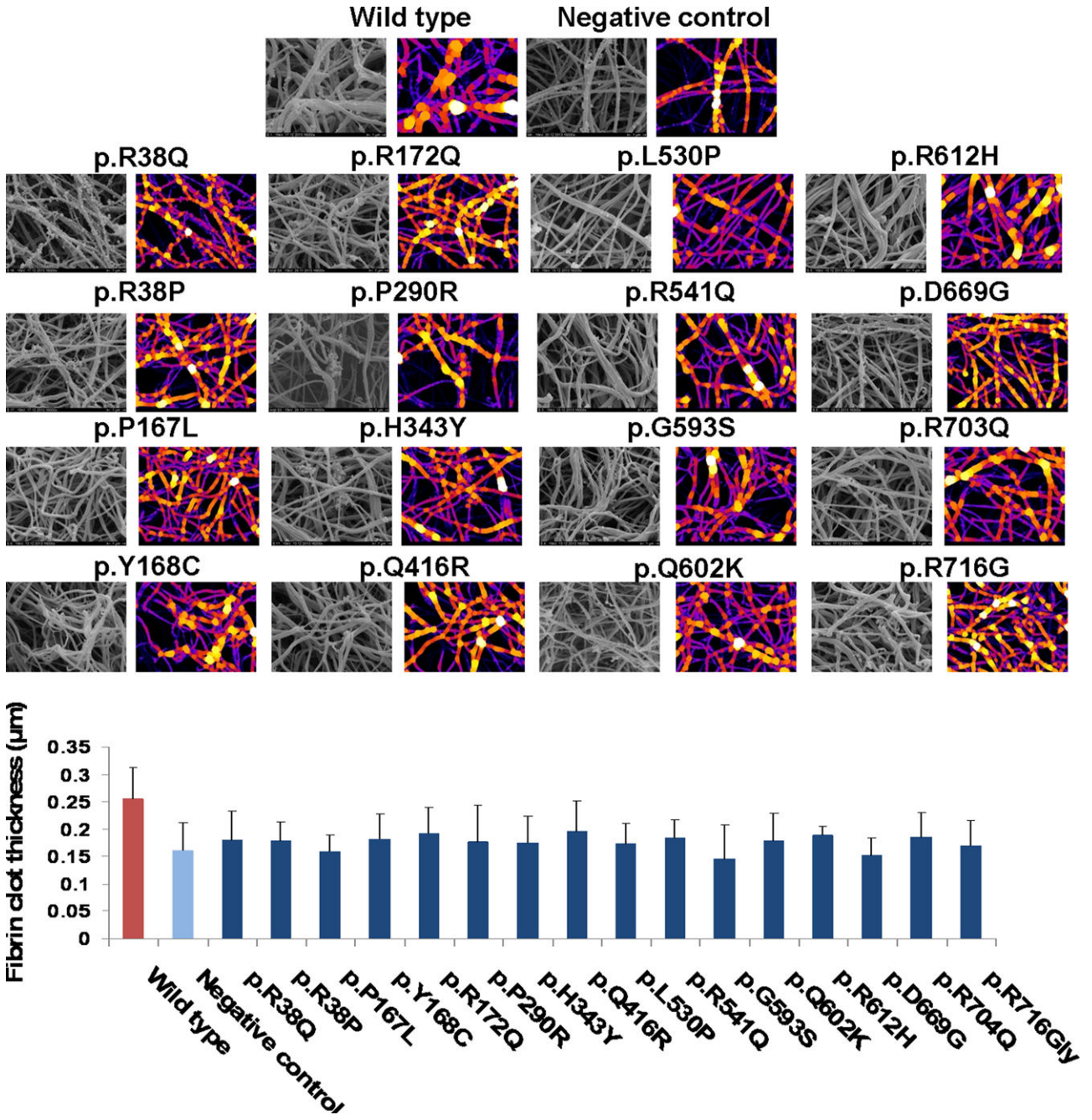

Figure 5. SEM analysis for clots generated from the expressed cell lysates of variants and wild type. The above figure has been split into two panels. The above panel represents scanning electron micrographs at 16,000× resolution for the clots generated from each of the variants, wild type, and negative control. Each micrograph is depicted with two images representing the same clot. In gray color (left), the original SEM picture is shown, which was converted to a colored binary image (right) with the BoneJ Plugin. The lower panel depicts the quantitative analysis of fiber thickness calculated for the SEM micrographs shown in the upper panel. Calculation is based on the colored thickness map produced by the binary image. The blue bars represent clots for the variants; light blue bars represent deficient plasma based clots, whereas the wild-type clot is shown with a dark blue bar.

common dominating factor in the interactions observed in all these interactions is the presence of residues belonging mainly to the core domain and to a lesser extent to the β-sandwich domain in the respective interfaces. Amongst all the reported mutated residues, only the *p.His343* and *p.Pro290 residues* from the core domain were observed to be directly on any of the docking interfaces, that is, both mutations on the *p.Gln223* FXIIIA constrained dock with α fibrinogen chain (Fig. 7C; Supp. Table S3). Certain mutated residues in the beta sandwich domain like the *p.Pro167*, *p.Tyr168*, and *p.Arg172* were observed to be proximal to the docking interface for one of the docks but not directly on the interface, that is, *p.Gln237* FXIIIA constrained dock with α fibrinogen chain (Fig. 7C; Supp. Table S4). The *p.Gln415* residue was also observed to be proximal to one of the docking interfaces, that is, *p.Gln328* FXIIIA constrained dock with α-fibrinogen chain (Fig. 7C, Supp. Table S6). No participant interaction residues were observed from the β-barrel-1 and β-barrel-2

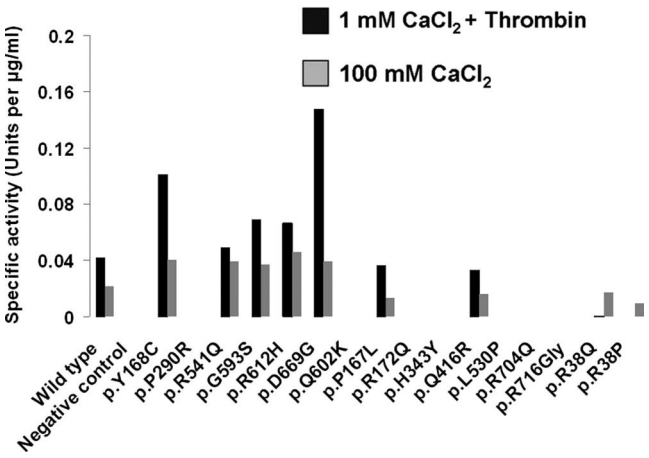

Figure 6. Incorporation assay results for the expressed variants and wild-type cell lysates. This bar graph represents the specific activity levels for the variants and the wild type measured with incorporation assay under low calcium/thrombin (black bars) and high calcium/no thrombin (light gray bars) conditions.

domains of activated FXIIIA in any of the docks/orientations. The interface residue interaction chart for all FXIIIA–fibrinogen interfaces is presented in Supp. Tables S3–S7.

Activation Pathway for FXIII

The contact map for the modeled activation pathway of FXIII shows a number of residues heterogeneously distributed between the N and C terminal domains of activated FXIIIA and its core domain which were in close contact (<5 Å) during the process of activation but not in contact post activation (>5 Å). Amongst the reported mutated residues *p.Leu530*, *p.Gln602*, and *p.Arg716* are the ones sharing this characteristic. Apart from these, some mutated residues like *p.His343* (stretch 331–342), *p.Arg612* (stretch 608–619), were observed proximal to stretches of residues which lose close contact upon activation (Supp. Fig. S3). Interestingly, with the exception of *p.His343*, all these residues belong to the two β-barrel domains.

Discussion

Although traditionally FXIII deficiency has not been classified on the basis of severity but there have been literature based suggestions that a "hemophilia" like distinction between mild, moderate, and severe FXIII deficiency based on measured FXIII activity and the degree of clinical bleeding might be possible [Peyvandi et al., 2012]. This type of classification is in concordance with our results which also reflect these differences in the expression phenotype of the evaluated missense mutations. It is also necessary to stress that this type of classification observed in our in vitro expression phenotype cannot automatically be translated into a symptom-based clinical phenotype because many mild/moderate FXIII-deficient patients are primarily asymptomatic unless they are exposed to some kind of physical trauma. Notably, the differences in the expression phenotype do not always perfectly correlate with the observed clinical phenotype (Supp. Table S8) because of the following reasons: (1) differences between the in vitro and in vivo scenario, (2) clinically it has been observed that FXIII activity > 10 % is sufficient to prevent spontaneous bleeding, (3) the variant reported might not be the real causative mutation and could just be in linkage disequilibrium with the real mutation which might lie in a region that was not screened for in earlier studies from which these mutations are reported (i.e., deep intronic mutation, and so on).

Activation Peptide Mutations (*p.Arg38Pro* and *p.Arg38Gln*)

As expected, *p.Arg38Pro* and *p.Arg38Gln* are not cleaved by thrombin in the presence of 1 mM calcium as observed before also [Ivaskevicius et al., 2012]. Their adverse influence on thrombin cleavage is quite evident, precisely because a correction in their expression phenotype in non-proteolytic conditions (high calcium; no thrombin) was possible (Fig. 6). Interestingly, these two substitutions also show a mild effect on stability and inhibition of activated FXIIIAa, that is, the substitution of the positively charged arginine residue to a neutral charged glutamine leads to a mild effect on protein stability, whereas the substitution with an imino-group, that is the non-polar proline residue does not alter the antigen levels but influences the rate of activated FXIIIAa inhibition. This can be expected because both mutations are semi to non-conservative and likely to have a structural effect on the protein as well. Interestingly both these mutations showed close to normal γ-γ dimer generation (Fig. 4), but that might be attributed to the high levels of calcium used for fibrin clot generation.

ß-Sandwich Domain Mutations (*p.Pro167Leu*, *p.Tyr168Cys*, and *p.Arg172Gln*)

The β-sandwich mutations *p.Pro167Leu* and *p.Tyr168* showed qualitative reduction in α-α crosslinking (Fig. 4) which could be the consequence of impaired binding to fibrinogen. Our in silico docking between the α-fibrin chain and activated FXIII showed (Fig. 7B) that these two residues as well as *p.Arg172* are proximal to the interaction sites for these two proteins. The mutant *p.Arg172Gln* unlike *p.Pro167Leu* and *p.Tyr168Cys* leads to severely decreased antigen and activity levels (Fig. 1), which is possibly caused by a structural defect as a consequence of the loss of positive charge in this substitution. These three residues were also predicted previously to be part of putative interface between fibrin and activated FXIII by Smith et al. [2013]. The clinical picture (Supp. Table S8) for the patient's carrying these three mutations differ, that is, the patients with *p.Tyr168Cys* and *p.Arg172Gln* mutations showed asymptomatic phenotypes, whereas the patient with *p.Pro167Leu* suffered from bleeding after dental extraction. A plausible explanation for the asymptomatic phenotype of *p.Tyr168Cys* mutation/patient could be the low rate of elimination (Kb) of the activated FXIII (Fig. 3B) while that for the *p.Arg172Gln* mutation/patient could be that this patient was not exposed to any trauma which is often the primary trigger for bleeding in a heterozygous scenario.

Core Domain Mutations (p.Pro290Arg, p.His343Tyr, and p.Gln416Arg)

Core domain mutations especially ones which critically influence structure are expected to have a strong influence on protein stability as well as activity owing to their proximity to the catalytic triad. The *p.Pro290Arg* mutation is a highly non-conservative substitution from a rigid non-polar proline residue to a large polar positive charged arginine which is likely to have a deleterious effect on the

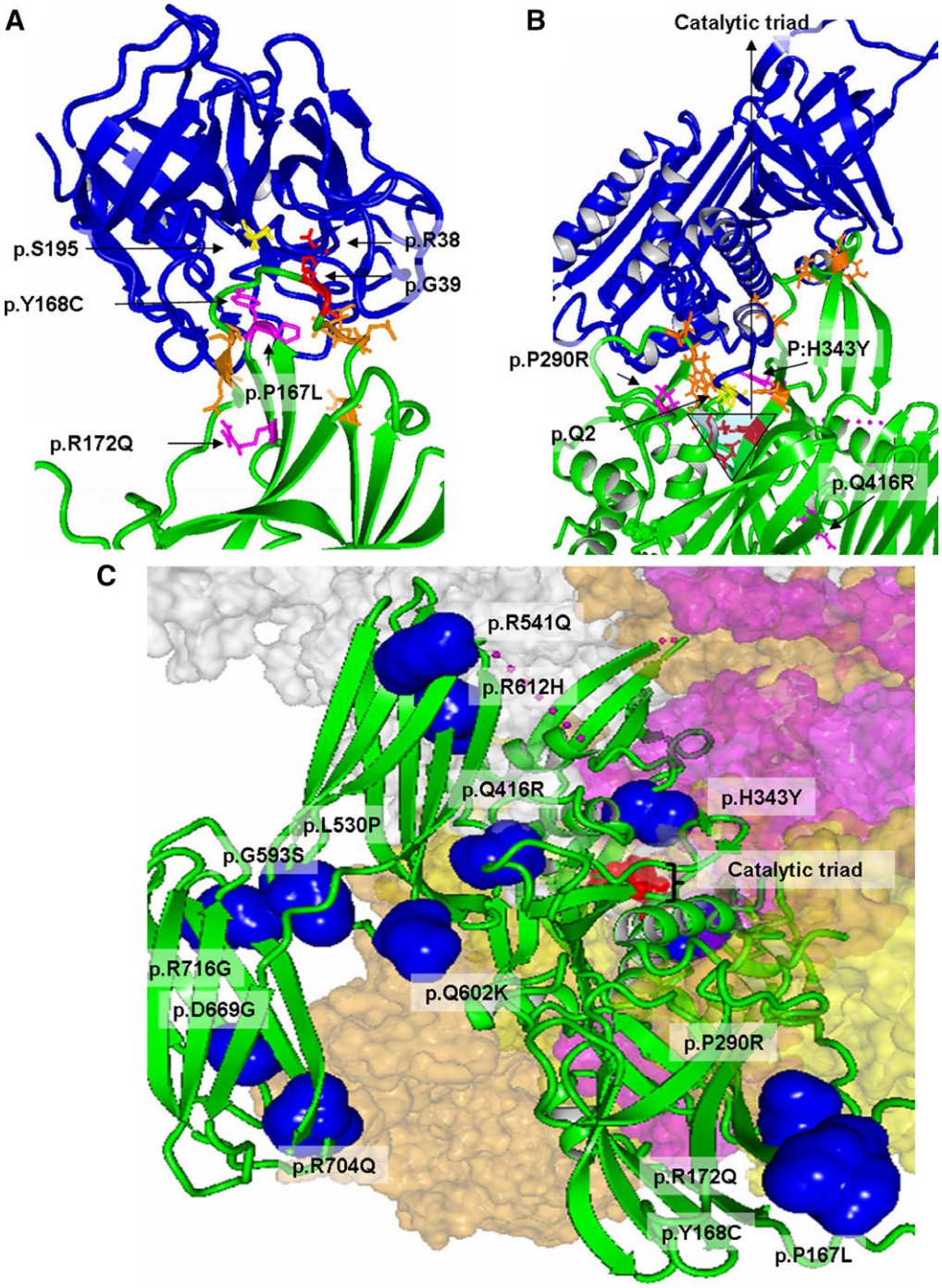

Figure 7. The in silico docking representations of various docking complexes. Panel **A** illustrates the in silico generated dock of activated thrombin crystal structure on a monomer of the zymogenic FXIIIA crystal structure, whereas panel **B** depicts the in silico generated dock of the human α-2-antiplasmin model on a monomer of the activated FXIIIA crystal structure. The protein backbone in panels **A** and **B** are presented in ribbon format. Thrombin is colored blue and the zymogenic FXIIIA is colored green in panel **A**. Interface residues on FXIIIA have been depicted in stick format. The catalytic Ser195 residue in thrombin also has been depicted in yellow colored stick format. Amongst the interface residues the residues on which mutations have been reported in this study are colored magenta, the activation peptide cleavage site residues are colored red, whereas the remaining residues are colored camel. The human α-2-antiplasmin model is colored blue and the activated FXIIIA is colored green in panel **B**. The reactive Gln2 residue in the human α-2-antiplasmin model has been depicted in yellow colored stick format. Amongst the interface residues, the residues on which mutations have been reported in this study are colored magenta, the FXIIIA catalytic triad residues are colored red, whereas the remaining residues are colored camel in panel **B**. The panel **C** depicts the four models generated from the docking of partly modeled fibrinogen α-chain on the activated FXIIIA crystal structure using reactive Gln residues on fibrinogen α-chain as guiding constraints. The activated FXIIIA monomer is depicted in green ribbon format. The four fibrinogen α-chain orientations with respect to the activated FXIIIA monomer are represented by the molecular surfaces in different colors (Gln223 orientation: camel, Gln237: yellow, Gln366: pink, Gln328: gray). The FXIIIA catalytic triad is depicted in red ball format. The mutations reported in this study are represented by their accessible surfaces in blue color.

protein fold and therefore also on protein stability as is seen in our activity and antigen values (Fig. 1) as well as other expression phenotype evaluations for this mutation. The mutation *p.His343Tyr* involves the loss of charge as well as polarity. This residue has been shown to be of critical importance since the *p.His343*/*p.Glu402* hydrogen bonded duplet in activated FXIII structure guides the substrate to the proximal catalytic triad [Stieler et al., 2013]. Another group by Jang et al. [2015] described a mutation (although in compound heterozygous state) on the *p.His343*residue (*p.His343Gln*) leading to severe bleeding episodes. The mutation *p.Gln416Arg* is the only core domain mutation which did not show a strong effect on FXIII activity or antigen levels (Fig. 1) in most of the expression based evaluations in spite of the mutation being a biochemically non-conservative substitution. In fact it is the only core domain mutation which shows no influence on α2-antiplasmin incorporation despite its relative proximity to the activated FXIIIA–α 2-antiplasmin interface in the respective dock.

β-Barrel-1&2 Mutations (p.Arg541Gln, p.Gly593Ser, p.Arg612His, p.Asp669Gly, p.Gln602Lys, p.Leu530Pro, p.Arg704Gln, and p.Arg716Gly)

A large number of functional missense mutations were found on the surface of the β-barrel-1 and β-barrel-2 domains. With the present disclosure of the activated FXIII structure [Stieler et al., 2013], it is clear that the transition of inactivated to an activated open FXIIIA structure involves the movement of these two domains. Our model of the activation path clearly shows that at least four of the reported mutated residues, that is, *p.Leu530*, *p.Gln602*, *p.Arg612*, and *p.Arg716* are on regions of the protein that undergo critical conformational changes during activation (Supp. Fig. S3) and therefore could influence the flexibility of these domains to adopt an activated open structure. Three of these mutations (*p.Leu530*, *p.Gln602,* and *p.Arg716*) show severe reduction in almost all expression phenotype evaluations (Fig. 1). The *p.Arg612His* shows a moderate decrease in FXIII activity/antigen levels but also a delay in activation (TTP) which might explain its putative influence on the activation pathway (Figs. 1 and 3). Interestingly, the mutations *p.Leu530Pro*, *p.Arg704Gln*, and *p.Arg716Gly* despite poor antigenic stability showed comparatively (to their low antigen values) higher values of α 2-antiplasmin incorporation (although much lower than wild type) indicating relatively higher affinity of these variant for α2-antiplasmin. The activated FXIIIA–α-2-antiplasmin complex dock however does not suggest any direct influence of these residues at the activated FXIIIA–α 2-antiplasmin interface although an allosteric influence cannot be ruled out. Amongst the remaining mutations, the severest expression phenotype was observed for *p.Arg704Gln* which could be explained by the biochemically non conservative nature of this substitution. Interestingly one missense mutation the *p.Gly593Ser* substitution showed wild type like or at times a better expression phenotype in certain evaluations (Fig. 1). It seems that the mutation leads to a higher quantitative generation of activated FXIIIA (k_a and CP higher than wild type; Fig. 6) which is similar to the *p.Val35Leu* variant which gets activated more rapidly by thrombin resulting in altered fibrin with reduced tensile strength [Ariens et al., 2000].

One major aspect of our expression phenotype was that for all missense mutations evaluated in this study irrespective of their effect on activity and antigen we observed a difference in fibrin clot thickness when compared with the wild type. All mutations showed reduced fiber thickness (shown in Fig. 5) which is surprising since current literature suggests that FXIII contributes to thinner and denser clots [Hethershaw et al., 2014; Kurniawan et al., 2014]. Since from our SEM´s we are not able to comment on the density of the clots that we analyzed, it might still be that the mutations result in thinner but more perfuse clots which are less stiff and therefore more prone to degradation. The other possibility might be that the image analysis technique used by us (BoneJ) was originally developed and validated for porous or spongy continua in trabecular research and its use for fibrin clots might not have influenced the final outcome adequately. The fact that even mutations which show normal expression phenotype have thinner clots suggests that there might be other variables at play for the mutations which were not part of the current experimental set up and therefore could not be evaluated. One major variable that has not been touched upon in this study is the influence of these mutations on the interaction between FXIIIA and FXIIIB subunits. Since comprehensive structural information on their respective interfaces is still awaited, future resolution of the $FXIIIA_2B_2$ heterotetrameric structure will provide more insight in the putative influences of these mutations. To finally conclude, we have determined the causality of 16 missense mutations which had previously been reported in heterozygous form from patients with mild FXIII deficiency.

Acknowledgments

A.B. and J.O. are the principle investigators of this study. A.T. conducted and collected the experimental data. H.P. and E.S. performed α-2-antiplasmin incorporation assay and helped in setting up the FXIII incorporation assays. H.J.E. performed the SEM experiments. J.D. performed the FXIIIAa generation assays. A.B. performed and collected the in silico data. V.I. and J.O. provided clinical support to the study. A.B. and A.T. analyzed the data. A.B. and A.T. cowrote the article, and J.O. edited the article. A.B. designed the study. A.B. and J.O. supervised the study. The authors would like to acknowledge Sophie Lyonga for technical assistance. The manuscript is a retrospective mutation (previously reported) based functional study that does not require ethics committee approval at that institution.

Disclosure statement: The authors declare no conflict of interest.

References

Ariens RA, Philippou H, Nagaswami C, Weisel JW, Lane DA, Grant PJ. 2000. The factor XIII V34L polymorphism accelerates thrombin activation of factor XIII and affects cross-linked fibrin structure. Blood 96:988–995.

Biswas A, Ivaskevicius V, Seitz R, Thomas A, Oldenburg J. 2011. An update of the mutation profile of Factor 13 A and B genes. Blood Rev 25:193–204.

Biswas A, Thomas A, Bevans CG, Ivaskevicius V, Oldenburg J. 2013. In vitro secretion deficits are common among human coagulation factor XIII subunit B missense mutants: correlations with patient phenotypes and molecular models. Hum Mutat 34:1490–1500.

Biswas A, Ivaskevicius V, Thomas A, Oldenburg J. 2014a. Coagulation factor XIII deficiency. Diagnosis, prevalence and management of inherited and acquired forms. Hamostaseologie 34:160–166.

Biswas A, Ivaskevicius V, Thomas A, Varvenne M, Brand B, Rott H, Haussels I, Ruehl H, Scholz U, Klamroth R, Oldenburg J. 2014b. Eight novel F13A1 gene missense mutations in patients with mild FXIII deficiency: in silico analysis suggests changes in FXIII-A subunit structure/function. Ann Hematol 93:1665–1676.

Chen R, Jiang X, Sun D, Han G, Wang F, Ye M, Wang L, Zou H. 2009. Glycoproteomics analysis of human liver tissue by combination of multiple enzyme digestion and hydrazide chemistry. J Proteome Res 8:651–661.

Das A, Gur M, Cheng MH, Jo S, Bahar I, Roux B. 2014. Exploring the conformational transitions of biomolecular systems using a simple two-state anisotropic network model. PLoS Comput Biol 10:e1003521.

Dodt J, Volkers P, Seitz R. 2013. Factor XIIIa generation assay: a tool for studying factor XIII function in plasma. Anal Biochem 439:145–151.

Duckert F, Jung E, Shmerling DH. 1960. A hitherto undescribed congenital haemorrhagic diathesis probably due to fibrin stabilizing factor deficiency. Thromb Diath Haemorrh 5:179–186.

Fraser SR, Booth NA, Mutch NJ. 2011. The antifibrinolytic function of factor XIII is exclusively expressed through alpha(2)-antiplasmin cross-linking. Blood 117:6371–6374.

Hethershaw EL, Cilia La, Corte AL, Duval C, Ali M, Grant PJ, Ariens RA, Philippou H. 2014. The effect of blood coagulation factor XIII on fibrin clot structure and fibrinolysis. J Thromb Haemost 12:197–205.

Ichinose A, Davie EW. 1988. Characterization of the gene for the a subunit of human factor XIII (plasma transglutaminase), a blood coagulation factor. Proc Natl Acad Sci USA 85:5829–5833,

Ichinose A, McMullen BA, Fujikawa K, Davie EW. 1986. Amino acid sequence of the b subunit of human factor XIII, a protein composed of ten repetitive segments. Biochemistry 25:4633–4638,

Ivaskevicius V, Biswas A, Bevans C, Schroeder V, Kohler HP, Rott H, Halimeh S, Petrides PE, Lenk H, Krause M, Miterski B, Harbrecht U, et al. 2010a. Identification of eight novel coagulation factor XIII subunit A mutations: implied consequences for structure and function. Haematologica 95:956–962.

Ivaskevicius V, Biswas A, Loreth R, Schroeder V, Ohlenforst S, Rott H Krause M, Kohler HP, Scharrer I, Oldenburg J. 2010b. Mutations affecting disulphide bonds contribute to a fairly common prevalence of F13B gene defects: results of a genetic study in 14 families with factor XIII B deficiency. Haemophilia 16:675–682.

Ivaskevicius V, Biswas A, Thomas A, Schroeder, V, Kohler H, Huetker S, Oldenburg J 2012. First case of inherited FXIII-A type II deficiency. Haemophilia 18:185–185.

Jang MA, Park YS, Lee KO, Kim HJ. 2015. Novel and recurrent mutations in the F13A1 gene in unrelated Korean patients with congenital factor XIII deficiency. Blood Coagul Fibrinolysis 26:46–49.

Kohler HP, Ichinose A, Seitz R, Ariens RA, Muszbek L, 2011 Factor XIII And Fibrinogen SSC Subcommittee Of The ISTH. Diagnosis and classification of factor XIII deficiencies. J Thromb Haemost 9:1404–1406.

Kollman JM, Pandi L, Sawaya MR, Riley M, Doolittle RF. 2009. Crystal structure of human fibrinogen. Biochemistry 48:3877–3886.

Komaromi I, Bagoly Z, Muszbek L. 2011. Factor XIII: novel structural and functional aspects. J Thromb Haemost 9:9–20.

Kozakov D, Hall DR, Beglov D, Brenke R, Comeau SR, Shen Y, Li K, Zheng J, Vakili P, Paschalidis I, Vajda S. 2010. Achieving reliability and high accuracy in automated protein docking: ClusPro, PIPER, SDU, and stability analysis in CAPRI rounds 13-19. Proteins 78:3124–3130.

Kozakov D, Beglov D, Bohnuud T, Mottarella SE, Xia B, Hall DR, Vajda S. 2013. How good is automated protein docking? Proteins 81:2159–2166.

Krieger E, Vriend G. 2014. YASARA view—molecular graphics for all devices—from smartphones to workstations. Bioinformatics 30:2981–2982.

Kurniawan NA, Grimbergen J, Koopman J, Koenderink GH. 2014. Factor XIII stiffens fibrin clots by causing fiber compaction. J Thromb Haemost 12:1687–1696.

Lorand L, Losowsky MS, Miloszewski KJ. 1980. Human factor XIII: fibrin-stabilizing factor. Prog Hemost Thromb 5:245–290.

Muszbek L, Bereczky Z, Bagoly Z, Komaromi I, Katona E. 2011. Factor XIII: a coagulation factor with multiple plasmatic and cellular functions. Physiol Rev 91:931–972.

Peyvandi F, Di Michele D, Bolton-Maggs PH, Lee CA, Tripodi A, Srivastava A. 2012. Project on Consensus Definitions in Rare Bleeeding Disorders of the Factor VFIXS, Standardisation Committee of the International Society on T, Haemostasis. Classification of rare bleeding disorders (RBDs) based on the association between coagulant factor activity and clinical bleeding severity. J Thromb Haemost 10:1938–1943.

Philippou H, Rance J, Myles T, Hall SW, Ariens RA, Grant PJ, Leung L, Lane DA. 2003. Roles of low specificity and cofactor interaction sites on thrombin during factor XIII activation. Competition for cofactor sites on thrombin determines its fate. J Biol Chem 278:32020–32026.

Schroeder V, Vuissoz JM, Caflisch A, Kohler HP. 2007. Factor XIII activation peptide is released into plasma upon cleavage by thrombin and shows a different structure compared to its bound form. Thromb Haemost 97:890–898.

Schwartz ML, Pizzo SV, Hill RL, McKee PA. 1973. Human Factor XIII from plasma and platelets. Molecular weights, subunit structures, proteolytic activation, and cross-linking of fibrinogen and fibrin. J Biol Chem 25;248:1395–1407.

Smith KA, Pease RJ, Avery CA, Brown JM, Adamson PJ, Cooke EJ, Neergaard-Petersen S, Cordell PA, Ariens RA, Fishwick CW, Philippou H, Grant PJ. 2013. The activation peptide cleft exposed by thrombin cleavage of FXIII-A(2) contains a recognition site for the fibrinogen alpha chain. Blood 121:2117–2126.

Stieler M, Weber J, Hils M, Kolb P, Heine A, Buchold C, Pasternack R, Klebe G. 2013. Structure of active coagulation factor XIII triggered by calcium binding: basis for the design of next-generation anticoagulants. Angew Chem Int Ed Engl 52:11930–11934.

Thomas A, Biswas A, Ivaskevicius V, Oldenburg J. 2015. Structural and functional influences of coagulation factor XIII subunit B heterozygous missense mutants. Mol Genet Genomic Med 3:258–271.

van Giezen JJ, Minkema J, Bouma BN, Jansen JW. 1993. Cross-linking of alpha 2-antiplasmin to fibrin is a key factor in regulating blood clot lysis: species differences. Blood Coagul Fibrinolysis 4:869–875.

Webb GC, Coggan M, Ichinose A, Board PG. 1989. Localization of the coagulation factor XIII B subunit gene (F13B) to chromosome bands 1q31-32.1 and restriction fragment length polymorphism at the locus. Hum Genet 81:157–160.

Weiss MS, Metzner HJ, Hilgenfeld R. 1998. Two non-proline cis peptide bonds may be important for factor XIII function. FEBS Lett 423:291–296.

Xu D, Zhang Y. 2012. *Ab initio* protein structure assembly using continuous structure fragments and optimized knowledge-based force field. Proteins 80:1715–1735.

Yang J, Yan R, Roy A, Xu D, Poisson J, Zhang Y. 2015. The I-TASSER Suite: protein structure and function prediction. Nat Methods 12:7–8.

Human mutation

Supplementary section

Coagulation Factor XIIIA subunit missense mutations affect structure and function at the various steps of factor XIII action

Anne Thomas[1†], Arijit Biswas[1†]*, Johannes Dodt[2], Helen Philipou[3], Emma Hethershaw[3], Ensikat[4], Vytautas Ivaskevicius[1], Johannes Oldenburg[1*]

[1]Institute of Experimental Haematology and Transfusion Medicine, University Clinic Bonn, 53127 Bonn, Germany
[2]Paul Ehrlich Institut, 63225 Langen, Germany.
[3]Leeds Institute of Cardiovascular and Metabolic Medicine, University of Leeds, Leeds, UK.
[4]Nees Institute for Biodiversity of Plants, University of Bonn, Bonn, Germany.

Running head title: Molecular defects underlying FXIIIA missense mutations

[†]These authors contributed equally to this work.

***Correspondence should be addressed to:**

Dr. rer. nat. Arijit Biswas, Institute of Experimental Haematology and Transfusion Medicine, University Clinic Bonn, Sigmund Freud Str. 25, 53127 Bonn, Germany.
Email: arijit.biswas@ukb.uni-bonn.de
Phone: +49 228 287 19428
Fax: +49 228 287 14320

or

Prof. Dr.(med.) Johannes Oldenburg, Director, Institute of Experimental Haematology and Transfusion Medicine,
University Clinic Bonn, Sigmund Freud Str. 25, 53105 Bonn, Germany.
Email: johannes.oldenburg@ukb.uni-bonn.de
Phone: +49 228 287 15175
Fax: +49 228 287 14783

FXIIIA Activity measurement on FXIIIA expressed cell lysates with a photometric Assay

Determination of the FXIII activity for the expressed cell lysates was conducted with the Technochrom® FXIII Kit (Technoclone GmbH, Austria) according to the manufacturer's instructions. The monitoring of the FXIII activity is based on the detection of ammonia release during activation process by spectrophotometric measurement. FXIIIA levels from normal pooled plasma were measured as a control. Samples above 300 % were diluted and recalculated.

FXIIIA Activity measurement on FXIIIA expressed cell lysates with a pentylamine incorporation Assay

FXIII Activity measurement based on amine incorporation was additionally performed with all the mutants at different time points (0, 10, and 20 mins). For detection of the wild type and mutant FXIII activity an assay with fibrinogen (40 µg/ml) (Sigma Aldrich, Germany) coated microtiter plate was used. Non-specific binding was prevented with 1 % BSA (bovine serum albumin, Roth, Germany) blocking buffer. 15 µl of each sample was mixed with 85 µl of an reaction mix containing 100 µM DTT (Dithiothreitol, Sigma Aldrich, Germany), 2,7 µM 5-(biotinamido) pentylamine (BAPA, Fisher Scientific, Germany), 1 U/ml thrombin (Sigma Aldrich, Germany) and 1 mM $CaCl_2$ (Roth, Germany). Detection of the FXIII activity was conducted using the streptavidin alkaline phosphatase (Sigma Aldrich, Germany) (2 µg/ml) conjugate, which binds to the incorporated BAPA and is proportional to the FXIII activity and was measured photometrical at 405 nm. Additionally, the mutants and wild type were measured with higher calcium concentrations of 100 mM without adding thrombin (to observe non proteolytic activation) into the reaction mix. For evaluation a standard curve was produced with different concentrations of the coagulation reference (Technoclone, Austria) at 2.5, 1.8, 0.18, 0.04, and 0 Units dissolved in TBS (Tris-buffered Saline) (pH 8.3).

FXIIIA antigen quantitation for FXIIIA expressed cell lysates

FXIIIA antigen was quantified for cell lysates in cell lysis buffer using the Technozym FXIII-A:Ag Sub ELISA kit (Technoclone, Austria) according to the manufacturer's instructions. The standard assay detection limit is 0.35 µg/ ml. FXIIIA levels from normal pooled plasma and from high/ low controls were measured as controls. All FXIIIA variant protein concentrations are reported in µg/ ml.

α-2-antiplasmin incorporation assay evaluated for FXIIIA expressing cell

Fibrinogen coated microtiter plates were activated with thrombin and calcium to convert the fibrinogen to fibrin and a mixture of thrombin, calcium, DTT and α-2-antiplasmin before the expressed FXIIIA subunit cell lysates were introduced into the wells. The reaction was stopped over a time course of 50 mins with Ethylenediaminetetraacetic acid (EDTA) from Sigma (Germany). Detection of the cross-linked α 2-antiplasmin was done using anti-human α 2-antiplasmin antibody. The measured OD for each of the samples was used to calculate the % activity relative to $FXIIIA_2B_2$ (Fibrogammin, CSL Behring, Germany) which was also evaluated along with FXIIIA subnit expression lysates. Additionally the value for the negative control was subtracted from the final value for each of the mutants and the wild type.

Activated FXIIIA (FXIIIAa) Activity measurement on FXIIIA expressed cell using a FXIIIAa generation assay

For the measurement 25 µl of the diluted samples were mixed with 35 µl reagent solution containing 100 mM glycinmethylester in HBS (containing 1% human serum albumin), 2 mM fluorogenic FXIIIA substrate A101 (Zedira, Germany) in DMSO, recombinant TF Innovin (Dade Behring, Germany) diluted in phospholipids (from PTT reagent kit, Roche, Germany). The

reaction is started with 20 mM HBS containing 25 mM $CaCl_2$ and the fluorescence is continuously measured during 1 h reflecting the FXIIIa generation. Since only one set of transfection was used to generate these results, therefore to avoid differences of transfection efficiency, only the transfection set showing non-significant differences in the reporter control between mutant and wild type expressed FXIIIA subunit cell lysates was used for this evaluation.

Western Blotting of FXIIIA expressed cell lysates

Western blotting was performed with 15 µl of expressed FXIIIA subunit cell lysates which were denatured in a 1:1 ratio with laemmli sample buffer (BioRad, Germany) and run on a 10 % tris-glycine gel (BioRad, Germany) by 140 V for 95 min. After the protein transfer to a PVDF (polyvinylidene fluoride) membrane (Amersham Hybond-P GE Healthcare, Germany) detection of FXIIIA protein was done with 4 µg of a FXIIIA polyclonal IgG goat antibody (Santa Cruz Biotechnology, Germany) labeled with 2 µg of donkey anti goat IgG-HRP (Santa Cruz Biotechnology, Germany). ß-actin detection was used as an internal control and was performed using a mouse monoclonal anti-ß actin HRP coupled antibody (Abcam, England). Signal development was done with the BM Chemiluminescence kit (Roche, Germany).

Fibrin clots run on a SDS PAGE

A 1:1 solution for each cell lysates sample with FXIII deficient plasma was activated with thrombin (0.5 U) and calcium (50 mM) to form clots. The reaction was stopped at several time points (0 min, 10 min, 30 min, 60 min and 90 min) using 100 µl EDTA (50 mM). Furthermore, normal pooled plasma and rFXIIIA (recombinant FXIIIA, Zedira, Germany) (5 ng/ µl) mixed with FXIIIA deficient plasma were used. Clots were washed in 15 µl PBS and denatured with 15 µl laemmli buffer (BioRad, Germany) for 8 min, 96°C. Samples were run on a 10 % tris-glycine-gel under denaturing conditions with SDS for 95 min under 140 Volt. Protein staining on the gels

was performed with BioSafe Coomassie (Biorad, Germany). To avoid differences of transfection efficiency, only the transfection set showing non-significant differences in the reporter control between mutant and wild type expressed FXIIIA subunit cell lysates was used for this evaluation.

Scanning electron microscopy and fibrin clot thickness evaluation of clots generated from FXIIIA expressed cell lysates

Washed clots were fixed in 4 % glutaraldehyde (Sigma, Germany) and dehydration in a graded ethanol solution (20 %, 40 %, 60 %, 80 % and 99 %) followed. All clots were stored at 4°C in 99 % ethanol till analysis was performed. Critical Point drying (CPD), sample mounting, gold coating and viewing of the specimens in the SEM was performed in a DPD 020 CP dryer (Balzers AG, Liechtenstein) using carbon dioxide as drying medium. The dry samples were mounted on conductive adhesive tabs and sputter-coated with a 30 nm gold layer, using a SCD 040 sputter coater (Balzers AG, Liechtenstein). Scanning electron microscopy was done on a Cambridge S 200 Stereoscan (Cambridge, UK) microscope. Images were obtained at 4000X and 16000X resolution. Quantitative analysis of fiber thickness for the expressed clot sample images was performed with the BoneJ plugin embedded in the Fiji (ImageJ) image visualization and analysis package. The original images with resolutions of 4000X and 16000X were first converted into a binary image using the BoneJ Plugin to generate a colored thickness map. Calculations of thickness were performed on the colored thickness map with uniform threshold ratio of 78/200 (adjusting the minimum and maximum threshold value) for all images.

Modeling and docking analysis for FXIIIA and its interacting partners

A) Interaction with α-2-antiplasmin

A threaded model for human α-2-antiplasmin was generated on the ITASSER server (http://zhanglab.ccmb.med.umich.edu/I-TASSER/ accessed on 22.11.2014) using the murine α-

2-antiplasmin (PDB ID: 2r9y; 2.65 Å resolution) as a guiding constraint. Since the murine α-2-antiplasmin differs from the human α-2-antiplasmin in the N-terminal region (missing in Bovine) and because the N-terminal region carries the reactive glutamine for the human α-2-antiplasmin, an *ab initio* based model of a 65 amino acid long N-terminal region of 2-antiplasmin was generated on the Quark ab initio server (http://zhanglab.ccmb.med.umich.edu/QUARK/; accessed on 27.11.2014). The generated model was used for docking analysis on the activated FXIII (FXIIIAa) structure using Q2 and Q4 residues of α-2-antiplasmin and the catalytic triad residues of FXIII as guiding constraints. All dockings were performed on the cluspro docking server (http://cluspro.bu.edu/login.php; accessed between 08.12.2014 and 24.12.2014). The best dock was determined to be the one with least distance between the Q2 residue of α-2-antiplasmin for putative interactions between α-2-antiplasmin and activated FXIIIAa. The complete docked structure was subsequently recreated by joining the rest of human α-2-antiplasmin model onto the docked 65 amino acid long N-terminal region of human α-2-antiplasmin. Model joining was done by replacing the last two amino acid residues common to both models so as to keep the dihedral angles for the full model at the point of joining the same. The entire structure was energy minimized during a model refining solvated simulation lasting 500 ps (using the YAMBER force field) to remove any bumps and stereo chemical clashes occurring as a result of model joining (Krieger et al, 2004). The model with the energetic minimum in the simulation trajectory was chosen as the final model and used for further analysis.

B) Interaction with fibrinogen

The fibrinogen crystal structure (PDB ID: 3GHG; 2.9 Å resolution) was used for studying interaction between activated FXIIIAa and fibrinogen. Missing parts of alpha and gamma chain residues in the crystal structure of fibrinogen which carry the reactive glutamines *ab initio* based

modeled on the Quark *ab initio* server (http://zhanglab.ccmb.med.umich.edu/QUARK/; accessed on 03.12.2014). These models were docked on the activated FXIII (FXIIIAa) structure using different known reactive glutamine donor residues as guiding restraints, one dock at a time. Docking was performed on the cluspro server (http://cluspro.bu.edu/login.php ; accessed between 08.12.2014 and 24.12.2014). The best dock was determined to be the one with least distance between the particular reactive donor glutamine used as a guiding restraint in that dock and the reactive Cys314 residue of the activated FXIII (FXIIIAa) structure. The complete docked structure was subsequently recreated by joining the rest of the chain structure taken from the PDB file: 3GHG (2.9 Å resolution) on the respective fibrinogen chain already docked on the activated FXIII (FXIIIAa) structure. Model joining was done by replacing the last two amino acid residues common to both models so as to keep the dihedral angles for the full model at the point of joining the same. The docked structure was further refined using a similar protocol as for the α-2-antiplasmin: activated FXIII (FXIIIAa) dock.

C) Interaction with thrombin

The active thrombin; FXIII complex was recreated by docking in order to analyze any position influences of one of our variants on this interaction. The active thrombin heavy chain structure (PDB ID: 1PPB; chain: H; 1.92 Å resolution) was used to dock on the monomeric chain zymogenic crystal structure of FXIII (PDB ID: 1f13; 2.1 Å resolution). The Arg37-Gly38 sessile bond is unresolved in the crystal structure of zymogenic FXIII (1f13). Therefore before docking the loop corresponding to this sessile bond was modeled on the Fread loop modeling server (http://opig.stats.ox.ac.uk/webapps/fread/php/ accessed on 05.12.2014) and joined to the zymogenic FXIII crystal structure. Residues which are known to be important or participate in this interaction were used as guiding constraints for this docking. The best docked model was chosen on the basis of the least distance between the catalytic Ser195 residue of Thrombin and

the Arg37-Gly38 sessile bond. The docked structure was further refined using a similar protocol as for the α-2-antiplasmin: activated FXIII (FXIIIAa) dock.

Supplementary Tables and Images

Table S1. Interaction chart for the t**hrombin-zymogenic FXIII dock.**

	Zymogenic FXIII						**Thrombin**				
Atom	**Atom no.**	**Atom name**	**Res name**	**Res no.**	**Chain**	**Atom no.**	**Atom name**	**Res name**	**Res no.**	**Chain**	**Distance (in Å)**
1	221	OE2	GLU	31	B	945	NH1	ARG	97	H	2.71
2	221	OE2	GLU	31	B	948	NH2	ARG	97	H	2.75
3	224	N	LEU	32	B	952	O	ARG	97	H	2.98
4	232	O	LEU	32	B	434	OH	TYR	60	H	2.62
5	273	N	ARG	38	B	1991	OE2	GLU	192	H	2.98
6	282	NH1	ARG	38	B	1967	OD1	ASP	189	H	2.82
7	282	NH1	ARG	38	B	1976	O	ALA	190	H	2.6
8	285	NH2	ARG	38	B	1967	OD1	ASP	189	H	2.82
9	285	NH2	ARG	38	B	2257	O	GLY	219	H	2.64
10	285	NH2	ARG	38	B	2317	O	LYS	224	H	2.8
11	290	N	GLY	39	B	1991	OE2	GLU	192	H	2.97
12	313	O	ASN	41	B	1761	NH2	ARG	178	H	2.64
13	320	OE1	GLN	43	B	2312	NZ	LYS	224	H	2.73
14	321	NE2	GLN	43	B	1739	O	SER	171	H	2.87
15	332	OE1	GLU	44	B	2286	NH2	ARG	221	H	2.79
16	362	OD1	ASN	47	B	1758	NH1	ARG	173	H	2.75

Table S2. Interaction chart for the α-2-antiplasmin-activated FXIII dock.

	FXIIIa´						**α -2-antiplasmin**				
Atom	**Atom no.**	**Atom name**	**Res name**	**Res no.**	**Chain**	**Atom no.**	**Atom name**	**Res name**	**Res no.**	**Chain**	**Distance (in Å)**
1	4186	NE1	TRP	280	A	10733	OE1	GLN	2	B	2.7
2	4220	ND2	ASN	282	A	11130	O	GLY	29	B	3.07
3	5391	N	ASN	360	A	15106	OG	SER	280	B	2.73
4	5428	ND2	ASN	362	A	15042	O	LEU	276	B	2.73
5	5493	NZ	LYS	367	A	11446	O	PHE	50	B	3.29
6	5579	O	TYR	373	A	10734	NE2	GLN	2	B	3.25
7	5593	OH	TYR	373	A	10716	OD1	ASN	1	B	2.53
8	6111	OH	TYR	408	A	12093	NH2	ARG	93	B	2.56
9	6111	OH	TYR	408	A	15772	NE2	GLN	319	B	2.94
10	6666	O	ALA	445	A	15068	N	ASN	278	B	1.41
11	6708	O	THR	450	A	15075	ND2	ASN	278	B	3.08

Table S3. Interaction chart for the fibrinogen **α-chain** -activated FXIII dock based on the Glutamine 223 residue constraint.

	FXIIIa´					**Fibrinogen (α-chain 223 Glutamine residue)**					
Atom	**Atom no.**	**Atom name**	**Res name**	**Res no.**	**Chain**	**Atom no.**	**Atom name**	**Res name**	**Res no.**	**Chain**	**Distance (in Å)**
1.	2175	O	GLY	229	A	9728	NZ	LYS	208	D	3.12
2.	2541	N	ALA	269	A	11664	O	SER	373	D	2.91
3.	2568	O	ASP	271	A	11329	N	ARG	348	D	1.44
4.	2578	N	GLU	273	A	11262	O	ASN	342	D	2.75
5.	2587	O	GLU	273	A	11668	OG	SER	373	D	3.14
6.	2609	O	LEU	276	A	11690	N	ARG	375	D	1.95
7.	2610	N	VAL	277	A	11646	O	SER	371	D	2.15
8.	2630	O	SER	279	A	10024	NH1	ARG	239	D	1.90
9.	2666	O	ASN	282	A	12259	NZ	LYS	413	D	2.54
10.	2675	O	ILE	283	A	12111	N	ARG	406	D	2.46
11.	2710	N	GLY	287	A	12102	O	THR	405	D	2.94
12.	2710	N	GLY	287	A	12105	OG1	THR	405	D	3.08
13.	2714	O	GLY	287	A	12105	OG1	THR	405	D	2.50
14.	2715	N	VAL	288	A	12172	OE1	GLU	408	D	2.01
15.	2736	O	PRO	290	A	9387	NZ	LYS	183	D	1.96
16.	2741	OG	SER	291	A	9799	OD1	ASN	217	D	3.27
17.	2741	OG	SER	291	A	9830	N	SER	220	D	3.04
18.	2766	O	TRP	293	A	9387	NZ	LYS	183	D	3.08
19.	2771	OG1	THR	294	A	9306	OH	TYR	178	D	3.25
20.	2805	O	ASP	298	A	9604	NE	ARG	197	D	3.28
21.	2814	O	ILE	299	A	9610	NH2	ARG	197	D	2.65
22.	2886	OG	SER	306	A	9607	NH1	ARG	197	D	2.86
23.	2926	N	ARG	311	A	11603	O	HIS	368	D	2.59
24.	2938	NH2	ARG	311	A	11556	O	GLY	365	D	2.61
25.	2938	NH2	ARG	311	A	11624	OG S	ER	369	D	2.27
26.	2956	O	TYR	312	A	12174	N T	YR	409	D	2.30
27.	2968	OE1	GLN	314	A	9850	N	LEU	222	D	2.29
28.	2969	NE2	GLN	314	A	12179	O	TYR	409	D	2.82
29.	2978	SG	CYS	315	A	12193	OH	TYR	409	D	3.23
30.	3254	O	HIS	343	A	10079	NH1	ARG	244	D	1.96
31.	3270	ND2	ASN	345	A	10066	OE1	GLU	243	D	3.24
32.	3527	N	ASN	372	A	9891	O	VAL	225	D	2.36
33.	3548	OH	TYR	373	A	12193	OH	TYR	409	D	3.14
34.	3829	N	ASN	403	A	11078	OE1	GLN	328	D	2.65
35.	3857	N	GLY	406	A	11003	O	THR	322	D	2.11
36.	3871	N	TYR	408	A	11365	O	SER	350	D	2.26
37.	3881	OH	TYR	408	A	11078	OE1	GLN	328	D	3.18

Table S4. Interaction chart for the fibrinogen **α-chain** -activated FXIII dock based on the glutamine 237 residue constraint.

	FXIIIa´						**Fibrinogen (α-chain 237 Glutamine residue)**				
Atom	**Atom no.**	**Atom name**	**Res name**	**Res no.**	**Chain**	**Atom no.**	**Atom name**	**Res name**	**Res no.**	**Chain**	**Distance (in Å)**
8.	574	N	LYS	74	A	12149	OG1	THR	405	D	2.69
9.	930	O	VAL	105	A	11256	N	GLY	339	D	2.40
10.	939	O	ILE	106	A	11345	OG	SER	345	D	3.20
11.	957	NH2	ARG	108	A	10923	OG	SER	311	D	3.12
12.	1419	O	VAL	155	A	11734	N	ARG	375	D	2.18
13.	1432	NZ	LYS	157	A	11585	O	THR	364	D	2.92
14.	1462	NH2	ARG	159	A	11684	OE2	GLU	370	D	2.28
15.	1685	O	THR	171	A	11696	N	GLY	372	D	3.18
16.	1708	O	ILE	173	A	11714	N	PHE	374	D	2.80
17.	1708	O	ILE	173	A	11752	NH1	ARG	375	D	2.97
18.	2034	N	GLY	216	A	9899	OD1	ASN	217	D	2.60
19.	2039	N	GLU	217	A	9340	O	GLN	181	D	2.61
20.	2067	O	ASN	219	A	9138	N	LEU	169	D	3.28
21.	2063	ND2	ASN	219	A	9109	O	ARG	167	D	3.26
22.	2074	OD2	ASP	220	A	9038	SG	CYS	161	D	2.70
23.	2077	N	ILE	221	A	9232	OD1	ASP	174	D	3.08
24.	2093	NZ	LYS	222	A	9038	SG	CYS	161	D	2.97
25.	2093	NZ	LYS	222	A	9280	O	ASP	177	D	2.21
26.	2108	N	ARG	214	A	9321	OE1	GLU	179	D	2.77
27.	2215	OD1	ASP	233	A	12155	N	ARG	406	D	2.36
28.	2255	OG1	THR	238	A	12285	N	LYS	413	D	3.06
29.	2260	N	CYS	239	A	12223	O	TYR	409	D	1.94
30.	2286	OH	TYR	241	A	12762	OG	SER	443	D	2.01
31.	2307	N	ASP	244	A	11777	O	ASP	377	D	2.33
32.	2345	OE1	GLN	247	A	10282	OG1	THR	256	D	2.93
33.	2346	NE2	GLN	247	A	10277	O	SER	255	D	2.50
34.	2346	NE2	GLN	247	A	10764	O	THR	299	D	2.87
35.	2400	NH1	ARG	253	A	11777	O	ASP	377	D	2.49
36.	2403	NH2	ARG	253	A	11420	O	ALA	351	D	2.82
37.	2540	O	ASN	268	A	10210	ND2	ASN	248	D	2.23
38.	2574	OD1	ASP	272	A	10210	ND2	ASN	248	D	2.39
39.	2863	NE	ARG	304	A	11815	O	GLY	380	D	3.05
40.	2896	OE1	GLU	307	A	238	OG1	THR	251	D	2.52
41.	2906	ND2	ASN	308	A	12769	O	LYS	444	D	3.26
42.	3035	O	VAL	321	A	12237	OH	TYR	409	D	2.41
43.	3217	N	PHE	340	A	9888	O	PRO	215	D	2.10
44.	3532	OD1	ASN	372	A	9938	N	GLN	221	D	2.73
45.	3563	O	HIS	374	A	9655	NH1	ARG	199	D	2.03
46.	3568	SG	CYS	375	A	9658	NH2	ARG	199	D	3.28
47.	4129	OE1	GLU	435	A	9622	NH2	ARG	197	D	2.78

48.	4374	NZ	LYS	447	A	9635	OD1	ASP	198	D	2.35
49.	4467	O	ASP	457	A	9271	NZ	LYS	176	D	2.58

Table S5. Interaction chart for the fibrinogen **α-chain** -activated FXIII dock based on the glutamine 366 residue constraint.

	FXIIIa´						**Fibrinogen (α-chain 366 Glutamine residue)**				
Atom	**Atom no.**	**Atom name**	**Res name**	**Res no.**	**Chain**	**Atom no.**	**Atom name**	**Res name**	**Res no.**	**Chain**	**Distance (in Å)**
1.	3295	N	VAL	218	A	16518	OG1	THR	393	D	2.72
2.	3320	ND2	ASN	219	A	16511	O	GLY	392	D	2.69
3.	4260	OD2	ASP	281	A	15942	OG	SER	350	D	2.19
4.	4272	ND2	ASN	282	A	15319	O	THR	301	D	3.05
5.	4272	ND2	ASN	282	A	15979	O	HIS	353	D	2.63
6.	4296	N	TYR	284	A	15942	OG	SER	350	D	3.12
7.	4316	O	TYR	284	A	15553	OG	SER	319	D	2.77
8.	4313	OH	TYR	284	A	15701	OG	SER	332	D	3.09
9.	4313	OH	TYR	284	A	15822	NE1	TRP	341	D	3.00
10.	4347	O	TYR	286	A	15920	NH1	ARG	348	D	3.01
11.	4348	N	GLY	287	A	15553	OG	SER	319	D	3.02
12.	4778	SG	CYS	315	A	15738	NH2	ARG	334	D	3.00
13.	5621	N	VAL	370	A	16092	O	SER	361	D	3.04
14.	5636	O	VAL	370	A	16111	N	THR	364	D	2.33
15.	5636	O	VAL	370	A	16125	N	GLY	365	D	2.61
16.	5695	O	TYR	373	A	15735	NH1	ARG	334	D	2.60
17.	6099	O	PRO	400	A	15773	N	THR	338	D	2.77
18.	6815	O	LYS	447	A	13160	N	LYS	157	D	2.61
19.	7127	NE2	GLN	469	A	18313	O	PHE	514	D	2.39
20.	7157	O	GLY	471	A	18353	N	MET	517	D	2.54

Table S6. Interaction chart for the fibrinogen **α-chain** -activated FXIII dock based on the glutamine 563 residue constraint.

	FXIIIa´					**Fibrinogen (α-chain 563 Glutamine residue)**					
Atom	**Atom no.**	**Atom name**	**Res name**	**Res no.**	**Chain**	**Atom no.**	**Atom name**	**Res name**	**Res no.**	**Chain**	**Distance (in Å)**
1.	2925	O	VAL	310	A	14606	NZ	LYS	556	D	2.09
2.	2968	OE1	GLN	314	A	14520	N	GLY	547	D	2.73
3.	2978	SG	CYS	315	A	14533	O	ILE	548	D	1.60
4.	3183	N	THR	337	A	14337	O	GLY	529	D	2.67
5.	3191	O	THR	337	A	14382	N	ILE	534	D	2.92
6.	3202	O	ASN	338	A	14413	N	THR	536	D	2.31
7.	3197	OD1	ASN	338	A	14023	NZ	LYS	508	D	3.20
8.	3197	OD1	ASN	338	A	14401	N	PHE	535	D	2.91
9.	3198	ND2	ASN	338	A	14485	OG	SER	543	D	3.31
10.	3389	O	GLU	357	A	10813	OG	SER	275	D	2.80
11.	3386	OE1	GLU	357	A	10839	N	ASN	277	D	1.32
12.	3398	O	ASP	358	A	14871	OH	TYR	582	D	2.91
13.	3415	N	VAL	361	A	14797	OG	SER	575	D	1.49
14.	3503	N	VAL	370	A	14716	OG	SER	567	D	2.01
15.	3510	O	VAL	370	A	14712	N	SER	567	D	3.18
16.	3551	O	TYR	373	A	14501	N	HIS	545	D	2.64
17.	3552	N	HIS	374	A	14369	O	SER	532	D	3.18
18.	3560	NE2	HIS	374	A	14646	OH	TYR	560	D	2.94
19.	3560	NE2	HIS	374	A	14646	OH	TYR	560	D	2.94
20.	3605	OE2	GLU	378	A	14331	N	GLY	529	D	2.80
21.	3779	OD1	ASP	397	A	14550	N	PHE	551	D	2.01
22.	3819	N	GLU	402	A	14573	OG	SER	553	D	2.34
23.	3942	O	VAL	415	A	14267	N	THR	525	D	2.95
24.	3961	N	ILE	418	A	14275	OG1	THR	525	D	2.84
25.	4104	O	VAL	432	A	14325	NH1	ARG	528	D	1.65
26.	4130	OE2	GLU	435	A	14509	NE2	HIS	545	D	3.06
27.	4232	NZ	LYS	446	A	10862	OG	SER	278	D	2.99
28.	4326	N	ALA	458	A	13726	OD2	ASP	488	D	3.09
29.	4332	N	THR	459	A	13726	OD2	ASP	488	D	1.99
30.	4388	O	LEU	464	A	14382	N	ILE	534	D	1.86
31.	4398	N	VAL	466	A	14337	O	GLY	529	D	2.73
32.	4587	N	GLU	486	A	14004	O	GLY	507	D	2.74
33.	4597	N	GLY	487	A	14035	OG1	THR	509	D	2.81
34.	4634	N	GLU	491	A	14046	O	PHE	510	D	2.95
35.	4669	O	LEU	493	A	14147	N	MET	517	D	2.13
36.	4676	N	LEU	495	A	14081	O	GLY	512	D	2.83
37.	4676	N	LEU	495	A	14127	O	SER	515	D	2.25

Table S7. Interaction chart for the fibrinogen **γ-chain** -activated FXIII dock based on the glutamine 398 residue constraint.

	FXIIIa´						**Fibrinogen (γ chain 398 Glutamine residue)**				
Atom	**Atom no.**	**Atom name**	**Res name**	**Res no.**	**Chain**	**Atom no.**	**Atom name**	**Res name**	**Res no.**	**Chain**	**Distance (in Å)**
1.	2019	O	PHE	214	A	12093	N G	LY	404	C	2.79
2.	2030	OH	TYR	215	A	11623	N S	ER	358	C	2.66
3.	2124	O	ARG	224	A	11962	ND2	ASN	390	C	2.73
4.	2117	NH1	ARG	224	A	11805	O	ARG	375	C	3.00
5.	2120	NH2	ARG	224	A	11835	O	TYR	377	C	2.82
6.	2149	N	SER	227	A	11784	OG1	THR	374	C	3.31
7.	2153	OG	SER	227	A	11784	OG1	THR	374	C	3.35
8.	2153	OG	SER	227	A	11795	NE	ARG	375	C	2.17
9.	2206	OE1	GLU	232	A	11005	N	ASP	294	C	3.21
10.	2600	O	VAL	275	A	10660	NH1	ARG	256	C	2.65
11.	2686	OH	TYR	284	A	12026	N	GLY	397	C	3.13
12.	2709	O	TYR	286	A	10646	N	GLY	255	C	1.96
13.	2714	O	GLY	287	A	11533	OH	TYR	348	C	2.20
14.	2736	O	PRO	290	A	11913	NZ	LYS	385	C	2.87
15.	2741	OG	SER	291	A	11568	N	GLY	352	C	3.26
16.	2751	N	TRP	293	A	11572	O	GLY	352	C	3.24
17.	2780	O	GLY	295	A	11780	N	THR	374	C	3.17
18.	2797	N	ASP	298	A	11741	O	ALA	370	C	3.29
19.	2806	N	ILE	299	A	11766	O	TRP	372	C	2.50
20.	2839	OE1	GLU	302	A	11760	NE1	TRP	372	C	2.14
21.	2932	NE	ARG	311	A	10612	O	ASP	252	C	3.01
22.	2932	NE	ARG	311	A	10617	OD1	ASP	252	C	3.23
23.	2935	NH1	ARG	311	A	10650	O	GLY	255	C	2.76
24.	2938	NH2	ARG	311	A	10617	OD1	ASP	252	C	2.75
25.	2974	N	CYS	315	A	12146	OD2	ASP	410	C	2.07
26.	3182	O	VAL	336	A	12075	NE2	HIS	401	C	2.16
27.	3191	O	THR	337	A	12104	N	LYS	406	C	1.75
28.	3229	N	SER	341	A	12128	O	GLN	407	C	2.67
29.	3551	O	TYR	373	A	12067	N	HIS	401	C	2.88
30.	3552	N	HIS	374	A	12116	O	LYS	406	C	3.09
31.	3563	O	HIS	374	A	12088	N	GLY	403	C	3.25
32.	3557	ND1	HIS	374	A	12067	N	HIS	401	C	2.63
33.	3557	ND1	HIS	374	A	12134	O	ALA	408	C	1.48
34.	3568	SG	CYS	375	A	11966	O	ASN	390	C	2.29
35.	3586	O	TRP	376	A	12075	NE2	HIS	401	C	3.06
36.	4398	N	VAL	466	A	12092	O G	LY	403	C	3.06

Table S8. Summary of the patient's genotype and phenotype.

Patient ID/ Sex/ Age	Genotype	Affected domain	Exon	Phenotype	Bleeding score	FXIII %	FXIII %	Ag*: FXIII A %	Ag*: FXIII B %
U/M/5	Arg38Gln	Activation peptide	1	AS*	-	29-35	18-38	85-121	81-120
V/F/30	Arg38Pro	Activation peptide	1	Menorrhagia and a large haematoma after a caesarean section	-	20	n.d.*	42	97
A/F/22	Pro167Leu, c.500C>T	Beta-Sandwich	4	Delayed bleeding after wisdom tooth extraction	3	52-55	63	77	83
B/F/29	Tyr168Cys, c.503>G	Beta-sandwich	4	AS	n.d.	57-70	n.d.	n.d.	n.d.
C/F/30	Arg172Gln, c.515G>A	Beta-Sandwich	4	No history of risk exposure (e.g. major trauma, surgery, etc.)	0	45	n.d.	n.d.	n.d.
D/M/10	Pro290Arg, c.869C>G	Core	7	Subcutaneous shank hematoma due to trauma	n.d.	46	n.d.	n.d.	n.d.
E/M/37	His343Tyr, c.1027C>T	Core	8	No bleeding after appendectomy, inguinal herniotomy, right hand surgery or arthroscopy of right knee	-1	40	50	38	72
F/F/36	Gln416Arg, c.1247A>G	Core	10	Postpartum bleeding	4	55-57	63	55	60
G/F/41	Leu530Pro, c.1589T>C	Barrel1	12	AS	0	67	n.d.	n.d.	n.d.
H/F/32	Arg541Gln, c.1622G	Barrel1	12	AS	n.d.	50-61	n.d.	n.d.	n.d.
I/F/28	Gly593Ser, c.1777G>A	Barrel1	13	Postpartum bleeding	n.d.	61	n.d.	n.d.	n.d.

J/F/42	Gly593Ser, c.1777G>A			Menorrhagia, postpartum bleeding, bleeding after dental extraction		71			
K/F/35	Gly593Ser, c.1777G>A			Bleeding after breast fibrioadenoma surgery		60			
L/F/50	Gln602Lys, c.1804C>A	Barrel1	13	Subcutaneous Haemorrhages	1	38-40	n.d.	n.d.	n.d.
M/F/32	Gln602Lys, c.1804C>A			Postpartum (massive blood loss)	4	52-54	39	59	137
N/M/59	Arg612His, c.1835G>A	Barrel1	13	Postoperative bleeding due to facial trauma	n.d.	49	n.d.	n.d.	n.d.
O/M/27	Arg612His, c.1835G>A			AS		43			
P/F/24	Arg612His, c.1835G>A			AS		43			
Q/M/3	Asp669Gly, c.2006A>G	Barrel2	14	Bleeding due to craniostenosis surgery, mucous and subcutaneous bleeds, impaired wound healing	n.d.	23-40	n.d.	n.d.	n.d.
R/F/22	Asp669Gly, c.2006A>G			AS		n.d.			
S/F/20	Arg704Gln, c.2111G>A	Barrel2	15	Delayed bleeding after wisdom tooth extraction	3	58	63	61	73
T/M/46	Arg716Gly, c.2146A>G	Barrel2	15	-	0	50-55	n.d.	n.d.	n.d.

*Abbreviations: AS: asymptomatic at presentation, n.d.: not done, Ag: antigen, %: percentage of normal pool plasma. [&]FXIII Behrichrom activity assay [%]FXIII Technoclone activity assay

Figure S1. The western blotting image for all the expressed FXIIIA variants and controls. Wild type FXIIIA, rFXIIIA and non-transfected cell lysates served as controls.

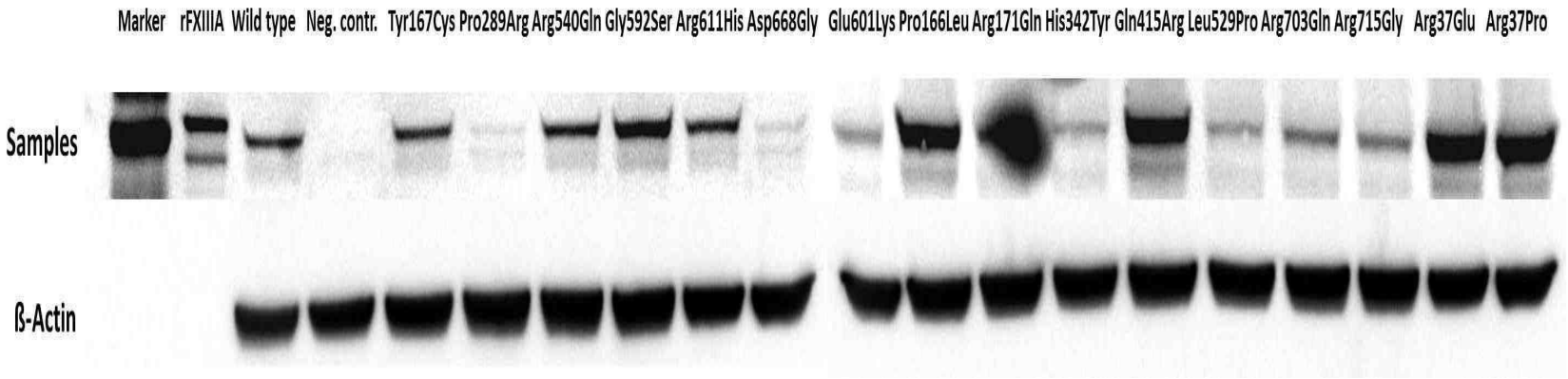

Figure S2. This figure shows the plotted curves for the variants with detection levels above the detection limit. Apart from the recombinant expressed variants, also depicted in this figure is the curve of FXIIIa generation in normal pool plasma. The area under the curve (AUC), time to peak (TTP) and concentration at peak (CP) for wild type as well as some variants has been calculated from these curves and some of these variables have been shown in **Figure 3**.

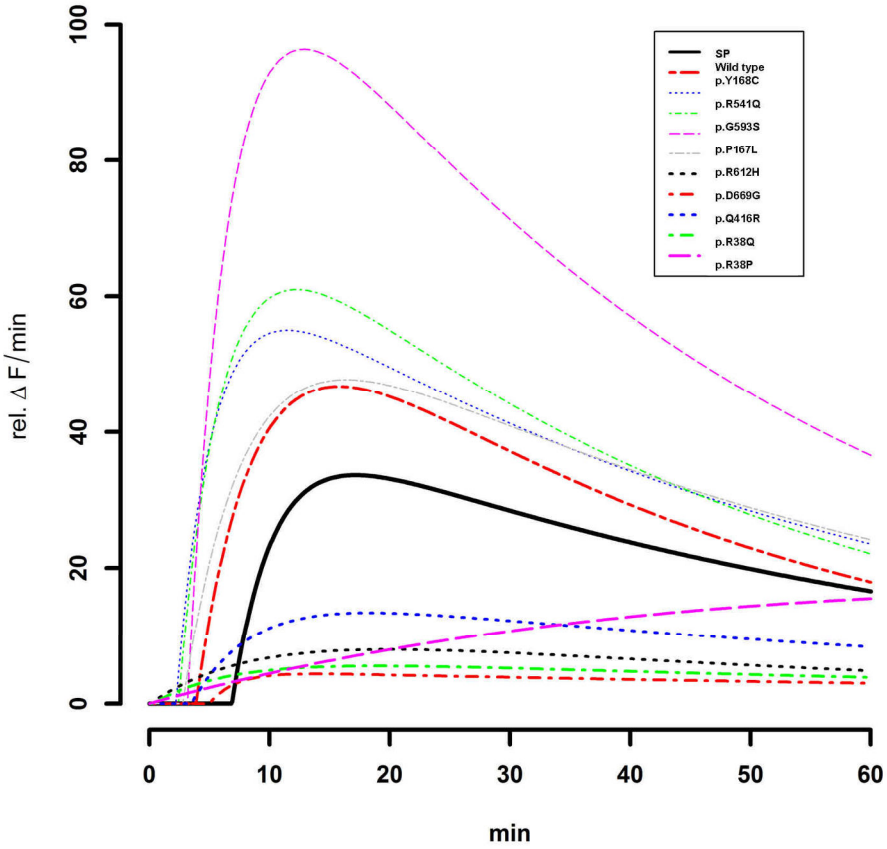

Figure S3. The modelled activation pathway for the FXIIIA subunit
This image is split up into two panels. The right panel shows multiple coarse grained transition forms (the number of intermediate forms for the sake of clarity has been reduced from 463 to only 10) between the activated and zymogenic FXIIIA unit monomer. The activated and zymogenic FXIIIA unit monomer is coloured red and blue respectively. All intermediate forms are coloured yellow. The left panels also shows the multiple coarse grained transition forms in the background. As an example two sets of residues have been colour coded specifically in the activated and the zymogenic forms in order to depict the conformational transition occurring during this change. The colour coding goes as:
Green: Residues close to the p.Lys222 residue in the zymogenic form. **Red:** The p.Lys222 residue in the zymogenic form. **Blue:** Reported mutations from our study close to the p.Lys222 residue in the zymogenic form. **Yellow:** Residues which were earlier close to the p.Lys222 residue now their position in the activated form. **Magenta:** The p.Lys222 residue in the activated form. **Purple:** Reported mutations (from our study) which were earlier close to the Lys221 residue now in the activated form.
From the above description it is evident that the residues close to p.Lys222 residue in the zymogenic FXIIIA (more importantly the ones on which the mutations have been reported in this study i.e. p.Arg716Gly, p.Leu530Pro and p.Gln602Lys) move away (>5Å) in the activated FXIIIA following conformational changes.

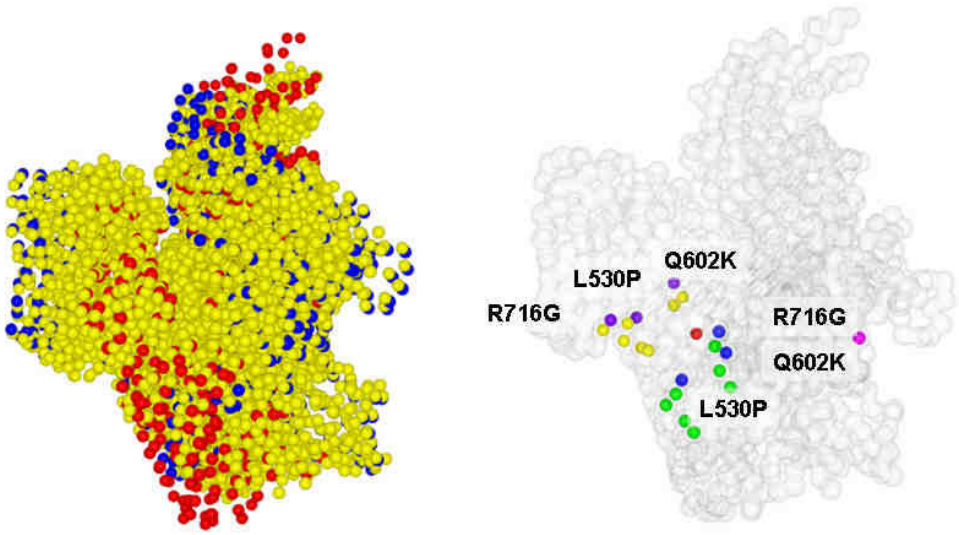

Chapter III: Supplementary

3.1 References

1. Lewis, B. A., Freyssinet, J. M. & Holbrook, J. J. An equilibrium study of metal ion binding to human plasma coagulation factor XIII. *Biochem. J.* **169,** 397–402 (1978).
2. Page, M. J. & Di Cera, E. Serine peptidases: classification, structure and function. *Cell. Mol. Life Sci. CMLS* **65,** 1220–1236 (2008).
3. Lippi, G., Favaloro, E. J., Franchini, M. & Guidi, G. C. Milestones and perspectives in coagulation and hemostasis. *Semin. Thromb. Hemost.* **35,** 9–22 (2009).
4. Gale, A. J. Continuing education course #2: current understanding of hemostasis. *Toxicol. Pathol.* **39,** 273–280 (2011).
5. Jennings, L. K. Role of platelets in atherothrombosis. *Am. J. Cardiol.* **103,** 4A–10A (2009).
6. Osterud, B. & Rapaport, S. I. Activation of factor IX by the reaction product of tissue factor and factor VII: additional pathway for initiating blood coagulation. *Proc. Natl. Acad. Sci. U. S. A.* **74,** 5260–5264 (1977).
7. Nieswandt, B. & Watson, S. P. Platelet-collagen interaction: is GPVI the central receptor? *Blood* **102,** 449–461 (2003).
8. Moroi, M. *et al.* Analysis of the involvement of the von Willebrand factor-glycoprotein Ib interaction in platelet adhesion to a collagen-coated surface under flow conditions. *Blood* **90,** 4413–4424 (1997).
9. Savage, B., Almus-Jacobs, F. & Ruggeri, Z. M. Specific synergy of multiple substrate-receptor interactions in platelet thrombus formation under flow. *Cell* **94,** 657–666 (1998).
10. Goodeve, A. C. The genetic basis of von Willebrand disease. *Blood Rev.* **24,** 123–134 (2010).
11. Luo, G.-P., Ni, B., Yang, X. & Wu, Y.-Z. von Willebrand factor: more than a regulator of hemostasis and thrombosis. *Acta Haematol.* **128,** 158–169 (2012).
12. Miura, Y., Takahashi, T., Jung, S. M. & Moroi, M. Analysis of the interaction of platelet collagen receptor glycoprotein VI (GPVI) with collagen. A dimeric form of GPVI, but not the monomeric form, shows affinity to fibrous collagen. *J. Biol. Chem.* **277,** 46197–46204 (2002).
13. Wörner, P. & Brossmer, R. Platelet aggregation and the release induced by inophores for divalent cations. *Thromb. Res.* **6,** 295–305 (1975).
14. Feinstein, M. B. & Fraser, C. Human platelet secretion and aggregation induced by calcium ionophores. Inhibition by PGE1 and dibutyryl cyclic AMP. *J. Gen. Physiol.* **66,** 561–581 (1975).
15. Feinstein, M. B., Becker, E. L. & Fraser, C. Thrombin, collagen and A23187 stimulated endogenous platelet arachidonate metabolism: differential inhibition by PGE1, local anesthetics and a serine-protease inhibitor. *Prostaglandins* **14,** 1075–1093 (1977).
16. Bevers, E. M., Comfurius, P. & Zwaal, R. F. Changes in membrane phospholipid distribution during platelet activation. *Biochim. Biophys. Acta* **736,** 57–66 (1983).
17. Rink, T. J. & Sage, S. O. Calcium signaling in human platelets. *Annu. Rev. Physiol.* **52,** 431–449 (1990).
18. Berridge, M. J., Bootman, M. D. & Roderick, H. L. Calcium signalling: dynamics, homeostasis and remodelling. *Nat. Rev. Mol. Cell Biol.* **4,** 517–529 (2003).
19. Hathaway, D. R. & Adelstein, R. S. Human platelet myosin light chain kinase requires the calcium-binding protein calmodulin for activity. *Proc. Natl. Acad. Sci. U. S. A.* **76,** 1653–1657 (1979).
20. Shattil, S. J. & Brass, L. F. Induction of the fibrinogen receptor on human platelets by intracellular mediators. *J. Biol. Chem.* **262,** 992–1000 (1987).
21. Silverberg, S. A., Nemerson, Y. & Zur, M. Kinetics of the activation of bovine coagulation factor X by components of the extrinsic pathway. Kinetic behavior of two-chain factor VII in the presence and absence of tissue factor. *J. Biol. Chem.* **252,** 8481–8488 (1977).
22. Kirchhofer, D. & Nemerson, Y. Initiation of blood coagulation: the tissue factor/factor VIIa complex. *Curr. Opin. Biotechnol.* **7,** 386–391 (1996).
23. Kaplan, A. P. & Ghebrehiwet, B. The plasma bradykinin-forming pathways and its interrelationships with complement. *Mol. Immunol.* **47,** 2161–2169 (2010).
24. Renné, T., Schmaier, A. H., Nickel, K. F., Blombäck, M. & Maas, C. In vivo roles of factor XII. *Blood* **120,** 4296–4303 (2012).
25. Anwar, R. & Miloszewski, K. J. Factor XIII deficiency. *Br. J. Haematol.* **107,** 468–484 (1999).
26. Huq, F. Y. & Kadir, R. A. Management of pregnancy, labour and delivery in women with inherited bleeding disorders. *Haemoph. Off. J. World Fed. Hemoph.* **17 Suppl 1,** 20–30 (2011).
27. Mandle, R. J., Colman, R. W. & Kaplan, A. P. Identification of prekallikrein and high-molecular-weight kininogen as a complex in human plasma. *Proc. Natl. Acad. Sci. U. S. A.* **73,** 4179–4183 (1976).
28. Adams, T. E. & Huntington, J. A. Thrombin-cofactor interactions: structural insights into regulatory mechanisms. *Arterioscler. Thromb. Vasc. Biol.* **26,** 1738–1745 (2006).

29. Suzuki, K., Dahlbäck, B. & Stenflo, J. Thrombin-catalyzed activation of human coagulation factor V. *J. Biol. Chem.* **257,** 6556–6564 (1982).
30. Tanaka, K. A., Key, N. S. & Levy, J. H. Blood coagulation: hemostasis and thrombin regulation. *Anesth. Analg.* **108,** 1433–1446 (2009).
31. Lövgren, A. *et al.* Characterization of thrombin derived from human recombinant prothrombin. *Blood Coagul. Fibrinolysis Int. J. Haemost. Thromb.* **26,** 545–555 (2015).
32. Esmon, C. T. & Owen, W. G. Identification of an endothelial cell cofactor for thrombin-catalyzed activation of protein C. *Proc. Natl. Acad. Sci. U. S. A.* **78,** 2249–2252 (1981).
33. Dahlbäck, B. Protein S and C4b-binding protein: components involved in the regulation of the protein C anticoagulant system. *Thromb. Haemost.* **66,** 49–61 (1991).
34. Bajaj, M. S., Birktoft, J. J., Steer, S. A. & Bajaj, S. P. Structure and biology of tissue factor pathway inhibitor. *Thromb. Haemost.* **86,** 959–972 (2001).
35. Barkan G. Zur Frage der Reversibilität der Fibringerinnung II. 291–301 (1923).
36. Robbins KC. A study on the conversion of fibrinogen to fibrin. *Am J Physiol* 581–588 (1944).
37. Laki, K. & Lóránd, L. On the Solubility of Fibrin Clots. *Science* **108,** 280 (1948).
38. Lorand, L. A study on the solubility of fibrin clots in urea. *Hung. Acta Physiol.* **1,** 192–196 (1948).
39. Lorand, L. Fibrin clots. *Nature* **166,** 694–695 (1950).
40. Duckert, F., Jung, E. & Shmerling, D. H. A hitherto undescribed congenital haemorrhagic diathesis probably due to fibrin stabilizing factor deficiency. *Thromb. Diath. Haemorrh.* **5,** 179–186 (1960).
41. Loewy, A. G., Dahlberg, A., Dunathan, K., Kriel, R. & Wolfinger, H. L. Fibrinase. II. Some physical properties. *J. Biol. Chem.* **236,** 2634–2643 (1961).
42. Loewy, A. G., Dunathan, K., Gallant, J. A. & Gardner, B. Fibrinase III. Some enzymatic properties. *J. Biol. Chem.* **236,** 2644–2647 (1961).
43. Loewy, A. G., Dunathan, K., Kriel, R. & Wolfinger, H. L. Fibrinase. I. Purification of substrate and enzyme. *J. Biol. Chem.* **236,** 2625–2633 (1961).
44. Loewy, A. G., Gallant, J. A. & Dunathan, K. Fibrinase. IV. Effect on fibrin solubility. *J. Biol. Chem.* **236,** 2648–2655 (1961).
45. Loewy, A. G., Veneziale, C. & Forman, M. Purification of the factor involved in the formation of urea-insoluble fibrin. *Biochim. Biophys. Acta* **26,** 670–671 (1957).
46. Buluk, K., Januszko, T. & Olbromski, J. Conversion of fibrin to desmofibrin. 1093–1094 (1961).
47. Wright, I. . The International Committee on Blood Clotting Factors: the past, present and future. In: Fibrinogen and Fibrin. Turnover of Clotting Factors. Transactions of the conference held under the auspices of the International Committee on Blood Clotting Factors. (1963).
48. Takahashi, N., Takahashi, Y. & Putnam, F. W. Primary structure of blood coagulation factor XIIIa (fibrinoligase, transglutaminase) from human placenta. *Proc. Natl. Acad. Sci. U. S. A.* **83,** 8019–8023 (1986).
49. Ichinose, A., McMullen, B. A., Fujikawa, K. & Davie, E. W. Amino acid sequence of the b subunit of human factor XIII, a protein composed of ten repetitive segments. *Biochemistry (Mosc.)* **25,** 4633–4638 (1986).
50. Grundmann, U., Nerlich, C., Rein, T. & Zettlmeissl, G. Complete cDNA sequence encoding the B subunit of human factor XIII. *Nucleic Acids Res.* **18,** 2817–2818 (1990).
51. Grundmann, U., Amann, E., Zettlmeissl, G. & Küpper, H. A. Characterization of cDNA coding for human factor XIIIa. *Proc. Natl. Acad. Sci. U. S. A.* **83,** 8024–8028 (1986).
52. Yee, V. C. *et al.* Three-dimensional structure of a transglutaminase: human blood coagulation factor XIII. *Proc. Natl. Acad. Sci.* **91,** 7296–7300 (1994).
53. Stieler, M. *et al.* Structure of Active Coagulation Factor XIII Triggered by Calcium Binding: Basis for the Design of Next-Generation Anticoagulants. *Angew. Chem. Int. Ed.* **52,** 11930–11934 (2013).
54. Brand-Staufer, B. *et al.* Pharmacokinetic characterization of recombinant factor XIII (FXIII)-A2 across age groups in patients with FXIII A-subunit congenital deficiency. *Haemoph. Off. J. World Fed. Hemoph.* **21,** 380–385 (2015).
55. Iismaa, S. E., Mearns, B. M., Lorand, L. & Graham, R. M. Transglutaminases and disease: lessons from genetically engineered mouse models and inherited disorders. *Physiol. Rev.* **89,** 991–1023 (2009).
56. KomáRomi, I., Bagoly, Z. & Muszbek, L. Factor XIII: novel structural and functional aspects: FXIII: structure and function. *J. Thromb. Haemost.* **9,** 9–20 (2011).
57. Kim, S. Y., Chung, S. I. & Steinert, P. M. Highly active soluble processed forms of the transglutaminase 1 enzyme in epidermal keratinocytes. *J. Biol. Chem.* **270,** 18026–18035 (1995).
58. Liu, S., Cerione, R. A. & Clardy, J. Structural basis for the guanine nucleotide-binding activity of tissue transglutaminase and its regulation of transamidation activity. *Proc. Natl. Acad. Sci. U. S. A.* **99,** 2743–2747 (2002).

59. Ahvazi, B., Kim, H. C., Kee, S.-H., Nemes, Z. & Steinert, P. M. Three-dimensional structure of the human transglutaminase 3 enzyme: binding of calcium ions changes structure for activation. *EMBO J.* **21,** 2055–2067 (2002).
60. Weiss, M. S., Metzner, H. J. & Hilgenfeld, R. Two non-proline cis peptide bonds may be important for factor XIII function. *FEBS Lett.* **423,** 291–296 (1998).
61. Rallapalli, P. M., Orengo, C. A., Studer, R. A. & Perkins, S. J. Positive selection during the evolution of the blood coagulation factors in the context of their disease-causing mutations. *Mol. Biol. Evol.* **31,** 3040–3056 (2014).
62. Board, P. G., Webb, G. C., McKee, J. & Ichinose, A. Localization of the coagulation factor XIII A subunit gene (F13A) to chromosome bands 6p24----p25. *Cytogenet. Cell Genet.* **48,** 25–27 (1988).
63. Ichinose, A. & Davie, E. W. Characterization of the gene for the a subunit of human factor XIII (plasma transglutaminase), a blood coagulation factor. *Proc. Natl. Acad. Sci. U. S. A.* **85,** 5829–5833 (1988).
64. Schwartz, M. L., Pizzo, S. V., Hill, R. L. & McKee, P. A. Human Factor XIII from Plasma and Platelets MOLECULAR WEIGHTS, SUBUNIT STRUCTURES, PROTEOLYTIC ACTIVATION, AND CROSS-LINKING OF FIBRINOGEN AND FIBRIN. *J. Biol. Chem.* **248,** 1395–1407 (1973).
65. Hwang, C.-S., Shemorry, A. & Varshavsky, A. N-terminal acetylation of cellular proteins creates specific degradation signals. *Science* **327,** 973–977 (2010).
66. Ichinose, A., Hendrickson, L. E., Fujikawa, K. & Davie, E. W. Amino acid sequence of the a subunit of human factor XIII. *Biochemistry (Mosc.)* **25,** 6900–6906 (1986).
67. Lahav, J. *et al.* Coagulation factor XIII serves as protein disulfide isomerase. *Thromb. Haemost.* **101,** 840–844 (2009).
68. Lorand, L., Jeong, J. M., Radek, J. T. & Wilson, J. Human plasma factor XIII: subunit interactions and activation of zymogen. *Methods Enzymol.* **222,** 22–35 (1993).
69. Lai, T. S., Slaughter, T. F., Peoples, K. A. & Greenberg, C. S. Site-directed mutagenesis of the calcium-binding site of blood coagulation factor XIIIa. *J. Biol. Chem.* **274,** 24953–24958 (1999).
70. Lai, T. S., Achyuthan, K. E., Santiago, M. A. & Greenberg, G. S. Carboxyl-terminal truncation of recombinant factor XIII A-chains. Characterization of minimum structural requirement for transglutaminase activity. *J. Biol. Chem.* **269,** 24596–24601 (1994).
71. Muszbek, L., Bereczky, Z., Bagoly, Z., Komaromi, I. & Katona, E. Factor XIII: A Coagulation Factor With Multiple Plasmatic and Cellular Functions. *Physiol. Rev.* **91,** 931–972 (2011).
72. Ichinose, A. *et al.* Arg260-Cys mutation in severe factor XIII deficiency: conformational change of the A subunit is predicted by molecular modelling and mechanics. *Br. J. Haematol.* **101,** 264–272 (1998).
73. Souri, M. *et al.* Novel Y283C mutation of the A subunit for coagulation factor XIII: molecular modelling predicts its impaired protein folding and dimer formation. *Br. J. Haematol.* **113,** 652–654 (2001).
74. Iismaa, S. E. *et al.* Evolutionary specialization of a tryptophan indole group for transition-state stabilization by eukaryotic transglutaminases. *Proc. Natl. Acad. Sci. U. S. A.* **100,** 12636–12641 (2003).
75. Pedersen, L. C. *et al.* Transglutaminase factor XIII uses proteinase-like catalytic triad to crosslink macromolecules. *Protein Sci. Publ. Protein Soc.* **3,** 1131–1135 (1994).
76. Yee, V. C., Pedersen, L. C., Bishop, P. D., Stenkamp, R. E. & Teller, D. C. Structural evidence that the activation peptide is not released upon thrombin cleavage of factor XIII. *Thromb. Res.* **78,** 389–397 (1995).
77. Fox, B. A. *et al.* Identification of the calcium binding site and a novel ytterbium site in blood coagulation factor XIII by X-ray crystallography. *J. Biol. Chem.* **274,** 4917–4923 (1999).
78. Ortner, E., Schroeder, V., Walser, R., Zerbe, O. & Kohler, H. P. Sensitive and selective detection of free FXIII activation peptide: a potential marker of acute thrombotic events. *Blood* **115,** 5089–5096 (2010).
79. Bode, W., Turk, D. & Karshikov, A. The refined 1.9-A X-ray crystal structure of D-Phe-Pro-Arg chloromethylketone-inhibited human alpha-thrombin: structure analysis, overall structure, electrostatic properties, detailed active-site geometry, and structure-function relationships. *Protein Sci. Publ. Protein Soc.* **1,** 426–471 (1992).
80. Harris, J. L., Peterson, E. P., Hudig, D., Thornberry, N. A. & Craik, C. S. Definition and redesign of the extended substrate specificity of granzyme B. *J. Biol. Chem.* **273,** 27364–27373 (1998).
81. Schechter, I. & Berger, A. On the active site of proteases. 3. Mapping the active site of papain; specific peptide inhibitors of papain. *Biochem. Biophys. Res. Commun.* **32,** 898–902 (1968).
82. Huntington, J. A. How Na+ activates thrombin--a review of the functional and structural data. *Biol. Chem.* **389,** 1025–1035 (2008).
83. Di Cera, E. Thrombin. *Mol. Aspects Med.* **29,** 203–254 (2008).
84. Isetti, G. & Maurer, M. C. Employing Mutants to Study Thrombin Residues Responsible for Factor XIII Activation Peptide Recognition: A Kinetic Study †. *Biochemistry (Mosc.)* **46,** 2444–2452 (2007).

85. Isetti, G. & Maurer, M. C. Thrombin Activity Is Unaltered by N-Terminal Truncation of Factor XIII Activation Peptides †. *Biochemistry (Mosc.)* **43,** 4150–4159 (2004).
86. Webb, G. C., Coggan, M., Ichinose, A. & Board, P. G. Localization of the coagulation factor XIII B subunit gene (F13B) to chromosome bands 1q31-32.1 and restriction fragment length polymorphism at the locus. *Hum. Genet.* **81,** 157–160 (1989).
87. Carrell, N. A., Erickson, H. P. & McDonagh, J. Electron microscopy and hydrodynamic properties of factor XIII subunits. *J. Biol. Chem.* **264,** 551–556 (1989).
88. Skerka, C., Chen, Q., Fremeaux-Bacchi, V. & Roumenina, L. T. Complement factor H related proteins (CFHRs). *Mol. Immunol.* **56,** 170–180 (2013).
89. Patthy, L. Detecting homology of distantly related proteins with consensus sequences. *J. Mol. Biol.* **198,** 567–577 (1987).
90. Patthy, L. Evolution of the proteases of blood coagulation and fibrinolysis by assembly from modules. *Cell* **41,** 657–663 (1985).
91. Bottenus, R. E., Ichinose, A. & Davie, E. W. Nucleotide sequence of the gene for the b subunit of human factor XIII. *Biochemistry (Mosc.)* **29,** 11195–11209 (1990).
92. Kaetsu, H., Hashiguchi, T., Foster, D. & Ichinose, A. Expression and release of the a and b subunits for human coagulation factor XIII in baby hamster kidney (BHK) cells. *J. Biochem. (Tokyo)* **119,** 961–969 (1996).
93. Ichinose, A., Bottenus, R. E. & Davie, E. W. Structure of transglutaminases. *J. Biol. Chem.* **265,** 13411–13414 (1990).
94. Lockwood, C. R. & Frayling, T. M. Combining genome and mouse knockout expression data to highlight binding sites for the transcription factor HNF1alpha. *In Silico Biol.* **3,** 57–70 (2003).
95. Chen, R. *et al.* Glycoproteomics analysis of human liver tissue by combination of multiple enzyme digestion and hydrazide chemistry. *J. Proteome Res.* **8,** 651–661 (2009).
96. Liu, T. *et al.* Human plasma N-glycoproteome analysis by immunoaffinity subtraction, hydrazide chemistry, and mass spectrometry. *J. Proteome Res.* **4,** 2070–2080 (2005).
97. Katona, E. *et al.* Interaction of factor XIII subunits. *Blood* **123,** 1757–1763 (2014).
98. Souri, M., Kaetsu, H. & Ichinose, A. Sushi Domains in the B Subunit of Factor XIII Responsible for Oligomer Assembly †. *Biochemistry (Mosc.)* **47,** 8656–8664 (2008).
99. Polgár, J., Hidasi, V. & Muszbek, L. Non-proteolytic activation of cellular protransglutaminase (placenta macrophage factor XIII). *Biochem. J.* **267,** 557–560 (1990).
100. Souri, M., Osaki, T. & Ichinose, A. The Non-catalytic B Subunit of Coagulation Factor XIII Accelerates Fibrin Cross-linking. *J. Biol. Chem.* **290,** 12027–12039 (2015).
101. Lopaciuk, S., Lovette, K. M., McDonagh, J., Chuang, H. Y. & McDonagh, null. Subcellular distribution of fibrinogen and factor XIII in human blood platelets. *Thromb. Res.* **8,** 453–465 (1976).
102. Sixma, J. J., van den Berg, A., Schiphorst, M., Geuze, H. J. & McDonagh, J. Immunocytochemical localization of albumin and factor XIII in thin cryo sections of human blood platelets. *Thromb. Haemost.* **51,** 388–391 (1984).
103. Adány, R., Kiss, A. & Muszbek, L. Factor XIII: a marker of mono- and megakaryocytopoiesis. *Br. J. Haematol.* **67,** 167–172 (1987).
104. Lorand, L. & Graham, R. M. Transglutaminases: crosslinking enzymes with pleiotropic functions. *Nat. Rev. Mol. Cell Biol.* **4,** 140–156 (2003).
105. Credo, R. B., Curtis, C. G. & Lorand, L. Ca2+-related regulatory function of fibrinogen. *Proc. Natl. Acad. Sci. U. S. A.* **75,** 4234–4237 (1978).
106. De Backer-Royer, C., Traoré, F. & Meunier, J. C. Purification and properties of factor XIII from human placenta. *Int. J. Biochem.* **24,** 91–97 (1992).
107. Hornyak, T. J. & Shafer, J. A. Interactions of factor XIII with fibrin as substrate and cofactor. *Biochemistry (Mosc.)* **31,** 423–429 (1992).
108. Nakano, Y., Al-Jallad, H. F., Mousa, A. & Kaartinen, M. T. Expression and Localization of Plasma Transglutaminase Factor XIIIA in Bone. *J. Histochem. Cytochem.* **55,** 675–685 (2007).
109. Cohen, I., Blankenberg, T. A., Borden, D., Kahn, D. R. & Veis, A. Factor XIIIa-catalyzed cross-linking of platelet and muscle actin. Regulation by nucleotides. *Biochim. Biophys. Acta* **628,** 365–375 (1980).
110. Kiesselbach, T. H. & Wagner, R. H. Demonstration of factor XIII in human megakaryocytes by a fluorescent antibody technique. *Ann. N. Y. Acad. Sci.* **202,** 318–328 (1972).
111. Buluk, K. [An unknown action of blood platelets; preliminary communication]. *Pol. Tyg. Lek.* **10,** 191 (1955).
112. Muszbek, L., Yee, V. C. & Hevessy, Z. Blood coagulation factor XIII: structure and function. *Thromb. Res.* **94,** 271–305 (1999).

113. Adány, R. & Bárdos, H. Factor XIII subunit A as an intracellular transglutaminase. *Cell. Mol. Life Sci. CMLS* **60,** 1049–1060 (2003).
114. Cordell, P. A. *et al.* Association of coagulation factor XIII-A with Golgi proteins within monocyte-macrophages: implications for subcellular trafficking and secretion. *Blood* **115,** 2674–2681 (2010).
115. Schwartz, M. L., Pizzo, S. V., Hill, R. L. & McKee, P. A. The subunit structures of human plasma and platelet factor XIII (fibrin-stabilizing factor). *J. Biol. Chem.* **246,** 5851–5854 (1971).
116. Katona E, E., Ajzner, E., Tóth, K., Kárpáti, L. & Muszbek, L. Enzyme-linked immunosorbent assay for the determination of blood coagulation factor XIII A-subunit in plasma and in cell lysates. *J. Immunol. Methods* **258,** 127–135 (2001).
117. Mitchell, J. L. *et al.* Functional factor XIII-A is exposed on the stimulated platelet surface. *Blood* **124,** 3982–3990 (2014).
118. Bohn, H. & Schwick, H. G. [Isolation and characterization of a fibrin-stabilizing factor from human placenta]. *Arzneimittelforschung.* **21,** 1432–1439 (1971).
119. Chung, S. I. Comparative studies on tissue transglutaminase and factor XIII. *Ann. N. Y. Acad. Sci.* **202,** 240–255 (1972).
120. Orosz, Z. Z., Katona, E., Facskó, A., Berta, A. & Muszbek, L. A highly sensitive chemiluminescence immunoassay for the measurement of coagulation factor XIII subunits and their complex in tears. *J. Immunol. Methods* **353,** 87–92 (2010).
121. Orosz, Z. Z. *et al.* Factor XIII subunits in human tears; their highly elevated levels following penetrating keratoplasty. *Clin. Chim. Acta Int. J. Clin. Chem.* **412,** 271–276 (2011).
122. Kappelmayer, J., Bacskó, G., Kelemen, E. & Adány, R. Onset and distribution of factor XIII-containing cells in the mesenchyme of chorionic villi during early phase of human placentation. *Placenta* **15,** 613–623 (1994).
123. Adány, R. & Muszbek, L. Immunohistochemical detection of factor XIII subunit a in histiocytes of human uterus. *Histochemistry* **91,** 169–174 (1989).
124. Wolberg, A. S. Plasma factor XIII: understanding the 99%. *Blood* **123,** 1623–1624 (2014).
125. Poon, M. C. *et al.* Hemopoietic origin of factor XIII A subunits in platelets, monocytes, and plasma. Evidence from bone marrow transplantation studies. *J. Clin. Invest.* **84,** 787–792 (1989).
126. Wölpl, A. *et al.* Coagulation factor XIII A and B subunits in bone marrow and liver transplantation. *Transplantation* **43,** 151–153 (1987).
127. Inbal, A. *et al.* Platelets but not monocytes contribute to the plasma levels of factor XIII subunit A in patients undergoing autologous peripheral blood stem cell transplantation. *Blood Coagul. Fibrinolysis Int. J. Haemost. Thromb.* **15,** 249–253 (2004).
128. Kappelmayer, J. *et al.* Consecutive appearance of coagulation factor XIII subunit A in macrophages, megakaryocytes, and liver cells during early human development. *Blood* **86,** 2191–2197 (1995).
129. Griffin, K. *et al.* Use of a novel floxed mouse to characterise the cellular source of plasma coagulation FXIII-A. *Lancet Lond. Engl.* **385 Suppl 1,** S39 (2015).
130. Adány, R. & Antal, M. Three different cell types can synthesize factor XIII subunit A in the human liver. *Thromb. Haemost.* **76,** 74–79 (1996).
131. Nagy, J. A., Henriksson, P. & McDonagh, J. Biosynthesis of factor XIII B subunit by human hepatoma cell lines. *Blood* **68,** 1272–1279 (1986).
132. Yorifuji, H., Anderson, K., Lynch, G. W., Van de Water, L. & McDonagh, J. B protein of factor XIII: differentiation between free B and complexed B. *Blood* **72,** 1645–1650 (1988).
133. Board, P. G., Pierce, K. & Coggan, M. Expression of functional coagulation factor XIII in Escherichia coli. *Thromb. Haemost.* **63,** 235–240 (1990).
134. Bishop, P. D. *et al.* Expression, purification, and characterization of human factor XIII in Saccharomyces cerevisiae. *Biochemistry (Mosc.)* **29,** 1861–1869 (1990).
135. Jagadeeswaran, P., Reddy, S. V. & Haas, P. Synthesis of human coagulation factor XIII in yeast. *Gene* **86,** 279–283 (1990).
136. Bröker, M. & Bäuml, O. New expression vectors for the fission yeast Schizosaccharomyces pombe. *FEBS Lett.* **248,** 105–110 (1989).
137. Gao, J., Hooker, B. S. & Anderson, D. B. Expression of functional human coagulation factor XIII A-domain in plant cell suspensions and whole plants. *Protein Expr. Purif.* **37,** 89–96 (2004).
138. Kristiansen, G. K. & Andersen, M. D. Reversible Activation of Cellular Factor XIII by Calcium. *J. Biol. Chem.* **286,** 9833–9839 (2011).
139. Ando, Y. *et al.* Platelet factor XIII is activated by calpain. *Biochem. Biophys. Res. Commun.* **144,** 484–490 (1987).

140. Greenberg, C. S. & Shuman, M. A. The zymogen forms of blood coagulation factor XIII bind specifically to fibrinogen. *J. Biol. Chem.* **257,** 6096–6101 (1982).
141. Greenberg, C. S., Enghild, J. J., Mary, A., Dobson, J. V. & Achyuthan, K. E. Isolation of a fibrin-binding fragment from blood coagulation factor XIII capable of cross-linking fibrin (ogen). *Biochem J* **256,** 1013–1019 (1988).
142. Schroeder, V., Durrer, D., Meili, E., Schubiger, G. & Kohler, H. P. Congenital factor XIII deficiency in Switzerland: from the worldwide first case in 1960 to its molecular characterisation in 2005. *Swiss Med. Wkly.* **137,** 272–278 (2007).
143. Hornyak, T. J. & Shafer, J. A. Role of calcium ion in the generation of factor XIII activity. *Biochemistry (Mosc.)* **30,** 6175–6182 (1991).
144. Radek, J. T., Jeong, J. M., Wilson, J. & Lorand, L. Association of the A subunits of recombinant placental factor XIII with the native carrier B subunits from human plasma. *Biochemistry (Mosc.)* **32,** 3527–3534 (1993).
145. Lewis, S. D., Janus, T. J., Lorand, L. & Shafer, J. A. Regulation of formation of factor XIIIa by its fibrin substrates. *Biochemistry (Mosc.)* **24,** 6772–6777 (1985).
146. Schroeder, V., Vuissoz, J.-M., Caflisch, A. & Kohler, H. P. Factor XIII activation peptide is released into plasma upon cleavage by thrombin and shows a different structure compared to its bound form. *Thromb. Haemost.* (2007). doi:10.1160/TH06-08-0458
147. Kohler, H. P. Interaction between FXIII and fibrinogen. *Blood* **121,** 1931–1932 (2013).
148. Smith, K. A. *et al.* The activation peptide cleft exposed by thrombin cleavage of FXIII-A(2) contains a recognition site for the fibrinogen α chain. *Blood* **121,** 2117–2126 (2013).
149. Philippou, H. *et al.* Roles of low specificity and cofactor interaction sites on thrombin during factor XIII activation. Competition for cofactor sites on thrombin determines its fate. *J. Biol. Chem.* **278,** 32020–32026 (2003).
150. Wouwer, M. V. de, Collen, D. & Conway, E. M. Thrombomodulin-Protein C-EPCR System Integrated to Regulate Coagulation and Inflammation. *Arterioscler. Thromb. Vasc. Biol.* **24,** 1374–1383 (2004).
151. Bagoly, Z. *et al.* Cleavage of factor XIII by human neutrophil elastase results in a novel active truncated form of factor XIII A subunit. *Thromb. Haemost.* **99,** 668–674 (2008).
152. Kopeć, M., Latallo, Z. S., Stahl, M. & Wegrzynowicz, Z. The effect of proteolytic enzymes on fibrin stabilizing factor. *Biochim. Biophys. Acta* **181,** 437–445 (1969).
153. Walter, M., Nyman, D., Krajnc, V. & Duckert, F. The activation of plasma factor XIII with the snake venom enzymes ancrod and batroxobin marajoensis. *Thromb. Haemost.* **38,** 438–446 (1977).
154. Niewiarowski, S., Kirby, E. P., Brudzynski, T. M. & Stocker, K. Thrombocytin, a serine protease from Bothrops atrox venom. 2. Interaction with platelets and plasma-clotting factors. *Biochemistry (Mosc.)* **18,** 3570–3577 (1979).
155. McDonagh, J. & McDonagh, R. P. Alternative pathways for the activation of factor XIII. *Br. J. Haematol.* **30,** 465–477 (1975).
156. Krarup, A., Gulla, K. C., Gál, P., Hajela, K. & Sim, R. B. The action of MBL-associated serine protease 1 (MASP1) on factor XIII and fibrinogen. *Biochim. Biophys. Acta* **1784,** 1294–1300 (2008).
157. Mosesson, M. W., Siebenlist, K. R., Amrani, D. L. & DiOrio, J. P. Identification of covalently linked trimeric and tetrameric D domains in crosslinked fibrin. *Proc. Natl. Acad. Sci. U. S. A.* **86,** 1113–1117 (1989).
158. Bagoly, Z., Haramura, G. & Muszbek, L. Down-regulation of activated factor XIII by polymorphonuclear granulocyte proteases within fibrin clot. *Thromb. Haemost.* **98,** 359–367 (2007).
159. Hur, W. S. *et al.* Coagulation factor XIIIa is inactivated by plasmin. *Blood* (2015). doi:10.1182/blood-2015-07-650713
160. Shen, L. & Lorand, L. Contribution of fibrin stabilization to clot strength. Supplementation of factor XIII-deficient plasma with the purified zymogen. *J. Clin. Invest.* **71,** 1336–1341 (1983).
161. Henschen, A., Lottspeich, F., Kehl, M. & Southan, C. Covalent Structure of Fibrinogen. *Ann. N. Y. Acad. Sci.* **408,** 28–43 (1983).
162. Mosesson, M. W., Siebenlist, K. R. & Meh, D. A. The structure and biological features of fibrinogen and fibrin. *Ann. N. Y. Acad. Sci.* **936,** 11–30 (2001).
163. Mosesson, M. W., Siebenlist, K. R., Meh, D. A., Wall, J. S. & Hainfeld, J. F. The location of the carboxy-terminal region of gamma chains in fibrinogen and fibrin D domains. *Proc. Natl. Acad. Sci. U. S. A.* **95,** 10511–10516 (1998).
164. Riedel, T. *et al.* Fibrinopeptides A and B release in the process of surface fibrin formation. *Blood* **117,** 1700–1706 (2011).
165. Pechik, I., Yakovlev, S., Mosesson, M. W., Gilliland, G. L. & Medved, L. Structural basis for sequential cleavage of fibrinopeptides upon fibrin assembly. *Biochemistry (Mosc.)* **45,** 3588–3597 (2006).

166. Tsurupa, G. *et al.* Structure, stability, and interaction of the fibrin(ogen) alphaC-domains. *Biochemistry (Mosc.)* **48,** 12191–12201 (2009).
167. Standeven, K. F. *et al.* Functional analysis of the fibrinogen Aalpha Thr312Ala polymorphism: effects on fibrin structure and function. *Circulation* **107,** 2326–2330 (2003).
168. Hethershaw, E. L. *et al.* The effect of blood coagulation factor XIII on fibrin clot structure and fibrinolysis. *J. Thromb. Haemost. JTH* **12,** 197–205 (2014).
169. Greenberg, C. S. & Miraglia, C. C. The effect of fibrin polymers on thrombin-catalyzed plasma factor XIIIa formation. *Blood* **66,** 466–469 (1985).
170. Ariens, R. A. S. Role of factor XIII in fibrin clot formation and effects of genetic polymorphisms. *Blood* **100,** 743–754 (2002).
171. Chen, R. & Doolittle, R. F. - cross-linking sites in human and bovine fibrin. *Biochemistry (Mosc.)* **10,** 4487–4491 (1971).
172. Standeven, K. F. *et al.* Functional analysis of fibrin {gamma}-chain cross-linking by activated factor XIII: determination of a cross-linking pattern that maximizes clot stiffness. *Blood* **110,** 902–907 (2007).
173. Richardson, V. R., Cordell, P., Standeven, K. F. & Carter, A. M. Substrates of Factor XIII-A: roles in thrombosis and wound healing. *Clin. Sci.* **124,** 123–137 (2013).
174. Matsuka, Y. V., Migliorini, M. M. & Ingham, K. C. Cross-linking of fibronectin to C-terminal fragments of the fibrinogen alpha-chain by factor XIIIa. *J. Protein Chem.* **16,** 739–745 (1997).
175. Sobel, J. H. & Gawinowicz, M. A. Identification of the Chain Lysine Donor Sites Involved in Factor XIIIa Fibrin Cross-linking. *J. Biol. Chem.* **271,** 19288–19297 (1996).
176. Wang, W. Identification of respective lysine donor and glutamine acceptor sites involved in factor XIIIa-catalyzed fibrin α chain cross-linking. *J. Biol. Chem.* **286,** 44952–44964 (2011).
177. Siebenlist, K. R. & Mosesson, M. W. Evidence of intramolecular cross-linked A alpha.gamma chain heterodimers in plasma fibrinogen. *Biochemistry (Mosc.)* **35,** 5817–5821 (1996).
178. Brennan, S. O. Variation of fibrinogen oligosaccharide structure in the acute phase response: Possible haemorrhagic implications. *BBA Clin.* **3,** 221–226 (2015).
179. Aeschlimann, D., Mosher, D. & Paulsson, M. Tissue transglutaminase and factor XIII in cartilage and bone remodeling. *Semin. Thromb. Hemost.* **22,** 437–443 (1996).
180. Piercy-Kotb, S. A. *et al.* Factor XIIIA transglutaminase expression and secretion by osteoblasts is regulated by extracellular matrix collagen and the MAP kinase signaling pathway. *J. Cell. Physiol.* **227,** 2936–2946 (2012).
181. Myneni, V. D., Hitomi, K. & Kaartinen, M. T. Factor XIII-A transglutaminase acts as a switch between preadipocyte proliferation and differentiation. *Blood* **124,** 1344–1353 (2014).
182. Nikolajsen, C. L., Dyrlund, T. F., Poulsen, E. T., Enghild, J. J. & Scavenius, C. Coagulation factor XIIIa substrates in human plasma: identification and incorporation into the clot. *J. Biol. Chem.* **289,** 6526–6534 (2014).
183. Cohen, I., Young-Bandala, L., Blankenberg, T. A., Siefring, G. E. & Bruner-Lorand, J. Fibrinoligase-catalyzed cross-linking of myosin from platelet and skeletal muscle. *Arch. Biochem. Biophys.* **192,** 100–111 (1979).
184. Asijee, G. M., Sturk, A., Bruin, T., Wilkinson, J. M. & Ten Cate, J. W. Vinculin is a permanent component of the membrane skeleton and is incorporated into the (re)organising cytoskeleton upon platelet activation. *Eur. J. Biochem. FEBS* **189,** 131–136 (1990).
185. Serrano, K. & Devine, D. V. Intracellular factor XIII crosslinks platelet cytoskeletal elements upon platelet activation. *Thromb. Haemost.* **88,** 315–320 (2002).
186. Francis, R. T., McDonagh, J. & Mann, K. G. Factor V is a substrate for the transamidase factor XIIIa. *J. Biol. Chem.* **261,** 9787–9792 (1986).
187. Hada, M., Kaminski, M., Bockenstedt, P. & McDonagh, J. Covalent crosslinking of von Willebrand factor to fibrin. *Blood* **68,** 95–101 (1986).
188. Mutch, N. J. *et al.* Model thrombi formed under flow reveal the role of factor XIII-mediated cross-linking in resistance to fibrinolysis. *J. Thromb. Haemost. JTH* **8,** 2017–2024 (2010).
189. Huh, M. M., Schick, B. P., Schick, P. K. & Colman, R. W. Covalent crosslinking of human coagulation factor V by activated factor XIII from guinea pig megakaryocytes and human plasma. *Blood* **71,** 1693–1702 (1988).
190. Roberts, W., Magwenzi, S., Aburima, A. & Naseem, K. M. Thrombospondin-1 induces platelet activation through CD36-dependent inhibition of the cAMP/protein kinase A signaling cascade. *Blood* **116,** 4297–4306 (2010).
191. Bale, M. D., Westrick, L. G. & Mosher, D. F. Incorporation of thrombospondin into fibrin clots. *J. Biol. Chem.* **260,** 7502–7508 (1985).

192. Brotchie, H. & Wakefield, D. Fibronectin: structure, function and significance in wound healing. *Australas. J. Dermatol.* **31,** 47–56 (1990).
193. Mosher, D. F. Cross-linking of fibronectin to collagenous proteins. *Mol. Cell. Biochem.* **58,** 63–68 (1984).
194. Sadler, J. E. Biochemistry and genetics of von Willebrand factor. *Annu. Rev. Biochem.* **67,** 395–424 (1998).
195. Takagi, J. *et al.* Identification of factor-XIIIa-reactive glutaminyl residues in the propolypeptide of bovine von Willebrand factor. *Eur. J. Biochem. FEBS* **232,** 773–777 (1995).
196. Dale, G. L. *et al.* Stimulated platelets use serotonin to enhance their retention of procoagulant proteins on the cell surface. *Nature* **415,** 175–179 (2002).
197. Szasz, R. & Dale, G. L. Thrombospondin and fibrinogen bind serotonin-derivatized proteins on COAT-platelets. *Blood* **100,** 2827–2831 (2002).
198. Kimura, S. & Aoki, N. Cross-linking site in fibrinogen for alpha 2-plasmin inhibitor. *J. Biol. Chem.* **261,** 15591–15595 (1986).
199. Valnickova, Z. & Enghild, J. J. Human procarboxypeptidase U, or thrombin-activable fibrinolysis inhibitor, is a substrate for transglutaminases. Evidence for transglutaminase-catalyzed cross-linking to fibrin. *J. Biol. Chem.* **273,** 27220–27224 (1998).
200. Ritchie, H., Robbie, L. A., Kinghorn, S., Exley, R. & Booth, N. A. Monocyte plasminogen activator inhibitor 2 (PAI-2) inhibits u-PA-mediated fibrin clot lysis and is cross-linked to fibrin. *Thromb. Haemost.* **81,** 96–103 (1999).
201. Jensen, P. H. *et al.* A unique interhelical insertion in plasminogen activator inhibitor-2 contains three glutamines, Gln83, Gln84, Gln86, essential for transglutaminase-mediated cross-linking. *J. Biol. Chem.* **269,** 15394–15398 (1994).
202. Sane, D. C. *et al.* Vitronectin is a substrate for transglutaminases. *Biochem. Biophys. Res. Commun.* **157,** 115–120 (1988).
203. Podor, T. J. *et al.* Type 1 plasminogen activator inhibitor binds to fibrin via vitronectin. *J. Biol. Chem.* **275,** 19788–19794 (2000).
204. Harpel, P. C. Alpha2-plasmin inhibitor and alpha2-macroglobulin-plasmin complexes in plasma. Quantitation by an enzyme-linked differential antibody immunosorbent assay. *J. Clin. Invest.* **68,** 46–55 (1981).
205. Wassmann, S. *et al.* Inhibition of diet-induced atherosclerosis and endothelial dysfunction in apolipoprotein E/angiotensin II type 1A receptor double-knockout mice. *Circulation* **110,** 3062–3067 (2004).
206. AbdAlla, S., Lother, H., Langer, A., el Faramawy, Y. & Quitterer, U. Factor XIIIA transglutaminase crosslinks AT1 receptor dimers of monocytes at the onset of atherosclerosis. *Cell* **119,** 343–354 (2004).
207. Donato, G. *et al.* Coagulation Factor XIIIA (F13A1): novel perspectives in treatment and pharmacogenetics. *Curr. Pharm. Des.* (2015).
208. Dardik, R. *et al.* Novel proangiogenic effect of factor XIII associated with suppression of thrombospondin 1 expression. *Arterioscler. Thromb. Vasc. Biol.* **23,** 1472–1477 (2003).
209. Dardik, R., Loscalzo, J. & Inbal, A. Factor XIII (FXIII) and angiogenesis. *J. Thromb. Haemost.* **4,** 19–25 (2006).
210. Gemmati, D. *et al.* Factor XIII-A dynamics in acute myocardial infarction: a novel prognostic biomarker? *Thromb. Haemost.* **114,** 123–132 (2015).
211. Kiss, F. *et al.* Leukemic lymphoblasts, a novel expression site of coagulation factor XIII subunit A. *Thromb. Haemost.* **96,** 176–182 (2006).
212. Deguchi, M., Aiba, S., Ohtani, H., Nagura, H. & Tagami, H. Comparison of the distribution and numbers of antigen-presenting cells among T-lymphocyte-mediated dermatoses: CD1a+, factor XIIIa+, and CD68+ cells in eczematous dermatitis, psoriasis, lichen planus and graft-versus-host disease. *Arch. Dermatol. Res.* **294,** 297–302 (2002).
213. Nickoloff, B. J. & Griffiths, C. E. Factor XIIIa-expressing dermal dendrocytes in AIDS-associated cutaneous Kaposi's sarcomas. *Science* **243,** 1736–1737 (1989).
214. Töröcsik, D. *et al.* Detection of factor XIII-A is a valuable tool for distinguishing dendritic cells and tissue macrophages in granuloma annulare and necrobiosis lipoidica. *J. Eur. Acad. Dermatol. Venereol. JEADV* **28,** 1087–1096 (2014).
215. Palla, R., Peyvandi, F. & Shapiro, A. D. Rare bleeding disorders: diagnosis and treatment. *Blood* **125,** 2052–2061 (2015).
216. Kohler, H. P. *et al.* Diagnosis and classification of factor XIII deficiencies. *J. Thromb. Haemost. JTH* **9,** 1404–1406 (2011).

217. Biswas, A., Ivaskevicius, V., Seitz, R., Thomas, A. & Oldenburg, J. An update of the mutation profile of Factor 13 A and B genes. *Blood Rev.* **25,** 193–204 (2011).
218. Tahlan, A. & Ahluwalia, J. Factor XIII: congenital deficiency factor XIII, acquired deficiency, factor XIII A-subunit, and factor XIII B-subunit. *Arch. Pathol. Lab. Med.* **138,** 278–281 (2014).
219. Ichinose, A. Hemorrhagic acquired factor XIII (13) deficiency and acquired hemorrhaphilia 13 revisited. *Semin. Thromb. Hemost.* **37,** 382–388 (2011).
220. Franchini, M., Frattini, F., Crestani, S. & Bonfanti, C. Acquired FXIII inhibitors: a systematic review. *J. Thromb. Thrombolysis* **36,** 109–114 (2013).
221. Souri, M. *et al.* Non-autoimmune combined factor XIII A and B subunit deficiencies in rheumatoid arthritis patients treated with anti-interleukin-6 receptor monoclonal antibody (tocilizumab). *Thromb. Res.* **140,** 100–105 (2016).
222. Pénzes, K. *et al.* Alloantibody developed in a factor XIII A subunit deficient patient during substitution therapy; characterization of the antibody. *Haemophilia* n/a–n/a (2015). doi:10.1111/hae.12786
223. Ichinose, A. & Japanese Collaborative Research Group (JCRG) on AH13 Hemorrhagic Acquired Coagulopathies. Inhibitors of Factor XIII/13 in older patients. *Semin. Thromb. Hemost.* **40,** 704–711 (2014).
224. Lorenz, R., Born, P. & Classen, M. [Substitution of factor XIII concentrate in treatment refractory ulcerative colitis. A prospective pilot study]. *Med. Klin. Munich Ger. 1983* **89,** 534–537 (1994).
225. Dorgalaleh, A. *et al.* Factor XIII deficiency in Iran: a comprehensive review of the literature. *Semin. Thromb. Hemost.* **41,** 323–329 (2015).
226. Hosseini, S. *et al.* First cases of severe congenital factor XIII deficiency in Southwestern Afghanistan in the vicinity of southeast of Iran. *Blood Coagul. Fibrinolysis Int. J. Haemost. Thromb.* (2015). doi:10.1097/MBC.0000000000000358
227. Anwar, R., Gallivan, L., Edmonds, S. D. & Markham, A. F. Genotype/phenotype correlations for coagulation factor XIII: specific normal polymorphisms are associated with high or low factor XIII specific activity. *Blood* **93,** 897–905 (1999).
228. Ivaskevicius, V. *et al.* International registry on factor XIII deficiency: a basis formed mostly on European data. *Thromb. Haemost.* **97,** 914–921 (2007).
229. Hsieh, L. & Nugent, D. Factor XIII deficiency: FXIII DEFICIENCY. *Haemophilia* **14,** 1190–1200 (2008).
230. Taeumer, T. *et al.* [The significance of bleeding disorders in patients with epistaxis]. *HNO* **59,** 582–587 (2011).
231. Peyvandi, F., Bolton-Maggs, P. H., Batorova, A. & De Moerloose, P. Rare bleeding disorders: RARE BLEEDING DISORDERS. *Haemophilia* **18,** 148–153 (2012).
232. Levy, J. H. & Greenberg, C. Biology of Factor XIII and clinical manifestations of Factor XIII deficiency. *Transfusion (Paris)* **53,** 1120–1131 (2013).
233. Asahina, T., Kobayashi, T., Okada, Y., Goto, J. & Terao, T. Maternal blood coagulation factor XIII is associated with the development of cytotrophoblastic shell. *Placenta* **21,** 388–393 (2000).
234. Doolittle, R. F. Step-by-step evolution of vertebrate blood coagulation. *Cold Spring Harb. Symp. Quant. Biol.* **74,** 35–40 (2009).
235. Ivaskevicius, V. *et al.* Mutations affecting disulphide bonds contribute to a fairly common prevalence of *F13B* gene defects: results of a genetic study in 14 families with factor XIII B deficiency. *Haemophilia* (2010). doi:10.1111/j.1365-2516.2010.02207.x
236. Andersen, M. D. *et al.* Coagulation factor XIII variants with altered thrombin activation rates. *Biol. Chem.* **390,** 1279–1283 (2009).
237. Trumbo, T. A. & Maurer, M. C. V34I and V34A substitutions within the factor XIII activation peptide segment (28-41) affect interactions with the thrombin active site. *Thromb. Haemost.* **89,** 647–653 (2003).
238. Ivaskevicius, V. *et al.* Identification of eight novel coagulation factor XIII subunit A mutations: implied consequences for structure and function. *Haematologica* **95,** 956–962 (2010).
239. Biswas, A. *et al.* Eight novel F13A1 gene missense mutations in patients with mild FXIII deficiency: in silico analysis suggests changes in FXIII-A subunit structure/function. *Ann. Hematol.* **93,** 1665–1676 (2014).
240. Mikkola, H. *et al.* Deficiency in the A-subunit of coagulation factor XIII: two novel point. *Blood* **84,** 517–525 (1994).
241. Mezei, Z. A. *et al.* Factor XIII B subunit polymorphisms and the risk of coronary artery disease. *Int. J. Mol. Sci.* **16,** 1143–1159 (2015).
242. Wells, P. S. Factor XIII Val34Leu Variant Is Protective against Venous Thromboembolism: A HuGE Review and Meta-Analysis. *Am. J. Epidemiol.* **164,** 101–109 (2006).
243. Vokó, Z., Bereczky, Z., Katona, E., Adány, R. & Muszbek, L. Factor XIII Val34Leu variant protects against coronary artery disease. A meta-analysis. *Thromb. Haemost.* **97,** 458–463 (2007).

244. Gallivan, L., Markham, A. F. & Anwar, R. The Leu564 factor XIIIA variant results in significantly lower plasma factor XIII levels than the Pro564 variant. *Thromb. Haemost.* **82,** 1368–1370 (1999).
245. Reiner, A. P. *et al.* Polymorphisms of coagulation factor XIII subunit A and risk of nonfatal hemorrhagic stroke in young white women. *Stroke J. Cereb. Circ.* **32,** 2580–2586 (2001).
246. Board, P. G. Genetic polymorphism of the B subunit of human coagulation factor XIII. *Am. J. Hum. Genet.* **32,** 348–353 (1980).
247. Komanasin, N. *et al.* A novel polymorphism in the factor XIII B-subunit (His95Arg): relationship to subunit dissociation and venous thrombosis. *J. Thromb. Haemost. JTH* **3,** 2487–2496 (2005).
248. Pruissen, D. M. O. *et al.* Prothrombotic gene variants and mortality after cerebral ischemia of arterial origin. *Neuroepidemiology* **37,** 109–113 (2011).
249. Reiner, A. P. *et al.* Genetic variants of coagulation factor XIII, postmenopausal estrogen therapy, and risk of nonfatal myocardial infarction. *Blood* **102,** 25–30 (2003).
250. Fadoo, Z., Merchant & Rehman. New developments in the management of congenital Factor XIII deficiency. *J. Blood Med.* 65 (2013). doi:10.2147/JBM.S32693
251. Kerlin, B. *et al.* Pharmacokinetics of recombinant factor XIII at steady state in patients with congenital factor XIII A-subunit deficiency. *J. Thromb. Haemost. JTH* **12,** 2038–2043 (2014).
252. Odame, J. E., Chan, A. K., Wu, J. K. & Breakey, V. R. Factor XIII deficiency management: a review of the literature. *Blood Coagul. Fibrinolysis Int. J. Haemost. Thromb.* **25,** 199–205 (2014).
253. Lovejoy, A. E. *et al.* Safety and pharmacokinetics of recombinant factor XIII-A2 administration in patients with congenital factor XIII deficiency. *Blood* **108,** 57–62 (2006).

Acknowledgement

First of all, i would like to thank my thesis supervisor Prof. Oldenburg for giving me the opportunity to be part of his institute for my PhD. I am also thankful to him inviting me to several congresses, giving me the chance to present the thesis work on international congresses in form of talks and posters and be part of the scientific community. He also gave me the possibility to do my medicine studies along with my thesis work. I would especially like to thank my post-doctoral supervisor PD Dr. Arijit Biswas for his scientific and personal guidance throughout all the challenges of my thesis work in the last five years. I am grateful to PD Dr. Vytas Ivaskevicius for assisting me with the clinical aspects of my thesis and for making it possible for me to work on FXIII deficiency patient samples.

I would like to thank and acknowledge our collaborators, Prof. Dr. Helen Philipou and Dr. Emma Hethershaw from Leeds, Dr. Johannes Dodt from the Paul-Ehrlich Institut and Mr. Hans-Jürgen Ensikat form the Nees-Institut für Biodiversität der Pflanzen for their invaluable co-operation guidance in several technical aspects of my thesis work. Without their expertise and help in several aspects of my work like the incorporation and generation assays and electron microscopy would not have been possible.

I would like to mention my friends and co-workers, Zaid (Dr. Aburubaiha) and Ursula, who both were most organized, kind and helpful co-workers in the lab. I thank you both so much for your encouragement, advices and helpful suggestions. I would like to thank our scientific –in-charge PD Dr. Rainer Schwaab for coordinating lab space and organisation. I would like to make a special mention for our lab technician, Sophie Lyonga. She was of great help to me during my lab work with her ever smiling

and warm presence. I will always admire you how you managed everything. I loved to have my coffee breaks with the friendliest MTAs from the genomic lab especially Inga, Steffi and Helena heartfull, smiling and always kind. Please stay like you are. Special thanks for Milda (always smiling) and Christina and having great fun together when ever we meet. Also I would like to thank Vero and Kapil from the Pharmacy Department whom I got to know as friends and with whom I could discuss my scientific problems. Christiane, Melli and Sarah I am very happy to be still in contact and especially Sarah I would like to thank you for helping me to read and correct my thesis.

At the end I would like to thank my family for their support with me and my scientific career. Thanks Alex for joining, listening and supporting me with your endless patience and love.

3.3 List of Publications of the author (all inclusive i.e. including also those not from thesis):

1. **Thomas A.*,** Biswas A.*, Dodt J., Philipou H., Smith E., Ensikat H.J., Ivaskevicius V., and Oldenburg J. Factor XIII A subunit missense mutations affect structure and function at the various steps of factor XIII action. Hum Mutat. 2016, 37(10):1030-1041

2. **Thomas A**., Ivaškevičius V., Zawadzki C., Goudemand J., Biswas A., Oldenburg J. Characterization of a novel large deletion caused by double stranded breaks in 6 bp microhomologous sequences of intron 11 and intron12 of the F13A1 gene. Human Genome Variation, 2016, 15059.

3. Ivaškevičius V.*, **Thomas A.***, Biswas A., Ensikat J., Schmitt U., Horneff S., Pavlova A., Pötzsch B., Oldenburg J. A novel fibrinogen γ chain frameshift deletion (c.637delT) in a patient with hypodysfibrinogenemia associated with thrombosis. Hamostaseologie 2015 Suppl 1:S27-31

4. Ivaškevičius V, Goldmann G, Biswas A, Westhofen P, **Thomas A**., Marquardt N, Horneff S, Klein C, Rühl H, Pötzsch B, Oldenburg J. Neoplasm-induced bleeding in inherited, heterozygous FXIII-A deficiency. Hamostaseologie. 2015;35 Suppl 1:S32-5.

5. **Thomas A.*,** Biswas A.*, Ivaškevičius V., Oldenburg J. Structural and functional influences of coagulation factor XIII subunit B heterozygous missense mutants. Mol Genet Genomic Med. 2015, 3(4):258-71.

6. Biswas A., Ivaškevičius V., **Thomas A**, Varvenne M, Brand B, Rott H, Haussels I, Ruehl H, Scholz U, Klamroth R, Oldenburg J. Eight novel F13A1 gene missense mutations in patients with mild FXIII deficiency: in silico analysis suggests changes in FXIII-A subunit structure/function. Ann Hematol. 2014, 93(10):1665-76.

7. Biswas A., Ivaškevičius V., **Thomas A.**, Oldenburg J. Coagulation factor XIII deficiency. Diagnosis, prevalence and management of inherited and acquired forms. Hamostaseologie. 2014, 34(2):160-6.

8. Biswas A.*, **Thomas A.*,** Bevans C.*, Ivaškevičius V., Oldenburg J. In vitro secretion deficits are common among human coagulation factor XIII subunit B missense mutants: correlations with patient phenotypes and molecular models. Hum Mutat. 2013, 34(11):1490-500.

9. Ivaškevičius V.*, Biswas A.*, **Thomas A.**, Lyonga S., Rott H., Halimeh S., Kappert G., Klammroth R., Scholz U., Eberl W., Harbrecht U., Gnida C., Hertfelder H., Marquardt N., Oldenburg J. A common F13A1 intron 1 variant IVS1+12(A) is associated with mild FXIII deficiency in Caucasian population. Ann Hematol. 2013, 92(7):975-9.

10. Biswas A, Ivaškevičius V., Seitz R, **Thomas A**, Oldenburg J. An update of the mutation profile of Factor 13 A and B genes. Blood Rev. 2011, 25(5):193-204.

*These authors contributed equally

3.4 Poster and Oral presentation

Poster presentation:

Thomas A., H.J. Ensikat, Biswas A., Ivaskevicius V., Oldenburg J. *FXIIIA heterozygous missense mutations decrease the fiber thickness in fibrin clots.* Gth Düsseldorf 2015

Thomas A., Biswas A., Ivaskevicius V., Oldenburg J. *Co-localization analysis of pathological FXIIIB subunit cysteine variants supports a varied but indirect effect on secretion.* Wien 2014

Thomas A., Biswas A., Ivaskevicius V., Lyonga S., Oldenburg J. *Co-localization analysis of a pathological FXIIIB subunit cysteine variant Cys5Arg does not suggest a direct effect on secretion*. Hamburg 2013

Thomas A., Biswas A., Ivaskevicius V., Oldenburg J. *Establishing causativity for isolated heterozygous mutations in F13A and B gene by in vitro expression.* ISTH Kyoto 2013

Thomas A., Biswas A., Ivaskevicius V., Aburubaiha Z., Lyonga S., Oldenburg J. *Structure-functional analysis of heterozygous missense mutations screened from the F13A gene supports their causality for mild FXIII deficiency*. GTH München 2013

Thomas A., Biswas A., Ivaskevicius V., Oldenburg J. *Establishing causativity for isolated heterozygous mutations in F13A and B gene by in vitro expression*. Sankt Gallen, 2012

Thomas A., Biswas A., Ivaskevicius V., Oldenburg J. *Establishing causativity for isolated heterozygous mutations in F13B gene by in vitro expression*. Hamburg 2011

Thomas A., Biswas A., Ivaskevicius V., Oldenburg J. 44. Jahreskongress der Deutschen Gesellschaft für Transfusionsmedizin und Immunhämatologie (DGTI): Hannover 2011

Thomas A., Biswas A., Ivaskevicius V., Oldenburg J. *In vitro expression of F13A heterozygous mutations and their effect on Factor XIII A activity and antigen levels*. Hamburg 2010

Oral poster presentation

Thomas A., Biswas A., Ivaskevicius V., Lyonga S., Oldenburg J. *Co-localization analysis of pathological FXIIIB subunit mutants confirms an indirect but varied effect on secretion.* World Federation of Haemophilia conference Melbourne, 2014

Talks

Thomas A., Biswas A., Ivaskevicius V., Oldenburg J. *Characterization of a rare large deletion found in the F13A1 gene spanning intron 11 to intron 12.* GTH Düsseldorf 2015

Thomas A., Biswas A., Ivaskevicius V., Aburubaiha Z., Lyonga S., Oldenburg J. *FXIIIB subunit mutations show differences in secretory pattern.* GTH Munich 2013

Thomas A., Biswas A., Ivaskevicius V., Oldenburg J. *In vitro expression of F13A and F13B heterozygous mutations and their effect on Factor XIII A and B activity and antigen levels.* Wiesbaden, 2011